

Genetic and Molecular Investigation of the Schnitzler Syndrome

Shelly Pathak

Submitted in accordance with the requirements for the degree
of Doctor of Philosophy

The University of Leeds
School of Medicine

November 2019

This copy has been supplied on the understanding that it is
copyright material and that no quotation from the thesis may be
published without proper acknowledgment

Intellectual Property and Publication Statement:

The candidate confirms that the work submitted is her own, except where work which has formed part of jointly-authored publications has been included. The contribution of the candidate and the other authors to this work has been explicitly indicated below. The candidate confirms that appropriate credit has been given within the thesis where reference has been made to the work of others.

Publication 1: 'Molecular genetic investigation, clinical features, and response to treatment in 21 patients with Schnitzler syndrome'.

Blood, 2018

Authors: Dorota M. Rowczenio, Shelly Pathak, Juan I. Arostegui, Anna Mensa-Vilaro, Ebun Omoyinmi, Paul Brogan, Dan Lipsker, Thomas Scambler, Roger Owen, Hadija Trojer, Anna Baginska, Julian D. Gillmore, Ashutosh D. Wechalekar, Thirusa Lane, Rene Williams, Taryn Youngstein, Philip N. Hawkins, Sinisa Savic, and Helen J. Lachmann.

Contributions

Conception and Study Design: Dorota M. Rowczenio, Sinisa Savic, Helen J. Lachmann.

Experimental Performance and Data Analysis: Dorota M. Rowczenio, Shelly Pathak, Anna Mensa-Vilaro, Ebun Omoyinmi, Thomas Scambler, Roger Owen, Hadija Trojer, Anna Baginska, Dan Lipsker, Paul Brogan.

Patient Recruitment and Care: Julian D. Gillmore, Ashutosh D. Wechalekar, Thirusa Lane, Rene Williams, Taryn Youngstein, Philip N. Hawkins, Sinisa Savic.

Manuscript Writing: Dorota M. Rowczenio and Helen J. Lachmann.

Publication 2: 'Exploratory study of MYD88 L265P, rare *NLRP3* variants and clonal hematopoiesis prevalence in patients with Schnitzler's Syndrome'.

Arthritis and Rheumatology, 2019

Authors: Shelly Pathak, Dorota M Rowczenio, Roger G Owen, Gina M Doody, Darren J Newton, Claire Taylor, Jan Taylor, Catherine Cargo, Philip N Hawkins, Karoline Krause, Helen J Lachmann, Sinisa Savic.

Contributions

Conception and Study Design: Shelly Pathak, Gina M Doody, Darren J Newton, Catherine Cargo, Philip N Hawkins, HelenJ Lachmann, Sinisa Savic.

Experimental Performance and Data Analysis: Shelly Pathak, Dorota M Rowczenio, Gina M Doody, Darren J Newton, Catherine Cargo, Roger G Owen, Claire Taylor, Philip N Hawkins, Jan Taylor, Karoline Krause, Sinisa Savic.

Patient Recruitment and Care: Helen J Lachmann, Karoline Krause, Sinisa Savic.

Manuscript Writing: Shelly Pathak and Sinisa Savic.

This copy has been supplied on the understanding that it is copyright material and that no quotation from the thesis may be published without proper acknowledgement.

© 2019 The University of Leeds and Shelly Pathak

Acknowledgements

For God, my parents and grandparents, for without whom this PhD would have been impossible.

Abstract

The Schnitzler Syndrome (SchS) is a rare, autoinflammatory condition with an unknown pathological mechanism, but treatment with IL-1 inhibition provides remarkable efficacy. Exhibiting two main defining features: (1) an urticarial rash and (2) an IgM gammopathy, this IL-1 mediated disease phenotypically bears stark resemblance to NLRP3-associated inflammatory disease. The latter monogenic entity is known to show gain-of-function and pathological mutations in the NACHT, LRR and PYD domains-containing protein 3 (NLRP3) inflammasome. Furthermore, 20% of SchS patients go on to develop overt lymphoproliferative diseases, namely Waldenström's Macroglobulinaemia (WM). This condition presents with a specific mutation in the Myeloid Differentiation Primary Response (*MYD88*) gene in over 90% of patients. Against the backdrop of these imperative findings, the work presented in this thesis therefore examines the role of these immunological constituents in SchS, via the assessment of mutations in *NLRP3* and *MYD88* alongside a panel of genes frequently mutated in haematological malignancies. Identification of a causative gene would not only improve molecular diagnosis, but allows for potential unearthing of genotype-phenotype correlations.

Since the identification of this condition in 1972, the features and consequences of the IgM gammopathy has remained elusive. In a bid to delineate the latter, examination of the heavy chain of the immunoglobulin repertoire would therefore indicate aspects of the adaptive immune response integral to formation of the monoclonal component. A biased repertoire would therefore indicate the existence of a clonal B-cell population. Additionally, isolation of SchS-IgM and interrogation of a protein array comprising of over 15,700 human proteins further indicates whether this element causes pathological effects.

Exploration of the genetic and molecular components did not expose a common mechanism through which SchS manifests, ruling out the notion that *NLRP3*, *MYD88* and other associated genes are universally causative of this enigmatic disease. Assessment of the IgH repertoire indicated that SchS patients show evidence of expanded B-cell populations, and together with protein array analysis demonstrating the preference of IgM binding to nuclear antigens, this study supports the theory that SchS is a clonal disorder. The breadth and depth of these findings broadens the currently limited scientific knowledge pertaining to SchS, forming the basis upon which further investigations can commence.

Contents

Chapter 1: Introduction	1
Systemic Auto-inflammatory Disorders	1
1.1.1 Broadening the spectrum of SAIDs and PFS.....	5
1.2 The Schnitzler Syndrome	6
1.2.1 Differential Diagnosis and Diagnostic Criteria.....	6
1.2.2 Genetics.....	9
1.2.3 Clinical Findings.....	9
1.2.4 Biological Findings.....	12
1.2.5 Unique Findings.....	14
1.2.6 Disease Course and Complications.....	14
1.2.7 Pathophysiology.....	15
1.2.8 Treatment	18
1.3 The NLRP3 Inflammasome.....	25
1.4 The Connection between Autoinflammation and Clonal Haematopoiesis	26
1.5 Schnitzler Syndrome and Lymphoproliferative Disorders	27
1.6 Binding Capacities of the Monoclonal Component	28
1.7 B-cell Repertoire Sequencing	29
1.8 Novelty of this PhD.....	30
1.9 Hypotheses of this PhD.....	31
Chapter 2 The Schnitzler Syndrome as an auto inflammatory disease	33
2.1 Introduction	33
2.1.1 Periodic Fever Syndromes.....	33
2.1.2 The Inflammatory Response of Schnitzler Syndrome.....	33
2.1.3 The role of the NLRP3 inflammasome in autoinflammatory disease.....	34
2.1.4 Chapter aims.....	38
2.2 Methods	39
2.2.1 Patients and ethical approval.....	39
2.2.2 Cytokine Detection.....	39
2.2.3 IL-18 ELISA.....	39
2.2.4 Statistical analysis.....	40
2.2.5 DNA extraction.....	40
2.2.6 PCR and agarose-gel electrophoresis	40

2.2.7	Galaxy.....	44
2.2.8	ASC specks	45
2.3	Results	46
2.3.1	Cytokine data	46
2.3.2	PCR and agarose-gel electrophoresis	50
2.3.3	Sample QC and pooling.....	52
2.3.4	Sequencing results	54
2.3.5	ASC specks are elevated in autoinflammatory diseases	57
2.3.6	Clinical Data summary of the SchS patients.....	58
2.4	Discussion.....	59
2.4.1	Cytokine data	59
2.4.2	NGS of the NLRP3 gene.....	60
2.4.3	ASC specks	61
2.4.4	Chapter conclusions	63
Chapter 3 Exploring the role of Clonal Haematopoiesis in Schnitzler Syndrome		64
3.1	Introduction	64
3.1.1	The MYD88 L265P mutation.....	64
3.1.2	Waldenström's Macroglobulinaemia	65
3.1.3	MDS and autoinflammatory disease	67
3.1.4	X inactivation.....	68
3.1.5	The Role of CH in SchS.....	69
A. Deep sequencing of 28 MDS related genes in 30 SchS patients		69
3.2	Methods	70
3.2.1	Primary fibroblast explant culture.....	70
3.2.2	Genetic investigation into <i>MYD88</i>	70
3.2.3	MDS sequencing.....	71
3.2.4	X inactivation.....	71
3.3	Results	73
3.3.1	The <i>MYD88</i> L265P mutation.....	73
3.3.2	Primary fibroblast explant culture & ASO PCR	75
3.3.3	HMDS Sequencing panel.....	77
3.3.4	XCI patterns at the <i>HUMARA</i> locus	78
3.4	Discussion.....	83
3.4.1	MYD88 L265P.....	84
3.4.2	MDS sequencing panel.....	87

3.4.3	X inactivation.....	88
3.4.4	Chapter conclusions	89
Chapter 4 IgM Isolation and Protein Microarray.....		90
4.1	Introduction	90
4.1.1	Protein isolation and purification	90
4.2	Methods	93
4.2.1	IgM isolation.....	93
4.2.2	Isolated IgM profiling on proteome microarray.....	96
4.3	Results	101
4.3.1	Isolated IgM levels	101
4.3.2	Protein microarray.....	105
4.3.3	Shared protein targets	124
4.4	Discussion.....	125
4.4.1	IgM isolation from serum.....	125
4.4.2	Chapter conclusions	130
Chapter 5 IgH sequencing		131
5.1	Introduction	131
5.1.1	Properties of the IgH region	132
5.1.2	Assessment of the immune repertoire	140
5.2	Methods	143
5.2.1	IgH NGS.....	143
5.3	Results	148
5.3.1	PCR and agarose gel-electrophoresis	148
5.3.2	Quality control of the libraries	150
5.3.3	Sequencing and quality scores	152
5.3.4	Repertoire diversity	153
5.3.5	CDR3 characteristics	154
5.3.6	VDJ usage	176
5.3.7	V-J recombination	183
5.4	Discussion.....	186
5.4.1	IgH	186
5.4.2	VH usage	190
Chapter 6 Main Discussion		196
6.1	Main findings	196
6.2	Future Experiments.....	197

6.2.1	Precise assessment of IL-1 and related cytokines.....	197
6.2.2	Screening for the MYD88 L265P mutation	198
6.2.3	The effect of IgM on SchS pathology.....	198
6.2.4	Follow up of VDJ usage and CDR3 aa expansion.....	199
6.3	Strengths and Limitations of this PhD project	199
6.4	Conclusions.....	201
Chapter 7 Appendices		202
7.1	Primer sequences	202
7.1.1	Results Chapter 2 primer sequences.....	202
7.1.2	IgH sequencing primers	203
7.2	Results Chapter 3 primer sequences.....	203
7.2.1	ASO-PCR primer sequences for <i>MYD88</i>	203
7.2.2	List of MDS genes sequenced.....	204
7.3	Genes sequenced as part of the UCL panel.....	205
7.4	Calculation of the frequency of CDR3 clones	206
7.4.1	10% B-cell assumption within gDNA.....	206
7.4.2	1% B-cell assumption in gDNA.....	209
References		212

List of Figures

Figure 1: The typical urticaria seen with SchS.	10
Figure 2: Histopathology of NUD.....	11
Figure 3: The NLRP3 inflammasome.	35
Figure 4: Workflow of DNA library preparation.	43
Figure 5: The customised Galaxy workflow used in this study.	44
Figure 6: IL-1 β and IL-6 cytokine levels.	46
Figure 7: IL-8, IL-10, IL-12p40 and IL-12p70 cytokine levels.	47
Figure 8: IL-17 α , IL-18, IFN- γ and TNF- α cytokine levels.	48
Figure 9: Schematic of the NLRP3 gene and primer coverage.....	50
Figure 10: Visualisation of <i>NLRP3</i> PCR products.	50
Figure 11: Bioanalyser results trace.	52
Figure 12: PicoGreen Assay curve.....	53
Figure 13: Sequencing coverage and alignment of the amplicon sequencing.	54
Figure 14: Representative QC figure generated by Galaxy.	55
Figure 15: IGV sequencing analysis.....	56
Figure 16: ASC specks per microlitre.....	57
Figure 17: The absence of a correlation between CRP and ASC specks.	62
Figure 18: MYD88 dependent pathway.....	64
Figure 19: Schematic of the MYD88 protein.	65
Figure 20: The link between MYD88 and NLRP3	66
Figure 21: The development of haematopoietic and mesenchymal stem cell lineages.	67
Figure 22: Schematic showing the rise of cell progeny with skewed XCI.	69
Figure 23: ASO-PCR results of 30 SchS patients.	74
Figure 24: ASO PCR results for the aNLRP3-AID patients.....	74
Figure 25: Primary fibroblast culture and ASO-PCR results.	75
Figure 26: Chromatogram showing the male DNA control.....	78
Figure 27: Chromatogram showing the healthy female DNA control.	79
Figure 28: Chromatogram showing skewing of SchS patient 9.....	80
Figure 29: Chromatogram showing skewing of acquired NLRP3-AID patient 3.....	81
Figure 30: Schematic of the research undertaken in Chapter 3.....	83
Figure 31: Schematic of the MYD88 ASO-PCR primer coverage.....	84
Figure 32: Stepwise summary of the IgM isolation procedure.	95
Figure 33: Summary of steps carried out for the HuProt™ protein microarray.	96

Figure 34: Layout of the HuProt™ protein microarray slide.	98
Figure 35: Representative chromatogram from the AKTA machine.....	102
Figure 36: Representative SDS PAGE blots.	103
Figure 37: Array visualisation for SchS patient 2.	106
Figure 38: Array visualisation for SchS patient 23.	109
Figure 39: Array visualisation for SchS-31.	112
Figure 40: Array visualisation for WM-1.	115
Figure 41: Array visualisation for WM-2.	118
Figure 42: Array visualisation for NLRP3-AID patient 7.	121
Figure 43: Overlapping IgM targets.	124
Figure 44: Percentage composition of proteins imprinted on the HuProt™ array slide.....	126
Figure 45: Overview of VDJ recombination.	133
Figure 46: Generation of the antigen binding section an antibody from the IgH locus.	134
Figure 47: Basic structure of an antibody.	135
Figure 48: The structure of IgM.	138
Figure 49: Amplification of the IgH region.	143
Figure 50: Workflow for processing IgH data.	146
Figure 51: Representative gel doc image of the first round of IgH PCR.	148
Figure 52: Representative PCR image denoting the second round of indexing.....	149
Figure 53: Representative bioanalyser trace.....	150
Figure 54: The 8 point standard curve obtained with the PicoGreen assay.....	151
Figure 55: Schematic showing the sequencing coverage of the VDJ region carried out. ..	152
Figure 56: Galaxy quality score boxplots.	152
Figure 57: The calculated number of input cells and reads per B cell.....	156
Figure 58: Ranking of unique CDR3 aa sequences.	159
Figure 59: Frequency distribution of all CDR3 aa sequences.	165
Figure 60: CDR3 clones as a proportion of all CDR3 aa sequences.	166
Figure 61: Box and whisker plots comparing CDR3 lengths across 10 SchS patients.	169
Figure 62: CDR3 length distribution.	171
Figure 63: CDR3 composition in SchS patients.	174
Figure 64: Comparison of 10 SchS CDR3 aa compositions.	175
Figure 65: V gene usage in 10 SchS patients.	176
Figure 66: D gene usage in 10 SchS patients.....	177
Figure 67: J gene usage in 10 SchS patients.....	178
Figure 68: VH, DH and JH gene usage.	180

Figure 69: Representative circos plots of V-J recombination.	183
Figure 70: Circos plots of HC, SchS-24 and CLL.	185

List of Tables

Table 1: Comparison table of monogenic SAIDs well studied in literature.	3
Table 2: Differential diagnosis of SchS.	7
Table 3: Comparison of the SchS diagnostic criteria.	7
Table 4: Clinical and biological findings in SchS.	8
Table 5: Clinical Data Summary of SchS patients.	58
Table 6: The composition of the restriction enzyme digestion.	72
Table 7: Composition of reagents required for PCR amplification.	72
Table 8: MDS sequencing panel.	77
Table 9: Summary of Results	82
Table 10: Resulting IgM concentrations from the isolation procedure (g/L).	101
Table 11: Top 20 hits from the protein microarray for sample SchS-2.	107
Table 12: Top 20 hits from the protein microarray for SchS patient 23.	110
Table 13: Top 20 hits from the protein microarray for SchS patient 31.	113
Table 14: Top 20 hits from the protein microarray for sample WM-1.	116
Table 15: Top 20 hits from the protein microarray for sample WM-2.	119
Table 16: Top 20 hits from the protein microarray for sample NLRP3-AID 7.	122
Table 17: Combinatorial diversity.	132
Table 18: Initial sequencing counts as computed by IMG-T.	153
Table 19: Inference of B-cell counts and reads.	157
Table 20: SchS patients included for the IgH research.	158
Table 21: CDR3 clones derived from the IgH sequencing data.	163
Table 22: Primer sequences for <i>NLRP3</i>	202
Table 23: List of primers used to amplify the IgH locus.	203
Table 24: The panel of 28 MDS associated genes.	204
Table 25: Panel of 32 genes associated with monogenic autoinflammatory diseases.	205

Abbreviations

AA: Amino Acid

ABC-DBCL: Activated B Cell Diffuse Large B-Cell Lymphoma

AD: Autosomal Dominant

AID: Associated Inflammatory Disease

AML: Acute Myeloid Leukaemia

AOSD: Adult-Onset Still's Disease

AR: Autosomal Recessive

ASC: Apoptosis-associated speck-like protein containing a CARD domain

ASO: Allele-Specific Nucleotide

AUC: Area Under the Curve

BALP: Bone Alkaline Phosphatase

BM: Bone Marrow

BMPs: Bone Morphogenic Proteins

BTK: Bruton's Tyrosine Kinase

CAD: Cold Agglutinins Disease

CAMPS: CARD14-Mediated Pustular Psoriasis

CANDLE: Chronic Atypical Neutrophilic Dermatitis with Lipodystrophy and Elevated Temperature Syndrome

CCL2: C-C Chemokine Ligand 2

CDR: Complementarity- Determining Region

CH: Clonal Haematopoiesis

CINCA: Chronic Infantile Neurological, Cutaneous, and Articular syndrome

CLL: Chronic Lymphocytic Leukaemia

COPD: Chronic Obstructive Pulmonary Disease

CPA: Cambridge Protein Arrays

CRP: C-Reactive Protein

CTX: C-Terminal Telopeptide

DADA2: Deficiency of Adenosine Deaminase 2

DAMPs: Damage-Associated Molecular Patterns

DIRA: Deficiency of Interleukin-1 Receptor Antagonist

DITRA: Deficiency of the IL-36 Receptor Antagonist

ESR: Erythrocyte Sedimentation Rate
FACS: Fluorescence Activated Cell Sorting
Fc: Fragment Crystallisable Region
FCAS: Familial Cold Autoinflammatory Syndrome
FCAS2: Familial Cold Autoinflammatory Syndrome 2
FcεRIα: IgE receptor alpha
FDA: Food and Drug Administration
FMF: Familial Mediterranean Fever
FPLC: Fast Protein Liquid Chromatography
gDNA: Genomic DNA
GOF: Gain of Function
HC: Healthy Control
HLH: Haemophagocytic Lymphohistiocytosis
HMDS: Haematological Malignancy Diagnostic Service
HPLC: High Performance Liquid Chromatography
HSC: Haematopoietic Stem Cell
HSCT: Haematopoietic Stem Cell Transplantation
IFN-γ: Interferon Gamma
Ig: Immunoglobulin
IgE: Immunoglobulin E
IgG: Immunoglobulin G
IgH: Immunoglobulin Heavy Chain Locus
IgM: Immunoglobulin M
IgMκ: IgM kappa
IGV: Integrated Genome Viewer
IL: Interleukin
IL-1R: Interleukin-1 Receptor
IL-1Ra: IL-1 Receptor Antagonist
L265P: Leucine to Proline Substitution at AA position 265
LPD: Lymphoproliferative Disorder
LPL: Lymphoplasmacytic Lymphoma
LPS: Lipopolysaccharide

LUBAC: Linear Ubiquitin Chain Assembly Complex
mAb: Monoclonal Antibody
MAS: Macrophage Activation Syndrome
MCP-1: Monocytic Chemoattractant Protein-1
MDS: Myelodysplastic Syndrome
MGUS: Monoclonal Gammopathy of Unknown Significance
MKD: Mevalonate Kinase Deficiency
MM: Multiple Myeloma
MOI: Mode of inheritance
MWS: Muckle-Wells Syndrome
MYD88: Myeloid Differentiation Primary Response Gene 88
MZL: Marginal Zone Lymphoma
NF- κ B: Nuclear Factor Kappa-Light-Chain-Enhancer of Activated B Cell
NGS: Next-Generation Sequencing
NLR: Nod-Like Receptor
NLRC4: NLR Family CARD Domain – Containing Protein 4
NLRC4-AID: NLRC4-Associated Inflammatory Disease
NLRP3: NACHT, LRR and PYD domains-containing protein 3
NLRP3-AID: NLRP3 Associated Inflammatory Disease
NMR: Nuclear Magnetic Resonance
NSAIDs: Nonsteroidal Anti-Inflammatory Drugs
NUD: Neutrophilic Urticarial Dermatoses
OA: Osteoarthritis
OH: Oligoclonal Haematopoiesis
OPN: Osteoprotegerin
ORAS: Otulin-Related Autoinflammatory Syndrome
PAAND: Pyrin-Associated Autoinflammation with Neutrophilic Dermatitis
PAMPs: Pathogen-Associated Molecular Patterns
PAPA: pyogenic arthritis, pyoderma gangrenosum, and acne syndrome
PB: Peripheral Blood
PBMcs: Peripheral Blood Mononuclear Cells
PCR: Polymerase Chain Reaction

PFS: Periodic Fever Syndrome

POEMS: Polyneuropathy, Organomegaly, Endocrinopathy, Myeloma Protein, and Skin Changes

QoL: Quality of Life

RA: Rheumatoid Arthritis

RBCs: Red Blood Cells

RORyT: Rar-Related Orphan Receptor Gamma

ROS: Reactive Oxygen Species

SAA: Serum Amyloid A

SAID: Systemic Autoinflammatory Disorder

SAVI: Sting-Associated Vasculopathy with Onset in Infancy

SchS: Schnitzler Syndrome

SDS-PAGE: Sodium Dodecyl Sulphate Polyacrylamide Gel Electrophoresis

SJIA: Systemic Juvenile Idiopathic Arthritis

SLE: Systemic Lupus Erythematosus

SNV: Single Nucleotide Variant

SRANKL: Soluble Receptor Activator of NF- κ B Ligand

TA: Thiophilic Adsorption

TF: Transcription Factor

Th-17: T helper-17 cells

TIR: Toll/Interleukin 1 Receptor

TLR: Toll-Like Receptor

TNF α : Tumour Necrosis Factor alpha

TRAPS: TNF-associated Periodic Fever Syndrome

VDJ: Variable, Diversity and Junctional

VEGF: Vascular Endothelial Growth Factor

WES: Whole Exome Sequencing

WM: Waldenström's Macroglobulinaemia

WT: Wild-Type

XCI: X-Chromosome Inactivation

XLA: X-linked Agammaglobulinaem

Chapter 1: Introduction

Systemic Auto-inflammatory Disorders

Characteristically distinguished by recurrent outbreaks of sterile systemic inflammation, 'Systemic Auto-inflammatory Disorders' (SAIDs) are referred to as conditions of the innate immune system (1). The presence of high titre antibodies (Abs) or antigen-specific T cells characteristic of an adaptive immune response is absent in SAIDs. More particularly over the last decade and since the advent of Next Generation Sequencing (NGS), the SAIDs spectrum is broadening and included in this overarching term are Periodic Fever Syndromes (PFS), bearing a monogenetic basis. Being of a recurrent nature, the periodic fevers seen within PFS have no infectious basis (2). A majority of PFS have undergone comprehensive genetic and functional delineation, attributable to novel gene and mutation discovery. The NLRP3-associated autoinflammatory disease spectrum (NLRP3-AID); Familial Mediterranean Fever (FMF); and Tumour Necrosis Factor Associated Periodic Syndrome (TRAPS) form the more well-studied hereditary PFS.

Diagnosis of such hereditary PFS was entirely dependent upon the assessment of clinical manifestations and laboratory findings, up until the 1990's. Mutations within exon 10 of *MEFV*, encoding the inflammasome associated protein, pyrin, was deemed causative of FMF (3). This novel finding was closely followed by the discovery of TNF-receptor associated mutations causal of TRAPS (1). Alongside the Mendelian mode of inheritance and significant progression in genetic mapping techniques, identification of many monogenic forms of SAIDs ensued. (Table 1). The pathogenesis of these PFS can be attributed to the aberrant IL-1 β release due to inappropriate caspase 1 activation. Likewise, a large proportion of these conditions are successfully treated with IL-1 blockade (4).

General pathway	Disease	Gene	Affected protein	MOI	Age of onset	Key clinical features	Treatment
Inflammasomopathies	FMF	MEFV ¹	Pyrin	AR/AD	0-20 yrs	Peritonitis, joint attacks and joint pain	Colchicine/anti-IL1
	PAAND	MEFV ¹	Pyrin	AD	0-10 yrs	Neutrophilic dermatosis (Pyoderma gangrenosum) arthralgia, myalgia	Anti-IL-1/anti-TNF
	PAPA	PSTPIP1	CD2 binding protein-1	AD	1-16 yrs	Juvenile-onset arthritis, painful ulcers and acne	Prednisone/ anti-IL-1, anti-TNF
	MKD	MVK	Mevalonate kinase	AR	Variable ²	Lymphadenopathy, abdominal pain, joint pain, diarrhoea, skin rashes, and headache	NSAIDs/ prednisone/Anti-IL-1, Anti-TNF
	<i>NLRP3</i> -AID (spectrum) CINCA/NOMID, MWS, FCAS	NLRP3 ¹	NLRP3	AD*	Variable ²	Conjunctivitis, general malaise, headaches, rash, joint pain	Anti-IL-1
	<i>NLRP12</i> -AID	NLRP12	Monarch-1 protein	AD	Infancy	Skin rash, lymphadenopathy, aphthous ulcers, abdominal complaint	Anti-IL-1 /corticosteroids
	<i>NLR4</i> -AID	NLRC4	NLRC4	AD	Infancy	Infantile enterocolitis Macrophage activation syndrome	Anti-IL-1/anti-IL18
	<i>NLRP1</i> -AID	NLRP1	NLRP1	AD	6 mo-10 yrs	Dyskeratosis, arthritis	Acitretin, anti-IL-1
Interferonopathies	Aicardi Goutières syndrome	TREX1 RNASEH2A, RNASEH2B, RNASEH2C, SAMHD1	Exonuclease subunits of the RNase H2 endonuclease complex, Control of dNTP pool	AD/AR	Infancy-Childhood	Encephalopathy, hepatosplenomegaly, skin lesions	Symptomatic treatment JAK inhibition Reverse transcriptase inhibitors
	Proteasome-associated autoinflammatory syndrome (PRAAS), CANDLE	PSMB3, PSMB4, PSMB8, PSMB9, POMP	Proteasome	AR	Infancy	Skin eruptions, progressive lipodystrophy, hepatosplenomegaly, myositis,	Glucocorticoids JAK inhibition/
	SAVI	TMEM173	Stimulator of Interferon Genes (STING)	AD	Infancy-childhood	Vasculopathy, skin lesions (leading to ulcers and necrosis), Raynaud phenomenon	JAK inhibition
Relopathies	A20 haploinsufficiency	TNFAIP3	NF-κB regulatory protein, A20	AD*	Variable	Oral, gastrointestinal and genital ulcers; arthralgia	Colchicine, systemic corticosteroids, anti-IL-1, anti-IL-6, anti-TNF

	Biallelic RIPK1 mutations	RIPK1	Receptor interacting serine/threonine kinase 1	N/A	Infancy	Early-onset inflammatory bowel disease, and progressive polyarthritis	HSCT successful in 1 patient
	HOIL-1/HOIP deficiency	HOIL-1, HOIP	HOIP, HOIL-1, and SHARPIN (components of LUBAC)	AR	Infancy	Amylopectinosis, increased susceptibility to viral and bacterial infections	HSCT
	ORAS	OTULIN	Otulin (deubiquitinase protease)	AR	Infancy	Panniculitis, diarrhoea, swollen joints	Anti-TNF
	RELA (p65) haploinsufficiency	P65	REL-associated protein	AD	Variable	Abdominal pain, mucocutaneous ulceration vomiting, leucocytosis	Anti-TNF
Others	DADA2	CECR1	Adenosine Deaminase 2	AR	Variable	Mottled rash (livedo reticularis) anaemia, joint pain, fatigue	Anti-TNF, bone marrow transplantation
	DIRA**	IL-1RN	IL-1 Receptor Antagonist	AR	Infancy	Painful joint swelling, pustular rash, hepatosplenomegaly	IL-1 blockade
	DITRA	IL-36RN	IL-36 Receptor Antagonist	AR	Infancy	Pustular psoriasis, asthenia	IL-1 blockade, anti-TNF
	TRAPS	TNFRSF1A	Tumour Necrosis Factor	AD	Variable	Skin rash, abdominal pain, myalgia	Corticosteroids, anti-IL-1/anti-TNF
	<i>NOD2</i> -associated granulomatous disease, Blau Syndrome	NOD2	NOD2 inflammatory	AD*	Infancy-childhood	Granulomatous dermatitis, arthritis, uveitis	Anti-TNF

Table 1: Comparison table of monogenic SAIDs well studied in literature.

Aside from apparent high fever, other key clinical features are stated in Table 1 which was constructed using information from references (5-12).

CANDLE: Chronic Atypical Neutrophilic Dermatosi s with Lipodystrophy and Elevated Temperature Syndrome; **CAMPS**: CARD14-Mediated Pustular Psoriasis; **DADA2**: Deficiency of Adenosine Deaminase 2; **FMF**: Familial Mediterranean Fever; **DIRA**: Deficiency Of Interleukin-1 Receptor Antagonist; **DITRA**: Deficiency of the IL-36 Receptor Antagonist; **FCAS2**: Familial Cold Autoinflammatory Syndrome 2; **HSCT**: Haematopoietic Stem Cell Transplantation; **LUBAC**: Linear Ubiquitin Chain Assembly Complex; **MKD**: Mevalonate Kinase Deficiency; **ORAS**: Otulin-Related Autoinflammatory Syndrome; **NLRC4-AID**: NLRC4 Associated Inflammatory Disease; **NLRP3-AID**: NLRP3 Associated Inflammatory Disease; **PAAND**: Pyrin-Associated Autoinflammation with Neutrophilic Dermatosi s; **PAPA**: pyogenic arthritis, pyoderma gangrenosum, and acne syndrome; **SAVI**: Sting-Associated Vasculopathy With Onset In Infancy; **TRAPS**: TNF-associated Periodic Fever Syndrome.

AD: Autosomal Dominant; AID: Associated Inflammatory Disease; AR: Autosomal Recessive; MOI: Mode of inheritance; NSAIDs: Nonsteroidal Anti-Inflammatory Drugs.

¹ Genes that have been investigated in this study.

² Age of onset depends on disease severity.

* Reports of sporadic cases as well.

** Fever is not a typical feature in this condition.

1.1.1 Broadening the spectrum of SAIDs and PFS

Description of new clinical phenotypes alongside utilisation of Next Generation Sequencing (NGS) for causative gene discovery within increasing numbers of patients worldwide, has inevitably expanded the spectrum of PFS (2). Since the primary genetic basis of FMF and TRAPS was established, the focus of genetic testing in SAIDs has successfully rendered identification of several new PFS. Nevertheless, there are still an estimated 50-60% of patients testing negative for germline mutations in genes associated with such monogenic conditions (13). This is markedly relevant as there are growing numbers of sporadic cases recognised in the clinic where patients were not determined to carry such mutations. However, upon further examination facilitated through NGS technology, some of these cases were determined to carry somatic mutations of low frequency in SAID-associated genes, initially arising from the haematopoietic stem cell (HSC) lineage within the bone marrow (14-17). The first indication of this phenomenon was described in a Japanese patient 2005, initially presenting with the more severe NLRP3-AID entity known as Chronic Infantile Neurological, Cutaneous, and Articular Syndrome (CINCA). Sanger sequencing of genomic DNA (gDNA) derived from total peripheral blood mononuclear cells (PBMCs) and also sorted cells (i.e. neutrophils and T cells) revealed the *NLRP3* Y570C mutation appearing at around 20% in each of these subsets. Further cloning experiments established this variant alone to be 'potent in inducing ASC (apoptosis associated speck-like protein containing a CARD) dependent NF- κ B activation', sufficient to cause disease at low percentages (18). Since the publication of this study, several reports utilising NGS have indicated the occurrence of somatic mutations and somatic mosaicism within patients diagnosed with NLRP3-AID, TRAPS and FMF (14-17), where the genetic component was not initially apparent. Another example of a lesser known PFS where this concept was also hypothesised is the Schnitzler Syndrome (SchS). In 2015, de Koning *et al* employed NGS to carry out whole exome sequencing upon gDNA and further granulocytes and monocytes in 11 SchS patients (19), revealing pathological *NLRP3* mutations (F523L and K435E detected at less than 30%) in two SchS patients. Thus, novel insights into the genetics and pathology of these rare conditions through such investigations has not only confirmed appropriate treatment options (i.e. anti-IL-1 therapy for *NLRP3* mutation based conditions), but also revealed the heterogeneous characteristics of PFS.

1.2 The Schnitzler Syndrome

The Schnitzler Syndrome (SchS) is a rare, systemic disease bearing similarities with the monogenic SAID and PFS: NLRP3-AID (mainly Muckle Wells Syndrome (MWS)). The relatively late onset of SchS (presenting in the fifth decade of life) and the lack of positive family history portrays this as an acquired entity. Its main clinical features comprise of a chronic urticarial rash, periodic fevers, bone, joint and/or muscle pain and lymphadenopathy. With regards to biological indicators, a monoclonal immunoglobulin M (IgM) gammopathy is the hallmark of this condition. Prior to the introduction of the IL-1 antagonist anakinra with remarkable success, SchS was conventionally treated with anti-histamines for the chronic urticaria, with systemic and immunosuppressive agents for the systemic manifestations with limited effectiveness. Near to 20% of SchS patients develop overt lymphoproliferative diseases such as Waldenström's Macroglobulinaemia (WM) and Monoclonal Gammopathy of Undetermined Significance (MGUS), with both of the latter conditions presenting with a spike in the monoclonal component. Clinician unfamiliarity alongside the relatively unspecific phenotype of the condition renders SchS as an underdiagnosed entity (20).

1.2.1 Differential Diagnosis and Diagnostic Criteria

The rarity of the SchS combined with the absence of a biological or other confirmative assessment necessitates an extensive and differential diagnosis. Retrospective studies determined that obtaining a definite diagnosis of SchS takes an average of five years; attributed to the rarity of the disease combined with the absence of a biological or other confirmative assessment (21, 22). Given the overlapping features of autoimmune and autoinflammatory disorders with SchS (Table 1), exclusion of haematological, infectious and other immunological conditions, covering both acquired and inherited entities is advised prior to such diagnosis (23) (Table 2). The original diagnostic criteria were first developed by Lipsker *et al.*, in 2001 (24). Over the past decade there have been increased reports of SchS cases, especially beyond Europe where this condition was first documented. Such outcomes indicate that SchS is more common than previously considered (24), and better recognition may be attributed to the revised 'Strasbourg' criteria published in 2013 (Table 3). The notion that SchS is under-diagnosed in the clinic is further highlighted by the retrospective study carried out at Mayo Clinic USA, where 46 undiagnosed patients were identified to fulfil SchS criteria, by cross referencing chronic urticarial and dysproteinaemia databases (25). Notably, this identified cohort was originally stratified from 4,000 patients who presented with monoclonal IgM within that institution alone over 38 years (25).

<p>Periodic Fever syndromes</p> <ul style="list-style-type: none"> • NLRP3 autoinflammatory disease spectrum (NLRP3-AID) • TNFRS1 receptor associated periodic syndrome (TRAPS) • Hyper-IgD syndrome
<p>Immunological disorders</p> <ul style="list-style-type: none"> • Adult Onset Still's disease (AOSD) • Systemic Lupus Erythematosus (SLE)
<p>Haematological Disorders</p> <ul style="list-style-type: none"> • Monoclonal Gammopathy of unknown significance (MGUS) • Waldenström's macroglobulinemia (WM) • Multiple Myeloma (MM) • POEMS syndrome
<p>Infectious diseases</p> <ul style="list-style-type: none"> • Hepatitis (B,C) • Chronic meningococemia
<p>Other</p> <ul style="list-style-type: none"> • Chronic idiopathic urticaria • Mastocytosis • Cryoglobulinaemia • Erdheim-Chester disease

Table 2: Differential diagnosis of SchS.

The above conditions must be excluded before a clinical diagnosis of SchS can be made. This table was constructed using information from: Dingli *et al.*, and de Koning *et al.* (20, 23).

Lipsker 2001 guidelines	Strasbourg 2013 guidelines
Obligate criteria:	Obligate criteria:
<ul style="list-style-type: none"> • Urticarial rash • IgM component 	<ul style="list-style-type: none"> • Chronic urticarial rash • Monoclonal IgM or IgG
With at least two of the following:	With at least two of the following:
<ul style="list-style-type: none"> • Arthralgia or arthritis • Abnormal bone morphology • Bone pain • Elevated ESR • Fever • Leucocytosis • Liver or spleen enlargement • Palpable lymph nodes 	<ul style="list-style-type: none"> • Abnormal bone remodelling with or without bone pain (As assessed by bone scintigraphy, MRI, or elevation of bone alkaline phosphatase) <ul style="list-style-type: none"> • Leucocytosis and/or elevated CRP (Neutrophils >10,000/mm³ and/or CRP >30 mg/L) • Neutrophilic dermal infiltrate on skin biopsy (Corresponding to the entity described as "neutrophilic urticarial dermatosis": absence of fibrinoid necrosis and significant dermal oedema) • Recurrent fever (Must be >38 °C and otherwise unexplained. Occurs usually—but not obligatory—together with the skin rash)

Table 3: Comparison of the SchS diagnostic criteria.

The Lipsker 2001 diagnostic criteria (24) were revised by Simon *et al* in 2013 (22). A patient is diagnosed with SchS if they fulfil both of the obligate criteria and at least 2 of the minor criteria; however preceding this, a differential diagnosis must be made to exclude the more frequent disorders (Table 2). The obligate criteria were amended to denote the urticarial rash as 'chronic' and include the Immunoglobulin G (IgG) gammopathy occurring in approximately 10% of patients (known as variant type SchS). Three minor criteria from the Lipsker recommendations were further detailed (abnormal bone remodelling, leucocytosis/elevated CRP and recurrent fever), with the inclusion of a new guideline based on evaluation of 196 cases with 76% of these demonstrating a neutrophilic dermal infiltrate (Table 4). Nonetheless, the 2001 minor criterion not enlisted in the 2013 guidelines (i.e. palpable lymph nodes) is still a feature of SchS in a proportion of patients and should also be considered upon diagnosis.

Finding	Percentage of SchS patients (%)
Urticarial rash	100
Elevated ESR	95
Fever	93
Monoclonal IgM gammopathy	89
Kappa light chain	89
Arthralgia/Arthritis	77
Neutrophilic leucocytosis	76
Bone pain	68
Abnormal bone morphology	62
Palpable lymph nodes	47
Pruritus	45
Liver and/or spleen enlargement	34

Table 4: Clinical and biological findings in SchS.

Published by Simon *et al* in 2013 (22), Table 4 provides a summary of the clinical and biological findings in 196 patients with SchS. These findings, in association with the Lipsker 2001 diagnostic guidelines, formed the basis of the Strasbourg criteria which are currently implemented (Table 3).

1.2.2 Genetics

Despite sharing many common symptoms with inherited autoinflammatory diseases, the lack of familial clustering and later age of onset renders SchS as an acquired syndrome (26). There have been no genetic studies carried out prior to the brief report published in 2015 by Koning *et al* revealing NLRP3 mutations restricted to the myeloid population of cells in two out of seven patients with SchS (19). Further, two SchS patients were found to have a non-pathological variant in *NLRP3*, although since healthy family members also presented with the same mutation, it is unlikely that this is significant in the context of disease (23, 27)

1.2.3 Clinical Findings

As described, the fundamental clinical symptom of SchS is the chronic urticarial rash, accompanied by intermittent fevers; bone, muscle and joint pain; lymphadenopathy and hepatosplenomegaly. Exhaustion, fatigue and general malaise are also commonly reported. The following section describes the prevalence of SchS and further details the aforementioned observations.

1.2.3.1 Epidemiology

Since the initial description of an SchS patient in 1972 (later published as a single report in 1974 by Liliane Schnitzler (28, 29)), around 300 cases have been reported in literature until date. Though the early cases were European - largely attributable to the enhanced knowledge of the condition in this continent. The past two decades have seen SchS patients originating from the USA (30) to Japan (31) and Australia (32). Notably, SchS doesn't exhibit ethnic preferentiality unlike FMF where approximately a fifth of the Mediterranean and Middle Eastern populations are predicted to be carriers of the disease (4).

Although one SchS patient reported that their urticarial symptoms started at 13 years of age, no paediatric case has been reported until date. The average age of SchS onset is 55 years, with a slight bias of this condition among males, marking parallels with WM where males are affected 50% more than females (33, 34). However the SchS male bias is contrasted to autoimmune disorders which generally follow a female preponderance (35).

1.2.3.2 Chronic urticarial rash

Usually, the recurrent, urticarial rash is the primary clinical indication of SchS. Manifesting mainly on the trunk and limbs, this exanthema presents as rose pink or red macules, with slightly raised papules with a pruritic tendency (36, 37). A similar type of rash can be seen in other autoinflammatory conditions such as Adult-Onset Still's Disease (AOSD) and NLRP3-AID, but where a 'salmon-coloured maculopapular urticarial efflorescence' is observed, AOSD

is a highly likely designation (37, 38). Occasionally, vasoconstriction and dermographism can be seen (39). Although common in urticarial disorders, angioedema is a rare finding, likewise to other PFS (40) and autoimmune conditions such as Systemic Lupus Erythematosus (SLE) (41). Similar to the fever, the eruptions can be aggravated by stress and usually last around 24 to 48 hours. Interestingly, the lesions show a 'daytime dynamic', most 'pronounced' the evening (37, 40), comparable to non-SchS patients presenting with Neutrophilic Urticarial Dermatitis (NUD) and systemic inflammation (42). Appearance of the rash greatly varies individually. For example, the study by Gusdorf *et al* reported that within a 32 SchS patient cohort the rash appeared: daily (n=19), more than once a week (n=4), weekly (n=2) and monthly (n=1) (36). Without treatment, these skin flares tend to resolve under less than a month, though an immediate and 'dramatic' amelioration in the severity of the rash is witnessed within 48 hours upon administration of the IL-1 receptor (IL-1R) antagonist, anakinra (Figure 1) (43, 44).

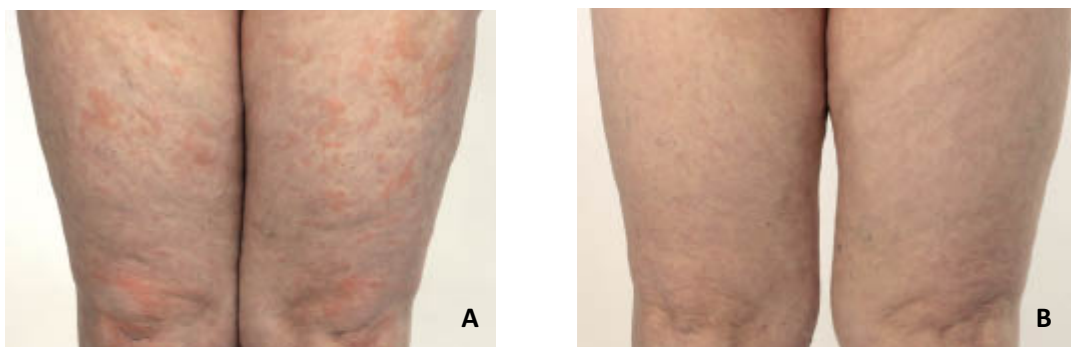


Figure 1: The typical urticaria seen with SchS.

(A) Prior to anti-IL-1 therapy and (B) 48 hours after daily subcutaneous administration of 100mg anakinra showing rapid clearance of the rash. Image taken from Volz *et al*, 2012 (45).

Imperatively, the histopathological analysis of a skin biopsy of a recent lesion is usually carried out to also search for evidence of neutrophilic urticarial dermatosis (NUD) - one of the newly included minor criteria in the revised Strasbourg 2013 guidelines (Table 3). The group of 'neutrophilic urticaria' has never been properly defined, with literature generally referring to this condition as a neutrophilic aseptic disease. In a bid to avoid confusion with NUD, Kieffer *et al* (46) delineated NUD as a separate entity from neutrophilic urticaria on the basis of two distinct histopathological patterns. Where the latter condition is exhibited as a perivascular neutrophilic and eosinophilic infiltrate with dermal edema not associated with systemic disease, NUD is defined as a perivascular and interstitial infiltrate of neutrophils, accompanied by leucocytoclasia but with the absence of vasculitis and edema strongly associated with systemic disease (36, 46).

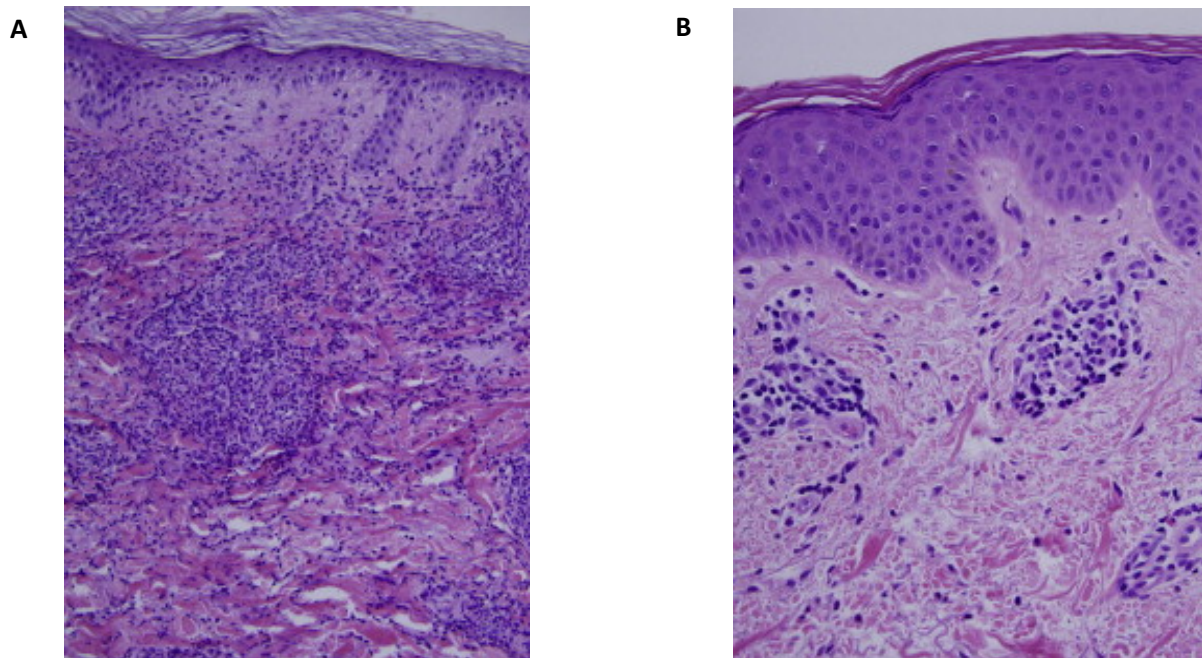


Figure 2: Histopathology of NUD.

Figure 2 (A&B) shows histopathological images of a patient affected with SchS demonstrating characteristic NUD patterns. (A) Principally neutrophilic perivascular and interstitial inflammation with evidence of leucocytoclasia and (B) mononuclear cell perivascular inflammation. Images A and B have been taken from Sokumbi *et al*, 2012 (21) and are stained with haematoxylin-eosin stain at a 20x magnification.

1.2.3.3 Fever

Nearly all SchS patients develop intermittent fever above 39°C, though the duration of the episodes varies per individual (24-48 hours) (33), akin to other PFS such as FMF (47) and NLRP3-AID (48). Interestingly, AOSD commonly reports elevated temperatures from the mid-afternoon to the evening (49) indicating unknown endogenous or external triggers, but an equivalent observation has not been recorded in SchS. Though, environmental and biological factors such as cold exposure, stress and infection can exacerbate fever flares and are commonly accompanied with fatigue (26). Out of 174 SchS patients presenting with urticaria as the predominant SchS symptom, 16 appeared to have this symptom three years prior to fever, with one case described as having fever a year before urticaria. The other 157 patients demonstrated both symptoms occurring simultaneously (20), thus, the onset of fever is usually concurrent with the dermal manifestations of the disease.

1.2.3.4 Organomegaly

Aside from the characteristic dermal manifestations, physical examination of SchS patients can also show abnormal organ enlargements. Evaluation of 281 cases by de Koning *et al* determined lymphadenopathy in a third of patients, with hepatomegaly and splenomegaly less common at around 10% (20). These swollen, palpable lymph nodes are largely in the axillary and inguinal regions, and can be permanently enlarged up to several centimetres presenting non-specific inflammation (23, 26, 37).

1.2.3.5 Kidney involvement

Five cases have been published where kidney involvement was presented alongside the SchS symptoms. O'Hare *et al* described the first known patient with renal insufficiency as measured by serum creatinine, followed by a kidney biopsy revealing tubulointerstitial nephritis associated with light chain deposition (50). This initial report was followed up by four more studies stating membranous nephropathy and membranoproliferative glomerulonephritis (51-54). The described renal issues were largely resolved upon treatment with either NSAIDs or IL-1 inhibition. Intriguingly, the study subjects were exclusively males and whether this is due to the male preponderance of the disease (39) or whether they are predisposed to renal ramifications in the context of SchS, is an observation yet to be examined. Nevertheless, reports of serum amyloidosis complications facilitates the recommendation of close kidney function monitoring as well, despite the infrequency of SchS kidney involvement (55).

1.2.4 Biological Findings

One of the two defining criteria of SchS is the existence of an IgM monoclonal component, alongside increased levels of inflammatory markers such as C - Reactive Protein (CRP), Erythrocyte Sedimentation Rate (ESR) and a raised neutrophilic count.

1.2.4.1 Monoclonal Component

The monoclonal IgM paraproteinaemia is a crucial feature of the syndrome, though in 10% of cases, an IgG component has been reported (24, 56). Generally, the IgM is associated with a kappa light chain in over 90% of patients and on primary diagnosis, the levels of this component can be present at trace amounts or at higher levels up to 41g/L (36). Such high levels (i.e. >10g/L raises suspicion of LPLs) and levels of the monoclonal component tend to increase at a rate of 0.5 to 1g/L annually. Intriguingly, there have been five instances where

SchS has been diagnosed without the gammopathy but have fulfilled the major and minor criteria for a diagnosis (57-60). As the presence of the aforementioned biological component is central to SchS, the nomenclature of 'variant-type Schnitzler Syndrome', denotes the IgG harbouring individuals.

A quarter of SchS patients have lowered levels of IgA and IgG (24), though one case report showed a polyclonal increase in the latter antibodies (61). Upon initial identification of the disease, bone marrow (BM) examination is usually normal in over 80% of patients, with the remaining individuals exhibiting unspecific or plasmocytic infiltrates (37).

Largely unaddressed experimentally, the query remains as to whether the paraproteinaemia seen is a consequence of continuous antigenic stimulation or is 'primitive in nature' (26) and is thus a by-product of the condition through unidentified mechanisms. In 2009, the clinical trial entitled 'Clinical Study, Physiopathological and Search for Genetic Factors' was launched in France and Italy, with the recruitment of 52 SchS patients led by Dan Lipsker (62). The study included the hypothesis that the monoclonal component 'fixes' IL-1 and lowers its clearance, however no results were posted or published and the trial was closed in 2017 (26, 62). There have been two cases where treatment of the underlying gammopathy was beneficial, substantiating the former stance (63, 64). No substantial change in IgM levels upon IL-1 inhibition is observed and could allude to the additional therapeutic capacity to halt clonal B cell growth – although not able to induce complete cessation (20).

1.2.4.2 Other Biological Observations

Inflammatory indicators CRP levels above 30mg/L (normal levels below 3mg/L) and an elevated ESR rate at 30 or above (healthy range between 0-20mm/hr) are frequent findings in over 95% of SchS patients (Table 4, (22)). Persistent neutrophilic leucocytosis ($>10,000\text{mm}^3$, normal range between 1,500 to 8,000/ mm^3) in the absence of any therapy appears in over two thirds of SchS affected individuals, providing clinical relevance through the lack of this occurrence in autoimmune diseases such as urticarial vasculitis and cryoglobulinaemia. Thus, the neutrophilia observed can be considered as a discriminating factor between this autoinflammatory disorder and support an autoimmune differential diagnosis (26).

Complement factor levels (C3 and C4) tend to be normal or raised, though a 1977 report alluded to two SchS patients harbouring genetic C4a deficiency (65), thus other associated conditions such as cryoglobulinaemia and hypocomplementic urticarial vasculitis should be

considered when complement levels found to be low. Other findings observed in less than 50% of SchS patients have included thrombocytosis, inflammatory anaemia and the presence of Bence-Jones proteins. More recently, biological indicators of abnormal bone remodelling and VEGF have also been observed with the latter component suggested to be included as a minor criterion for diagnosis of SchS (section 1.2.2.5, (66)).

1.2.5 Unique Findings

In 1991, Saurat *et al* discovered IgG antibodies directed at IL-1 α in six out of nine SchS patients tested (67), suggested by de Koning *et al* to prolong the half-life of IL-1 and sustain the systemic effects of this cytokine (68). However, these autoantibodies were not detected in subsequent studies, nor were serum levels of IL-1 β or IL-1Ra increased (68-72). Other auto antibody findings include anti phospholipid antibodies (73), IgG3 against microvascular endothelial and mast cells (74) and IgG2 directed against the high-affinity IgE receptor alpha (Fc ϵ RI α) – though not mediating histamine release (74).

Also a manifestation of the NLRP3-AID entities - MWS and CINCA, hearing loss observed in one SchS patient was successfully resolved with the commencement of anakinra (33), further highlighting the similarities seen between SchS and NLRP3-AID. There have been several reports of individual cases describing disease features unique to the affected SchS patient. These have included eye pain (75), aortitis (76), intercostal neuralgia (77) and pancreatitis (78), which were all resolved upon IL-1 blocking treatment. Hence, it is highly probable that this collateral damage is a consequence of IL-1 β dysregulation and its broad capacity to evoke inflammation through recruitment of additional proinflammatory mediators (79).

1.2.6 Disease Course and Complications

Besides a single case of spontaneous remission (80), SchS is a life-long, chronic disease with its complications largely attributable to existence of the monoclonal component. Prognosis of the condition depends on the potential advancement to lymphoproliferative disorders (LPDs), as those patients without LPDs have an 'unrestricted' life expectancy (37). Given the absence of a predictive marker to LPD evolution, it is thus challenging to specify the prognostic timeline of SchS. WM is acquired in approximately 20% of patients, with a median onset of eight years subsequent to the first signs of SchS. Progression to other lymphoproliferative disorders (LPDs) such as Chronic Lymphocytic Leukaemia (CLL) (0.1%), Lymphoplasmacytic Lymphoma (LPL) (3%) and Multiple Myeloma (MM) (0.5%) have also been detailed (20).

Literature development of serum amyloidosis (AA subtype) in seven cases (20, 81-85), with one of these patients dying of renal failure complications prior to anakinra therapy (85). In view of the chronic, proinflammatory milieu of SchS, there is a surprisingly small possibility of

developing amyloidosis. Interestingly, there have been no reports of immunoglobulin (Ig) light chain amyloidosis, given the underlying monoclonal gammopathy.

1.2.7 Pathophysiology

Many SchS features are shared with both genetically determined and acquired autoinflammatory syndromes and also rare haematological malignancies. The NLRP3-AID spectrum exhibits specific characteristics such as chronic urticaria (namely NUD), neutrophilia and with the ‘dramatic response to IL-1 inhibition’ strongly highlighting NLRP3 inflammasome involvement (26), these entities exhibit the most resemblances with SchS. However, a monoclonal component is not detected in NLRP3-AID, unlike in WM, LPL and polyneuropathy, organomegaly, endocrinopathy, myeloma protein, and skin changes (POEMS) where the gammopathy is a biological characteristic of the condition (86, 87), akin to SchS.

Mutations in the IL-1 β and IL-18 processing platform, NLRP3, were hypothesised to be the genetic determinant of this acquired disease, analogous to both hereditary and acquired forms of NLRP3-AID. Initially, de Koning *et al* reported the presence somatic *NLRP3* mutations in the myeloid lineage two subjects with variant type SchS (19). However it is the prerogative of experts in the field that these two cases should be considered as NLRP3-AID entities (39). Further investigation into the mutational status of this inflammasome is presented in Results Chapter 2 of this thesis.

1.2.7.1 IL-1

Deriving similarities to monogenic SAIDs such as NLRP3-AID, IL-1 β is the key inflammatory mediator in SchS, with previous research largely reporting increased levels of circulating IL-6 and IL-18 (88, 89). Gene expression of PBMCs taken during the symptomatic phase of SchS has demonstrated high levels of both IL-1 β and IL-6 mRNA transcripts, with IL-6 protein levels also high in sera (88). Quantification of IL-1 β remains challenging due to its short half-life (2 hours), though the central role IL-1 β plays in the pathophysiology of SchS is further reinforced by the high efficacy of anti-IL-1 treatment and subsequent suppression of the inflammatory response (85, 88). Migliorini *et al* established that there were raised levels of IL-18 in the serum of two SchS patients, despite low gene expression levels in monocytes (89). The latter findings also support the widely accepted concept that the IL-1 β /IL-18 producing inflammasome, NLRP3, is pivotal to the inflammatory manifestations of SchS (Figure 3).

Regulation of IL-1 is tightly controlled given the potential potent effects of this family of cytokines. Usually, IL-1 β and its sister cytokine, IL-1 α circulate the system at very low levels

and a few decoy receptors and soluble antagonists exist to support the regulation of both IL-1 α and IL-1 β (90). Both the latter cytokines bind to IL-1R1, which in turn forms a complex with the IL-1R3 accessory chain, initiating downstream signalling (91). The key antagonist, IL-1Ra, binds to IL-1R1 and blocks the formation of the complex required to initiating of IL-1 induced inflammatory activation. Whilst IL-1R2 is another IL-1 binding receptor, this essentially acts as a decoy receptor as binding to this receptor does not result in IL-1 mediated signalling (92). Interestingly, the extracellular domains of IL-1R1 and IL-1R2 can be soluble, with the ability to capture IL-1 cytokines in circulation (90, 93).

1.2.7.2 IL-6 and IL-18

The other two cytokines involved in SchS pathology are IL-6 and the NLRP3-inflammasome generated IL-18. The former is an acute phase reactant and is known to correlate with SchS disease activity (94), therefore its involvement maybe anticipated during systemic disease (26). However, given its additional role as an essential plasma cell growth factor (20, 95), it is highly likely that elevated amounts of this cytokine amplifies B cell growth in SchS and could be a factor promoting the underlying paraproteinaemia. Although successful remission of three SchS patients with anti-IL-6 therapy has been observed, high levels of the monoclonal component remained, but long-term follow up is required to confirm these findings (96). Raised levels of circulating IL-18 underscores the role of the overactive inflammasome in SchS, marking parallels to hereditary autoinflammatory diseases such as FMF (97) and NLRC4-AID (98). Thus, deducing that the systemic and autoinflammatory phenotype of SchS is largely due to the aberrant production of proinflammatory mediators based on the described data are the most relevant pathophysiological indications with regards to SchS. Nevertheless, the precise mechanisms underlying these defective pathways remain to be further investigated.

1.2.7.3 TNF- α

Aside from IL-1 β , other pro and anti-inflammatory cytokines have also been implicated within pathophysiology of SchS. The key role of TNF- α in monocyte proliferation and release of IL-1 β and IL-6, renders this effector molecule of interest in SchS pathology. Generally, TNF- α levels have not been widely described in SchS literature, though one 2007 report indicated significantly higher levels of TNF- α upon LPS stimulation of SchS PBMCs compared to HC (99). However, conflicting reports on the efficacy of TNF- α blockade further proves that its role in SchS is largely unclear. The 2010 report by Aikawa *et al* showed evidence of symptom amelioration with anti-TNF therapy (100), whereas this was conflicted with the 2007 report demonstrating disease exacerbation (101). Intriguingly, both reports used Adalimumab therefore the inconsistency observed could indicate TNF- α as a by-product of the proinflammatory SchS environment.

1.2.7.4 IL-10

Released by cells from both the innate and adaptive branches of the immune system (i.e. macrophages and B-cells), IL-10 is predominantly an anti-inflammatory cytokine with multiple effects. Where IL-10 enhances B-cell survival and antibody production (102), this molecule demonstrates inhibitory activity through the prevention of TNF- α release from macrophages (103). As SchS also involves the adaptive branch of the immune system through excessive IgM production, higher levels of IL-10 could be indicative of its potential contribution to the paraproteinaemia seen.

1.2.7.5 IFN- γ

IFN- γ is the vital mediator in two autoinflammatory syndromes: Haemophagocytic Lymphohistiocytosis (HLH) and Macrophage Activation Syndrome (MAS) and is produced by both the innate and adaptive immune systems (Natural Killer cells and T cells respectively) (104). This cytokine has also been implicated in the pathophysiology of several autoimmune conditions such as SLE, Sjögren's syndrome and polymyositis (105). Therefore, investigating levels of IFN- γ will indicate whether this cytokine plays a role in SchS pathophysiology.

1.2.7.6 IL-8

Although increased levels of IL-8 have not been documented previously in NUD, probing for this neutrophilic chemoattractant could partially explain the neutrophilic dermal infiltration. IL-8 primarily attracts neutrophils to sites of infection, with the secretion of this chemokine induced by TLR activation (more specifically TLR2 and TLR5) (106). Increased amounts of IL-1 β is noted to induce IL-8 transcription through NF- κ B activation, therefore probing for this cytokine is of great relevance to this work (107).

1.2.7.7 IL-17

IL-17 is chiefly produced by T helper 17 (Th-17) cells and is recognised as a cause of chronic inflammation through its stimulation of IL-1 β , IL-6, IL-8 and TNF- α production (108, 109). Although limited research has shown IL-17 levels not significantly raised in T_H17 cells, in comparison to healthy controls (HCs) (109), another report stated its significance in the keratinocytes of one SchS patient with variant type SchS (IgG instead of IgM) (110).

1.2.7.8 IL-12

Secretion of IL-12 has been associated with both innate and adaptive immunity, inducing IFN- γ production (111). Primarily produced by monocytes, macrophages and dendritic cells, IL-12p70 is the active form expressed when the subunits IL-12p35 and IL-12p40 are covalently

linked (111). Aside from IL-1 β , IL-6, IL-18 and TNF- α , levels of the other described cytokines have not been investigated before in the context of SchS and each of their presented roles within an inflammatory environment rationalises their investigation in the following research.

1.2.8 Treatment

Since the primary report of SchS, several treatment options have been outlined in literature. Prior to the introduction of successful amelioration of inflammatory manifestations in hereditary and autoinflammatory diseases with IL-1 blockade (112, 113), SchS patients were subject to an array of anti-inflammatory and immune-suppressing agents. Therapies such as alkylating agents, colchicine and cyclooxygenase inhibitors have been only partially effective (33, 55), with slight improvement in periodic fevers, ESR and CRP levels. Steroid administration has been 'highly' or 'partially' efficient in 64% of patients, though long-term management of SchS via this therapy is followed by adverse effects such as hypertension and osteoporosis and is therefore not indicated (20, 33, 39, 68). The largely non-pruritic urticarial eruption was typically resistant to such indications, and even antihistamines and ultraviolet therapy failed to resolve this manifestation, suggesting a 'histamine independent aetiology' (33). Nonetheless, the aforementioned drugs can be utilised in concert with IL-1 inhibition as a 'supportive' agent (37).

Given the inadequacy and safety concerns of the above-described treatments, the notion that alternative and systemic proinflammatory mediators were responsible for the characteristic manifestations of SchS was reinforced through the studies of both Hawkins *et al* in 2003 and 2004 (112, 113) and Hoffman *et al* in 2004 (114). Successful disease refraction in three MWS and four Familial Cold Autoinflammatory Syndrome (FCAS) patients using the IL-1 receptor antagonist (IL-1Ra), anakinra, underscored the imperative role of IL-1 β in NLRP3-AID pathophysiology. Following these revolutionary findings, administration IL-1Ra in an SchS patient yielding 'dramatic' remission (115), subsequently paved the way for IL-1 inhibition becoming the mainstay SchS therapeutic choice. Other IL-1 inhibitory agents utilised in SchS subjects include canakinumab, riloncept and gevokizumab (39, 55, 116).

Worldwide, a majority of SchS patients rely on off-label treatment or depend on the inclusion in clinical trials as there is no approved SchS indication (55). Though in the UK, anakinra was commissioned for SchS therapy in 2018 based on two retrospective studies (43, 117) highlighting the remarkable efficacy of IL-1Ra in a total of 38 SchS patients (118). In view of novel treatments for SchS, there are currently two alternative compounds being tested in clinical trials: Dapansutrile – an oral NLRP3 inhibitor (Clinical Trial ID: NCT03595371) and

ITF2357 – an oral histone deacetylase inhibitor (Clinical Trial ID: NCT00442182). Whilst the former drug is in the pilot stage in ten SchS patients and ideally abrogates release of active IL-1 β and IL-18, the latter compound is in phase two comprising of 20 subjects with autoinflammatory diseases, including SchS patients. ITF2357 is hypothesised to decrease gene expression of the acute phase response genes (IL-1 β , IL-6 and TNF α) and thus aid the reduction of disease severity (119).

1.2.8.1 Anakinra (Kineret®)

Human IL-1Ra is expressed systemically by a wide variety cells including immune (120, 121), skin keratinocytes (122) hepatocytes (123), and even by intestinal epithelial cells where IL-1 β was shown not to be secreted (124). The latter findings highlight the pivotal role of endogenous IL-1Ra, attempting to balance the proinflammatory effects of its competitive ligands, IL-1 α and IL-1 β . The pharmaceutical company Amgen generated the first non-glycosylated homologue of recombinant human IL-1Ra in 1993, known as ‘anakinra’ (Kineret®) in 1993, and in the same year trialled within RA patients (125). First approved for European use in March 2002, this antagonist competitively inhibits binding of the IL-1 receptor type 1 (IL-1R1) to both IL-1 α and IL-1 β (125). The recommended anakinra dosage is a once daily, subcutaneous administration of 100mg (22, 118), analogous to the suggested quantity for RA patients (113, 126). A few publications have demonstrated the safety and tolerability of the ‘modestly effective’ anakinra in RA (113) and the ‘remarkable sustained efficacy’ of anakinra in SchS (43). The first evaluative study of 472 RA patients in 1998 confirmed both the safety and moderate efficacy of the drug in question over a 24 week period (127) and subsequently followed by assessment of its long term over a longer duration of 76 weeks (128). Neel *et al* emulated the same in 29 SchS subjects, over the mean course of nine years and reported ‘no loss of effectiveness’ with a ‘favourable tolerance profile’ (43) and a recent account by de Koning and Krause determined a 95% efficacy of this drug in a further 94 cases (55). These clinical findings have also been mirrored ex-vivo, where increased IL-1 β secretion by SchS PBMCs were normalised by anakinra (99, 129). In spite of the clinical proficiency of this antagonist, an isolated case report in 2016 outlined the development of RA in concurrence with IL-1Ra treatment in one SchS patient suffering for nearly two decades (130). The initial response to anakinra was ‘immediate’ and ‘spectacular’ and was on this therapy eight years, prior to complaints of pain within hands, wrists and knees – but no appearance of a dermal rash (130). Whether the progression to autoimmunity was causally related or is a coincidental occurrence is yet to be determined, with this case further questioning the long term impact of IL-1 inhibition and its role in RA pathogenesis.

The rash and fever subside within the first few hours following the primary injection (30, 43, 68), with leucocyte counts and systemic markers of inflammation such as CRP generally returning to normal values within 48 hours (45). Common adverse effects of anakinra administration include neutropenia, upper respiratory tract infections and an erythematous reaction at the injection site (20). The 2014 follow up study reported the occurrence of the latter side effect in five patients, in whom four achieved complete remission. Three cases developed neutropenia, whilst a further five developed pneumonia and one complained of a severe sore throat. Of note, the latter six patients were all steroid dependent prior to commencement of anakinra and two of these patients had already developed chronic obstructive pulmonary disease (COPD). Therefore, it is likely that the aforementioned factors predisposed these patients to developing such infections. Nonetheless, all but one patient continued on IL-1Ra, with the researchers concluding the 'impressive clinical benefits' evidently outweighing the 'restrictive nature' of the regular injection regimen (43). Although anakinra monotherapy results in the effective clinical alleviation of SchS symptoms, long term remission from the disease itself is an extremely rare observation. There are two documented patients where spontaneous resolution of SchS symptoms occurred (26, 80), including the complete disappearance of the IgM component in one (80). Such unexplained remissions have also been reported in the NLRP3-AID entity, MWS (131).

1.2.8.1.1 Canakinumab (Ilaris®)

Despite the tremendous response to anakinra, the 'burden of painful daily injections' warrants the need of a longer acting agent (132). Originally developed by Novartis as a potential asthma treatment but later contraindicated, (133), this biologic has been trialled in many studies aside from SchS, looking at NLRP3-AID (134-136), MVK, TRAPS and colchicine resistant FMF (137). The largest clinical trial entitled 'CANTOS' assessed the therapeutic potential of canakinumab in 10,061 patients suffering from atherosclerotic disease, therefore the therapeutic potential of this drug has been assessed in approximately 10,400 patients worldwide (138). These trials generally reported the reasonable capacity of this treatment in successfully controlling and preventing disease flares and reducing the 'persistent proinflammatory response' as evaluated by CRP levels (138).

The evidence that IL-1 β was central to the pathophysiology of SchS was further underscored by two European clinical trials assessing the effects of canakinumab within a total of 28 patients (all previously on anakinra therapy) (132, 139, 140), a Russian study comprising of four patients (three on canakinumab) (141) and a further two patients in the USA (142). The patients were given 150mg subcutaneous doses of the drug every four to eight weeks (each

dependent upon the recurrence of clinical symptoms), with all four studies reporting the alleviation of symptoms within hours of the first injection and high clinical and laboratory efficiency as measured by CRP, Serum Amyloid A levels (SAA) and Quality of Life (QoL) assessments. The most common adverse side effect documented was 'mild' upper respiratory infections reported in a total of 15 patients from the two clinical trials (139, 140) and whether these were entirely as a consequence of treatment is more challenging to decipher. Requiring less injections, the 28 day half-life of canakinumab in comparison to anakinra (four to six hours) and rilonacept (seven days) is a key advantage of canakinumab. Conversely, the major drawback of prescribing canakinumab is its stark price in comparison to the other IL-1 inhibiting options. Where one dose of anakinra (100mg, Swedish Orphan Biovitrum AB) approximately costs £30, this mAb costs £9927.80 for one injection (150mg, Novartis) (143, 144).

The average time of relapsing symptoms in the trial by Krause *et al* was three months (139), whereas interestingly, de Koning *et al* reported the eight month, long-term remission in two patients after treatment discontinuation (140). SchS duration and indicators of disease activity for both these patients were similar to the other six patients included in the trial, therefore presuming that these particular individuals would be predisposed to sustaining longer remission periods could not have been anticipated. The 'vicious' autocrine IL-1 β generating cycle was clearly intercepted, though the mechanism behind this sustained efficacy remains elusive and such findings have not been discerned in the other therapeutic alternatives used for this ultra-rare condition (140). Although the paucity of data requires expansion with regards to long term ramifications of this drug in SchS, the decent safety and efficacy profile of canakinumab as indicated by the aforesaid studies, renders this treatment as a promising candidate for SchS therapy.

1.2.8.1.2 Rilonacept (Arcalyst®)

Several autoinflammatory and autoimmune disease based clinical trials have reported the general efficacy of rilonacept in ameliorating the symptoms associated with excessive IL-1 generation (145-149). In 2008, the orphan designation status was granted for the NLRP3-AID entities by the Food and Drug Administration (FDA) but was later withdrawn from the European market. Structurally resembling an antibody, rilonacept consists of the extracellular ligand binding domains of the human IL-1 receptor with the IL-1 receptor accessory protein fused to the Fragment Crystallisable Region (Fc) fragment of humanised IgG. Thus, this recombinant fusion protein enables the capture of both IL-1 α and IL-1 β blocking the downstream effects of these cytokines. The 2012 study by Krause *et al* signifies the single SchS trial comprising of

eight participants, where an initial subcutaneous injection of 320mg was followed by weekly administrations of 160mg (147). The 'effective, well tolerated' and 'safe' concluding remarks by Krause and co-workers outweighed the 'mild' and 'moderate' adverse events, none of which were considered related to riloncept administration. Such findings were emulated in the 2018 study assessing the pharmacokinetics of this drug in six DIRA patients (145), with Hoffman *et al* establishing injection site reaction as the most frequent adverse event within 47 NLRP3-AID cohort (149).

Akin to canakinumab, the benefits and drawbacks of this drug lie within its half-life and cost. The weekly injections (as opposed to daily with anakinra) is attributed to the seven day half-life of riloncept, thus reducing the need for injections and consequently decreasing the chance of injection site reactions and increasing QoL. However, the approximate cost of £4000 per 80mg (150) and relative lack of clinical data in comparison to both anakinra and canakinumab largely explains the infrequent use of riloncept in SchS.

1.2.8.1.3 Gevokizumab

Since the introduction of this compound in 2008 (XOMA/Novartis), limited trials of this mAb have been carried out in cancer (151), autoimmune (152, 153) and autoinflammatory settings (116), mainly yielding efficacious results. A French initiated study of gevokizumab in three SchS patients (one male, two females) over a two year period with a subcutaneous dosing strategy of 60mg each fortnight. The investigators reported 'markedly improved' global assessment of SchS disease activity as evaluated through clinical and biological parameters such as a 50% decrease in CRP levels prior to gevokizumab administration (116). Two of the SchS subjects were stated to develop diarrhoea, although this has not been documented as a side effect in the other studies (152, 153). Intriguingly, the results from the SchS trial are yet to be published and therefore this drug is not indicated for this autoinflammatory entity.

1.2.8.2 Alternative treatments

A handful of reports have reported benefit with tocilizumab (mAb against the IL-6 receptor) (96), B-cell depletion or modulatory agents such as rituximab (63, 154) and ibrutinib (64) and the antibiotic, pefloxacin (155, 156). These latter therapies are further detailed in the following sub-sections.

1.2.8.2.1 Tocilizumab (RoActemra®)

The particular success of IL-1 inhibition has rendered this line of therapy to be the mainstay treatment of SchS, however there have been a handful of cases where IL-1 inhibition has been ineffective. After failing a plethora of treatments including anakinra and riloncept, three typical

SchS patients were reported to achieve complete remission with tocilizumab monotherapy within three months of the initial intravenous infusion (96). Largely indicated for RA and Systemic Juvenile Idiopathic Arthritis (SJIA) in concurrence with other immunosuppressants such as methotrexate, tocilizumab competitively binds to both the soluble and membrane bound IL-6 receptor alpha chain (157), thereby preventing IL-6 signal transduction and diminishing the proinflammatory, acute-phase response. The three aforementioned SchS subjects were subject to a monthly dosing strategy of 8mg/kg, analogous to the effective dose in RA and SJIA (55, 157). Common side effects of this IL-6 mAb include abnormal liver function and neutropenia (157, 158), but these have not been stated in SchS tocilizumab research (96). Noted by the investigators of the latter study, the clinical parameters such as age at disease onset and duration of single dermatological lesions were comparable amongst those patients who responded to IL-1 inhibition and the trio responding to IL-6 inhibition. Therefore, these findings not only identify a sub-set of anti-IL-6 responding SchS patients, but highlights the imperative role of this acute-phase reactant in the pathogenesis of this rare condition. Interestingly, elevated circulating levels of IL-18 in SchS compared to healthy individuals is not only an indicator of inflammasome dysregulation (89, 93), but may also emphasise a treatment direction for those patients unresponsive to recommended SchS therapy. The success status of anti-IL-18 therapy autoinflammatory entities such as NLRP3-AID (159), accordingly warrants delineation of its role in SchS. However, such hypotheses are yet to be evaluated assessed in the setting of SchS.

1.2.8.2.2 Pefloxacin

Descriptions of antibiotics as a largely successful therapy in a handful of patients have emerged within the last two decades. The reports by Asli *et al* and Kastiritis *et al* totalled 12 SchS patients on an oral, daily pefloxacin mesylate 800mg regime (155, 156). Antibiotic therapy was administered alongside other drugs such as antihistamines and NSAIDs, but not IL-1 inhibitory agents and concluded 'dramatic' and 'sustained' improvements in the symptoms (155, 156). The reasonable success of this treatment in 11 out of 12 patients underscores the immunomodulatory role of pefloxacin against the backdrop of sterile inflammation in autoinflammatory disease. It is likely that this quinolone therapeutic modified the inflammatory response through mRNA regulation for the IL-1 cytokine superfamily and IL-6 (155, 160). The case report by Kastiritis *et al* observed a significant reduction in both the osteogenesis marker OPN and the angiogenesis-related VEGF (156), alluding to the musculoskeletal manifestations of SchS and indeed the role of these markers in autoinflammatory disease. These findings were emulated in 13 SchS patients assessed pre and post anakinra therapy a few years later in 2012 (66). Although the administrative route of this oral therapy facilitates

patient compliance with the agent, pefloxacin has not shown similar success in other cases. Thus, comparable to alternative therapies outlined, these cases may signify a subgroup of patients who respond well to antibiotics.

1.2.8.2.3 B cell depletion agents

In haematological diseases where the role of monoclonal gammopathy is also elusive but not associated with systemic inflammation, eradication of the plasma cell producing IgM population is highly effective (64). In 2013, SchS experts opposed the direction of treatment towards underlying gammopathy and highly recommended the focus to be on the autoinflammatory symptomatic alleviation (22). Nevertheless, a small number cases have been successfully treated with B cell modulatory agents such as the small molecule inhibitor, Ibrutinib and the mAb, rituximab (63, 64, 154, 161). The former agent is an irreversible Bruton's tyrosine kinase inhibitor (BTK) and an indicated therapy for WM and CLL – both of which are associated with the presence of plasma cells generating the IgM monoclonal component (64). Ibrutinib proved effective in the treatment of an 86 year old SchS patient, leading to 'resolution of existing lesions' and 'fewer new onset lesions', signifying the sole case employing anti-BTK therapy thus far (64). Targeting the CD20 antigen on both normal and malignant cells, rituximab was also an effective therapy in a few cases (63, 154, 161), but such favourable findings have been contradicted by other studies reporting the failure of this treatment using the same 375mg weekly dosing regimen (162, 163). Notably, IL-1 blockade later proved efficacious in these patients (162, 163). Taking the aforementioned evidence into consideration, the conflicting evidence and inconsistency of these atypical treatment options renders B-cell depleting therapies as less favoured in treating this heterogeneous syndrome.

1.2.8.3 Treatment effects on the Monoclonal Gammopathy

Elevated levels of the monoclonal IgM are one of the two main diagnostic criteria for SchS, a phenomenon also occurring in haematological malignancies such as CLL, WM and IgM-MGUS. The observation that SchS IgM paraprotein levels tend to increase by 0.5 to 1g/L per year (26), suggests that the SchS mainstay IL-1 inhibition therapy is unlikely to affect levels of the monoclonal component. The 10 year follow up study by Neel *et al*, demonstrating no significant difference seen upon IgM levels in 10 SchS patients treated with anakinra (43). These findings are corroborated in literature, aside from an isolated case where treatment with anakinra led to the 'disappearance' of the monoclonal component (164). Universally, both

alternative immunosuppressive agents (canakinumab, rilonacept, tocilizumab) and antibiotic therapy (pefloxacin) has demonstrated no significant effect upon the levels of the monoclonal component in each of the SchS cases presented (96, 139, 140, 147, 155, 156). Therefore based on this evidence, it is highly unlikely that the success of B-cell modulating agents in a limited number of cases is simply due to the removal of the monoclonal component. Rather, the favourable outcome may be attributed to the abrogation of IL-1 β mediated IL-6 upregulation within B cells (91). A similar occurrence was initially documented in the 2017 study looking at patients with NLRP3-AID (MWS) and X-linked agammaglobulinaemia (XLA), noting that PBMCs showed a markedly reduced release of IL-1 β upon BTK ablation (165).

1.3 The NLRP3 Inflammasome

Despite the rarity of SchS, there is significant emphasis on a more streamlined diagnosis as appropriate treatment dramatically improves QoL (section 1.2.7) (39, 55). The evidence that over 90% of SchS patients exhibit remarkable response to IL-1 blockade supports the involvement of the IL-1 β generating, NLRP3 inflammasome in SchS (20). Likewise, both inherited and acquired NLRP3-AID patients respond well to such blockade and present with either germline or somatic mutations in the *NLRP3* gene (2). The phenotypic similarity of SchS and NLRP3-AID raises the question as to whether the genetic findings in the latter entities are emulated in SchS. This line of enquiry in SchS was initially fuelled by the success of IL-1 antagonism (112, 113) and cases of late-onset, acquired NLRP3-AID (14, 166, 167). Saito *et al* first demonstrated somatic mutations in exon 3 of *NLRP3* in both the lymphoid and myeloid lineages in one CINCA patient (18). Subsequently, the advent of NGS coincided with several researchers investigating the prevalence of somatic mutations in those NLRP3-AID patients negative for mutations within the causative gene (166, 167), based on the initial discovery by Saito and colleagues (18). Such findings were later emulated in two SchS patients demonstrating myeloid cell-restricted somatic mosaicism in *NLRP3* (19). Notably, the other nine patients included in the SchS study were negative for *NLRP3* mutations (19) with other reports disclosing the same in a limited number of SchS cases (20). Moreover, mutations within this inflammasome are present in around five percent of the healthy population (168), therefore in this regard and in view of the *NLRP3* negative SchS patients (19, 20), it is highly plausible that pathogenic and somatic *NLRP3* mutations may not be discovered. Nevertheless, continuing the search within an increased number of SchS patients would ascertain or disprove the aforesaid phenomenon in this autoinflammatory entity. The variants sought may be universally present and even the limited presence in a subset of cases may indicate mutations in this gene as susceptibility factor to SchS development.

Abundant research establishes the inflammasome as the source of IL-1 β (91), therefore the augmented levels of this cytokine renders NLRP3 as a pivotal component in SchS disease pathophysiology. Exploring the involvement of other acute phase reactants such as IL-6 and TNF- α , and other (but not limited to) pro and anti-inflammatory cytokines such as IL-8, IL-10 and IFN- γ , provides comprehensive insight into the dynamics of the systemic inflammatory response. Furthermore, seeking proof of NLRP3 components extracellularly (i.e. Apoptosis-associated speck-like protein containing a CARD (ASC) specks) is not only indicative of autoinflammatory cell death (pyroptosis), but further explains high IL-1 β levels as such domains exhibit the capability of activating this cytokine outside the cell (169). Limited research has denoted the augmented circulating levels of IL-6, IL-18 and TNF- α largely *in-vitro* (88, 89, 99) but broad assessment of a large number of inflammatory mediators has not been investigated within the serum of active SchS. Irrespective of the genetic investigation, obtaining both direct and indirect evidence of upregulated inflammasome activity would reinforce its involvement in the disease and potentially reveal other pathological mediators in SchS. Thus, the work presented in the subsequent chapter investigates the extent of inflammasome dysregulation, interrogating both genetic and molecular aspects of the NLRP3 inflammasome within SchS patients.

1.4 The Connection between Autoinflammation and Clonal Haematopoiesis

Clonal Haematopoiesis (CH) is outlined as the preferential expansion of a population of blood cells originating from a single haematopoietic stem cell (HSC) lineage (170). The existence of these cells can be evidenced through the presence of somatic mutations in genes conferring selective growth and survival advantages, and can also be determined by X-chromosome inactivation (XCI) - in females only (171). Whilst CH is a 'relatively benign' phenomenon, its existence can be a precursory factor to the development of Myelodysplastic Syndromes (MDS) and subsequently Acute Myeloid Leukaemia (AML) (170). Although both disorders predominantly affect the myeloid lineage, MDS is considered to be a heterogeneous group of haematological disorders largely characterised by peripheral blood cytopenias (172). Whereas the abundant proliferation of immature myeloid cells in the bone marrow is emblematic of AML (172).

Emerging literature highlights the prevalence of autoinflammatory features present within a subset of MDS patients such as fever and a skin rash (173-175), with a further 10% of MDS cases being associated with autoinflammatory conditions, namely Sweet's Syndrome (176). The prospect of a shared mechanism between these entities is also denoted by several

investigators recommending the initiation of IL-1 blockade amongst MDS patients against the backdrop of preclinical studies indicating the pathogenic role of IL-1 β in haematological disease (176-178).

In addition to autoinflammatory diseases, extensive research has detailed the pathological consequences of NLRP3 inflammasome dysregulation in the context of haematological abnormalities (179, 180). The importance of these comprehensive investigations resides within establishing the inflammasome as a focus for therapeutic intervention. For example, inhibition of the enzyme BTK in CLL patients resulted in a significant reduction of NLRP3 activity, as assessed through quantification of IL-1 β in comparison to healthy controls (165). Use of this BTK inhibitor (ibrutinib) has also yielded a reduction in SchS disease activity, although only trialled in a single patient (Section 1.2.7.2) (64), thus demonstrating that NLRP3 is 'targetable' through this therapy.

In 2016, Basiorka *et al* reported the incidence somatic variants in epigenetic modifying genes resulting in NLRP3 activation due to excessive Reactive Oxygen Species (ROS) production (179, 180), thus provoking unwarranted stimulation of the inflammasome. These discoveries were verified through assessment of NLRP3 components such as extracellular ASC specks and pyroptosis with these elements being frequent findings in patients with autoinflammatory disease (181). Analogous to MDS, SchS is also an acquired, late onset and heterogeneous disease, therefore acquisition of somatic mutations in the bone marrow during both the ageing and disease processes may predispose and/or amplify the proinflammatory consequences perpetuated through NLRP3 over-activity.

1.5 Schnitzler Syndrome and Lymphoproliferative Disorders

Though the role of the monoclonal component in SchS pathogenesis remains unclear, twenty percent of patients go on to develop WM (section 1.2.5), an LPD also presenting with IgM gammopathy - of unknown significance (MGUS) (182). Whole Exome Sequencing (WES) by Treon *et al* in 2012 revealed a somatic mutation in the Myeloid-Differentiation Primary Response 88 (*MYD88*) gene in 91% of WM patients sequenced (n=54) (182), with these findings paralleled a year later within a different WM cohort (183). *MYD88* is an adaptor protein, relaying signals from the Toll/IL-1 Receptor (TIR), ultimately leading to nuclear NF- κ B activation. The somatic mutation detailed is a single nucleotide variation (SNV) at chromosomal position 3:38182641 in exon 5, resulting in the leucine to proline substitution at position 265 (L265P) (184). Located in the TIR domain of the *MYD88* protein, this gain-of-function mutation (GOF) leads to increased phosphorylation of IRAK1 and has also shown to

promote NF- κ B and JAK-STAT3 signalling to boost cell survival (184, 185). Other haematological malignancies such as activated B cell Diffuse Large B-cell Lymphoma (ABC-DLBCL) and IgM-MGUS also bear this mutation at frequencies of 29% and 50% within these patient cohorts respectively (185).

Granted that WM is not associated with systemic inflammation despite the universal occurrence of the aforesaid IL-1 facilitating mutation, acquisition of this somatic variant in the context of autoinflammation could represent a subset of those SchS patients who develop this LPD. Determination of the latter would also rationalise why those negative for *NLRP3* mutations are successfully treated with IL-1 inhibition. Uniting the concepts presented in 1.4 and this section, the work presented in the second results chapter questions the role of the ageing haematological compartment within the setting of SchS and assesses the presence of certain predisposing mutations which would theoretically endorse the evolution of SchS to WM and other LPDs.

1.6 Binding Capacities of the Monoclonal Component

The IgM monoclonal component is one of the two main criteria required for the diagnosis of SchS (section 1.2.1), yet the nature of the disease association remains unclear, akin to the aforesaid haematological malignancies. One case reported the onset of IgM paraprotein occurring four years after clinical symptom presentation (186), though there is insufficient data to determine whether this component precedes or follows the clinical signs. Hence, overproduction of this Ig could either be responsible for disease onset, or its establishment could be a result of the heightened inflammatory response. Either supposition renders IgM directly or indirectly perpetuating SchS disease manifestations through activation of the adaptive immune system and therefore supporting a proinflammatory milieu.

The theory of an underlying connection connecting B-cell neoplasms and potential antigenic stimulants have been proposed widely in literature (187, 188), therefore identification of the latter could reveal its effects upon disease manifestations. For example, the autoimmune Cold Agglutinins Disease (CAD) features mainly IgM autoantibodies directed at self-antigens present on red blood cells (RBCs) and subsequently causing their lysis (189). Conversely, the pathological function of the monoclonal component is dubious in haematological malignancies where B-cell neoplasms are a central trait of the condition. On the whole, research indicates a causal relationship between chronic antigenic stimulation in the pathogenesis of IgM-MGUS

and MM 'unlikely' (188), with no universal antigenic target discovered in WM (190). Also accounting the heterogeneity of the few targets detected in a small percentage of patients, the conclusions obtained are in spite of the elevated levels of the monoclonal component (188, 190). Nevertheless, identification of potential antigenic stimuli in SchS warrants investigation using an unbiased target approach.

Development of protein microarray technology has enabled the extensive detection of protein-protein interactions. This technology has been employed in the delineation of numerous disease pathophysiologies, including the widespread identification of autoantibody targets in autoimmune diseases (191, 192). For example in SLE and RA, anti-dsDNA and anti-citrullinated protein antibodies are a common finding (193, 194). Taking the aforementioned into consideration, probing the SchS-IgM protein interactions may provide clues to a potential antigenic target or group of related targets. Such experiments can be facilitated via the isolation of SchS IgM and subsequent application onto a protein microarray comprising of thousands of human antigens. Also supporting the genetic search for antigenic stimulation in SchS as explored in Results Chapter 4, execution of the protein microarray functionally addresses this concept through determining the binding capacity of SchS-IgM.

1.7 B-cell Repertoire Sequencing

The outcome of the adaptive immune response is influenced by the pool of available lymphocyte antigen receptors that constitute the immune repertoire. Understanding the composition and dynamics of immune repertoires is hence of relevance to characterising immunological and physiological processes, as well as understanding disease pathogenesis. In the context of SchS, the distinguishing paraproteinaemia of SchS highlights the role of the adaptive immune system in this autoinflammatory disorder, marking a very rare situation. The clonal expansion of B-cells is therefore implicated in the generation of the monoclonal component, akin to other conditions such as WM and ABC-DLBCL (182, 185). Largely of an IgM kappa (IgM κ) subtype, this element hence raises the query as to whether there is a predominant recombination pattern within the Ig genes of these patients. Biased usage of these Ig genes would not only indicate the existence of a clonal B cell population, but further questions the role of antigenic stimulation in the proliferation of a subset of SchS B cells.

A majority of the diversity lies within the IgH region, given the two rearrangement steps and non-templated additions and deletions within the junctional regions. Thus, analysis of the Ig heavy chain (IgH) region proves the most informative for the identification of B cell clones (195). The unique arrangement of V (Variable), D (Diversity) and J (Junctional) - (VDJ) segments enables the production of diverse sets of antibodies (196), with the amino acid (aa) sequences within the Complementarity Determining Region 3 (CDR3) of both the heavy and

light chains, mostly determining the specificity of an antibody. While repertoire sequencing has not been carried out before in this autoinflammatory disorder, SchS experts have recommended that 'immunoglobulin gene rearrangement study' should be carried out where a diagnosis is uncertain (22). The hypothesis that SchS is in fact a B-cell clonal disorder can be addressed via VDJ rearrangement and CDR3 analysis. The experiments performed in Results Chapter 5 therefore pertain to the aforementioned suppositions.

1.8 Novelty of this PhD

The rarity combined with the heterogeneity of this condition, renders many disparities within SchS pathology. The studies presented in this work pertain to uncovering the genetic and pathophysiological mechanisms through which SchS is established. Facilitated by the access to samples from a tenth of the total cases worldwide and the advent of novel scientific technology, the investigations shown in this work have addressed both new and original theories that were previously unachievable due to limited resources.

The first and second results chapters probe the mutational status of over 60 genes associated with autoinflammation, MDS and other haematological disorders in 30 SchS patients. Whilst previous work has questioned the genetic and functional role of the NLRP3 inflammasome in SchS, large scale genetic sequencing has not included the aforementioned categories. Likewise, analysis of 10 cytokines plus markers associated with the activated inflammasome has not been carried out previously in a relatively large cohort.

The third and fourth results chapters address the underlying monoclonal component. Central to the diagnosis of SchS, the notion that the underlying IgM gammopathy plays a role in SchS pathophysiology has been previously surmised but not examined. Isolation of IgM followed by application onto a protein microarray comprising of over 15,700 human proteins thus addresses if SchS derived IgM binds preferentially to a particular antigen and could therefore be implicated in SchS disease manifestations. To supplement these findings, comprehensive assessment of the IgH region seeks to detect if there are indications of clonality, hypothetically supporting the generation of the aforesaid component. Via the assessment of VDJ recombination and CDR3 aa sequences, determining whether there are indications of a monoclonal B-cell population, hence bridges the link between the innate and adaptive immune networks in SchS. The outcomes shown in each of the four results chapters not only adds to the limited literature on SchS and are informative for clinicians and research scientists alike, but also forms the initial basis upon which future research can be developed.

1.9 Hypotheses of this PhD

The work presented in this thesis endeavours to address concepts related to the pathogenesis of SchS, suggested through previous research of this condition and observations in other related IL-1 mediated monogenic autoinflammatory diseases such as NLRP3-AID and haematological entities where paraproteinaemia is a central feature of the condition, such as Waldenstroms Macroglobulinaemia.

- (1) SchS patients have mutations in the IL-1 β /IL-18 molecular processing platform known as the NLRP3 inflammasome.

The central role of IL-1 β in SchS has been highlighted through the efficacious and remarkable response of SchS patients to IL-1 inhibition (22). Two somatic gain of function mutations in this gene have been detected in two patients with SchS leading to increased IL-1 β release (19). On this basis, the hypothesis was formed that somatic mutations within the NLRP3 inflammasome may be instigating increased levels of IL-1 β .

- (2) A proportion of SchS patients have the MYD88 L265P gain-of-function mutation.

Waldenstroms Macroglobulinaemia (WM) is a type of lymphoproliferative disease, of which 20% of SchS patients go onto develop. Over 90% of WM patients were discovered to have the single nucleotide variation (T>C) at position 38182641 at 3p22.2 within exon 5 of *MYD88*, resulting in the L265P mutation (182). Based on these findings, the second hypothesis addresses if this variant is indeed present in SchS patients.

- (3) Oligoclonal Haematopoiesis (OH) is a feature of SchS, evident through the presence of additional 'passenger' mutations associated with myelodysplastic syndromes (MDS).

Recently, upregulation of the NLRP3 inflammasome has been implicated in the pathology of MDS (179, 180). This latter condition is known to bear mutations in a set of genes associated with OH. Given the central role of IL-1 in this condition and therefore involvement of NLRP3 in SchS, the notion that further mutations in genes frequently mutated in conditions where NLRP3 is also implicated is addressed with this third hypothesis.

Whilst the first three hypotheses address the genetic aspect of SchS, the further two hypotheses focus on the characteristics of the IgM paraproteinaemia.

(4) Serum derived SchS IgM binds a common antigen.

One previous study demonstrated the infiltration of IgM in the skin lesions of three SchS patients (197). However, since this study, the potential pathological role of IgM generated by SchS patients is yet to be addressed. In other haematological and autoimmune diseases, the paraproteinemia may be directed towards a specific antigen. For example, in Cold Agglutinin Disease (CAD), the IgM generated binds a specific component of red blood cells. In a similar manner, it is possible that SchS derived IgM binds a common antigen or set of antigens that are different to other disease entities.

(5) SchS bears characteristics of a clonal B cell disorder.

Given the generation of IgM from B cells, it is considerable that there is a defect within these cells responsible for the paraproteinaemia. Although the paraproteinaemia seen with WM is not known to be pathological, there is a bias in the usage of genes used for the generation of antibodies (IgH region). This usage bias is indicative that the antibody repertoire of these WM patients are skewed towards producing antibodies generated from specific V, D and J genes (198). Likewise, it is possible that such bias is seen in SchS, indicating a preponderance of SchS patients towards producing a more constricted repertoire of antibodies.

Chapter 2 The Schnitzler Syndrome as an auto inflammatory disease

2.1 Introduction

2.1.1 Periodic Fever Syndromes

PFS are a group of disorders characterised by recurrent episodic fevers accompanied by systemic or organ-specific sterile inflammation, encompassed by the umbrella term 'Systemic Autoinflammatory Disorders' (SAIDs). The clearly identifiable PFS include the NLRP3-AID associated FCAS, MWS; FMF, and TRAPS (Table 1) (199). The pathogenesis of such PFS can be ascribed to the release of IL-1 β due to inappropriate caspase 1 activation (200), with a large proportion of monogenic and polygenic SAIDs effectively treated with anti-IL-1 blockade (2). The diagnostic process of PFS relied wholly upon laboratory findings and clinical manifestations of the disease, until the assignment of *MEFV* mutations causative of FMF in 1997 (3). The Mendelian mode of inheritance of such diseases permitted the identification of additional monogenic SAIDs (5), allowing for a more 'definite diagnosis' (6). SchS is classified as a periodic fever, given the recurrent episodes of fever and sterile inflammation ascribable to IL-1 β mediated pathology (22, 26) .

2.1.2 The Inflammatory Response of Schnitzler Syndrome

Aside from fevers of a periodic nature, the diagnosis of SchS relies on the fulfilment of two main components: NUD and IgM paraproteinaemia, in accordance with the SchS Strasbourg criteria (Table 3, Introduction) (22). Other symptoms of this adult-onset condition usually include arthralgia, myalgia and ostealgia with clinical findings comprising of elevated CRP, leucocytosis and lymphadenopathy (22). The imperative role of IL-1 β upon manifestations of this condition has been widely corroborated, though whether this proinflammatory cytokine has effects on the IgM paraproteinaemia remains elusive. Quantification of this IL-1 β alongside nine other cytokines (IL-6, IL-18, TNF- α , IL-10, IFN- γ , IL-8, IL-17 and IL-12) (described in section 1.2.7) in the serum of SchS patients is explored in this chapter.

2.1.3 The role of the NLRP3 inflammasome in autoinflammatory disease

Constituents of the NLRP3 (Nod-like receptor – NLR) inflammasome are phylogenetically conserved molecules and play an important role in the recognition and subsequent response to danger within innate immunity (201). Unlike Toll-like receptors (TLRs), NLRs are intracellular sensors, forming macromolecular complexes termed ‘inflammasomes’, eventually mediating the maturation and release of IL-1 β and IL-18 via caspase 1 (201). Under normal, healthy conditions, the NLRP3 inflammasome requires both a ‘priming signal’, which can be Pathogen-Associated Molecular Patterns (PAMPs) or endogenous cytokines such as IL-1 β or TNF- α , followed by an ‘activation’ signal, provided by a wide range of reported stimuli such as ATP or particulate matter (202). Gain-of function mutations within *NLRP3* lead to spontaneous assembly of the inflammasome (203, 204). For example, mutations in the *NLRP3* gene in NLRP3-AID constitutively activates the inflammasome which has been shown to spontaneously oligomerise, providing a platform for pro - IL-1 β processing, due to increased activity of caspases 1 and 5 (13, 203) (Figure 3). Non germline mutations have also been reported in NLR domains and pyrin domains of NLRP3, thus causing ‘acquired NLRP3-AID’ (15, 17). Additionally, several reports of both the NLRP3 inflammasome and the pyrin and CARD domains (together forming the macromolecule ASC) have been detected in serum of NLRP3-AID and FMF patients (169, 205, 206). Not only is this indicative of pyroptosis (auto-inflammatory cell death) (207), but could also serve as a biomarker of NLRP3 activation within inflammatory disease.

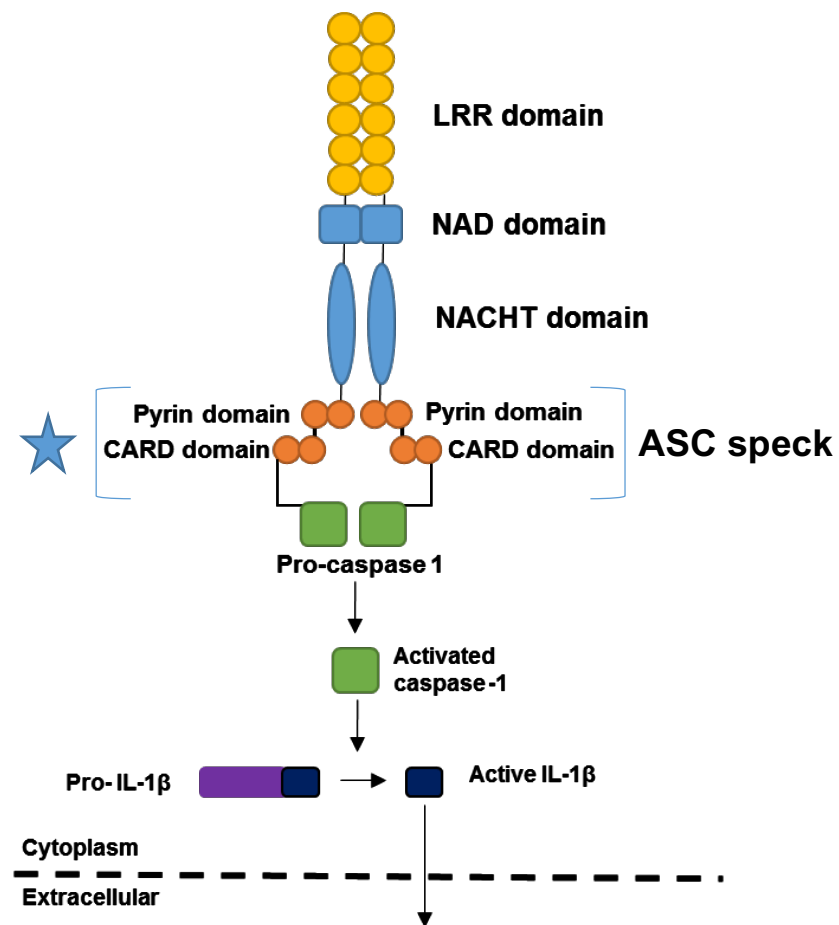


Figure 3: The NLRP3 inflammasome.

This inflammasome consists of the NLRP3 sensor molecule, the adaptor ASC (comprising of the Pyrin and CARD domains) and the effector molecule, pro-caspase 1. The assembly of this inflammasome results in the formation of active caspase-1 further cleaving proinflammatory cytokines such as IL-1 β and IL-18 (not shown) into their mature forms.

Figure 3 created with information from: Rubartelli, 2012 (208), Eitel *et al.*, 2010 (209), Tschopp and Schroder, 2010 (210).

2.1.3.1 Somatic mosaicism in *NLRP3*

Initially reported in 2005, a patient with CINCA (Chronic Infantile Neurologic Cutaneous Articular syndrome), the most severe phenotype of the *NLRP3*-AID spectrum, presented with negative family history for this condition. Further evaluation by sub-cloning and subsequent Sanger sequencing revealed the presence of a disease-causing *NLRP3* variant in 16.7% of whole blood derived DNA (18), though such precise quantification is debatable given the difficulty of detecting lower frequency mutations (especially below 20%) with this technique (211, 212). Evidently this variant, even in a lower percentage of cells was sufficient to cause the disease phenotype (18). Following this, a case-control study on the same condition, comprising of 26 patients was published, showing 70% of probands harbouring *NLRP3* mutations with high grade mosaicism; which were completely absent in the healthy controls (15). The aforementioned study carried out deep amplicon sequencing of gDNA; where the mutations were all present at varying degrees. Contrastingly, in 2015, Zhou *et al.* carried out *NLRP3* sequencing from the myeloid and lymphoid lineages of a suspected MWS patient (*NLRP3*-AID spectrum), who initially was reported as *NLRP3* mutation negative via Sanger sequencing (14). Using targeted deep sequencing, these researchers identified a somatic mutation which was present in 15% of the myeloid lineage, underscoring the significance of deep sequencing as a diagnostic method in auto-inflammatory conditions (14).

Reports of this genetic concept in auto-inflammatory disease is not limited to *NLRP3*-AID. Recently, Shinar *et al* reported the first case of 'acquired' FMF, usually an inherited disorder, with again the somatic variant present in 27% of the myeloid lineage (17). Interestingly, this R652H mutation in the FMF disease causative gene pyrin [an integral part of the inflammasome (Figure 3)], was present at 'negligible' levels prior to disease commencement; however after the onset of fever, the mutant allele was present at a 46% percent frequency in gDNA. This study also emphasised the mutated cell-dosage effect whereby the increasing number of cells harbouring the mutant allele correlated with disease activity (17). In line with these findings, 47 patients suffering from FMF who were mutation negative in pyrin by Sanger sequencing, were reported to have a milder phenotype than those patients harbouring the pyrin mutations (213). The mutation-negative patients showed milder acute and chronic manifestations with requiring a reduction in Colchicine therapy, as compared to mutation positive patients, indicating a marginal difference in phenotype. It is likely that there are in fact, mutations in pyrin but only present in a subset of small cells (likely the myeloid cells), which were not detected due to the absence of sensitive deep sequencing.

2.1.3.2 ASC specks

Inflammasome sensors such as NLRP3 comprise of a pyrin domain (PYD) and a CARD domain, together forming the apoptosis-associated speck like protein containing a caspase recruitment domain (henceforth known as ASC specks) (169). Detection of danger signals or microbes (i.e. ATP, Nigericin) by inflammasome sensors induces the rapid polymerisation of PYD and CARD into a speck, which in turn activates pro-caspase-1; stimulating the latter's autoproteolysis into mature caspase 1 (214). The enzymatic activity of active caspase-1 is employed through the cleavage of IL-1 β and IL-18 from their immature forms to their active structures. Thus, ASC specks provide a platform by which caspase-1 is recruited, thereby facilitating the inflammatory response (214). Aside from NLRP3, six other inflammasomes (AIM2, IFI-16, Pyrin, NLRC4 and NLRP1 and RIG1) can facilitate the assembly of an ASC speck (169, 214, 215).

In the context of autoinflammation, cellular release of ASC specks upon pyroptosis augments the inflammatory response through dissemination of these adaptor molecules through the extracellular environment. ASC specks demonstrated their ability to facilitate the cleavage of pro-IL-1 β to activated IL-1 β in the cell-free supernatant of NLRP3 primed and activated macrophages (169). Franklin *et al* further revealed that these extracellular specks were taken up by other surrounding macrophages into their phagolysosomal compartments, where ASC remained stable for over several hours. Baroja-Mazo *et al* corroborated these findings, detecting ASC specks in sera obtained from 18 NLRP3-AID patients with active disease and CRP levels over 10mg/l. In comparison to six healthy controls, levels of these specks were deemed significant in NLRP3-AID patients during active disease, but not significant during non-flare periods in these patients (214). Since the release of these papers, several publications have suggested the use of extracellular inflammasome components as biomarkers for traumatic brain injury (216), Multiple Sclerosis (217) and MDS (218). Accordingly, quantifying levels of ASC in sera and extracellular fluids can be an indicator of inflammasome activation whilst acting as supplementary marker of potential inflammation.

2.1.4 Chapter aims

Supporting the concept of SchS as an autoinflammatory disease, assessment of the SchS inflammatory milieu through measurements of cytokines and ASC specks serve as additional markers of inflammasome activation and NLRP3 involvement respectively. Emulating previous experimental strategies based on NLRP3-AID, utilising NGS technology to search for somatic *NLRP3* mutations in PB derived DNA. Therefore, the aims of this chapter are as follows:

- A.** Deep sequencing of *NLRP3* in 32 patients
- B.** Detection of ASC specks present in serum as an additional marker of NLRP3 activation
- C.** Serum quantification of ten interleukins associated with the NLRP3 inflammasome and general autoinflammation

2.2 Methods

2.2.1 Patients and ethical approval

Informed and written consent was obtained from all participants included in this thesis and subsequent published research papers. Samples were collected from three centres: St James' University Hospital, Leeds, UK; The National Amyloidosis Centre - University College London and Department of Dermatology and Allergy - Universitätsmedizin Berlin, Germany. Samples were also taken from healthy donors working in the department with informed consent, to serve as controls for this project. Ethical approval was granted by the Leeds (East) Research Ethics Committee (04/Q1206/107), Royal Free Hospital and University College Medical School Research Ethics (06/Q0501/42) and the Universitäts-medizin Berlin ethics committee (EA4/005/15, EA1/007/17).

2.2.2 Cytokine Detection

The Meso Scale Discovery (MSD) platform was utilised to detect the following cytokines in their active form: IL-1 β , TNF- α , IFN- γ , IL-6, IL-8, IL-10, IL-12p40, IL-12p70, and IL-17 α . MSD platform allows for the detection of nine separate cytokines within a single well of a 96-well plate, combining both electrochemiluminescence and spatial gridding technology. Subsequent detection of cytokines was achieved by the addition of an MSD ECL molecule (Sulfo-Tag™), which requires electrical stimulation for the activation of its chemiluminescence properties. Imaging of the resulting light signal was measured using the MSD Sector Imager instrument.

2.2.3 IL-18 ELISA

IL-18 levels were measured using ELISA: Human IL-18 Matched Antibody Kit (Catalogue no. BMS267-2MST, Thermo Fisher Scientific, UK). Ninety-six well plates were pre-coated with human monoclonal IL-18 antibody and incubated overnight at 4°C. Both the coating antibody and detection antibody detect the cleaved, mature form of IL-18. Serum samples and standards were added to the wells, followed by the addition of IL-18 antibodies labelled with biotin, in combination with Streptavidin-HRP in order to form immune complexes. Unbound material was washed away, with Chromogen solution added until the transformation of the colourless solution to blue. The latter steps were carried out at room temperature. The fluorescence was then measured using the Multiskan microplate reader (Thermo Fisher Scientific, UK) and results are expressed as pg/mL.

2.2.4 Statistical analysis

Statistical analysis was performed using GraphPad Prism software 8.0. The Shapiro-Wilks normality test was used to determine whether the resulting data was parametric or non-parametric. The Kruskal-Wallis one-way analysis of variance (ANOVA) test was used to derive significances between the non-parametric data obtained for comparing more than two datasets. If significance was determined across the groups, comparison between individual pairings and correction for multiple comparisons was carried out using the Dunn's multiple comparison test. A significant result was defined with a P value equal to or less than 0.05.

2.2.5 DNA extraction

Extraction of DNA was performed on 1 million PBMCs derived from lymphoprep (the latter carried from UCL and Berlin – not carried out at St James' Hospital). Based on column purification, the QIAmp DNA Mini Kit (Qiagen, Germany) was utilised according to the manufacturer's instructions. Purified DNA was eluted in 100µl of DNase free water (ThermoFisher, UK), with subsequent quantification and quality assessed using the Nanodrop spectrophotometer.

2.2.6 PCR and agarose-gel electrophoresis

The primary polymerase chain reaction (PCR) amplified *NLRP3* from leucocyte DNA derived from the previous section (2.2.5), including the untranslated regions according to the following method. The final PCR volume of 20µL consisted of 10 picomoles of each primer (section 7.7.1, appendix), 10µl of Phusion Green Hot Start II High-Fidelity DNA Polymerase master mix (Thermo-Fisher Scientific, USA) with 10-150ng of the DNA template. The reactions were carried out for 35 cycles: denaturation at 98°C for 10 seconds, annealing at 65°C for 5 seconds and elongation at 72°C for 4 minutes and 30 seconds, with 20µl of each PCR product plus 1µl of Midori Green Direct (Nippon Genetics, Germany), run on a 1% agarose gel in Tris-acetate-EDTA at 90 volts for 45 minutes. The gel was visualised using gel green and the GelDoc system, and Quantity-One software (BioRad, USA). Bands corresponding to the correct fragment sizes were excised and purified using the Zymogen Gel Recovery kit (Zymogen, USA) according to the manufacturer's protocol. DNA concentration was determined using the Nanodrop Spectrophotometer.

2.2.6.1 Sonication

Library preparations were performed using the NEBNext DNA Library Prep Kit for Illumina (NEB, USA), according to manufacturer's instructions. Equal amounts (20ng) of PCR products were pooled together. Purified amplicons were sonicated using the Bioruptor instrument (Diagnode, Belgium) with 0.25% SDS, at 4°C for 15 minutes using 1.5ml Eppendorf tubes, in order to fragment DNA as input for the following step. This was followed by column based purification method (Clean and Concentrate, Zymogen, UK), and the fragmented DNA eluted in 20µl of DNase free water (Thermo-Fisher, UK).

2.2.6.2 End repair and dA tailing

End repair and dA tailing was performed as a single reaction at room temperature for 30 minutes, then 65°C for a further 30 minutes to denature the enzymes and stop the reaction. End repair is necessary to fill in the blunt ended overhangs generated via the sonication step, containing 5' phosphate and 3' hydroxyl groups. For the ligation of Illumina sequencing adaptors, end repaired fragments require inclusion of a 5' deoxyadenosine, but also allowing for ligation with complementary adaptor dT overhangs (219). As DNA input was less than 100ng, index tagged adaptor ligation was carried out using a 1:10 dilution of the adaptor (originally at 15 µM) to prevent adaptor dimer formation; followed by the addition of the Ligation Master Mix and Ligation enhancer to the end-repaired and dA tailed amplicons from the previous step. Each tag was composed of a specific indexed primer sequence to enable identification of the patient.

2.2.6.3 Size selection

Due to the lower amounts of DNA derived from the initial PCR step, size selection and clean-up of adaptor ligated DNA was performed as one step prior to PCR enrichment. DNA size selection is imperative for successful sequencing, as surplus lower molecular weight fragments such as adaptor dimers and primer dimers can interfere with the sequencing run, essentially preventing reads on desired DNA fragments (219). The DNA products were purified using AxyPrep™ bead selection procedure (Axygen, CA, USA) in a 96 well plate. 0.9x AxyPrep beads were added to the adaptor ligation mix, preceded by an incubation time of 5 minutes, followed by placement onto a magnetic stand to allow for separation for a further 5 minutes, at room temperature. The amount of beads used are dependent upon desired

fragment length (250bp in this work), the lower the AxyPrep™ bead ratio to DNA ratio, the larger the eluted DNA fragments are. Addition of Polyethene-glycol (PEG) to DNA solution causes the DNA to form random coiled structures (220), with the addition of sodium chloride enabling DNA aggregation and adhesion to other molecules in the near vicinity, including the beads coated with carboxyl groups. With the addition of water, hydrating the DNA, the carboxyl groups on the beads repel the DNA, allowing for supernatant extraction.

2.2.6.4 PCR enrichment

The size-selected products were then subject to enrichment using NEBNext Q5 Master Mix and Universal Primer. PCR is carried out to amplify DNA fragments with 2 primers, one annealing to the ligated adaptor, and the other 'universal' primer ligating to the other end of the adaptor ligated DNA fragment. With fragments comprising of unique adaptor sequences at one end, this permits the first run within the flow cell to sequence the forward strand of the DNA, then synthesis of the reverse. The number of PCR cycles are limited to minimise generation of errors, and the PCR conditions were as follows: 98°C for 1 second, 65°C for 5 seconds and 72°C for 10 seconds, for a total of 6 cycles. A 250bp based 'size selection' procedure was additionally carried out before the final enrichment step. Figure 4 provides a summary of the DNA library preparation workflow.

2.2.6.5 Quality control and pooling

The size distribution of the resultant index tagged DNA libraries was measured using the Agilent 2200 TapeStation system and corresponding software; using 1µl of the DNA library and 3µl of the D1K buffer run on D1K screen tape (Agilent Technologies, UK).

Equal amounts of each library were pooled prior to the DNA library construction step, and for the final mix of all the uniquely tagged samples for loading onto the MiSeq was carried out following quantification by the Quant-iT™ dsDNA Assay Kit (Invitrogen, USA), which was utilised according to the manufacturer's instructions. Briefly, 2µl aliquots of each PCR product (or the final DNA libraries), were transferred into black Costar 96-well fluorimetry plates (to minimise background and absorb light) (Corning, USA), alongside 2µl of the manufacturer supplied standard curve. Quant-it dsBR reagent was diluted (1:200) using Quant-iT dsBR buffer (working solution), with 198µl of this transferred into each well containing the samples/standards. 20µl of each standard was transferred into a corresponding well, with another 180µl of working solution added to these wells to give a 1/10 standard curve. The PicoGreen probe within this working solution is fluorescent, binding double-stranded DNA and forming a highly fluorescent complex in comparison to dye in solution. Fluorescence was measured using the FluoStar plate reader, with comparison to the 2 standard curves generated by the given standards.

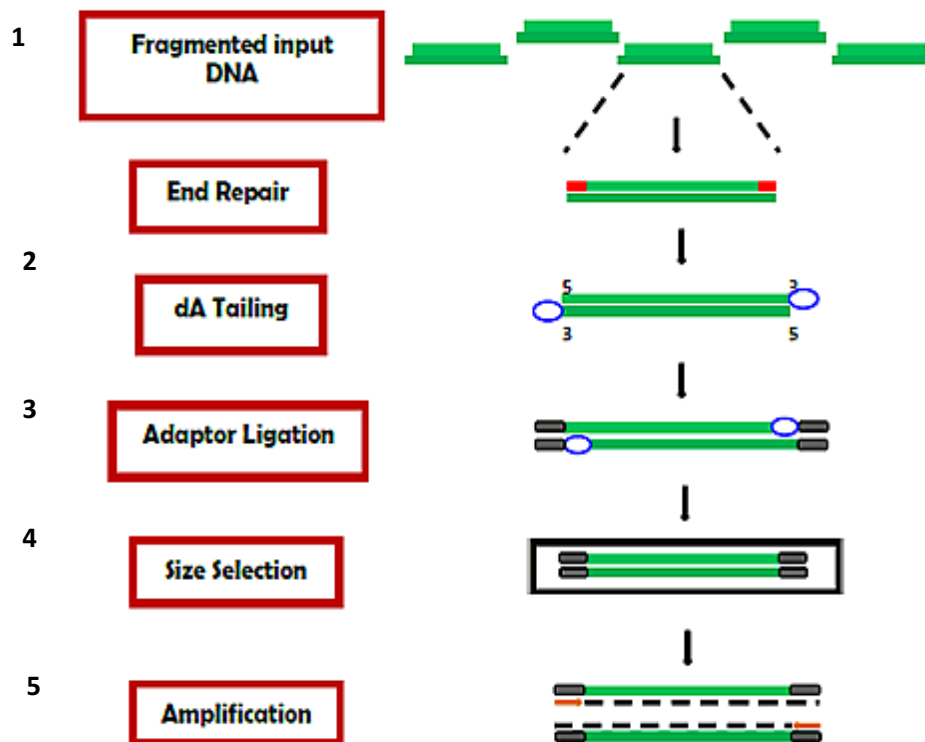


Figure 4: Workflow of DNA library preparation.

Step 1 - DNA is first fragmented to around 250bp-300bp. Step 2 - end repair and dA tailing is carried out. Step 3 - adaptors are ligated to the end repaired and dA tailed fragments. Step 4 - fragments are then size-selected and purified with AxyPrep™ beads. 5. PCR enrichment allows for increased DNA yields and accurate amplification using a high fidelity master mix. Following the above steps, the amplicons are subject to pooling and QC as described in section 2.2.6.5.

Figure 4 derived and modified from: BioCat Online (221).

2.2.6.6 MiSeq run

Sequencing was carried out by the NGS facility within the Leeds Institute of Medical Research at St James. Sequencing was performed on an Illumina MiSeq™ instrument, with a 2 x 150 bp paired end run. The sequencing result itself generating over 3 million reads, with the depth of sequencing average at 5000 reads per sample.

2.2.7 Galaxy

Using the Galaxy platform bioinformatics interface www.usegalaxy.org (222), the sequencing data files were analysed, subject to a customized workflow as outlined in Figure 5 below.

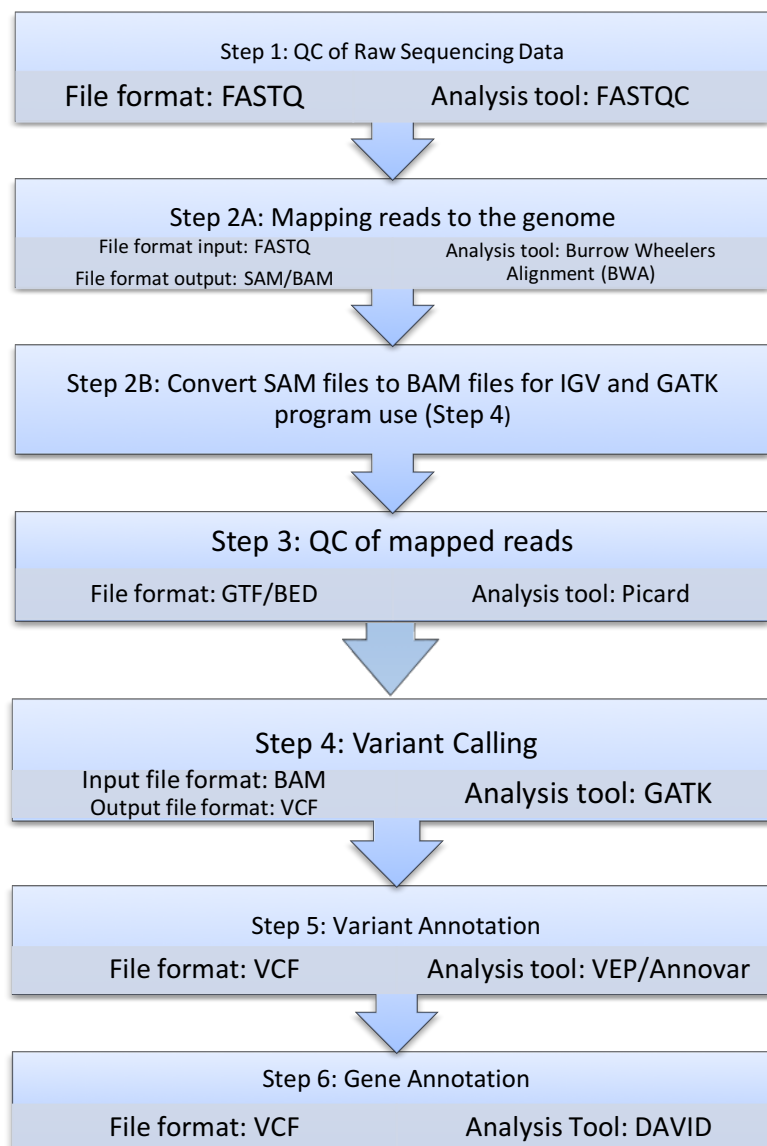


Figure 5: The customised Galaxy workflow used in this study.

Each step in Figure 5 shows the file format, analysis step and tools used to analyse the data. Integrated Genome Viewer (IGV) allows visualisation of the processed data.

Briefly, the paired end fastq files were subject to quality control analysis using fastqc. The 'Trimmomatic' tool was used to low quality data, as well as remove adaptors. Quality control checks on raw sequence data provided quality scores across all bases, where Q30 was deemed as 'good' based on a 1 in 1000 error probability. The Burrows Wheeler Alignment (BWA) allows for the alignment of short sequences less 400 nucleotides long to the selected reference genome (HG19). SAM files were converted to their binary format as BAM files and the conversion of SAM files to BAM files was required for the use of the downstream programme 'GATK'. Step 3 determined the percentage of aligned reads and coverage of target regions, step 4 involved variant calling using GATK to minimise false positives, and to call SNVs & short indels. Variant annotation was step 5, and determined the potential biological action of SNVs and small indels; i.e. variant location, variant effect, phenotype and disease association. The final step was gene annotation, involving the examination of the biological function of the list of genes containing the SNPs and short indels obtained from the previous step. DAVID is an online database for analysing groups of genes.

2.2.8 ASC specks

200µl of healthy control (HC) or patient serum were incubated with 5µl of PE anti-ASC (TMS-1) antibody (Cat. Number 653904, Biolegend, UK) for 1 hour, and subsequently analysed on the LSRII flow cytometer instrument (BD Biosciences, UK). Non-fluorescent 1µm microspheres (Cat. Number F13838 Thermo-Fisher Scientific, UK) were used as a guide to gate around the 1µm ASC specks. ASC speck events were reported as total events in the set gate divided by 200 (ASC speck/µl).

2.3 Results

2.3.1 Cytokine data

Nine pro-inflammatory and anti-inflammatory cytokines were measured within sera using the MSD platform, with IL-18 levels measured using an ELISA. All graphs are representative of healthy controls (n=12), SchS patients (n=19) and NLRP3-AID patients (n=7), except for IL-18, where 21 healthy controls were included in the experiment. The Kruskal-Wallis one way ANOVA test was used to derive significances between the non-parametric data obtained, and P values of equal to or <0.05 were regarded as significant.

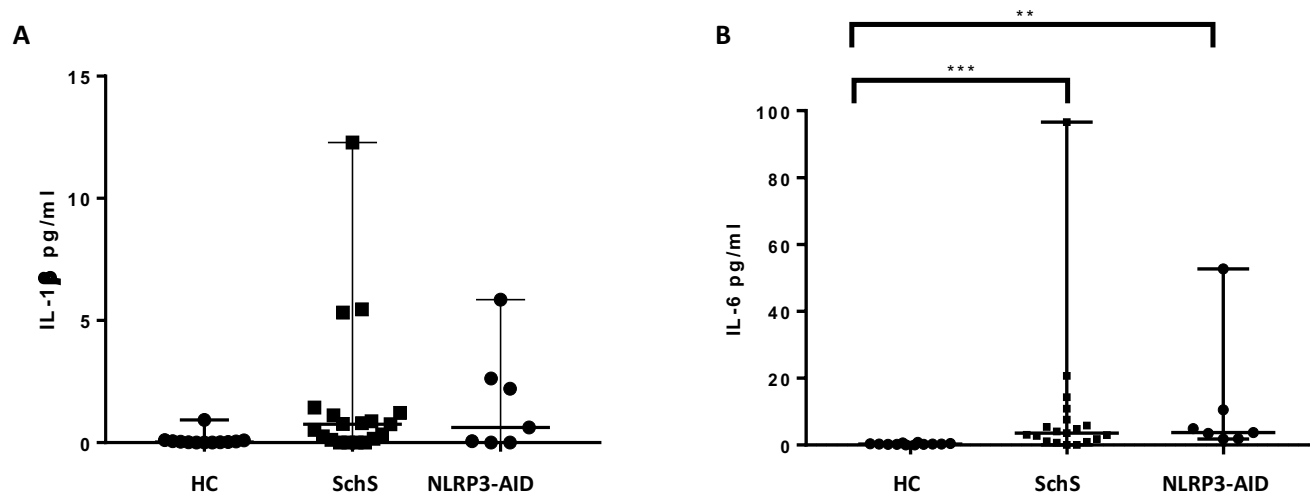


Figure 6: IL-1 β and IL-6 cytokine levels.

A – IL-1 β levels no significant differences observed. B - IL- 6 levels. Significant difference observed between the HC and SchS groups (***p=0.0005) and between HC and NLRP3-AID groups (**p = 0.0016).

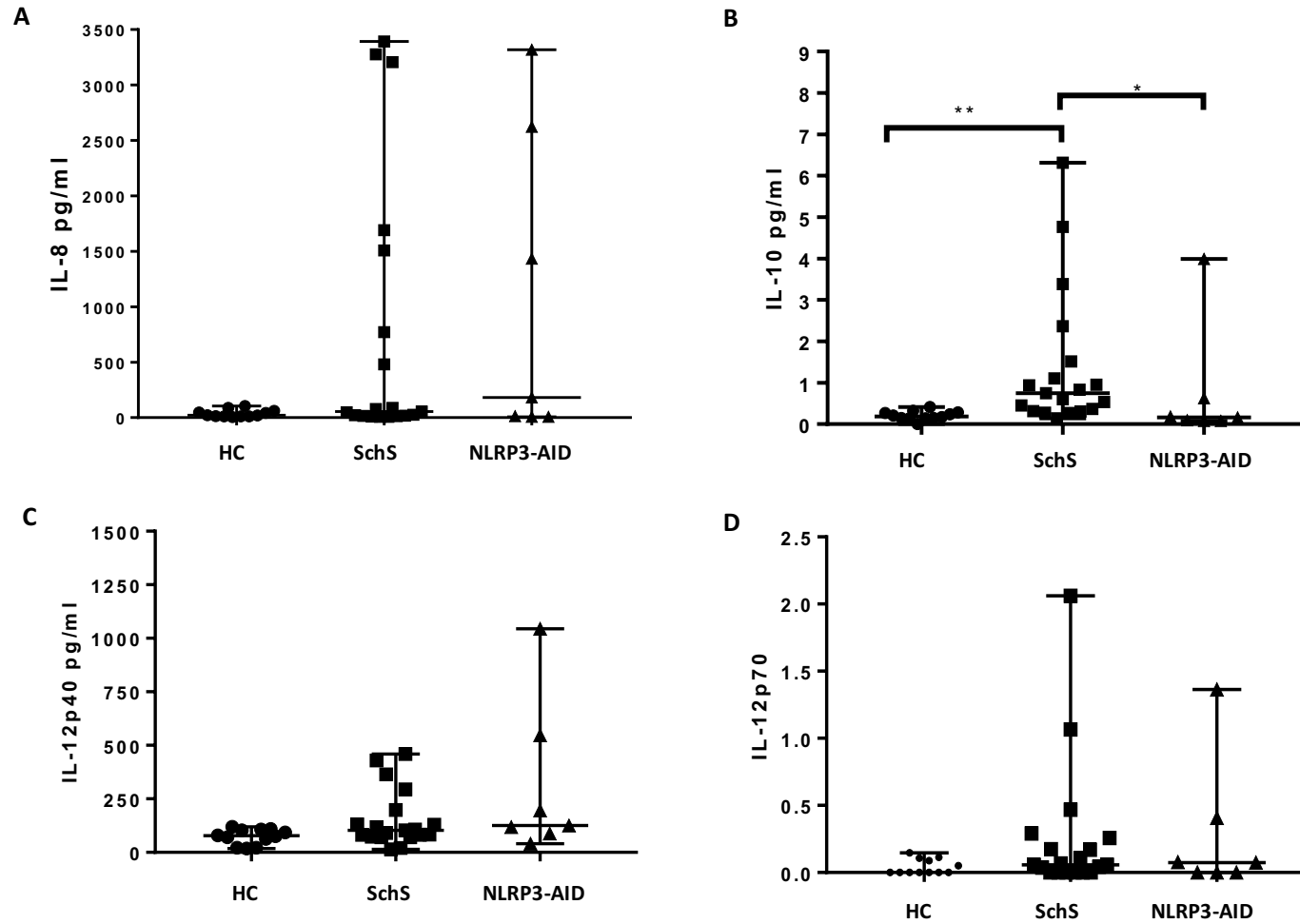


Figure 7: IL-8, IL-10, IL-12p40 and IL-12p70 cytokine levels.

A – IL- 8, no differences observed between the three groups. B – IL-10, significant difference was observed between the HC and SchS groups (** $p=0.0016$) and also between the SchS and NLRP3-AID patients (* $p=0.0254$). C & D: IL-12p40 and IL-12p70 respectively, no significant differences observed.

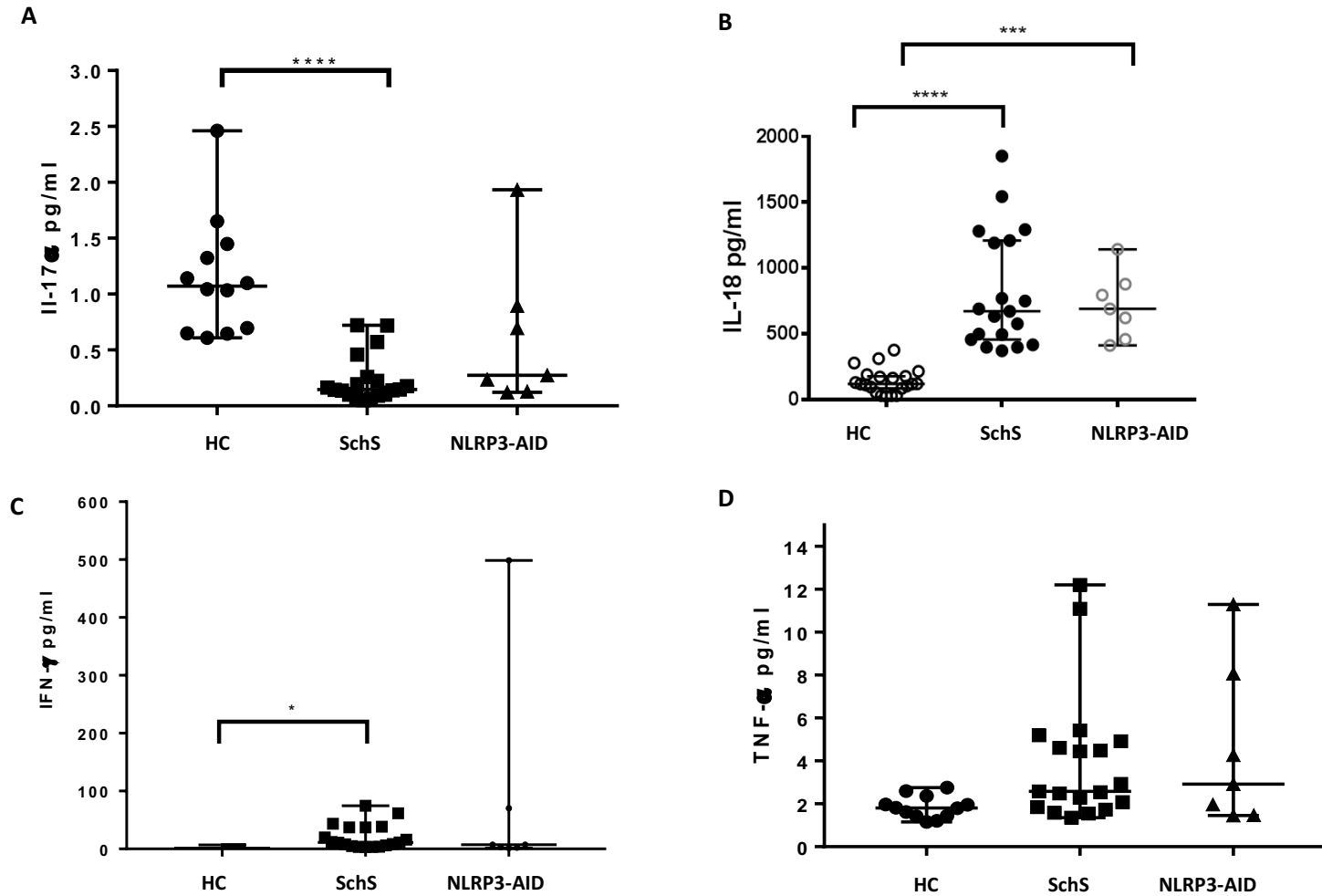


Figure 8: IL-17 α , IL-18, IFN- γ and TNF- α cytokine levels.

A – IL-17 α , significant difference was observed between the HC and SchS groups (**** $p=0.0001$). B – IL-18, significant difference observed between HC and NLRP3-AID patients (***) $p < 0.0003$), and between HC and SchS patients (**** $p < 0.0001$). C – IFN- γ , significant difference was observed between the HC and SchS groups (* $p=0.016$). D – TNF- α , no significant difference observed.

Previously investigated cytokines in SchS have included IL-6, IL-18 and TNF- α , though these studies were limited to between three to ten patients. In this work, 19 SchS patients were subject to their serum being probed for the following ten cytokines: IL-1 β , IL-6, IL-8, IL-10, IL-12p40, IL-12p70, IL-18, IFN- γ and TNF- α . Conferring statistical power, this in contrast to previous studies where access to large SchS cohorts was not possible. No significant differences were determined between HC, SchS and the NLRP3-AID cohorts with IL-1 β , IL-8, IL-12p40, IL-12p70 and TNF- α .

The median concentration of IL-6 in HC, SchS and NLRP3-AID groups were: 0.3 pg/ml (range 0.2-0.8), 4 pg/ml (range 1-97) and 3.7pg/ml (range 1.8-52.6) respectively. Significant difference was observed between HC and SchS (***p= 0.0005) and between HC and NLRP3-AID (**p = 0.0016) patients, but no significant difference of IL-6 was observed between the SchS and NLRP3-AID patients.

The median concentration of IL-10 in HC, SchS and NLRP3-AID groups were 0.19pg/ml (range 0-0.41), 0.75pg/ml (range: 0.14 to 6.3) and 0.16pg/ml (range: 0.08-4.0) respectively. Significant difference was observed between the HC and SchS groups (**p=0.0016) and also between the SchS and NLRP3-AID patients (*p=0.0254). No significant difference was observed between the HC and NLRP3-AID groups.

The median concentration of IL-17 α in HC, SchS and NLRP3-AID groups were 1.07pg/ml (range: 0.6 – 2.46), 0.15pg/ml (range 0.05 – 0.72) and 0.27pg/ml (range: 0.12-1.9) respectively. Significant difference was observed between the HC and SchS groups (****p=0.0001), but not between the SchS and NLRP3-AID patients, or between the HC and NLRP3-AID groups.

IL-18 levels were measured in healthy controls (HC, n=21), SchS patients (n=19) and NLRP3-AID patients (n=7). The median concentration of IL-18 in these three groups were: 119 pg/ml (range 23-278), 750 pg/ml (range 371-1852); and 688 pg/ml (range 411-1141) respectively. The levels of IL-18 were similar between SchS and NLRP3-AID patients, with no significant difference observed between these two cohorts. However, both SchS and NLRP3-AID had significantly higher levels in comparison to HC.

The median concentration of IFN- γ in HC, SchS and NLRP3-AID groups were 3.9pg/ml (range: 2.7-6.9), 11.2pg/ml (range: 3.3-74.5) and 7.0pg/ml (1.4-498p). Significant difference was observed between the HC and SchS groups (*p=0.016), but not seen between HC and NLRP3-AID, or between SchS and NLRP3-AID.

2.3.2 PCR and agarose-gel electrophoresis

The initial aim was to generate amplicons from PB DNA, with the primers used corresponding fragment length are shown in section 7.7.1, Appendix. PCR optimisation was carried out previously for each primer pair to determine the best PCR composition and thermocycling conditions in order to generate a clear, defined band. Amplicon size and primer coverage of the gene are further described below in the figure legends.

2.3.2.1 Amplification of *NLRP3*

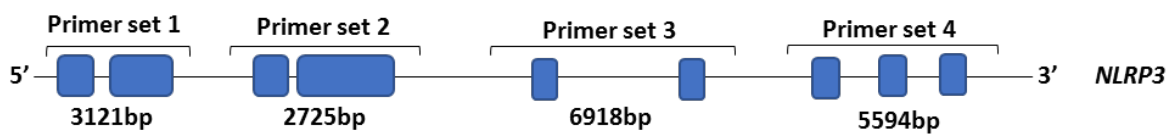


Figure 9: Schematic of the *NLRP3* gene and primer coverage.

NLRP3 is located on the long arm of chromosome one (base pairs 247,416,156 to 247,449,108). Primers were designed to encompass each of the nine exons of this gene. The sizes of the products generated from these primer sets are denoted below.

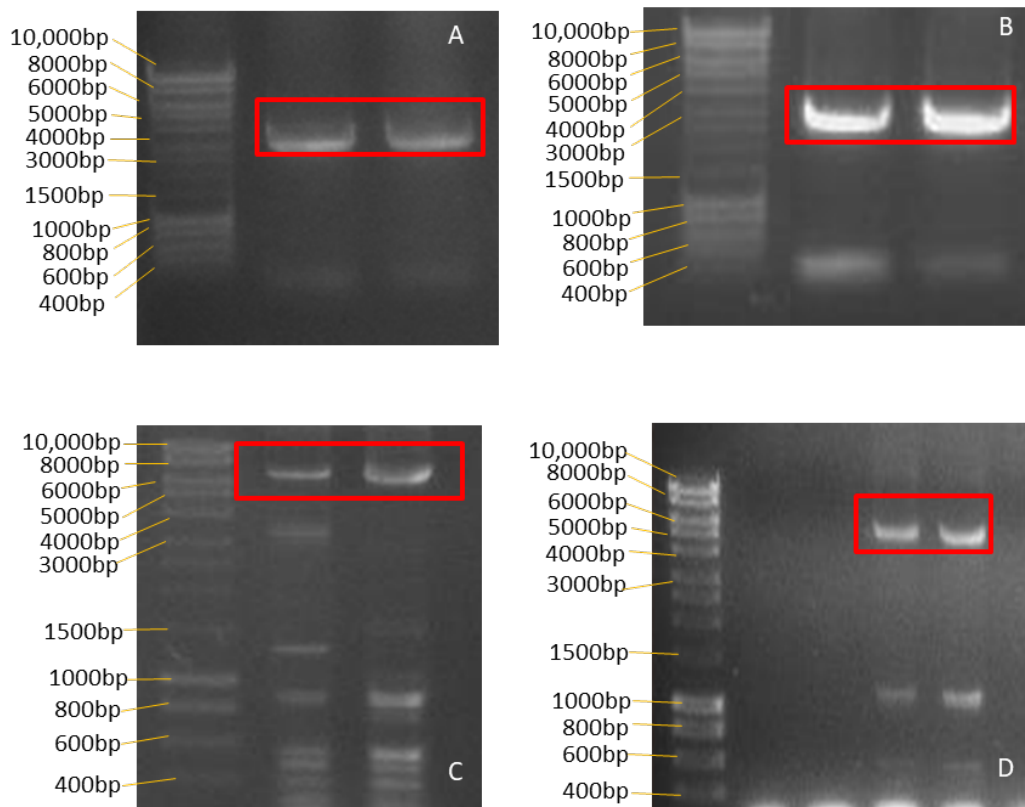


Figure 10: Visualisation of *NLRP3* PCR products.

Figure 10 - A,B,C & D are representative gel electrophoresis images showing the PCR products obtained for *NLRP3* amplification run on a 1% gel . The products were run on 0.5% agarose gel to allow for better resolution for the larger sized amplicons. Four sets of PCR primers for *NLRP3* were designed. Lane 1 on images A, B C and D correspond to the 1kb ladder used. (A): Primer set 1 amplified *NLRP3* from the 5' UTR to the end of exon 2 – 3121bp product (lanes 2 and 3). (B): Primer set 2 amplified *NLRP3* from the end of exon 2 to the beginning of exon 4 – 2725bp product (lanes 2 and 3). (C): Primer set 3 amplified *NLRP3* from the beginning of exon 4 to the end of exon 8 – 6918bp product (lanes 2 and 3). (D): Primer set 4 amplified *NLRP3* from the end of exon 8 to the 3' UTR – 5594bp product (lanes 2 and 3).

2.3.3 Sample QC and pooling

Prior to pooling the samples for MiSeq loading, two QC steps were carried out in order to quantitate and assess the purity of the indexed libraries: (1) TapeStation analysis to determine the size of the libraries, followed by (2) Quant-iT™ assay to assess the concentration of each sample.

2.3.3.1 TapeStation

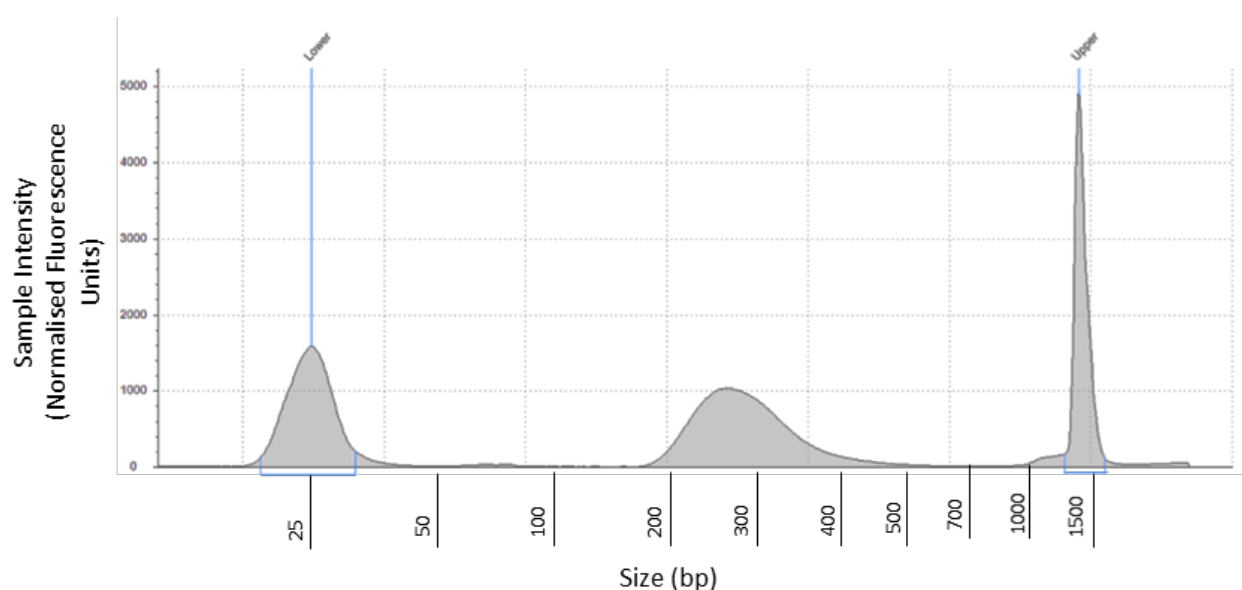


Figure 11: Bioanalyser results trace.

Figure 11 depicts a representative bioanalyser trace demonstrating the average size and distribution of the indexed library constructed from the steps described (Figure 4).

The above trace was acquired using the Agilent D1000 DNA screen tape assay in conjunction with Agilent 2200 TapeStation system (Agilent Technologies, UK). Figure 11 shows the size fragment distribution of an indexed library for *NLRP3* sequencing. The X axis refers to the size in base pairs of the DNA library, with the Sample Intensity (normalised fluorescence units) on the Y axis. The lower marker (left peak) and the upper marker (rightmost peak) correspond to the size markers of 25bp and 1500bp respectively. The average size of the library was 280bp, thus this broad peak is expected to cover the sonicated gene fragments with the adaptors ligated onto the DNA. The absence of other peaks (i.e. primer dimer at 50bp) within the sample, indicates there are no other artefacts which would interfere with the sequencing of the library.

2.3.3.2 Quant it™ PicoGreen assay

The purpose of carrying out Quant-iT™ assay was to accurately assess the amount of the DNA library per sample, in order to ultimately pool together the samples for sequencing in equimolar amounts.

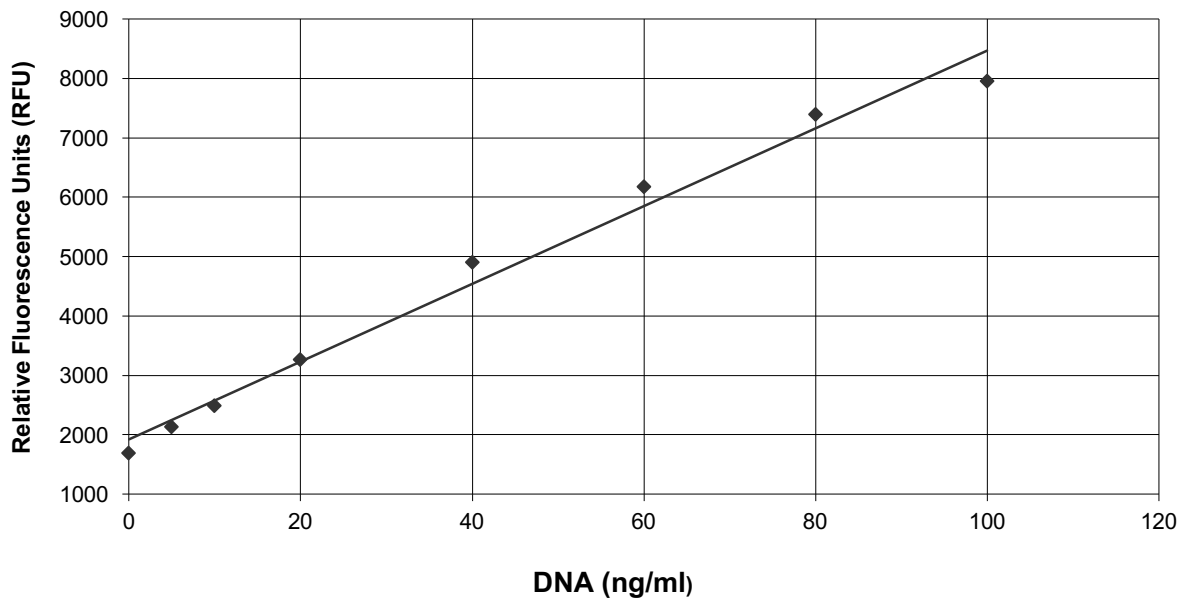


Figure 12: PicoGreen Assay curve.

Figure 12 demonstrates the 8 point standard curve obtained with the assay (0-100ng/ml). The X-axis demonstrates the concentration of DNA in ng/ml with relative fluorescence units on the Y-axis (arbitrary).

The samples were excited at 480nm with the fluorescence emission intensity measured at 520nm. Per DNA library, equimolar amounts of each sample were pooled to generate a combined library with equal amounts of DNA for sequencing to prevent disproportionate sequencing of each of the samples.

2.3.4 Sequencing results

In the context of this thesis, targeted *NLRP3* amplicon sequencing was carried out from the PB DNA of 32 SchS patients. No pathological variants were found in *NLRP3* of 32 SchS patients. Eighteen SchS patients were also subject to additional sequencing against a genetic panel comprised of autoinflammatory associated genes, carried out at UCL (85) section 7.3, Appendix).

2.3.4.1 Sequencing Coverage, QC and Alignment

The number of unique reads covering a given DNA base is referred to as the 'sequencing coverage', and deep sequencing aims to generate a substantial number of individual reads for a given DNA sequence. In the data obtained for this chapter, the number of unique reads varied from 0 to 7340 per sample. The QC step assessed the quality of these unique reads obtained (Galaxy). Alignment to the reference Human Genome, GRCh37, permitted detection of potential variants in the genes analysed. This latter step was carried out by BWA and visualised using Integrated Genome Viewer (IGV) (Figure 15).

2.3.4.1.1 Sequencing Coverage



Figure 13: Sequencing coverage and alignment of the amplicon sequencing.

Schematic showing the sequencing coverage and alignment of the amplicon sequencing carried out in this chapter. Yellow (indices), blue (DNA fragment). Employment of paired end sequencing enabled both ends of the input DNA fragment to be sequenced. As the distance between each end was known (250bp-300bp), alignment to the reference sequence was more precise given the abundance of repetitive regions within the input DNA.

2.3.4.1.2 Galaxy QC

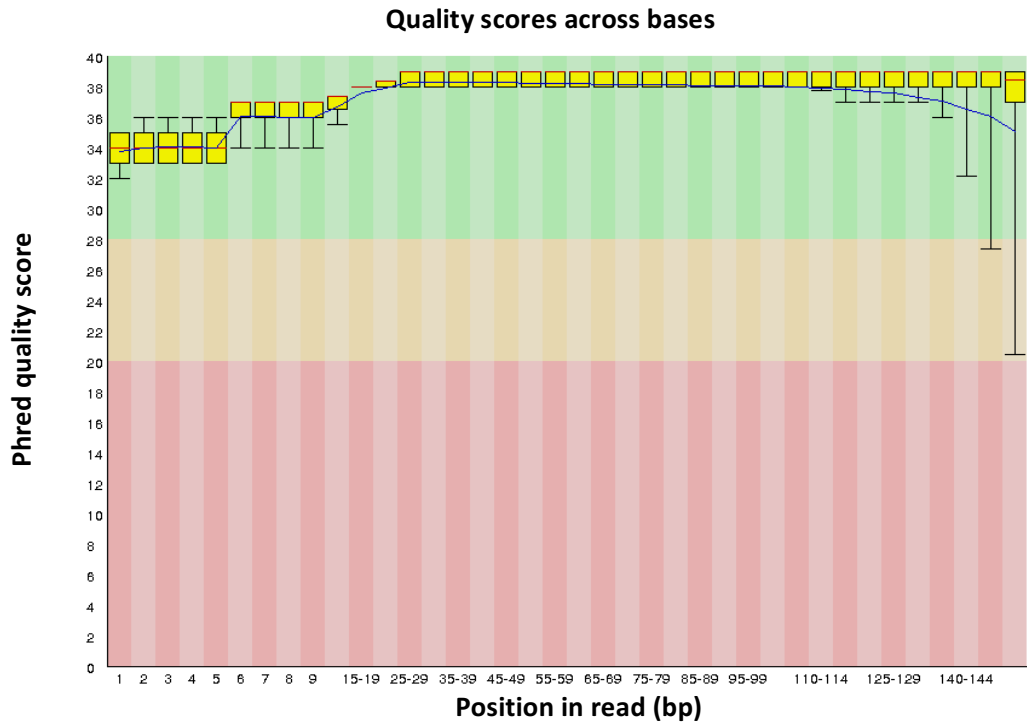


Figure 14: Representative QC figure generated by Galaxy.

Box plots are generated by Galaxy for each sample, indicating the quality scores across the bases. The yellow boxes represent the 25th to 75th percentiles, with the upper and lower whiskers demonstrating the 10th and 90th percentiles respectively. The Y-axis refers to the Phred quality scores, with the X-axis showing the results in correlation to the position in the read (1-150). A Phred score of 30 implies that the probability of an incorrect base call is 1 in 1000, and a 99.99% base call accuracy. Whereas a decreased Phred quality score of 20 implies the probability of an incorrect base call is 1 in 100, with a 99% base call accuracy. In this sample, all QC scores are above a Phred score of 20, therefore indicative of a 99% to 99.99% base call accuracy.

2.3.4.1.3 Alignment to the Reference Genome

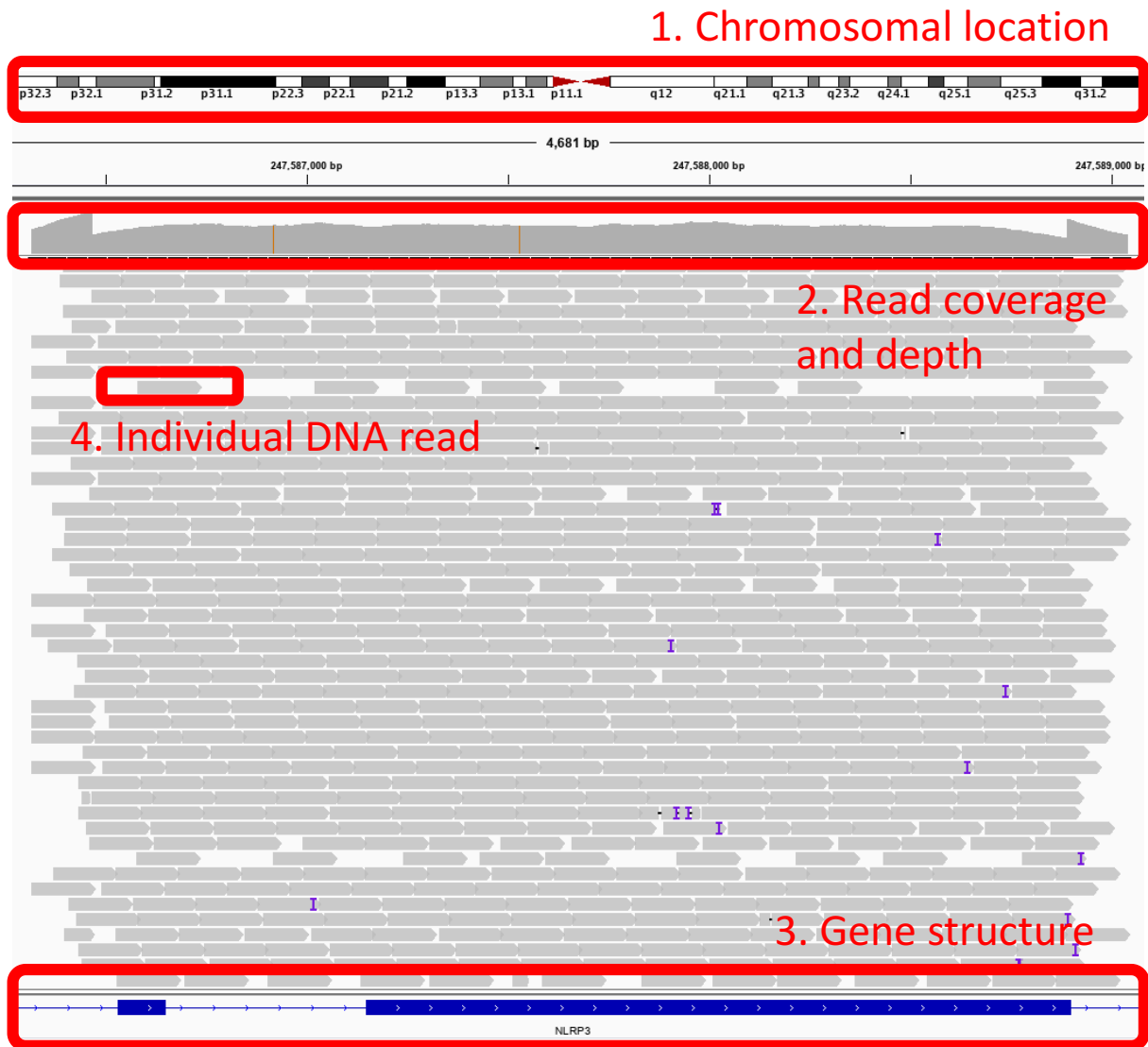


Figure 15: IGV sequencing analysis

Figure 15 is a representative snapshot of sequencing analysis from Integrated Genome Viewer (IGV - Broad Institute, Boston, USA). The image portrays the sequencing results obtained first two exons of *NLRP3* (position 1:247,585,750 to 1:247,590,451 for SchS sample one, aligned against the reference genome: GRCh37). The portion of the chromosome displayed is shown in the top box, the read coverage is shown by the track in the second box and the third box specifically indicates the coverage across the exonic and intronic regions of the gene being analysed. Here, *NLRP3* exons one and two are shown. The fourth box shows a grey bar which is representative of an individual read, with the sizes of the inserts varying from 200bp to 300bp in the sample shown. These grey bars change colour if there are 20% of the nucleotide reads in the sequenced sample that differ to the reference nucleotide. Nucleotide insertions are shown in this sample and are denoted by 'I' (purple).

2.3.4.2 Additional sequencing panel at UCL

These negative genetic results were further strengthened by the simultaneous findings of 18 SchS patients (patient 12 - 28, 32, Table 5), involving the sequencing of hot spots within genes associated with autoinflammatory disease. The aim to identify a common genetic susceptibility factor to SchS was pursued by Rowzcenio and colleagues at UCL. The panel comprised of genes such *NLRC4*, *NOD2* and *TNFRSF1A*, (section 7.3 Appendix), but failed to identify any unifying variants causative of SchS. These outcomes, alongside the results of this chapter were published as a regular article in Blood (85).

2.3.5 ASC specks are elevated in autoinflammatory diseases

Upon their activation, inflammasome forming receptors nucleate ASC molecules, instigating a prion-like aggregation event, forming ASC ‘specks’. These specks are 1µm in diameter, enabling the subsequent activation of caspase-1 (223). High levels of these specks have been previously identified in NLRP3-AID patients, thus determination of levels of ASC in 16 SchS patients was of relevance in this work.

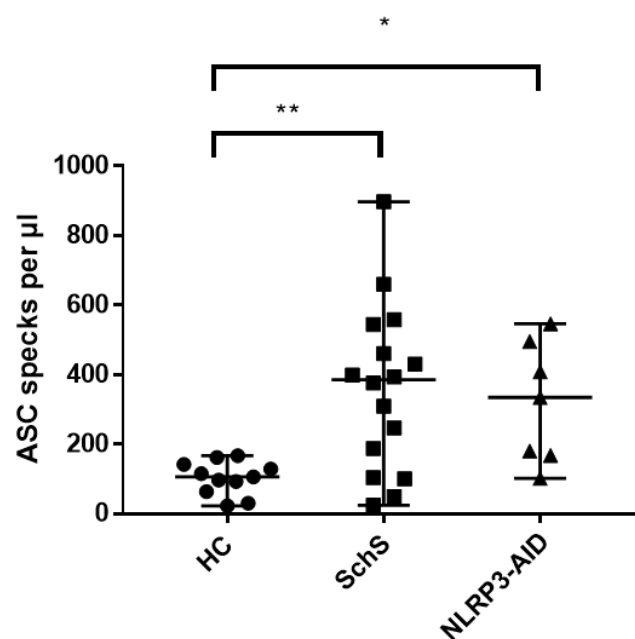


Figure 16: ASC specks per microlitre.

Extracellular ASC protein aggregates and cytokines levels were measured in the serum collected from 16 SchS patients, 7 NLRP3-AID patients who had germline mutations in the *NLRP3* gene and 11 HC, before administration of IL-1 blocking therapy. Significance was determined between HC and SchS (* $p = 0.0069$) and also between HC and NLRP3-AID (* $p = 0.0309$) No significant difference was observed between the NLRP3-AID and SchS cohorts.

2.3.6 Clinical Data summary of the SchS patients

Patient number	Sex	Age at Symptom onset (years)	M protein	IgMk paraprotein levels (g/l)	Rash (Y/N)	Response to IL-1 inhibition***	CRP mg/l	ASC specks (per µl)	<i>NLRP3</i> variants
1	M	62.0	IgMk	6	Y	complete	79.6	ND	
2	W	43.5	IgMk	17	Y	good	60.9	ND	
3	M	51.5	IgMk	8	Y	good	44.0	ND	
4	M	67.0	IgMk	8	Y	complete	8.0	ND	
5	W	54.5	IgMk	3	Y	good	254.0	ND	
6	W	72.5	IgMk	11	Y	complete	86.0	ND	
7	W	55.5	IgMk	5	Y	complete	92.5	ND	
8	W	53.0	IgMk	5	Y	complete	12.0	ND	
9	W	60.0	IgGk	N/A	Y	good	70.0	ND	
10	W	72.5	IgMk	3	Y	good	14.0	ND	Q703K**
11	M	62.0	IgMk	3	Y	good	26.0	ND	
12* [‡]	M	36.8	IgMk	3	Y	Partial	40.0	49.3	
13* [‡]	F	37.9	IgMk	3	Y	complete	257.0	24.4	
14* [‡]	M	43.9	IgGλ	N/A	Y	complete	60.0	376.2	
15* [‡]	F	44.8	IgMk	1	Y	complete	120.0	247.2	
16* [‡]	F	49.6	IgMk	4	Y	complete	89.0	460.6	
17* [‡]	M	49.9	IgMk	9	Y	complete	19.0	ND	
18* [‡]	M	52.8	IgMλ (IF)	N/A	Y	complete	45.0	309.3	
19* [‡]	M	57.1	IgMk	7	Y	complete	18.0	430.6	V198M**
20* [‡]	M	58.1	IgMk	3	Y	complete	49.0	87.5	
21* [‡]	M	59.6	IgMλ	7	Y	died before treatment	79.0	544.7	
22* [‡]	M	61.7	IgMk	5	Y	complete	40.0	ND	
23* [‡]	F	60.7	IgMk	9	Y	complete	112.0	897.2	
24* [‡]	F	68.4	IgMk	8	Y	complete	140.0	398.8	
25* [‡]	M	78.9	IgMk	7	Y	complete	143.0	659.5	
26* [‡]	F	39.7	IgMk	16	Y	complete	26.0	ND	
27* [‡]	M	40.7	IgMk	4	Y	complete	20.0	558.1	
28* [‡]	M	61.2	IgMk	8	Y	complete	80.0	104.2	
29 [‡]	M	43.6	IgMk	6	Y	complete	75.2	394.1	
30 [‡]	F	59.0	IgMk	5	Y	complete	110.0	100.2	
31	F	51.0	IgMk	14	Y	complete	ND	ND	
32*	M	41.9	IgMk	12	Y	complete	18.0	ND	

Table 5: Clinical Data Summary of SchS patients.

Table 5 indicates the clinical data obtained for the SchS patients included in this chapter, alongside ASC speck levels and *NLRP3* status. [‡]Patients included in the cytokine analysis using the MESO platform and IL-18 ELISA. *These patients underwent further sequencing at UCL. ND: Not done. **common non-pathogenic *NLRP3* variants unlikely to be disease causative and have shown to be present in healthy individuals.

***Complete: no symptoms Good: symptoms rarely reoccur Partial: symptoms reoccur sporadically

2.4 Discussion

The purpose of the work undertaken in this chapter was to assess the inflammatory milieu of SchS patients and investigate the presence of somatic mosaicism in two genes imperative to inflammasome functioning. The MSD platform was employed to detect cytokine levels and use of flow cytometry enabled quantification of ASC speck levels. For the genetics part of this chapter, NGS was used to assess if the phenomenon of somatic mosaicism was applicable to the cohort of SchS patients included in this research.

To summarise, the main findings in this chapter were:

- i. IL-6 and IL-10 levels were significantly raised in 19 SchS patients
- ii. IL-18 levels were also significantly elevated in 19 SchS patients
- iii. No causative *NLRP3* variants identified in 32 SchS patients
- iv. ASC specks detected in the serum of 16 SchS patients are significantly elevated in comparison to healthy controls, and similar in values to those in NLRP3-AID patients

2.4.1 Cytokine data

The cytokine profiles obtained from 19 SchS patients, prior to the commencement of IL-1 blocking therapy, supports the concept of SchS as an autoinflammatory disease. Though the complete remission of SchS through inhibition of IL-1 strongly supports the role of IL-1 in the pathophysiology of this disease, assessing endogenous levels of the latter cytokine has proved challenging. For example, IL-1 β was virtually undetectable in seven patients with active NLRP3-AID (135), in part owing to its short half-life of two hours. Further, unlike TNF- α or IL-6, large amounts of the inactive, pro-IL-1 β remains within the cell. Once released, active IL-1 β binds to large carrier proteins such as α 2 macroglobulin (720kDa) and can therefore escape detection (224). Thus, the lack of significance seen with IL-1 β in this work rather pertains to the difficulties in cytokine quantification.

Contrastingly, IL-6 and IL-18 and can be regarded as biomarkers of disease severity given that elevated levels of these cytokines have been previously established in SchS (89, 225), RA (226) and other autoinflammatory disorders such as AOSD (227). In this work, levels of both of these cytokines were found significantly raised in comparison to HC, but at similar

quantities to those found in NLRP3-AID. Similar to IL-1 β , IL-18 undergoes caspase-1 processing for biological activation, whilst IL-6 production is under the strict control of IL-1 β .

Although TNF- α may contribute to the inflammatory status of SchS, its lack of significance indicates that it does not play a central role and could support the little evidence in literature indicating the limited efficacy of anti-TNF therapy (100).

Deficiency of IL-10 and lack of IL-10 receptor mediated signalling causes proinflammatory disease (i.e. severe early-onset enterocolitis) (228), thus high levels of this cytokine documented in SchS patients prior to inflammatory resolution, indicates its anti-inflammatory role within the immune system. Inferring that the insignificant amounts of TNF- α seen in this data is in support of previous findings demonstrating IL-10 mediated suppression of TNF- α and IL-17 secretion from macrophages and T cells (103, 229). Moreover, as referred to in section 2.1.2 - raised levels of IL-10 could be maintained through its active role in B-cell proliferation and its autocrine release from these cells (102).

Although no significance was seen between the three groups, seven SchS patients alongside three NLRP3-AID patients demonstrated increased levels of IL-8 in comparison to HCs. The production of this neutrophilic chemoattractant from macrophages is understood to be stimulated by IL-1 β and TNF- α (107).

Interestingly, IL-17 levels were significantly lower in SchS in comparison to the HCs, but demonstrated similar values to NLRP3-AID. Though IL-17 was found elevated in the keratinocytes of one SchS patient (110), assessment of this cytokine in a larger group of SchS patients rendered no significant values whilst assessing T_H17 secretions (109). The patient mentioned in the former paper was a variant IgG type SchS patient and thus more SchS patients (IgM type) are necessary to strengthen and corroborate these findings. Further, the significantly high amounts of IL-10 within these patients could explain the IL-17 results. Literature has shown macrophage-producing IL-10 negatively regulating IL-17 generation through suppression of the Th-17 promoter and transcription factor: RAR-related orphan receptor gamma (ROR γ t) (229).

2.4.2 NGS of the NLRP3 gene

The emergence of SAIDs with a genetic basis rationalised the experimental approach taken in this section. Implication of the NLRP3 inflammasome in SchS pathophysiology through detection of its elevated components in serum and cytokine analysis, validated searching for variants within its gene. The emergence of aNLRP3-AID demonstrated that low level somatic mutations in *NLRP3* can lead to development of acquired SAID (167), but this is not the

apparent case for SchS. Sequencing the entire *NLRP3* gene excluded the notion that *NLRP3* mutations are responsible for SchS pathology within a total cohort of 32 SchS patients (Table 5). The prospect that aNLRP3-AID may be attributed to somatic *NLRP3* mutations with its close clinical similarity to SchS, raised the likelihood of somatic *NLRP3* mosaicism as a potential contributor or cause of SchS disease manifestations. This hypothesis was originally investigated by de Koning *et al* in 2015, reporting that two out of seven SchS patients harboured two different *NLRP3* mutations, F523L and K435E, restricted to the myeloid lineage only (19). This hypothesis has proved incorrect in this presented work, although the disparity between these findings could be due to the fact that the patients involved in the 2015 report had variant IgG, whereas this cohort of patients largely present with the typical IgM gammopathy seen with SchS. Nevertheless, no link has been made with *NLRP3* mutations and gammopathy in published literature as yet.

2.4.2.1 UCL panel

Forming a panel of genes associated with auto-inflammatory disease not only statistically increases the chances of finding a causative mutation with all types of sequencing, but association of the clinical findings with genetic status can enable focused treatment (230, 231). Taking the latter into consideration, further research by Rowczenio *et al* (85) revealed that 18 SchS patients (patients 12-28, 32, Table 5), did not harbour disease-causing mutations within hotspots of 32 genes associated with the inflammasome and inherited autoinflammatory diseases. The complete list of the 32 gene hotspots are outlined in section 7.3 within the Appendix.

2.4.3 ASC specks

Activation of the inflammasome ultimately leads to caspase-1 activation through the action of nucleated ASC specks around 1µm in diameter. Activation of caspase-1 enables the proteolytic cleavage of the proinflammatory cytokines (IL-1β and IL-18) into their active form, as well as facilitating pyroptosis (232). ASC specks are believed to be released into the cellular milieu through the aforementioned form of regulated cell death, though its recruitment of caspase 8 and subsequent apoptotic cell death has been noted (233).

Quantitative assessment of ASC specks in the sera of 16 SchS patients prior to the commencement of IL-1 blocking therapy demonstrated significantly elevated levels of this component in comparison to 11 HC's, but similar amounts to 7 NLRP3-AID patients. Thus, acquisition of indirect evidence that SchS is associated with upregulated inflammasome activation also reinforces the notion that SchS bears a similar pathophysiology to NLRP3-AID.

In 2014, Baroja-Mazo *et al* published data showing that ASC specks found in the sera of NLRP3-AID patients were significantly high in comparison to healthy controls (214). Building upon this work, high levels of ASC specks were reported within the serum of 6 untreated NLRP3-AID patients harbouring germline or somatic *NLRP3* mutations as opposed to 3 healthy volunteers (167). In the latter paper, follow up of ASC specks during the course of a year showed a gradual decrease in those patients whose CRP remained in the reference range (i.e. below 3g/l), with previous research demonstrating values of ASC comparable to those seen in HCs during remission periods (214). Although the ASC data shown in this work do not appear to correlate with CRP levels (Figure 17), further quantification before, during and after a disease flare with the corresponding CRP levels may reveal a correlation. Should the latter notion prove correct, this would strengthen the value of ASC as a biomarker of SchS and NLRP3-AID, and potentially disease severity.

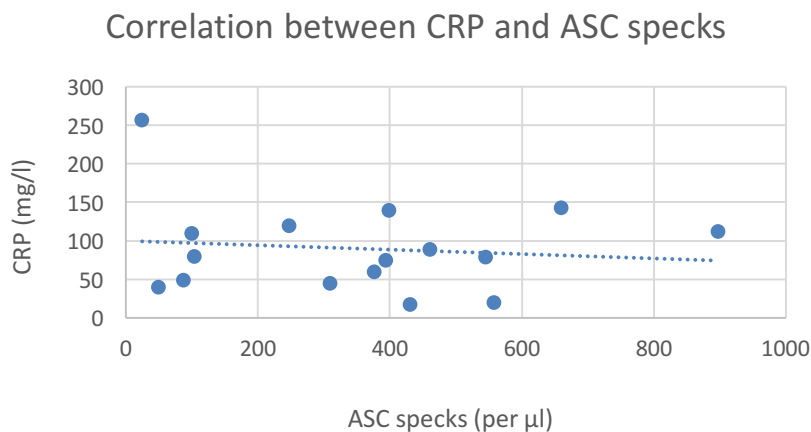


Figure 17: The absence of a correlation between CRP and ASC specks.

There are several limitations for the determination of ASC specks, thus the results shown are not conclusive, but are rather considered as another indicator of inflammasome activation. One such limitation is the absence of data pertaining to the long term stability of ASC specks in frozen sera samples. There is a likelihood that degradation occurred during the storage period and thus ASC speck levels could be higher when utilising this assay on freshly obtained sera, although this speculation remains clarification.

Elevated ASC speck levels are unlikely to be characteristic of either SchS or NLRP3-AID alone, or where inflammasome activation is integral to the pathophysiology of a given condition (i.e. Gout). Though discrimination in view of SchS/NLRP3-AID versus other autoinflammatory disorders may be possible, as both FMF and TRAPS have demonstrated very low amounts of ASC specks (214).

2.4.4 Chapter conclusions

In summary, levels of IL-6, IL-10, IL-18 and IFN- γ were significantly raised in SchS, with similar levels of IL-6 and IL-18 observed in the NLRP3-AID control group. IL-17 was significantly decreased, with levels of IL-8, IL-12p40, IL-12p70 and TNF- α comparable to HCs. Comparison of these cytokines during periods of inflammatory flares versus remission would further indicate the interplay between these that have not been reported in literature. Likewise, in view of ASC specks, comparisons of levels between flare and non-flare periods would demonstrate the levels of these inflammasome components released likely due to auto-inflammatory cell death (pyroptosis), thereby contributing to the augmented inflammatory phenotype.

Though the sequencing results of this chapter indicate the absence of *NLRP3* variants in 32 SchS patients and absence of somatic mosaicism in the *NLRP3* and *MEFV* gene within 2 SchS patients whom were subject to cellular sorting, indirect evidence of inflammasome activation was sought through the detection of extracellular ASC specks. Notably, DNA and serum samples were obtained from SchS patients prior to starting therapy with anakinra, thus the results obtained in this chapter are representative of a disease state (cytokine and ASC analyses). The novelty of the research presented in this chapter is largely attributed to the access to the relatively large cohort of SchS patient samples, given the rarity of this condition (less than 300 cases worldwide reported in entire literature).

Chapter 3 Exploring the role of Clonal Haematopoiesis in Schnitzler Syndrome

3.1 Introduction

3.1.1 The MYD88 L265P mutation

The Myeloid Differentiation Primary Response 88 gene (*MYD88*) codes for the critical adaptor protein required for the downstream signalling of the Toll-like receptors (TLRs) and IL-1 superfamily within immune cells (234). Initially described as a protein integral to terminal differentiation of myeloid cells upon IL-6 induction (235), this adaptor has since been documented to play a key role in early haematopoiesis. TLR exposure to PAMPs results in MYD88 dependent signalling (Figure 18 below), leading to proliferation of HSCs and precursor myeloid and lymphoid cells (236). Besides the latter, TLR/MYD88 is found in mesenchymal stem cells (MSCs), giving rise to several cell types including osteocytes and fibroblasts (236). MYD88 signalling directly and indirectly influences the development of both HSC and non-HSC lineages. Upon receptor stimulation by microbes or viral proteins for example, the MYD88 protein subsequently phosphorylates downstream proteins, ultimately leading to nuclear factor-kappa-B (NF- κ B) mediated transcription (Figure 18, below). Regulating the activity of multiple genes, NF- κ B controls immune responses and inflammatory reactions (237, 238).

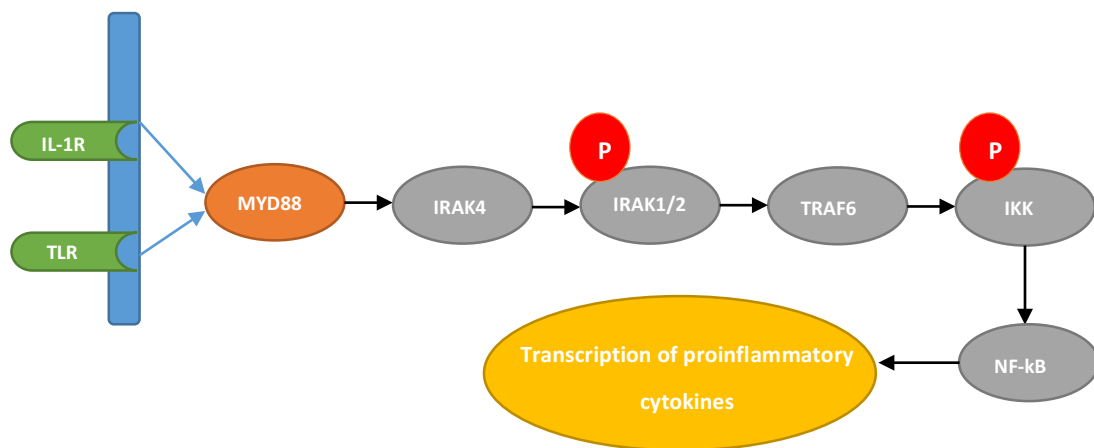


Figure 18: MYD88 dependent pathway.

Following IL-1R or TLR stimulation, MYD88 forms complexes with IRAK4, together phosphorylating IRAK1 and IRAK2 (denoted by 'P' in Figure 18). Phosphorylated IRAK1 interacts with tumour necrosis factor receptor-associated factor 6 (TRAF6) leading to IKK phosphorylation and subsequent activation of the transcription factor, NF- κ B activation (239).

Alterations in MYD88 activity are associated with both haematopoietic and non-haematopoietic conditions. For example, MYD88 was shown to be fundamental to tumour development during skin carcinogenesis (240). Conversely, genetic variants in *MYD88* are also found in a subset of patients with B-cell LPDs such as ABC-DBCL and IgM-MGUS (185). Although several mutations in *MYD88* have been identified (184), the leucine to proline substitution at position 265 of MYD88 due to a single nucleotide variation (SNV) in exon 5 (38182641 at 3p22.2) is of particular clinical significance. Situated in the Toll receptor/IL-1 interaction domain (TIR domain) (Figure 19, below), the substitution triggers the spontaneous formation of the MYD88-IRAK complex, leading to enhanced NF- κ B signalling and has shown to encourage cell survival (184, 185). Hence, this mutation is referred to as ‘gain-of-function’ (182, 241).

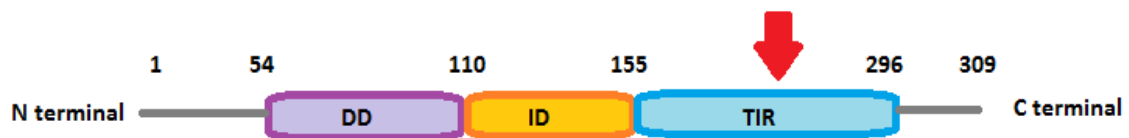


Figure 19: Schematic of the MYD88 protein.

MYD88 has a death domain (DD), an intermediary death domain (ID) and a TIR domain. The L265P variant sits within the TIR (approximate position indicated by red arrows) and affects IL-1 signalling.

3.1.2 Waldenström’s Macroglobulinaemia

As mentioned previously (Section 1.2.5), 20% of SchS patients develop Waldenström’s macroglobulinaemia (WM), a type of non-Hodgkin lymphoma characterised by IgM gammopathy due to uncontrolled proliferation of B cell progeny (182). Over 90% of WM patients carry the L265P gain-of-function mutation in *MYD88* (182, 242), though the consequence of this variant in WM is yet to be fully delineated in terms of the associated IgM paraproteinemia (182, 243). WM cell lines harbouring the L265P variant show increased activation of the NF- κ B pathway, ultimately leading to elevated production of proinflammatory cytokines such as IL-1 β (Figure 20) (244). Therefore, presence of this mutation could be explanatory of the elevated IL-1 β release witnessed in SchS patients, also rationalising why those negative for *NLRP3* mutations are successfully treated with IL-1 inhibitors. This notion has also been previously addressed in the review by de Koning *et al* in 2014, proposing that the aforementioned mutation might be present in a subset of SchS patients, hence contributing to the IL-1 β -dependent character of SchS (20).

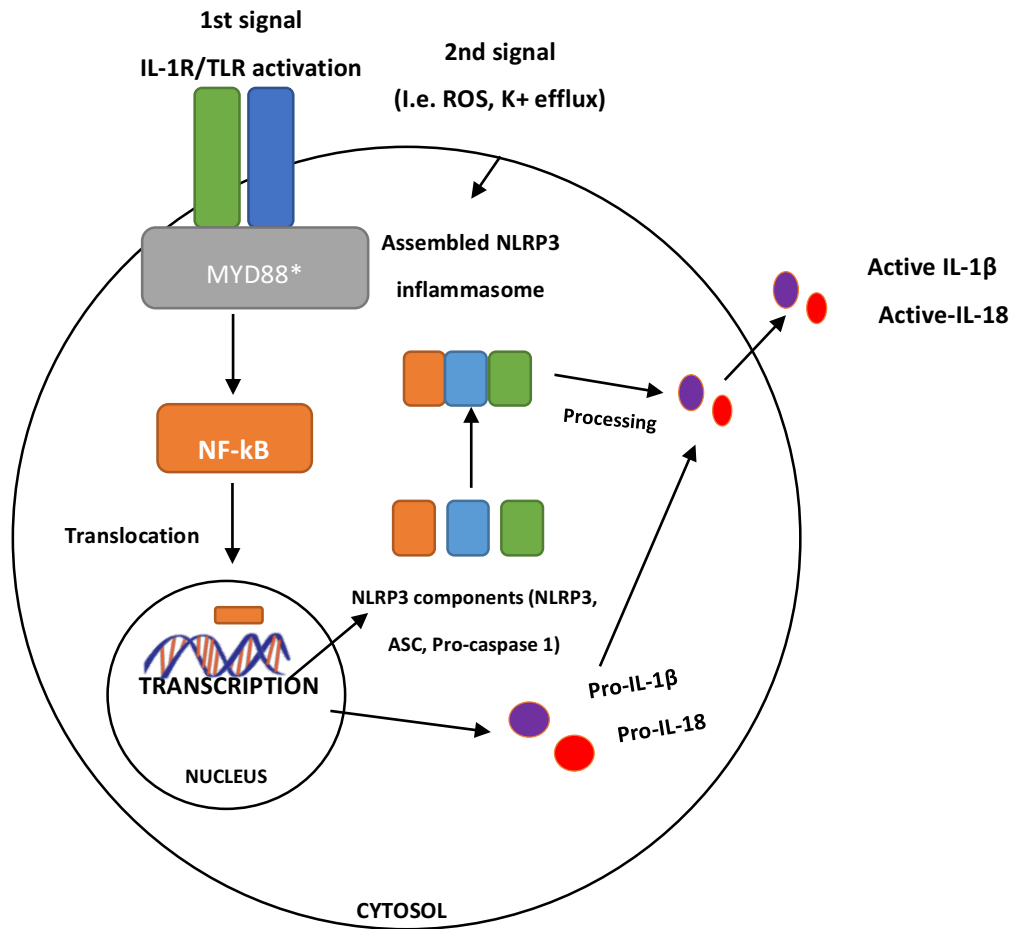


Figure 20: The link between MYD88 and NLRP3

Figure 20 illustrates the proposed mechanism by which the mutant MYD88 L265P augments the inflammatory milieu of SchS. Activation of mutant MYD88 can cause constitutive downstream signalling, resulting in the increased translocation of NF-κB to the nucleus and subsequent transcription of components of the inflammasome, as well as the inactive forms of the proinflammatory cytokines, IL-1β and IL-18. Upon signalling (requiring two hits), inflammasome assembly and subsequent activation causes release of the active forms of the aforesaid cytokines and also ASC specks.

Probing for this mutation in a non-HSC derived cell population would confirm whether this somatic mutation is confined to the HSC lineage or not. Given the varied proinflammatory and cell survival effects of this mutation in HSC derived cells, its presence in fibroblasts could augment the local inflammatory dermal manifestations of SchS.

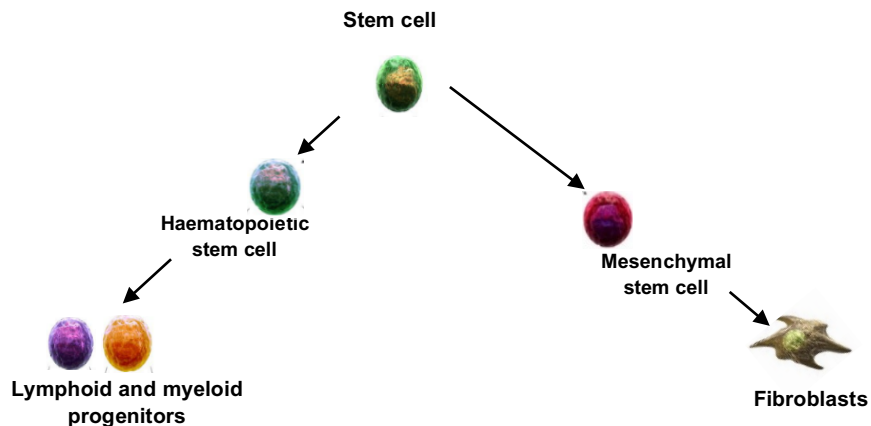


Figure 21: The development of haematopoietic and mesenchymal stem cell lineages.

DNA from lymphoid and myeloid progenitors, and fibroblasts were sequenced in the following work for the MYD88 L265P mutation in 30 SchS patients.

3.1.3 MDS and autoinflammatory disease

An altered HSC compartment is a feature of the ageing bone marrow and an increased incidence of myeloid malignancies is a common finding after the 5th decade of life (170). Analogous to autoinflammatory disease, activation of the NLRP3 inflammasome and TLR upregulation has been implicated in the pathology of myelodysplastic syndromes (MDS) (179, 180). Research has shown that MDS-related somatic mutations in *TET-2* and *U2AF1*, genes encoding for transcription and splicing factors respectively, stimulate the generation of reactive oxygen species (245). In turn, this triggers NLRP3 inflammasome formation and caspase-1 activation, as evaluated by the presence of ASC specks and consequential pyroptosis.

The preferential growth of the myeloid lineage can be substantiated by the clonal expansion of myeloid-biased HSCs, the latter largely due to the accumulation of somatic mutations within certain genes involved with growth and differentiation of these cells (246). On average, MDS tends to present in the 6th decade of life with symptoms of SchS tending to establish a decade earlier (55, 246). Therefore, it is reasonable to consider that mutations driving the MDS phenotype may also contribute to the pathological manifestations observed in SchS.

3.1.4 X inactivation

An altered HSC compartment has already been established as the leading feature of the ageing haematopoietic system, with analyses of large populations demonstrating that somatic mutations in HSCs, leading to expansion of a subset of cells (referred to as clonal haematopoiesis, CH), are commonly acquired during ageing (247). A clonally restricted haematopoietic compartment is associated with increased prevalence of myeloid or lymphoid malignancies and such malignancies can be associated with X chromosome inactivation (XCI). Though only relevant in females, such assessment of XCI has identified skewing as an age-related occurrence, particularly prominent in the myeloid compartment (248).

The X chromosome is approximately 150MB in size, harbouring over 1250 genes such as Bruton's Tyrosine Kinase, (BTK - crucial role in B-cell development) and NEMO (downstream signalling protein in the MYD88 pathway) (249). Primarily hypothesised by Mary Lyon in 1961 (250), XCI is an event occurring early in embryogenesis, where one of the two X chromosomes in each cell is subjected to specific modifications. Ultimately, this epigenetic phenomenon results in the dosage compensation of X-linked proteins between males and females through the random silencing of one X chromosome in females (249). Non-random silencing, either caused by chance or directed by genetics, can lead to the under or overrepresentation of genes. For example, tumour suppressor genes (i.e. *FOXP3*) located on the X chromosome maybe subject to under or overexpression dependent upon the XCI status (251). Hypothetically, the presence of XCI could then predispose or diminish the chance of developing malignancy.

Particular genes located on the X chromosome (i.e. *G6PD* and *HUMARA*), are highly polymorphic amongst individuals and molecular analysis techniques permit resolution of these alleles (252). Recent data from five studies have suggested employing the HUMARA assay alongside use of NGS sequencing within frequently mutated genes associated with CH, may aid the identification of those at higher risk of haematological malignancy (171, 248, 253-255). Therefore, application of the HUMARA assay to determine the XCI status is alternative way to seek further evidence that SchS shares features with haematological malignancies.

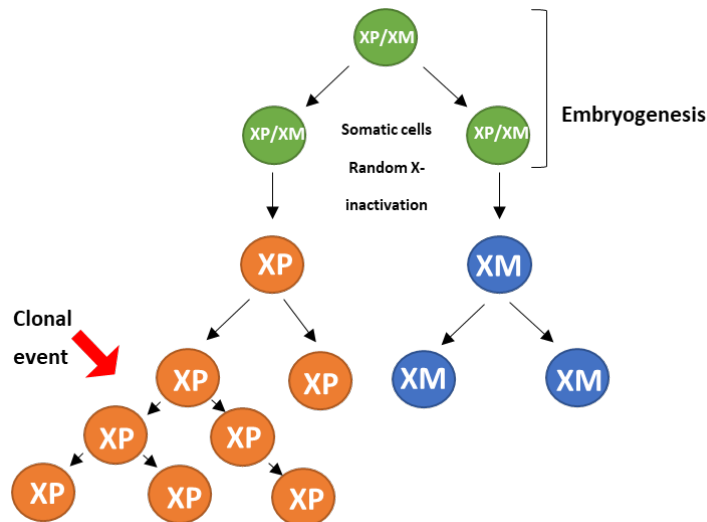


Figure 22: Schematic showing the rise of cell progeny with skewed XCI.

Normal female somatic cells comprise of one maternal (M) chromosome and one paternal (P) derived chromosome (XP/XM). During embryogenesis, one X chromosome is randomly inactivated, leaving one active X chromosome (XP or XM). The pattern of inactivation is then passed onto the cell populations derived from the originating cell. Hence, females are heterozygous for the polymorphic X chromosome.

3.1.5 The Role of CH in SchS

A handful of research papers have explored the possibility of variants within certain genes involved within SchS pathology (19, 85). Despite the identification of mutations likely to be disease contributing, no universal mutation has been found within autoinflammatory gene panels. Finding a causative gene will not only be extremely indicative of downstream SchS pathology, but would also facilitate reducing the average time of diagnosis, currently around 5 years (20, 33). Therefore, the research in this chapter largely focuses on further investigations into the genetics behind this intriguing condition in search for a common genetic component unifying all 30 SchS patients included in this work. Taking the detailed concepts (Sections 3.1.1, 3.1.3 and 3.1.4) into consideration, the hypothesis was formed that SchS patients may harbour the MYD88 L265P mutation, whilst demonstrating evidence of clonality in the form of MDS associated mutations, as a consequence of a shrinking pool of HSC's. Therefore, the aims of this chapter are as follows:

- A.** Deep sequencing of 28 MDS related genes in 30 SchS patients
- B.** Detection of the MYD88 L265P mutation via ASO-PCR in 30 SchS patients
- C.** Investigate the status of XCI to determine if this is a feature of female SchS patients

3.2 Methods

3.2.1 Primary fibroblast explant culture

Under aseptic conditions, fresh skin punch biopsies were transferred into PBS supplemented with antibiotics (penicillin/streptomycin). Using forceps, the dermis was separated from the epidermis and cut into 1mm diameter fragments using surgical blades and placed into T25 flasks. The fragments were left for 10 minutes to allow for flask adherence before addition of 5mls of DMEM supplemented with 10% fetal calf serum and antibiotics (ThermoFisher, UK). The culture was maintained at 37°C, 5% CO₂ in a humidified incubator, with media changes every 7 days. Cultured fibroblasts were then trypsinised and further lysed for the purposes of allelic variation detection (ASO PCR method, carried out by HMDS), 4 weeks after the initial culture set-up to allow for optimal fibroblast expansion for DNA extraction (Results Chapter 2, section 2.2.5).

3.2.2 Genetic investigation into *MYD88*

Genomic DNA samples from 30 SchS patients and five NLRP3-AID patients with acquired mutations (aNLRP3-AID), and fibroblast DNA samples from two SchS patients were investigated for the presence of the *MYD88* L265P mutation by allele-specific PCR (ASO-PCR). Two forward primers were utilised to discriminate between the wild-type allele (T) and the mutant allele (C), with a common reverse primer (Section 7.2.1, appendix). PCR was performed with a final volume of 28µl. The reactions were carried out for 35 cycles: denaturation at 95°C for 30 seconds, annealing at 59.5°C for 30 seconds and elongation at 72°C for 30 seconds. The final extension step was carried out at 72°C for 7 mins. The resulting PCR products plus 1µl of Midori Green Direct (Nippon Genetics, Germany), were run on a 2% agarose gel, 75 volts for 45 minutes. The gel was visualised using the GelDoc system and Quantity-One software (BioRad, USA). This technique is commonly used for the diagnostic assessment of WM and other B cell chronic LPDs across laboratories worldwide (183, 256, 257).

3.2.3 MDS sequencing

Sequencing was outsourced to the Haematological Malignancy Diagnostic Service (HMDS), a laboratory serving a population of over 6 million across the UK. For each patient, DNA was extracted as outlined in Section 2.2.5. Amplicons were designed using the D3™ Assay Design service (Fluidigm®, San Francisco, USA), with DNA libraries constructed using Fluidigm® technology. Forty-eight barcoded patient samples were pooled and subjected to 150bp paired-end sequencing. Both library preparation and sequencing were performed as per the manufacturer's instructions. Sequencing of the DNA libraries were performed on MiSeq (Illumina, UK), with an average read depth of 1500x. The panel of 28 genes, associated with myeloid malignancies, are listed within Section 7.2.2 (Appendix), alongside exon coverage and the reference sequences utilised for primer design.

3.2.4 X inactivation

The *HUMARA* assay was used to identify X-allelic skewing in female patients. The first exon of the *HUMARA* gene contains highly polymorphic 'CAG' repeats, and within 100bp from the start of this gene and the CAG repeats lies a site of differential methylation between the inactive and active X chromosome. Within this methylation area are two restriction sites for the methylation sensitive endonucleases (258). The enzyme *HpaII* is one such restriction endonuclease, cleaving unmethylated, active X alleles. Therefore, within this assay, a PCR product is only generated from the inactive X chromosome. In a mixed population of cells, the maternal and paternal X inactivated alleles, will both be amplified, thus two peaks are visualised on gene scanning software. Whereas for those cells arising from a single, common progenitor cell, only the maternal or paternal X inactivated allele PCR product will generated, giving rise to a single peak (258). Whilst the aforementioned is applicable to females, it should be noted that performance of this assay on a male derived sample will yield no peaks due to the existence of only one, active X chromosome.

The techniques stated below used to determine X inactivation were originally based on the methodologies published by Allen *et al* in 1992 (259). However, these were modified to enhance the quality of results obtained. Genomic DNA was utilised for this part of the study from 14 female SchS patients and 3 female aNLRP3-AID patients, at a starting concentration of 50ng. One male control and one female control were also included in the assay.

3.2.4.1 Restriction enzyme digestion

Reaction A (undigested DNA), and reaction B (restriction enzyme digested DNA) were prepared from each subject according to the following table (Table 6). The reactions were then subject to incubation in a thermocycler at for 2 hours to destroy the unmethylated HUMARA allele.

REACTION A	REACTION B
50ng genomic DNA	50ng genomic DNA
2µl of Buffer a	2µl of Buffer A
0.2µl acetylated bsa	0.2µl acetylated BSA
	0.5µl HpaII restriction enzyme digestion

Table 6: The composition of the restriction enzyme digestion.

Table 6 describes the compositions of reactions A and B, with a final volume adjusted to 20µL, using nuclease free water.

3.2.4.2 PCR amplification of the HUMARA gene

The AccuPrime™ Taq DNA Polymerase High Fidelity Kit (Invitrogen, Loughborough, UK), was used for the primary PCR amplification of the HUMARA gene. The forward primer was labelled with fluorescein amidite (FAM), in order for detection on the genetic analyser.

Undigested or digested DNA	5µl
10X AccuPrime™ PCR Buffer II	5µl
Molecular-grade water	37.8µl
10 µmol/l fluorescein amidite (FAM)-labeled forward primer FAM 5' TCC AGA ATC TGT TCC AGA GCG TGC 3'	1µl
10 µmol/l reverse primer 5' GCT GTG AAG GTT GCT GTT CCT CAT 3'	1µl

Table 7: Composition of reagents required for PCR amplification.

Using the stated composition, the following thermocycling conditions for AR gene amplification were used: denaturation at 94°C, annealing at 56°C and extension at 68°C for a total of 34 cycles.

3.2.4.3 Capillary reaction

Succeeding the previous steps, reactions were diluted in molecular-grade water, at a 1:50 ratio. Plated out in a 96 well plate, 8.5µl of Hi-Di formamide and 0.5µl of GeneScan™ 600 LIZ® dye Size Standard v2.0 (Life Technologies, UK), was added to 1µl of the diluted reaction. These PCR products were further subject to a denaturation cycle for 5 minutes at 95°C before subject to testing on the ABI 3100 DNA analyser (Applied Biosystems, UK).

3.2.4.4 Determination of X-skewing ratios

The resulting FSA files generated by the DNA analyser in the previous step were subject to evaluation using GeneMapper software version 2.0). Although the exact sizes (base pairs) of the peaks differ between individuals, two peaks were sought to appear close together (around a 20bp proximity). Assessing area under the curve (AUC) from both the HpaII digested and undigested reactions, facilitated the generation of ratios of X-inactivation. (A) Undigested reaction - left peak; (B) undigested reaction - right peak; (C) digested reaction - left peak; (D) digested reaction - right peak. XCI was thus determined by the following calculation: $(C/A)/((C/A)+(D/B))*100\%$. The values for the HpaII digested samples were normalised by assessing values of the undigested samples, thus accounting for preferential allele amplification (260). Percentages equal to or above 80% were deemed indicative of skewing.

3.3 Results

3.3.1 The *MYD88* L265P mutation

Since the somatic *MYD88* L265P mutation is present in over 90% WM patients (182) and in over 50% of IgM-MGUS patients (261), the following work explored the possibility that this mutation was present within gDNA of 30 SchS patients and in the fibroblasts of two patients. Within the PCR setup, a mixture of the wild-type (WT) primer binding to the WT allele, alongside a mutant primer, binding to the mutant allele produces two different sized bands. This *MYD88* mutation can be detected in DNA dilutions down to a mutant clone size of 0.1-0.5% (256, 262).

3.3.1.1 ASO-PCR

As a preliminary screening, the aim of undertaking ASO-PCR assay was to determine if the L265P mutation within *MYD88* was present within 30 patients with SchS. This assay was further carried out in five aNLRP3-AID patients.

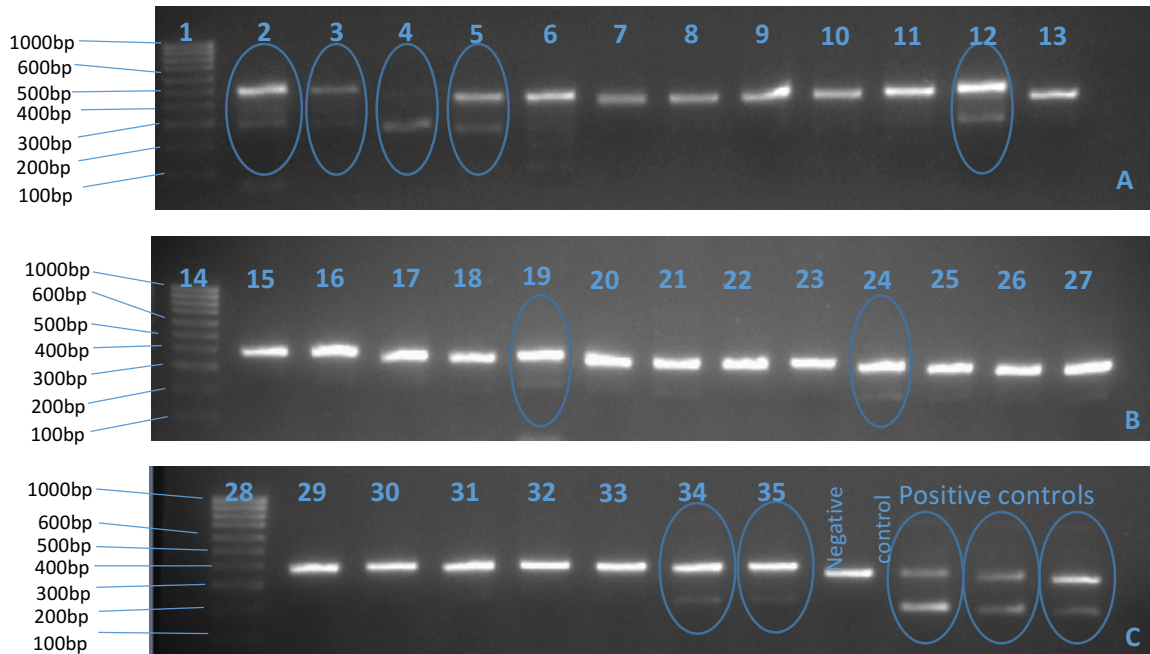


Figure 23: ASO-PCR results of 30 SchS patients.

Wells 1, 14 and 28 are 100bp ladders, wells 2-13; 15-27 and 29-35 correspond to SchS patients (results summarised in Table 9). The wild type allele – normal 400bp product whereas the mutant product has a size of around 200bp. Negative controls and positive controls were included (labelled within panel C). NB: 13 and 29 are repeated; 14 and 23 are repeated.

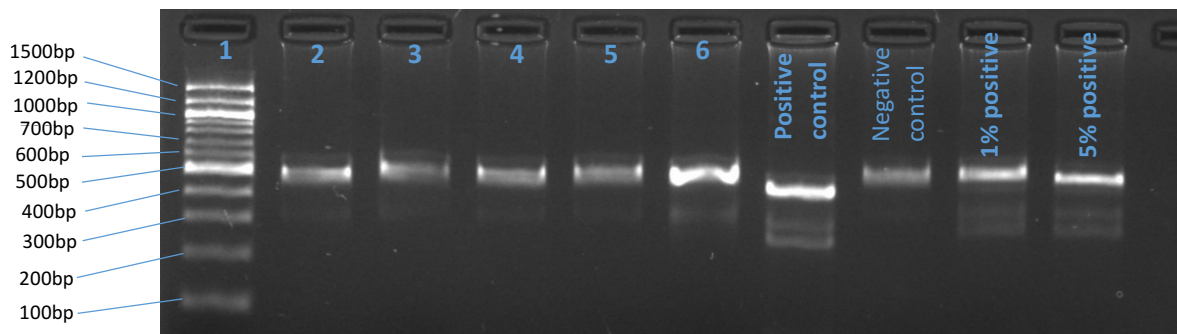


Figure 24: ASO PCR results for the aNLRP3-AID patients.

Wells 2-6 – negative for the *MYD88* L265P mutation. Lane 1: 100bp ladder, 2-6 aNLRP3-AID samples, positive & negative controls were also included in the experimental setup.

3.3.2 Primary fibroblast explant culture & ASO PCR

The aim of obtaining skin biopsies and culturing fibroblasts was to obtain DNA and carry out ASO-PCR in order to detect the *MYD88* mutant allele (C).

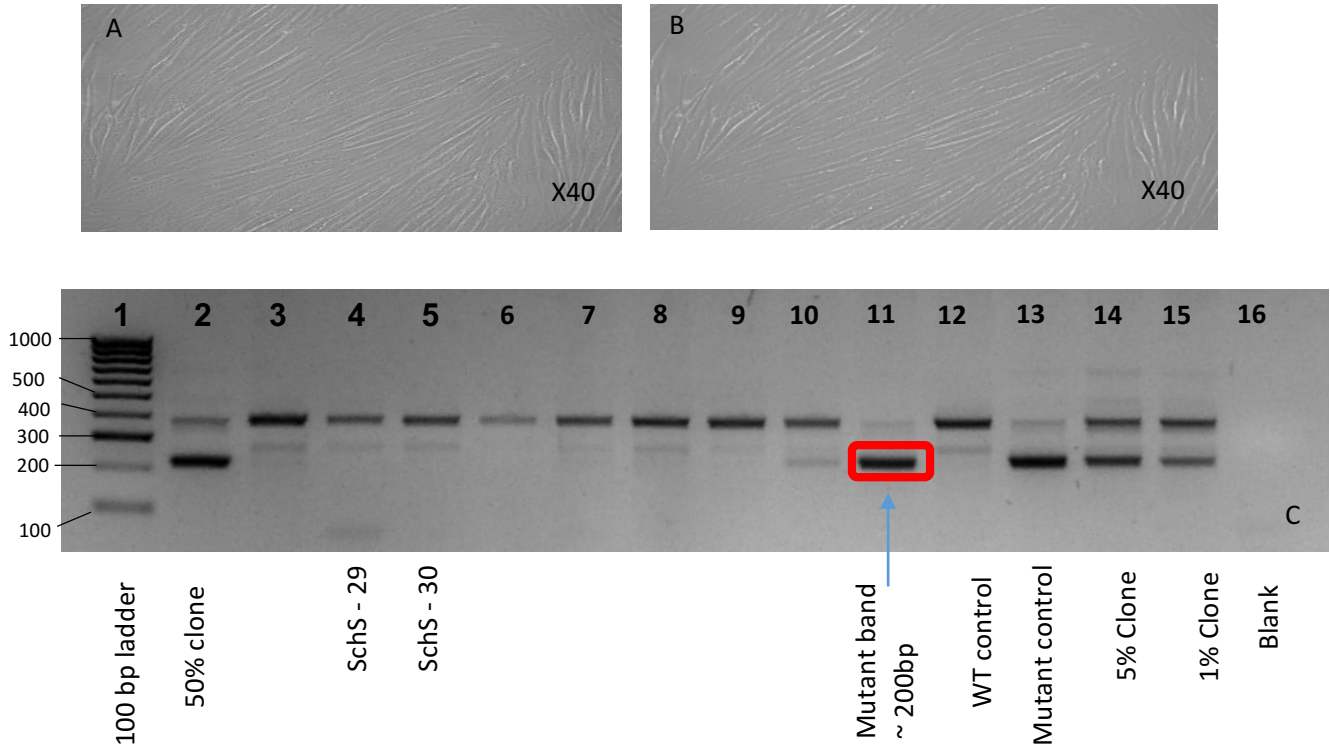


Figure 25: Primary fibroblast culture and ASO-PCR results.

Primary fibroblasts were cultured for SchS patients 29 and 30 in this study, followed by ASO PCR for *MYD88* L265P mutant detection. (A and B) Skin biopsies (1mm diameter) were cultured for 4 weeks using DMEM prior to DNA extraction and ASO PCR. Images are shown at x40 magnification. The two SchS patients showed absence of the mutant PCR band (~200bp) but presence of the normal band (~400bp). Lanes 3, 6-11 correspond to patients not included in this study. The results shown in panel C were provided by HMDS.

Using the *MYD88* reference sequence NM_001172567.1, employing the ASO-PCR technique permitted identification of the SNV at chromosomal location 3:38141150. The allelic change from T to C results in the leucine to proline substitution at position 265 of *MYD88*, producing a 'gain-of-function' protein. Significantly, this variant was detected in nine out of the 30 SchS patients included in this work, a novel genetic finding with regards to the condition.

No aNLRP3-AID patients harboured the T>C change, eliminating the prospect of *MYD88* bearing influence on this *NLRP3* mediated disease. Though this SNV was present in subset of SchS patients, the former outcome further discriminates SchS as a separate entity from aNLRP3-AID. Despite several shared features such as late disease onset and inflammasome involvement (Results Chapter 2) between the diseases, absence of this mutation in aNLRP3-AID reinforces that there is an alternative genetic component in SchS. Absence of the mutant band for the alternative germ layer derived fibroblasts demonstrates that the somatic pathogenic variant was generated after commitment of stem cells to the haematopoietic lineage.

3.3.3 HMDS Sequencing panel

The average age of symptom onset for the sequenced set of patients is 56.2 years, with SchS patients averaging at 55.2 years and aNLRP3-AID patients averaging at 61 years. The male-to-female ratio of the entire 36 patients was 1:1.5, identical for the SchS cohort. The aNLRP3-AID cohort had a 1:1 male-to-female ratio.

Functional Pathway	Gene
Chromatin Modification	<i>ASXL1, EZH2</i>
Cohesin Complex	<i>STAG2</i>
DNA Methylation	<i>DNMT3A, IDH1, IDH2, TET2</i>
Signalling	<i>CBL, cKIT, CSF3R, FLT3, JAK2, KRAS, MPL, NRAS, STAT3</i>
Splicing	<i>SF3B1, SRSF2, U2AF1, ZRSR2</i>
Transcription Factors	<i>BCOR, NPM1, RUNX1, TP53, WT1</i>
Other	<i>CALR, SETBP1, RHOA</i>

Table 8: MDS sequencing panel.

Genes and their corresponding functional pathways are shown in Table 8. Associated with the initiation and development of MDS, sequencing of 28 frequently mutated genes was carried out at the HMDS facility, using PB derived DNA from 30 SchS patients and 6 aNLRP3-AID patients. The latter cohort were included as disease controls, since they carry somatic mutations in *NLRP3*. The panel (Table 8) comprised of epigenetic modifiers, transcription factors, signalling and other genes known to play a role in MDS progression. The panel was designed by HMDS to detect somatic mutations and is consequently not suitable for inherited variants.

Solely one male SchS patient (20) had a nonsense mutation in the cohesion complex *STAG2* (c.559C>T p.Gln187), with a low variant allele fraction (VAF) of 0.081. This male patient was negative for both the presence of *NLRP3* variants and the *MYD88* L265P mutation, however BM histology examination showed LPL. Of the aNLRP3-AID cases, however, one female patient (3) had three pathogenic variants in 2 genes pertaining to DNA methylation: one mutation in *DNMT3-A* (c.2645G>A p.Arg882His), with two mutations in *TET-2* (c.4585C>T p.Gln1529; p.Gln1699*), all with a significant VAF (0.407, 0.388 and 0.402 respectively). This patient doesn't harbour the *MYD88* mutation, though bears the somatic A352T *NLRP3* mutation. Both of the aforementioned patients demonstrate a complete symptomatic response to IL-1 inhibition, thus these discovered mutations are more likely to be age-related findings.

3.3.4 XCI patterns at the *HUMARA* locus

The average age of symptom onset for the SchS female cohort (n=13) subject to the HUMARA assay was 53.7 years with a range between 37.9 years to 72.5 years. The aNLRP3-AID female cohort (n=3) included in the HUMARA assay had an average age of disease onset of 58.6 years ranging between 47 years to 67 years. Building upon the notion that MDS mutations may be a contributor to SchS disease manifestations, examination of the *HUMARA* gene to explore the possibility of XCI in 13 female SchS patients.

3.3.4.1 Male control

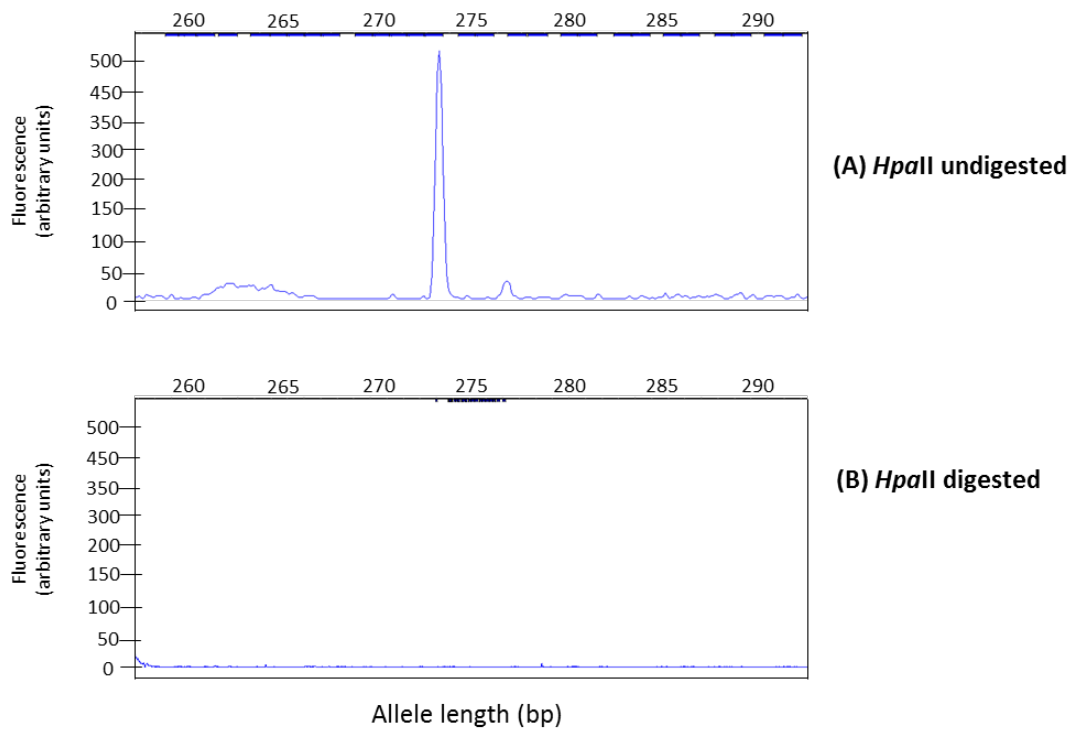


Figure 26: Chromatogram showing the male DNA control.

Figure 26 (A and B) are chromatograms showing the results for male control DNA probed with the HUMARA assay. (A) – Prior to digestion, the allelic peak at 274bp shown corresponds to the active X chromosome. (B) – Following digestion, the same allele is absent, indicating the active status of the male's one X chromosome. The absence of the peak in 23B also strengthens the data by excluding assay bias resultant of incomplete enzymatic digestion by *HpaII*.

3.3.4.2 Female control

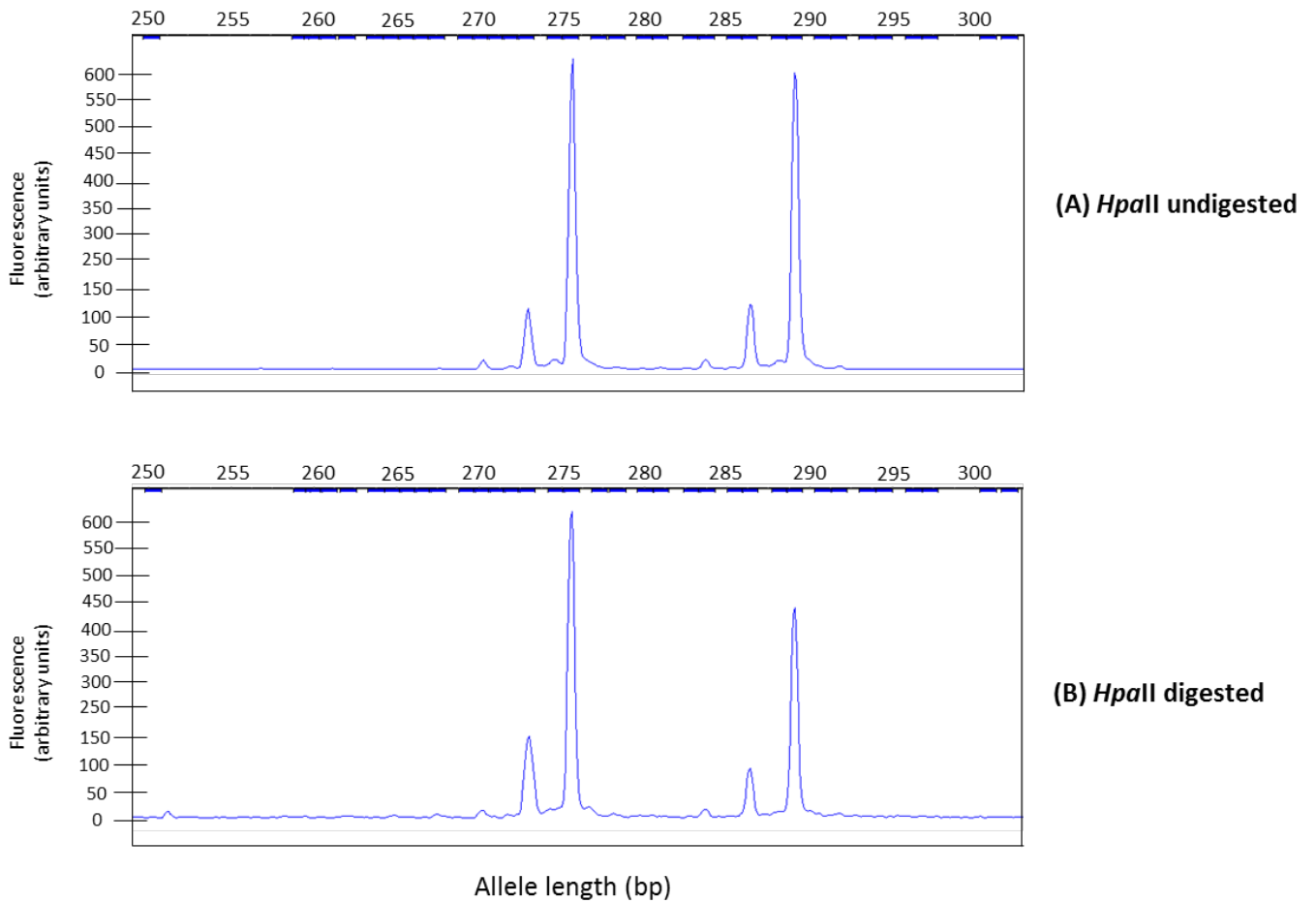


Figure 27: Chromatogram showing the healthy female DNA control.

Figure 27 A and B show chromatograms of the female healthy control probed for XCI.

Allelic peaks at 275bp and 290bp are present in both the undigested (A) and digested DNA samples (B), indicating the X chromosome's normal, active status.

NB: The stutter peaks present in this figure and the following two figures are likely to have arisen because of polymerase errors. Evaluation and subsequent calculations were based on the AUC of the major peak generated for each allele.

3.3.4.3 SchS - 9

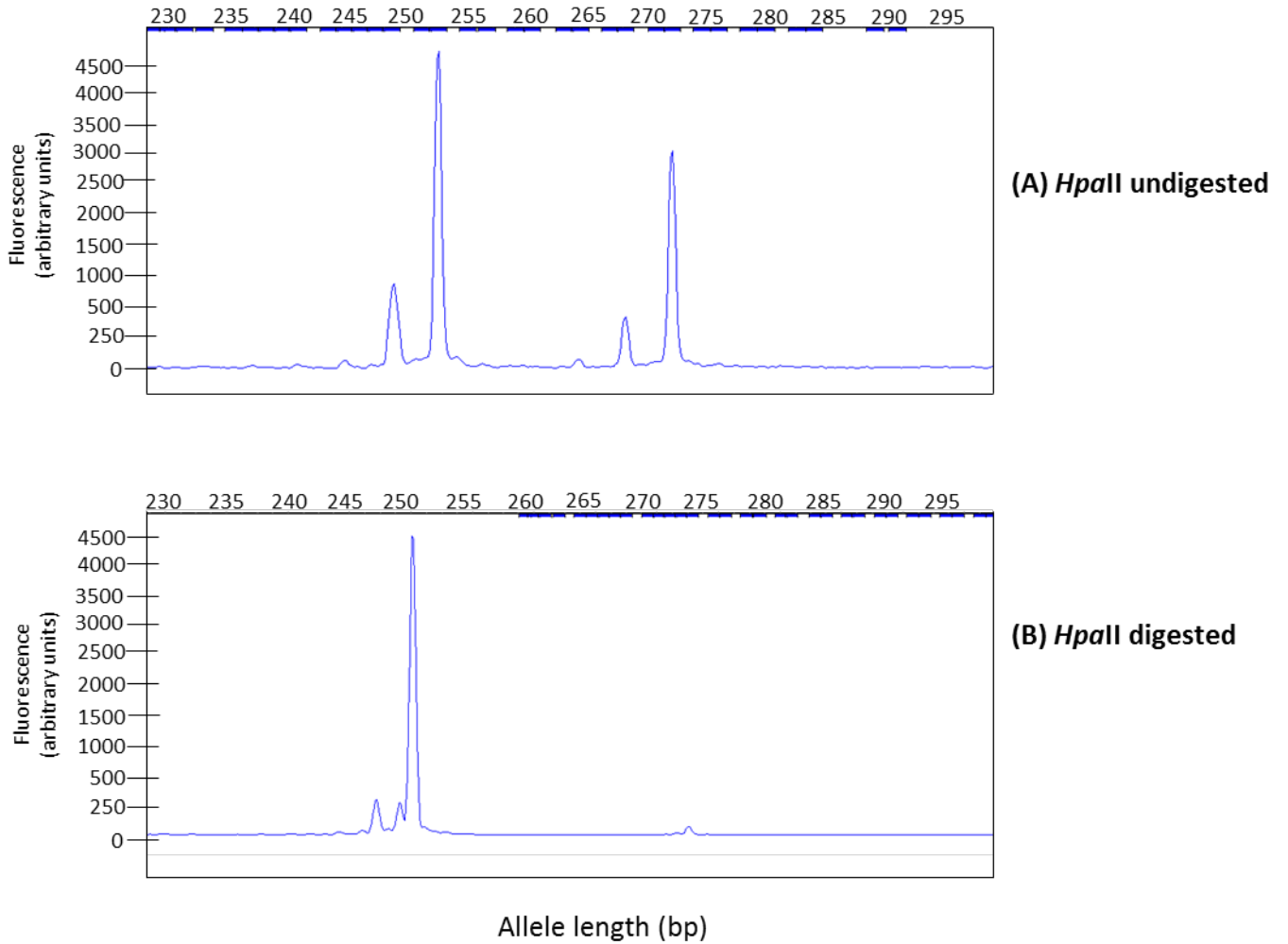


Figure 28: Chromatogram showing skewing of SchS patient 9.

Figure 28 A and B represent the chromatograms portraying the skewed XCI pattern in SchS female patient 9. (A) – The undigested DNA sample showing two peaks: 253bp and 271bp. (B) – The digested sample showing only one peak at 251bp. This is indicative of skewing, as the absence of the allelic peak at 271bp suggests use of only one of the HUMARA alleles and therefore preferential use of one of the two X chromosomes present in this female.

3.3.4.4 Acquired NLRP3-AID patient 3

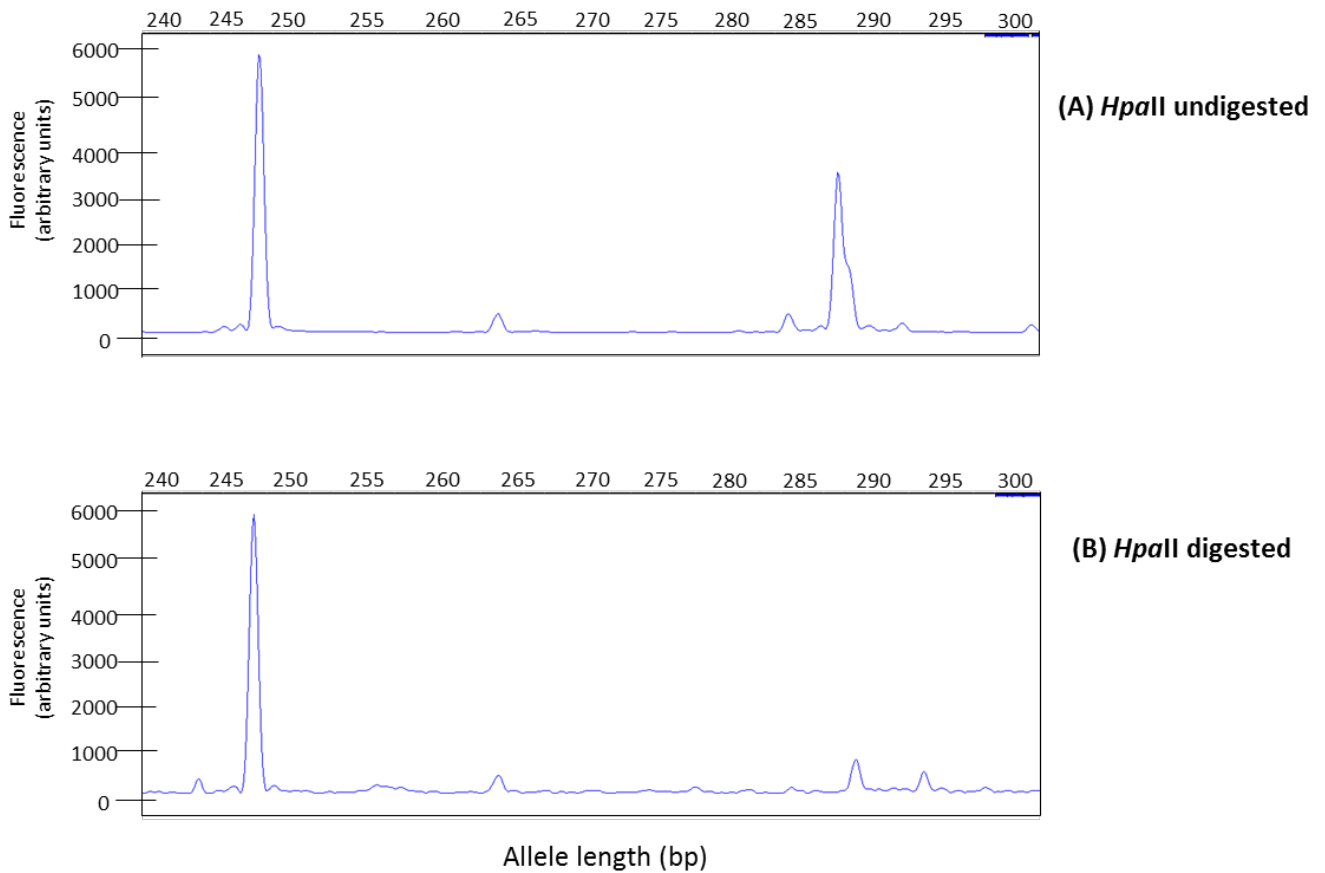


Figure 29: Chromatogram showing skewing of acquired NLRP3-AID patient 3.

Figure 29 A and B are chromatograms portraying the XCI pattern in aNLRP3-AID female patient 3. (A) – The undigested DNA sample shows two major peaks: 247bp and 286bp. (B) – The digested sample only appears to have one major peak at 247bp. The absence of the allelic peak in B, corresponding to the peak generated in A at 286bp indicates a non-random pattern of activation as one X-chromosome appears to be preferentially used in this sample.

XCI only occurred in one SchS patient and one aNLRP3-AID patient, suggestive that this event is not common to all female patients and therefore cannot be regarded as a marker of disease within this cohort.

SchS-9 had a skewed XCI. Despite age of disease onset being 60 years, not classed as elderly. May correspond to the low level myeloma already. Had a good response to IL-1 inhibition. Within the aNLRP3-AID cohort, previous findings were further confirmed given that allelic skewing was found in the patient with 3 pathogenic mutations; two of which were in *TET-2*.

Patient number	Sex	Age at symptom onset	Response to IL-1 inhibition	Bone marrow histology	Genes/variants identified by MDS panel Prediction/VAF	MYD88 L265P?	NLRP3 mutational status	X inactivation result (if applicable)
1	male	62.0	complete	No overt LPL		Yes		-
2	female	43.5	good	No overt LPL		Yes		random
3	male	51.5	good	No overt LPL		Yes		-
4	male	67.0	complete	No overt LPL		Yes		-
5	female	54.5	good	No overt LPL		No		random
6	female	72.5	complete	No overt LPL		No		random
7	female	55.5	complete	No overt LPL		No		random
8	female	53.0	complete	No overt LPL		No		random
9	female	60.0	good	Low-grade myeloma		No		non-random - skewed (80%)
10	female	72.5	good	No overt LPL		No	Q703K*	-
11	male	62.0	good	No overt LPL		Yes		-
12	male	36.8	Partial	No overt LPL		No		-
13	female	37.9	complete	No overt LPL		No		random
14	male	43.9	complete	15% BM plasma cell		No		-
15	female	44.8	complete	No overt LPL		No		random
16	female	49.6	complete	not done		No		random
17	male	49.9	complete	No overt LPL		No		-
18	male	52.8	complete	No overt LPL		No		-
19	male	57.1	complete	LPL		Yes	V198M*	-
20	male	58.1	complete	LPL	STAG-2 c.559C>T p.Gln187* Predicted: pathogenic VAF: 0.081	No		-
21	male	59.6	Died before treatment	No overt LPL		No		-
22	male	61.7	complete	No overt LPL		No		-
23	female	60.7	complete	low grade marginal zone lymphoma		No		random
24	female	68.4	complete	No overt LPL		No		random
25	male	78.9	complete	No overt LPL		Yes		-
26	female	39.7	complete	No overt LPL		No		random
27	male	40.7	complete	No overt LPL		No		-
28	male	61.2	complete	No overt LPL		No		-
29	male	43.6	complete	MGUS		Yes		-
30	female	59.0	complete	Marginal Zone Lymphoma		Yes		random
aNLRP3 - 1	male	48	complete	N/A		No	E567K	-
aNLRP3 - 2	male	79	complete	N/A		No	G569V	-
aNLRP3 - 3	female	67	complete	N/A	-DNMT3-A c.2645G>A p.Arg882His Predicted: pathogenic VAF: 0.407 -TET-2 c.4585C>T p.Gln1529* Predicted: pathogenic VAF:0.388 -TET-2 c.5095C>T p.Gln1699* Predicted: pathogenic VAF: 0.402	No	A352T	non-random – skewed (80%)
aNLRP3 - 4	male	63	complete	N/A		No	Y563C	-
aNLRP3– 5	female	62	complete	N/A		No	Y563C	random
aNLRP3 – 6	female	47	complete	N/A		N/D	Y536C	random

Table 9: Summary of Results

Table 9 is the summary of results found in this chapter showing the clinical and laboratory findings of 30 SchS patients and 6 aNLRP3-AID patients

LPL = lymphoproliferative lymphoma IF: immunofluorescence

*common non-pathogenic *NLRP3* variants unlikely to be disease causative and have shown to be present in healthy individuals

3.4 Discussion

The purpose of the work undertaken in this chapter was to investigate the presence of CH and initiating mutations within candidate genes of 30 SchS patients. Screening of the somatic L265P mutation within MYD88 (T > C (3:38182641) in exon 5) using ASO-PCR methodology was followed by assessment of the mutational status of 28 genes associated with MDS. Accompanying these genetic results, the functional HUMARA assay was employed to evaluate XCI within female subjects.

To summarise, the main findings in this chapter were:

- v. The somatic MYD88 L265P mutation was present within the gDNA of 9 patients with SchS, but not within the fibroblasts of two SchS patients
- vi. One SchS patient harboured a pathogenic *STAG-2* mutation
- vii. One aNLRP3-AID patient demonstrated three pathogenic mutations, one in *DNMT3-A* and two in *TET-2*
- viii. Skewed XCI was found in one female SchS patient

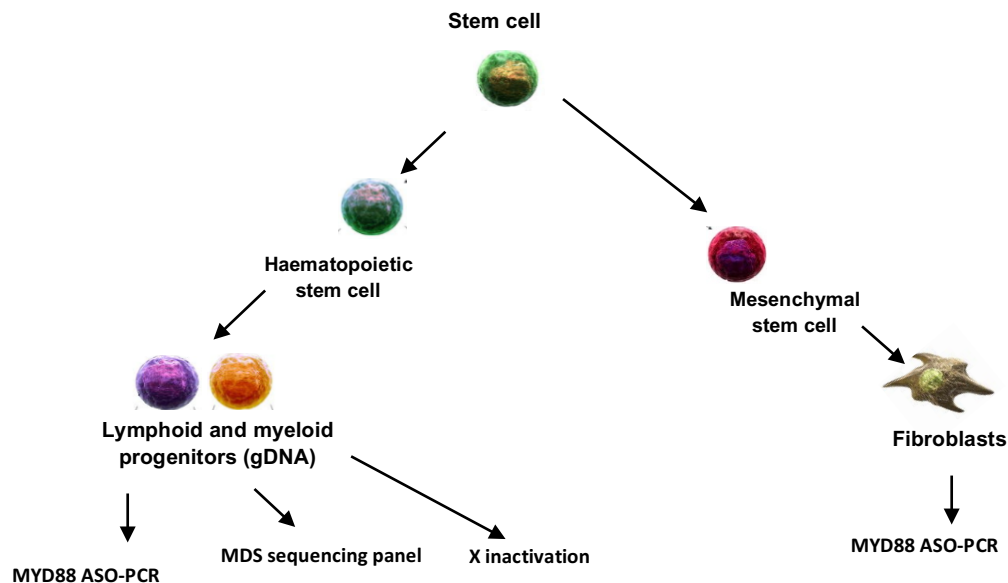


Figure 30: Schematic of the research undertaken in Chapter 3.

MYD88 ASO-PCR was carried out for the gDNA from 30 SchS patients, with material from a further two patients also subject to this technique using DNA from their cultured fibroblasts. Genomic DNA was also the starting material for assessment of the panel of genes associated with myeloid malignancies (HMDS). Lastly, gDNA from 12 female SchS patients was used to assess the status of X inactivation.

3.4.1 MYD88 L265P

The L265P variant was detected in the PB derived DNA in nine out of 30 SchS patients by ASO-PCR methodology as described in 3.2.2. In comparison to Sanger sequencing, ASO-PCR represents a highly sensitive technique, with the ability to detect the mutant allele down to 0.1-0.5% (256, 262). The original paper indicating that MYD88 L265P was a recurring somatic mutation in WM patients by Treon *et al* used Sanger sequencing to determine that mutation was present in 90% of WM patients and in 10% of IgM-MGUS patients (182). A year later, Varettoni *et al* developed an ASO-PCR assay to detect the mutant allele, demonstrating that 100% of their WM cohort harboured the mutation in question, alongside 47% of IgM-MGUS patients also showing the mutation (183). Not only did the latter study further confirm that this mutation is a hallmark of WM irrespective of their symptomatic features, but highlighted the efficacy of using such an assay for a large cohort. Therefore, utilisation of this method was a reliable approach to screen for this mutation within the gDNA of 30 SchS patients, fibroblast derived DNA from two SchS patients and five aNLRP3-AID patients in this work.

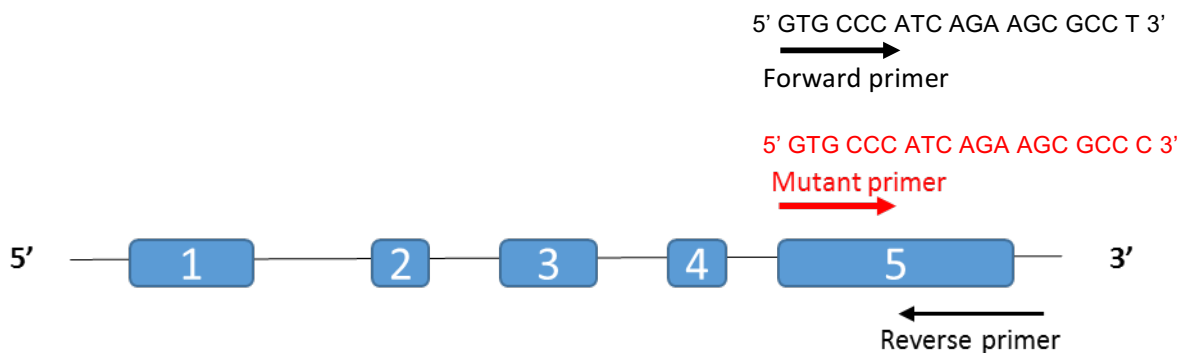


Figure 31: Schematic of the MYD88 ASO-PCR primer coverage.

MYD88 is comprised of 5 exons, with the T > C variation occurring in exon 5 at chromosome position 3:38182641. Both the forward primer and mutant primer anneal at the beginning of exon 5. The reverse primer located in the intronic region after exon 5. The mutant primer binds to the DNA and amplifies a product at 220bp if the T>C variant is present. Otherwise, a 400bp product is amplified and indicates the absence of this mutation.

3.4.1.1 SchS and MYD88 L265P

The frequency of SchS patients who develop WM (around 20%) is in line with those SchS patients positive for the MYD88 L265P variant (9/30) as described in this work. Although WM is not associated with inflammatory complications as those seen in SchS, establishing that a third of SchS patients bear this mutation could partially explain the clinical phenotype of systemic inflammation and NUD, with this novel finding in parallel with the frequency of those

SchS patients who go on to develop B cell malignancy. Certainly, in cases where SchS is speculated, screening of this mutation could corroborate a diagnosis. The absence of this mutation in cultured fibroblasts from patients 29 and 30, who have the mutation in their gDNA, indicates that this mutation must have occurred after the stem cell being committed to a HSC (Figure 30).

The MYD88 adaptor protein plays a pivotal role in innate immune signalling and is an activating component of NLRP3 (263). Several studies have established the requirement for two signals for NLRP3 inflammasome activation (210, 237, 264). The first signal requires microbial ligand or TLR activation, thereby activating the NF- κ B pathway resulting in the transcription and translation of inflammasome components. The second signal instigates assembly of the inflammasome, requiring DAMPs (Damage Associated Molecular Patterns) or PAMPs stimulation (265) (Figure 20). Conformational dynamics demonstrated that the TIR binding domain of MYD88 can exhibit two conformational states, one supporting homo-oligomerisation, with the other favouring hetero-oligomerisation (266). The leucine to proline substitution within MYD88 stabilises the homo-dimer interface of the MYD88-TIR domain (40), leading to spontaneous and increased homo-oligomerisation. The latter is imperative for protein activation downstream of MYD88. Those nine SchS patients harbouring the mutation in question are not likely to require TLR activation to prompt NF- κ B transcription, given that the 'priming' signal is spontaneously delivered by the mutant MYD88 protein. Thus in the context of SchS, one signal provided by the PAMP or DAMP would be sufficient to provoke NLRP3 inflammasome assembly. One way to test this hypothesis is to stimulate SchS derived PBMCs with LPS as the only signal, followed by probing mRNA transcripts of NLRP3 inflammasome components, IL-1 β and IL-18, via reverse-transcriptase PCR.

The negative status of the other 21 SchS patients included in this study could be explained by two reasons. Firstly, sequencing of gDNA derived from these patients presents the possibility of missing potential populations of cells bearing this somatic mutation. For example, those WM patients who were MYD88 L265P negative in the research by Petrikos *et al* had significantly low levels of lymphoplasmocytic cell infiltration in the bone marrow in comparison to mutation positive patients (198). The latter finding also raises the question as to whether this mutation is specific to the lymphoid or myeloid derived lineages. Nevertheless, probing bone-marrow derived DNA in place of gDNA would then categorically exclude these patients from harbouring the mutation. Secondly, it is possible that the remaining SchS patients harbour other variants in MYD88. Recent research has implicated a de-novo germline *MYD88* mutation as the cause of severe arthritis, intermittent fever and rash, of which the latter symptoms are frequent in SchS and other autoinflammatory conditions (267). Despite the difference in other clinical manifestations in the described patient, these findings emphasise the pathological effects *MYD88* variants can have. Likewise, Ngo *et al* revealed multiple *MYD88* mutations within the same gain-of-function domain as the T>C variant, in a cohort of

ABC subtyped DLBCL patients. Mirroring SchS, around 20%-30% of DLBCL patients also harbour the L265P somatic mutation. Hence, it is plausible to suspect the prevalence of other *MYD88* variants irrespective of the *MYD88* L265P status in SchS patients.

3.4.1.2 MYD88 L265P and disease burden

Presence of the *MYD88* L265P mutation in IgM-MGUS patients has been shown to correlate with a higher disease burden, with an increased risk to WM progression (183). Two papers also demonstrated the increased disease burden of those with WM is correlated with the presence of L265P as compared to those 10% of WM patients without the mutation (182, 242). Interestingly, IgM levels were found to be 'within range' and statistically 'insignificant' in the paper by Treon *et al.* However, the paper by Patkar *et al.*, found that those patients harbouring the L265P mutation with monoclonal gammopathy had a higher severity score on the International Prognostic Scoring System for WM. The nine patients harbouring the activating mutation in this study exhibit slightly higher levels of IgM in comparison to mutation negative SchS patients (7.5g/l versus 6g/l respectively). Nevertheless, deriving conclusions pertaining to presence of the mutation and increased monoclonal component levels in SchS patients is more difficult given the disparity between the average IgM values for the two groups. Varettoni *et al* further identified a subset of IgM-MGUS patients harbouring *MYD88* L265P alongside IgM levels above 15g/l, were at higher risk of progression to malignancy (261). Only SchS patient 2 had an IgM level above the aforementioned level in IgM-MGUS (17g/l), with bone marrow histology exhibiting no overt LPL. This female patient did not demonstrate a skewed XCI, nor did she have any detected *NLRP3* mutations.

Notably, the examined patients by Treon and colleagues had other mutations in genes such as *CXCR4*, likely to be factors contributing to these disease manifestations (182). Only SchS patient 19 demonstrated evidence of a non-pathogenic *NLRP3* variant (V198M), whereas SchS patient 20, who harboured the pathogenic *STAG2* variant did not harbour *MYD88* L265P.

In 2002, there was a report of two IgM multiple myeloma patients with neoplastic cells secreting elevated levels of IL-1 β , though this was not replicated in WM patients with the latter's IL-1 β levels as normal (268). Given the good (n=3) and complete (n=6) response to IL-1 inhibition in this mutation positive SchS subset, whether supposed 'neoplastic' cells are releasing excessive IL-1 β , or it is the consequence of an exacerbated innate inflammatory response would require further exploration. Cell sorting into myeloid and lymphoid lineages to detect IL-1 upregulation would be one way to address the latter proposal.

3.4.2 MDS sequencing panel

Genetic exploration into *NLRP3* and *MYD88* revealed that these genes are not disease causative within the patients probed in this thesis. Recent findings have implicated the NLRP3 inflammasome as ‘a driver of the MDS phenotype’ (179) and given the several indications that the latter inflammasome plays a key role in SchS, sequencing against a panel of MDS related genes was the next plausible step in search for a common causative or susceptibility marker. Significantly high levels of IL-18 and ASC specks alongside the successful remission of patients using IL-1 inhibition (Results Chapter 2), also substantiated the notion of NLRP3 involvement in this disease. In the context of SchS, bearing mutations in MDS associated genes would influence the shift to a proinflammatory milieu, with the potential to development of additional SAID-associated somatic mutations. However, gDNA sequencing of 30 SchS and six aNLRP3-AID patients against a 28 gene panel intended for the detection of somatic variants within MDS suspected patients did not detect a common genetic basis.

3.4.2.1 MDS variants

HSCs develop somatic mutations throughout their existence, a large proportion of which are non-pathogenic passengers without functional consequences (247). Age-related haematopoietic clones are a frequent occurrence in individuals after 55 years of age (269), with the median age of patients diagnosed with SchS in the cohort presented in this chapter at 56.3 years. The median ages of patients diagnosed with AML and myelodysplasia, 67 and 76 respectively (270, 271). Only SchS patient 20 presented with a pathogenic mutation in *STAG2*, thus, concluding that this is an incidental finding unrelated to the general pathology of SchS is probable. Interestingly, a 2014 study showed that MDS patients with *STAG2* mutations were correlated with poor survival (272), however the variant reported in this work (c.559C>T p.Gln187*) has not been reported in literature. There are eight subunits making up the protein cohesin, defined as a ‘ring-like structure that binds chromosomes together’ (273). *STAG2* is the most mutated cohesion subunit in cancer (274), with this discovered nonsense mutation is likely result in a loss of sister chromatid cohesion (273). In isolation, this variant may signify a ‘CHIP’ (clonal haematopoiesis of indeterminate potential) mutation. Originally described in 2015 by Steensma *et al*, CHIP represents the indolent phase of an individual demonstrating somatic mutation in their blood or bone marrow that is associated with haematological malignancy, but do not fulfil diagnostic criteria for a haematological malignancy (247).

Of the aNLRP3-AID cases however, three pathogenic variants were identified in patient three. HSCs shown to have mutations in *DNMT3-A* obtain self-renewing capacities and are thus are predisposed to clonal expansion over time (275). The *DNMT3-A* missense substitution found

in aNLRP3-AID patient 3 (c.2645G>A p.Arg882His), has been widely studied in the context of Acute Myeloid Leukaemia (AML) with several reports indicating the pathogenic nature of this specific mutation (276). Functional experiments demonstrate that cell lines harbouring the mutant R882H cause differentiation blockades in HSCs, by downregulation of differentiation-associated genes through binding with Polycomb Repressive Complex 1 (276). The *TET-2* gene encodes for a transcriptional regulator, catalysing the hydroxylation of 5-methylcytosines. The resulting loss of DNA methylation is constant with the findings that *TET-2* mutant AML patients demonstrate a genetically distinct hypermethylation profile (248). The two predicted pathogenic variants found in aNLRP3-AID patient 3 were nonsense c.4585C>T p.Gln1529* and c.5095C>T p.Gln1699*. *TET2* mutations are described in literature to render a global loss of protein function (177, 277), therefore implying a lack of genomic regulation and potential development of a milieu to acquire further mutations. The presence of three pathogenic mutations in aNLRP3-AID patient 3 consequently warrants close monitoring, though only a few cases of MDS development in autoinflammatory conditions have been documented (175, 278).

3.4.3 X inactivation

Clonal skewing in HSCs is a frequent finding over 55 years of age and though there are a few reports of late onset X-linked disorders in females (279), this phenomenon is rarely correlated with disease. During the course of embryonic development, random XCI occurs in females and stays a permanent feature of the cell's lifespan. Underlying a majority of haematological malignancies, somatic mutations have long been implicated as one of the major steering forces behind CH, though another probable cause of the CH is the presence of polymorphic genes on the X chromosome yielding selective attrition or fitness upon a HSC (171).

In this presented work, use of the HUMARA assay in female patients with autoinflammatory disease was substantiated by the findings that skewing is associated with MDS. First determined in 2012, Busque *et al* originally determined that CH is selectively enriched in women with *TET-2* mutations, with one in seven subjects with CH and a *TET-2* mutation developing haematological malignancy (248). These findings were corroborated with data demonstrated that XCI was more pronounced in samples with somatic mutations, typical of CH (171).

Certainly in agreement with literature, for aNLRP3-AID, the degree of HUMARA skewing was prominent in the sample with somatic mutations, though this was not emulated in SchS. The one patient (SchS-9) who demonstrated an abnormal XCI ratio did not have any variants identified by the MDS panel, nor the MYD88 L265P mutation or any detected *NLRP3* variants.

However, since bone marrow histology indicated low-grade myeloma within this patient, there is the increased probability that the skewed ratio observed is associated with the clonal restriction found within myeloma (280). Though, the latter statement could be contended given that SchS patients 23 and 30 demonstrated low grade MZL and MZL respectively, with normal XCI percentages. There is the likelihood that the gene panel employed did not target the change underlying the clonal process in SchS-9. Harboursing the pathogenic *STAG-2* variant, the male SchS patient 20 couldn't be investigated for XCI due to limitations of the HUMARA technique.

A preliminary trial showed that the HUMARA assay when performed on gDNA from both mononuclear cells and whole blood from the same individuals showed no difference in XCI ratios obtained. Not only does this corroborate the fact that inactivation patterns are determined during gestation, but strengthens the fact that gDNA used in this section of work is representative and the likelihood of alternate ratios from other cell types is low (171).

3.4.4 Chapter conclusions

Demonstrating that around a third of SchS patients have the activating *MYD88* mutation, is the most unifying genetic factor of SchS found to date, also in parallel with those SchS cases who develop WM. Though not present in all SchS samples, this novel finding provides clues to the pathogenesis of this heterogeneous disease. Exclusion of this somatic mutation from fibroblasts of two SchS patients further implies this pathogenic variant is confined to cells of the haematopoietic lineage.

Querying the mutational status of 28 genes associated with MDS was substantiated by several studies implicating the NLRP3 inflammasome as the mediator of CH and pyroptosis in MDS (179). Thus, harbouring initiating mutations in genes related to MDS could predispose SchS patients to maintain a generally pro-inflammatory environment, facilitating the development of additional SAID somatic mutations. Given that this hypothesis was proven incorrect, the few variants found are likely to be age-related. Values of the HUMARA assay provides little diagnostic benefit in SchS, though its use as a tool of predicting or corroborating CH findings within females suspected of haematological malignancy is of great significance. The results of this chapter were published as a brief report in *Arthritis and Rheumatology* (281).

Chapter 4 IgM Isolation and Protein Microarray

4.1 Introduction

With research in chapters two and three showing no common genetic basis to SchS, the work presented henceforth queries properties of the enigmatic paraprotein. The aim of the work presented in this chapter is to therefore investigate the hypothesis that elevated titres of monoclonal IgM contribute to the inflammatory phenotype seen within SchS patients through exhibiting preferential binding properties. Whether the gammopathy is an epiphenomenon or central to disease manifestations is explored.

The aim of this chapter was to explore the notion that SchS-IgM binds to a specific protein or set of related proteins, by utilising unbiased, proteome-wide methodology. Through employment of the HuProt™ V3.2 protein microarray and using isolated IgM as the probing sample, it was therefore possible to investigate the potential interactions of this antibody fraction with over 20,000 clones encoding human recombinant proteins. These represented more than 15,700 genes, encompassing around 75% of the annotated human protein coding genome. Nearly 90% of the expressed proteins are full-length, therefore representing a comprehensive emulation of the human proteome.

Antigen specific antibodies are generated and secreted by long-lived plasma cells in response to antigenic challenge and is a central role of the adaptive immune system (282). IgM antibodies differ to the other classes of Igs in that their production (by B1 cells predominantly) can be in the absence of apparent antigen encounter (283). Whilst featuring a broad specificity and a low affinity to foreign epitopes, IgM has a noted binding propensity to self-structures – such as the ‘phylogenetically’ conserved epitopes of nucleic acids, phospholipids, and carbohydrates (284).

4.1.1 Protein isolation and purification

With the aim to retain large concentrations of the target protein, separation involves two main steps: (1) protein isolation and (2) protein purification.

4.1.1.1 Antibody isolation

Isolating IgM from bodily fluids whilst retaining its biological activity is challenging, mostly attributed to its large size (970 kDa) as compared to other Igs (150kDa-190kDa), sensitivity to alterations in pH and salt conditions, susceptibility to denaturation and its tendency to bind DNA (285). In the past, purifying IgM was based on ammonium sulphate precipitation of the protein - followed by either gel filtration, ion-exchange chromatography or zone electrophoresis (286). These methods are time-consuming and still bear large fractions of

impurities. Isolation of high purity antibodies has been established through the availability of columns (referred to as the stationary phase), harbouring antibody binding proteins as immobilised ligands, for example, the bacterial wall derived protein A ligand which binds to the Fc region (287). The latter example and other commonly used reagents like Protein G do not work particularly well with IgM, as its pentameric conformation blocks access to the Fc region required for binding the ligand. However, the HiTrap™ IgM Purification HP (GE Healthcare, UK) is the sole commercially available IgM column manufactured for use with automated chromatography systems. For this column, the ligand is 2-mercaptopyridine attached to a sepharose resin and functions based on the concept of thiophilic adsorption (TA).

4.1.1.2 Antibody purification

Fast protein liquid chromatography (FPLC) is a type of High Performance Liquid Chromatography (HPLC) pushing through samples containing the protein of interest (mobile phase), through the stationary phase (described in 1.1.3.1) under high pressure. Such column chromatography can be performed with automated systems such as the GE Healthcare ÄKTA machines.

4.1.1.3 SchS IgM isolation

Application of these protein purification techniques to facilitate SchS IgM isolation from serum is a suitable approach given the commercial availability of the HiTrap™ IgM columns and access to the ÄKTA Pure machine at the University of Leeds. Though the total IgM component will be present in serum of SchS patients and thus subject to isolation and purification, acquisition of the potential 'pathological' SchS IgM is challenging given that the group of B-cells responsible for overproduction of a potentially pathogenic component is yet to be fully described.

4.1.1.4 Protein microarray

Protein microarrays were initially developed in the late 1990's to 2000's, based largely upon the work carried out by Roger Etkins in 1989 and the adaptation of DNA microarrays (288, 289). This technology is essentially the fixation of thousands of proteins onto a single surface, where peptide interactions can be investigated for numerous purposes. Key uses of this versatile and sensitive platform include assessment and validation of antibody specificity, evaluation of protein binding reagents employed in research and clinical applications, and the screening of molecular interactions using a protein of interest.

The HuProt™ v3.2 Human Proteome Microarray is the most extensive protein array available commercially, with this platform querying over 20,000 human recombinant proteins. This represents over 15,700 individual genes covering over 75% of the annotated protein coding

genome. These recombinant proteins are firstly expressed in the yeast, *S.cerevisiae*, and further subject to purification, conjugation to GST for adherence to glutathione on the array slide surface, followed by duplicate imprinting onto a glass slide.

4.1.1.5 IgM and SchS

The idea that IgM clonal diseases harbour the MYD88 L265P mutation was further developed through research by Varettoni *et al* in 2013, noting IgM-MGUS patients demonstrating 'significantly higher levels of IgM' carried the *MYD88* variant (183). The mutation in question is found in 50% to 80% of IgM-MGUS patients, 6% of patients with lymphomas such as Marginal Zone Lymphoma (MZL) and in 5% of chronic B-cell LPD (183, 290). As demonstrated in Results Chapter 3, approximately a third of SchS patients harbour the MYD88 L265P mutation. This novel finding was based on the hypothesis that since 20% of SchS patients go on to develop the IgM related WM, where over 90% of patients carry the aforementioned mutation, that this would be mirrored in SchS patients. However, in CAD, established monoclonal IgM binds to red blood cells activating the complement cascade, within the peripheral circulation due to cooler temperatures (189) - but patients don't harbour the MYD88 L265P mutation. Sequencing of the IgH regions determined that the IgHV4-34 gene segment encodes for the monoclonal cold agglutinin IgM molecule, indicative of particular aa sequences having an important role in antigen recognition (189). In CLL, the aa composition of the monoclonal component's binding region is shared amongst a third of patients, indicating antigenic specificity (291). Together with the hypothesis that the B-cell receptor in CLL is self-reactive, leading to clonal expansion of a B-cell progeny (292), highlights the potentiality pathological consequences due to a generation of a clonal Ig. The evidence of clonality sought in Results Chapter 5 (e.g. presence of highly expanded CDR3 aa clones) also supports the concept that a certain proportion of the monoclonal component in SchS may be directed towards a target, or group of related targets.

This chapter focuses on the hypothesis of a pathological Ig component, through isolating total IgM from the serum of three SchS patients, two WM patients and one NLRP3-AID patient, followed by application of these six isolated IgM samples to a protein microarray encompassing over 75% of the human proteome. Thus, the aims of this chapter are as follows:

- A.** Isolation of IgM from three SchS patients' serum using FPLC techniques
- B.** Application of isolated serum IgM to the HuProt™ protein microarray

4.2 Methods

4.2.1 IgM isolation

IgM paraprotein was isolated from three SchS patients, two WM patients and one NLRP3-AID patient (Table 10), alongside two healthy controls. I carried this section of work out at the Protein Production Facility at the University of Leeds (main campus), where the relevant laboratory equipment is available. First described in 1985 by Porath *et al* (293), 'Thiophilic Adsorption' (TA), forms the basis of Ig purification carried out in this work and is a salt dependent technique widely used to purify Igs. Having an affinity for sulfone groups that are near thioether groups (293), thiophilic proteins retain the ability to bind to an immobilised ligand. The protein of interest is subject to adsorption at a neutral pH, whilst its elution is attained by reducing the concentration of the salt components.

Implementation of this technique to isolate IgM in this work was facilitated by the use of the GE Healthcare HiTrap™ columns. Manufactured from polypropylene lacking interaction with biomolecules, the HiTrap™ column is an affinity medium, consisting of 2-mercaptopyridine at a concentration of 2mg/ml, acting as the 'ligand' binding only IgM. This ligand is coupled to a sepharose resin, with the bound protein (IgM) then released by decreasing the salt concentration. These HiTrap™ purification columns were used in conjunction with the fast protein liquid chromatography system (FPLC), ÄKTA Pure™ (GE Healthcare, UK). Controlling the rate at which the mobile phase passes through a small diameter stationary phase forms the basis of FPLC, a form of medium-pressure chromatography that was first introduced in 1982 (294). The advantages of using the ÄKTA Pure™ is primarily based on its high degree of automation, UV monitoring to determine protein separation and different wavelengths, with the system controlled by the Unicorn-6 software. Having the ability to purify micrograms to grams of protein, this machine operates at a maximum pressure of 5MPa.

Alternative antibody isolation ligands such as the bacterially derived proteins A, G and L work well for the purpose of isolating IgG, but not in the case of IgM (295). This is mainly attributable to the pentameric structure of IgM Fc receptor binding site - where the latter ligands would bind. Furthermore, TA works well for the 'selective depletion of immunoglobulins from complex biological fluids' (296), largely due to the pH neutral elution conditions of the bound protein. For example, protein A based affinity chromatography requires elution with a low pH that would affect the structure of the antibody. In view of the later objective to apply purified IgM to a protein microarray, the aforementioned benefits and commercial availability of the HiTrap™ columns with the ÄKTA Pure™ chromatography system is the most suitable approach to obtain substantial amounts of IgM from serum.

4.2.1.1 Buffer and sample preparation

High grade molecular water was used for making buffers and the following formulations were further passed through a 0.45µm filter, to ensure high purity. The following compositions were used for the buffers: (1) Binding buffer - 20mM sodium phosphate, 0.8M (NH₄)₂SO₄, pH7.5; (2) Elution buffer - 20mM sodium phosphate, pH7.5; (3) Regeneration buffer: 20mM sodium phosphate, pH7.5 with 30% isopropanol. Per 1ml of serum, 0.8M of crystallised ammonium sulphate (required to be the same concentration as in the binding buffer) was added gradually to avoid IgM precipitation and passed through a 0.45µm filter immediately prior to loading into the HiTrap™ column.

4.2.1.2 Experimental setup

IgM isolation was carried out using the ÄKTA™ Pure system (GE Healthcare, UK) at 4°C, using the prepacked HiTrap™ IgM Purification HP as the stationary phase and column. The column was washed with five column volumes (1ml) of each of the buffers: binding, elution and regeneration, subsequently followed by equilibration with five times (1ml) of binding buffer. A syringe was used to pump the sample into the column connected to the ÄKTA system, using a flow rate of 1ml/min, taking care to avoid bubble formation. The next step involved the use of 15mls of binding buffer, maintained at a flow rate of 2ml/min. The elution step was carried out subsequently, with 12mls of elution buffer. The automated feature of peak sensing via monitoring the conductivity and pressure values using real-time UV traces, enabled automatic peak fraction collection (2mls) into a 96 well plate. Following elution, regeneration and re-equilibration using wash buffer and binding buffer respectively, permitted reuse of the HiTrap™ column for subsequent IgM purification of a different serum sample.

4.2.1.3 Assessment of protein purity

Visualising the traces generated from the ÄKTA Pure™ machine facilitated identification of the fractions of interest. After pooling the protein fractions of relevance, protein purity was assessed by SDS-PAGE and further subject to fluorometric quantitation using the Qubit apparatus (ThermoFisher Scientific, UK).

4.2.1.3.1 Quantitation and sample storage

Setting aside 30ng for SDS-PAGE, purified IgM samples were aliquoted and stored in PBS at -80°C until use with the HuProt™ microarray (Section 4.2.2).

4.2.1.3.2 SDS-polyacrylamide gel electrophoresis (SDS-PAGE)

The objective of SDS-PAGE was to confirm the purification of IgM using a reducing gel. Polyacrylamide gels are formed by crosslinking of acrylamide and bis-acrylamide, and followed by electrophoresis, these gels serve to separate proteins based on their size. The 10% separation gels were made according to the following composition and order: 4.1ml dH₂O, 3.3ml acrylamide, 2.5ml Tris-HCL (1.5M, pH 8.8), 100µl SDS, 10µl TEMED, and 32µl APS (10%). The 4% stacking gels were made according to the following composition and order: 6.1ml dH₂O, 1.3ml acrylamide, 2.5ml Tris-HCL (0.5M, pH 6.8), 100µl SDS, 10µl TEMED, and 100µl APS (10%).

Equal volumes of sample buffer and 30ng of the isolated fractions (10µl each) were heated to 95°C for five minutes and then loaded into the gels. Ten microliters of the Precision Plus Protein marker™ (Bio-Rad, UK), was also loaded to determine the molecular weight of the isolated IgM and other fractions. After electrophoresis at 100V for an hour, the gel was subject to Coomassie Brilliant Blue staining and analysed using ImageLab software (Bio-Rad, UK).

4.2.1.4 Overview of IgM purification

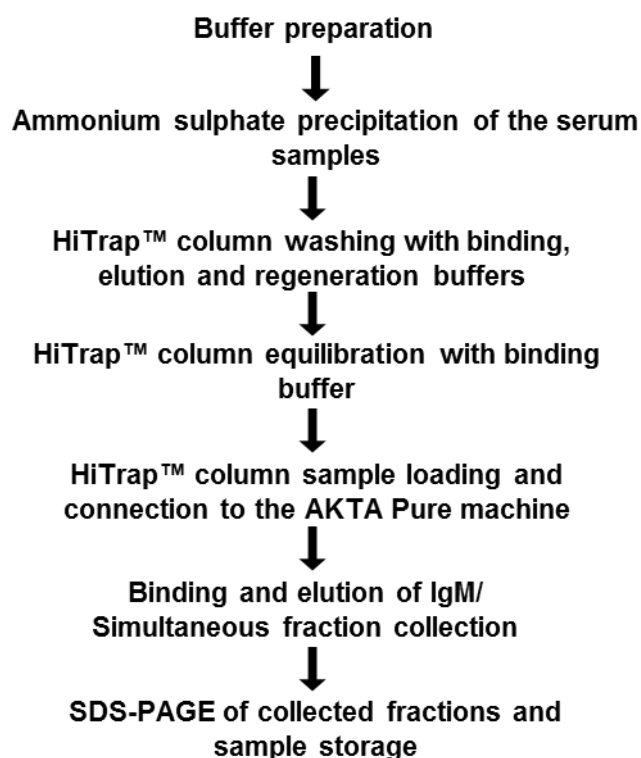


Figure 32: Stepwise summary of the IgM isolation procedure.

4.2.2 Isolated IgM profiling on proteome microarray

The following work was carried out with myself and the molecular biology scientists employed by Cambridge Protein Arrays Ltd (CPA) and carried out in the laboratory facility in Cambridge. Total IgM isolated from section 4.2.1 was used as the starting material for the following experiment. A total of six isolated IgM samples were included in this experimental procedure: three SchS patients, two WM patients and one NLRP3-AID patient. Of note, HC derived serum-IgM was not used as a control in the following work due to the professional advice obtained from CPA. They observed prior studies using IgM/IgG from HCs demonstrated increased reactivities to the protein array and suggested that HC derived IgM would likely bind a multitude of antigens given the reduced specificity and high binding capacity of IgM. Alternative controls were included and are described in the subsequent sections.

4.2.2.1 Overview of HuProt™ steps

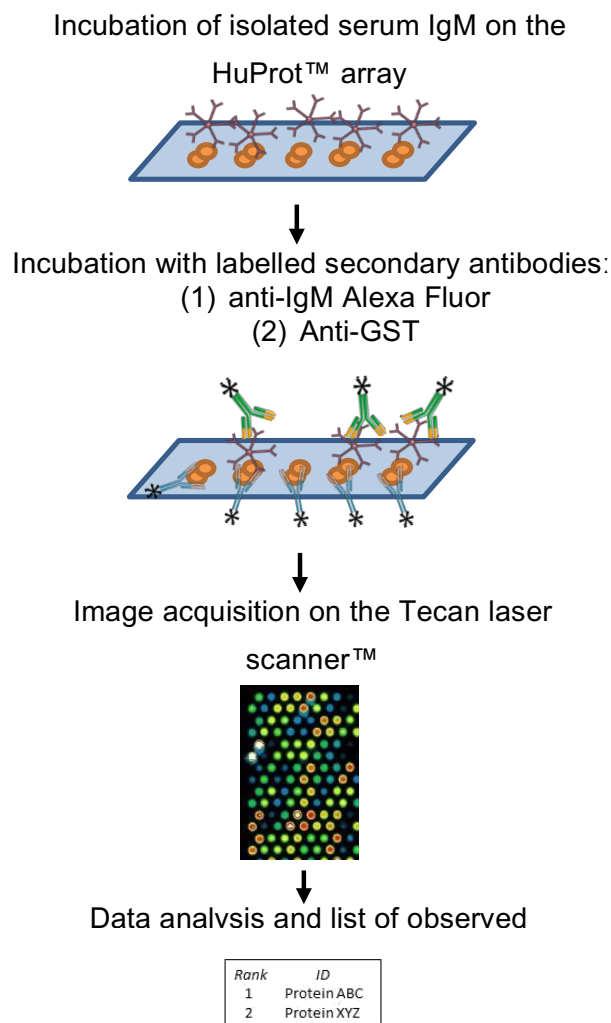


Figure 33: Summary of steps carried out for the HuProt™ protein microarray.

4.2.2.2 Sample probing

Four-well dishes were used for blocking the HuProt™ arrays by using 5ml of blocking buffer (2% BSA/PBS-Tween 0.05%) to each compartment, and kept at 4°C overnight. Isolated IgM was incubated on the HuProt™ human protein microarray (CDI Laboratories, USA), at a 15µg/ml concentration, in a final volume of 4ml in blocking buffer for 2 hours with gentle rocking. A negative control array was processed in parallel with the addition of blocking buffer, instead of isolated IgM.

4.2.2.3 Washing and antibody addition

The arrays were washed 3x with PBS-T (PBS, 0.05% Tween), followed by two 5 minute washes with PBS-T. The washing solution was removed by suction. Following washing, the fluorophore conjugated reagents were diluted. Anti-human Alexa Fluor IgM-488 (ug/ml) and anti-GST-Dylight-650 (0.5ug/ml) in blocking buffer. 4ml of the diluted antibodies were added to each incubation compartment of the 4-well plate. These were incubated for 2 hours at room temperature with gentle rocking. The arrays were further washed three times with PBS-T, followed by another 2 washes with PBS-T. One last wash with molecular grade water was performed to remove any residual PBS-T. The arrays were then centrifuged in order to dry the slides.

4.2.2.4 Imaging

The array slides were scanned immediately on a Tecan LS400 microarray scanner (Tecan Trading, Switzerland) at 535nm to detect the interaction of the samples, and again at 633nm to detect GST staining of all proteins, with a resolution of 10µm. Fluorescence data was collected and subject to analysis.

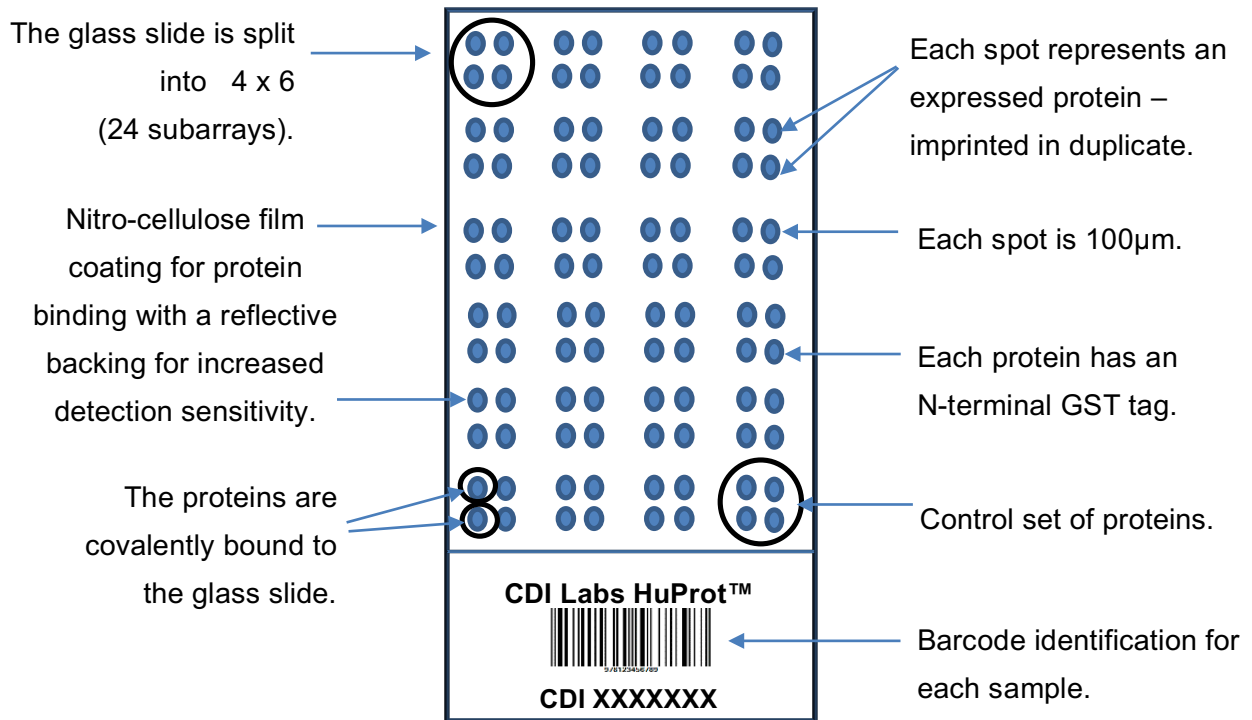


Figure 34: Layout of the HuProt™ protein microarray slide.

Each barcoded glass slide comprises of the expressed products from 20,000 clones encoding human recombinant proteins. These GST-His6 tagged proteins represent nearly 15,700 genes, covering 75% of the human protein coding genome. The slide is arranged into 24 subarrays, with each spot representing an expressed protein, imprinted in duplicate. The proteins are covalently bound to the glass slide, strengthening assay stability. The slide has a nitro-cellulose film coating for protein binding, including a reflective backing to increase the sensitivity of detection. The proteins are covalently bound to the glass slide, strengthening assay stability. A trio of experiments carried out by Hu *et al* at Johns Hopkins University determined that the ‘vast majority of proteins are in their native conformation’ (297). Retention of protein conformation is crucial for maintaining the physiological activity of the protein and in the context of this work, the status of IgM binding to a native protein is imperative to mimic *in-vivo* activity within the patient. For the purposes of grid alignment, fluorescent control spots are included within the slide. A set of control proteins (GST, BSA, Histones and IgG) are also incorporated.

4.2.2.5 Data analysis

Data analysis of the array aimed to identify specific proteins interacting with the purified IgM samples, and was segmented into the following steps: (A) image analysis; (B) numerical analysis; (C) data ranking and filtering based on the outputs from (A) and (B). For each step, outliers were excluded from further analysis.

4.2.2.5.1 Image analysis

Alignment of the human proteins spotted with the array positioning (.gal) file was carried out using GenePix software (Molecular Devices, USA). Following alignment of each of the 24 subarrays using fluorescently-conjugated control spots (labelled in Figure 34), the spots were repositioned and resized by the semi-automated software to garner best fit. The alignments were subject to visual confirmation and observable artefacts were manually flagged. Determination of the fluorescent intensity for each spot on the array was calculated by GenePix and further saved to a (.gpr) file.

4.2.2.5.2 Data analysis calculations

The following workflow to determine numerical values ascertaining to sample-protein binding is split into 2 steps:

1. Calculation of duplicate spot averages and subtraction of negative control array data
For each array slide (n=6 patients, n=1 negative control), the average fluorescence signal intensity and corresponding standard deviations were calculated from both the duplicate spots for each protein. The average fluorescence signal intensity obtained from the corresponding proteins on the negative control array were subtracted from the patient arrays, generating the corrected protein specific fluorescence signals. These values were further log₂ transformed.

2. Calculation of Z-scores for the evaluation of sample signals

For each protein present on the array, the Z-score was computed to define signal significance within the signal distribution according to the following formulae:

$$Z = \log_2(\text{sample-control}) - \text{average log}_2 / \text{SD log}_2$$

The values of the control spots (i.e. fluorescent markers) are not included in these calculations.

1. Data filtering and ranking

Positive 'hits' correspond to those proteins with statistically significant signals due to sample interaction. These 'hits' were established by filtering the entire data set according to the following parameters:

1. Relative Standard Deviation (rSD)

The rSD of the sample signal for duplicate spots must be below a set threshold of 0.35. Application of this parameter ensured that bright artefacts on the spot area did not influence a high, erroneous reading.

2. Signal to Noise ratio (S/N)

The S/N refers to the fluorescence signal in relation to the background signal. The value must have been above the threshold of 2.5 to ensure that only those spots clearly distinct from their background were examined.

3. Sample to Control ratio (S/C)

The S/C explored the relative change seen for the same spots on the sample array as compared to the negative control array. This parameter ensured the removal of protein signals which showed only a slight increase in signal relative to the control. This minor increase is considered as variation of the direct secondary reagent binding, rather than sample contribution.

Utilising the criteria above, data for the proteins were ranked by Z-score (corresponding to grading according to sample signal intensity). The top hits identified according to the outlined methods above were visually checked by inspection of the microarray images using ImageJ. Furthermore, spots manually flagged as artefacts during the initial step of grid alignment, were excluded from the analytical process.

4.3 Results

This chapter presents IgM isolation from two healthy controls, three SchS patients, two WM patients and one NLRP3-AID patient. Subsequently, the purified IgM from the previous step from the patients were then applied to a protein microarray consisting of over 75% of the human proteome to probe for preferential protein binding.

4.3.1 Isolated IgM levels

The following table portrays details of the HCs and patients who underwent serum IgM isolation.

Patient ID	Sex (M/F)	Age upon disease diagnosis	MYD88 L265P (Yes/No)	IgM subtype (kappa or lambda)	IgM levels upon diagnosis (g/L)	Isolated IgM levels (g/L)
HC – 1	M	30*	N/D	N/D	N/A	0.74
HC – 2	M	26*	N/D	N/D	N/A	0.26
SchS – 2	F	43	Yes	IgMk	17	0.55
SchS – 23	F	60	No	IgMk	9	0.73
SchS – 31	F	51	Yes**	IgMk	14	0.33
NLRP3-AID – 7	M	Unavailable	N/D	N/A	N/A	0.28
WM – 1	M	69*	Yes**	IgMk	Unavailable	0.33
WM – 2	F	81*	Yes**	IgMk	Unavailable	0.61

Table 10: Resulting IgM concentrations from the isolation procedure (g/L).

The normal range for IgM in healthy individuals ranges between 0.4 - 2.5g/L.

*Age upon obtaining serum

** Testing carried out at HMDS

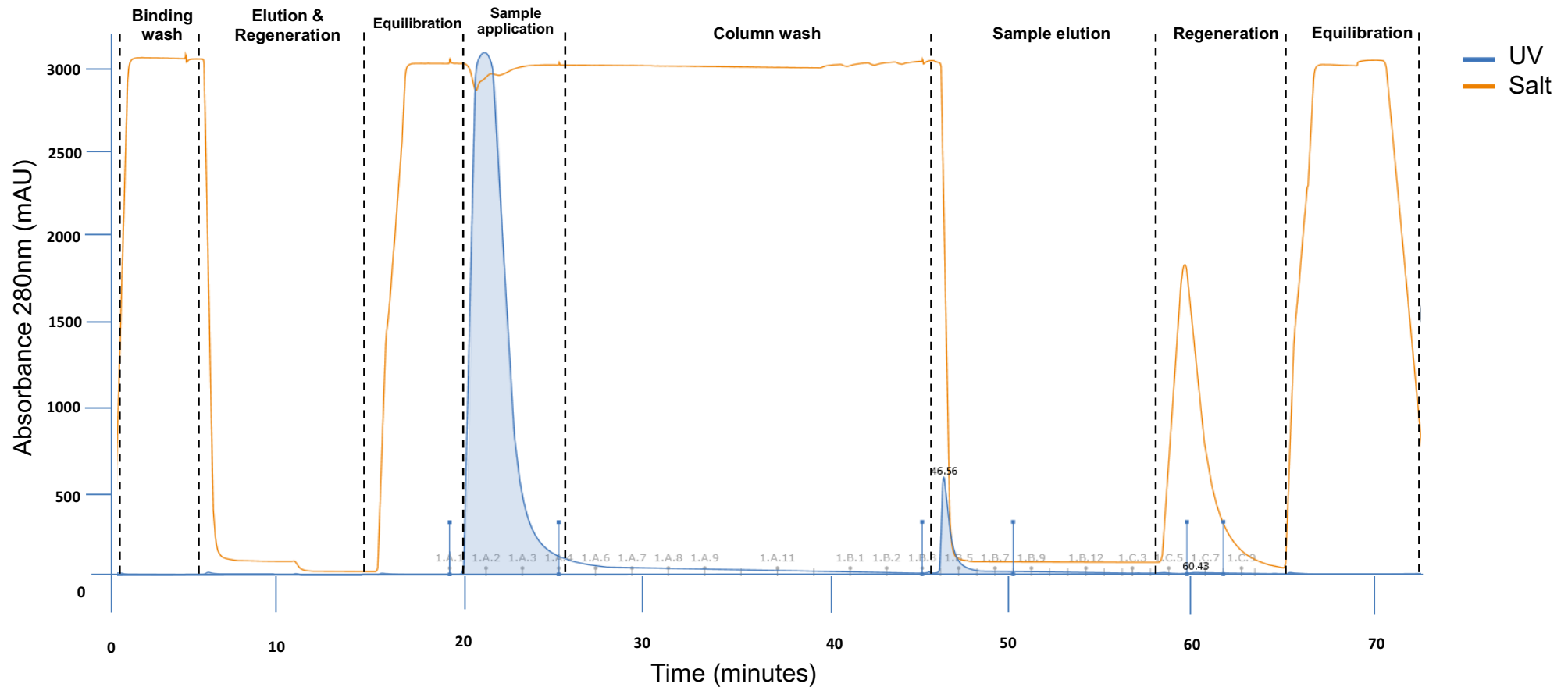


Figure 35: Representative chromatogram from the AKTA machine.

The trace above displays the eight stages of IgM isolation from 1ml of serum. (1) Binding wash ;(2) Elution and regeneration of the column; (3) Column equilibration; (4) Sample application; (5) Column wash; (6) Sample elution; (7) Regeneration; (8) Equilibration.

The blue lines show the UV absorbance values measured in (mili-Absorbance Units) with the orange lines corresponding to the salt levels.

The figure above was generated from Unicorn start software™.

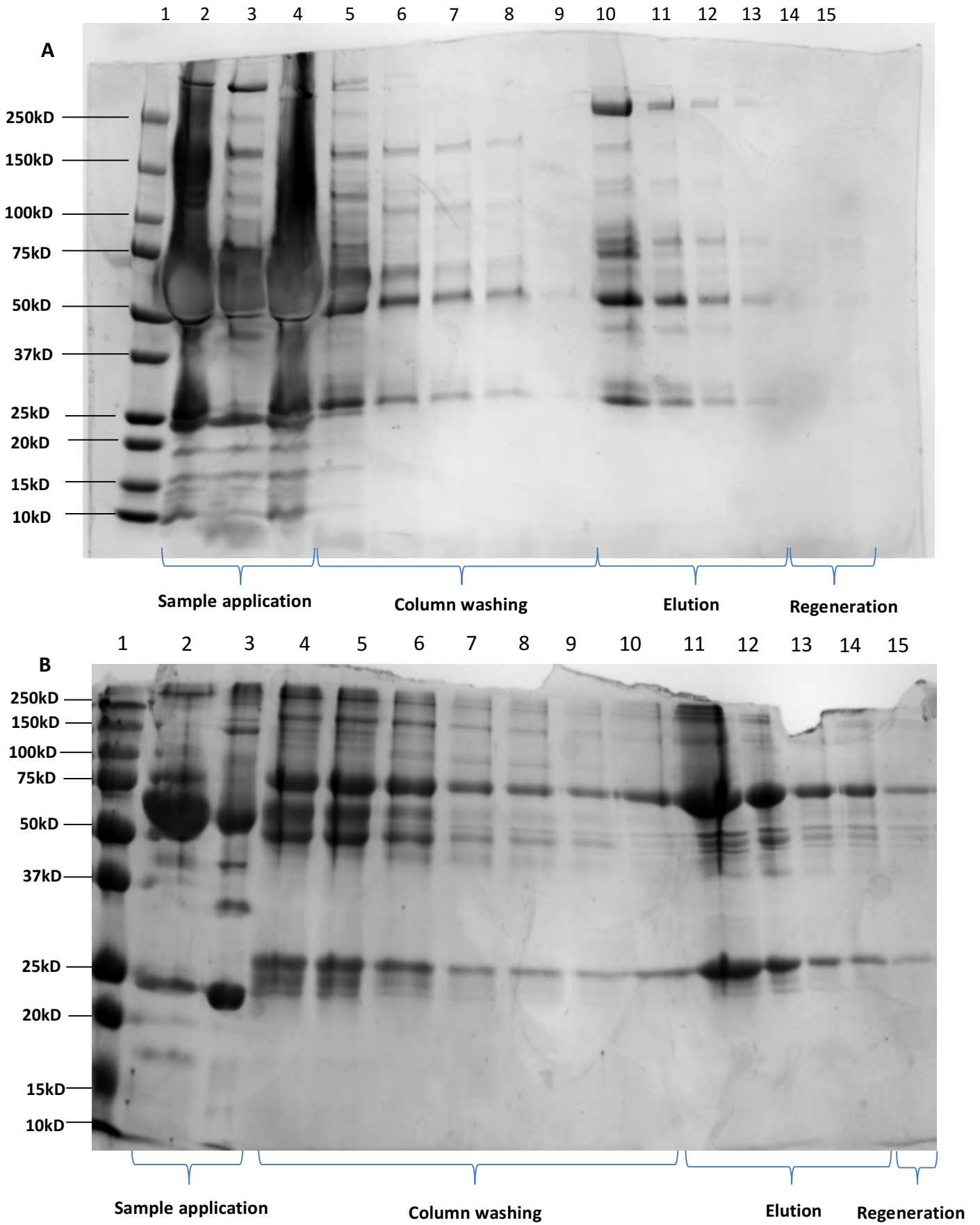


Figure 36: Representative SDS PAGE blots.

Figure 35 (A and B) is illustrative of the fractions collected via the AKTA machine. IgM isolation and purification from eight serum samples was a successful undertaking as demonstrated through this figure. Initially, serum containing IgM was precipitated with ammonium sulphate to deplete the majority of highly soluble contaminants in serum such as albumin and transferrin. The resulting partially purified precipitate was then subject to IgM HiTrap™ protein affinity column loading, previously washed and equilibrated with the buffers as described in section 4.2.1. HiTrap™ column attachment to the ÄKTA Pure™ system and initialisation of the Unicorn start software™ was followed by implementation of the purification strategy as outlined by Figures 35. The UV (blue line) and conductivity (orange) traces enabled automated collection of desalted fractions into a 96 well plate (Figure 35). The aforementioned workflow was an effective strategy for obtaining IgM yields using FPLC based separation as demonstrated by Figure 35, with the HiTrap™ column having a 5g/L IgM binding capacity. In this work, the purified antibody levels ranged between 0.28g/L to 0.74g/L.

The chromatogram and SDS-PAGE blots represent the stepwise purification procedure performed. Steps 1, 2 and 3 from the chromatogram correspond to the binding, elution & regeneration, and equilibration steps, aimed to prepare the HiTrap™ column for sample application. The equilibrating buffer was compatible with both IgM and the resin in the column (i.e. not denaturing IgM). Step 4 signifies application of the serum containing IgM sample, indicated by the high UV peak. This is reflected in Figure 35 where the high protein concentration is visually apparent through the density of the detected bands together showing a variety of different sized proteins. Following sample application, washing of the column was subsequently followed by IgM protein elution. The smaller peak on the trace indicates the generation of the purified IgM (Step 6), and correspondingly, these antibodies are portrayed Figures 35A and 35B in their denatured forms ('elution'). Whilst more prominent in Figure 35B, demonstration of the IgM heavy chain at around 70kDa and the light chain at around 23kDa indicates isolation of IgM was achieved using this strategy. The antibody containing fractions were pooled according to the stages of isolation and stored at -80°C until use with the HuProt™ array. Subsequent column regeneration and equilibration steps were successfully carried out to enable reuse of the IgM HiTrap™ columns. These stages are also indicated in the SDS-PAGE blots. Notably, the described procedures were first tested upon HC serum (35A) before proceeding to patient serum samples (35B).

4.3.2 Protein microarray

Using the material generated in 4.2.1, the following section of work investigates the hypothesis that SchS-IgM preferentially binds a protein or set of self-proteins belonging to a particular family. Three SchS, one NLRP3-AID and two WM samples were tested against the array (Table 10). Based upon previous experiments carried out by CPA, all six samples were diluted to a final concentration of 15 µg/ml when applied to the array. A seventh control sample was included as a negative control. PBS was added in lieu of a sample, but the array was incubated with both secondary antibodies. Likewise, a positive control (anti-GST staining) was performed in parallel for each of the sample arrays and negative control array. This served for overall array QC and assay performance, also providing data on the relative amount of all proteins on the slide. The samples tested gave good signal-to-background ratios and were determined suitable for investigation on the array, with no background issues observed on the HuProt™ 3.2 surface for either the samples or control slides. Relative to the negative control, data analysis for the examined samples identified numerous hits. The top 20 strongest interactors for each sample are presented in this chapter.

For each of the tables in the following sections, the top 20 interactors are ordered by their individual z-scores (calculations detailed in section 4.2.2.5.2). A hit pertaining to a z-score below 2.5 is unlikely to be an interaction. An additional value of interest is the Interaction Score (i-score), which is a measure of the signal strength obtained from the sample binding to a particular protein relative to the amount of immobilised protein, as judged by the staining intensity for the GST tag. Even for clearly detectable sample signals, the i-score can be relatively low in the case of strong anti-GST staining. Among proteins with a similar high z-score, an increased i-score can be an additional indication of strong specific binding. The 'sample – control' column indicates the difference of fluorescence between sample staining at 535nm and antihuman IgM staining alone; whereas the 'sample/control' pertains to the fluorescence ratio between sample staining at 535nm and anti-human IgM staining alone, indicative of the relative change upon sample incubation. Values of 1 demonstrate a low relative change. Protein ID, functionality and location are also included – together providing a comprehensive overview of the obtained results. Functional descriptions of the proteins were researched through the following websites: www.genecards.org; www.proteinatlas.org and www.uniprot.org.

4.3.2.1 Sample SchS-2

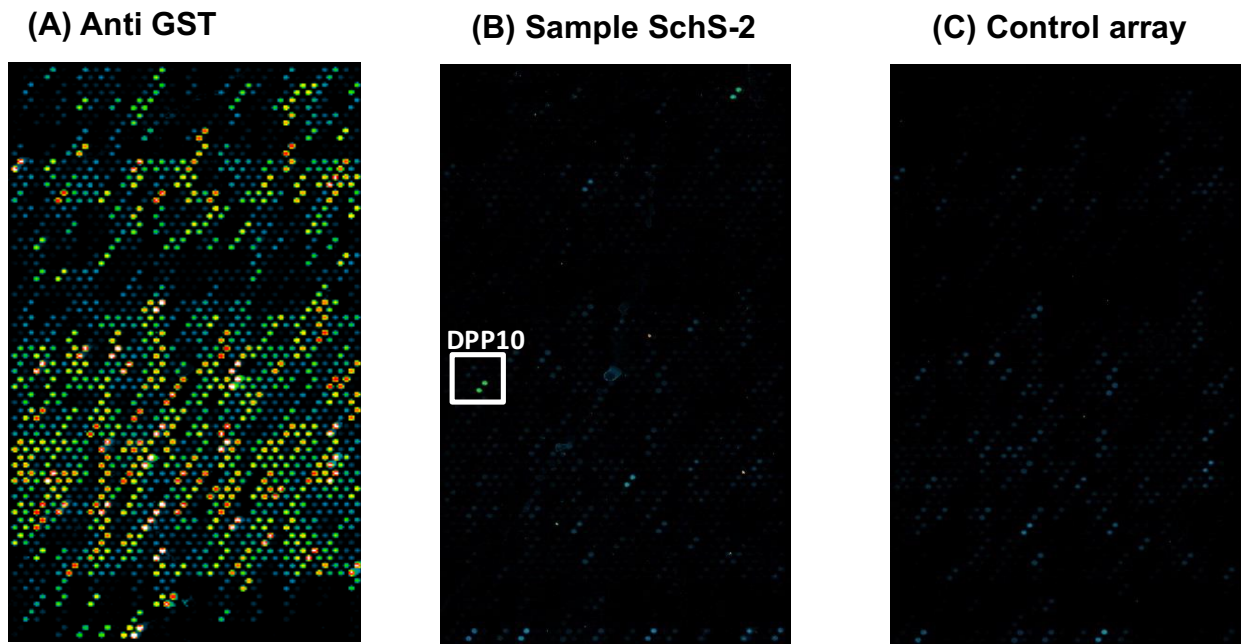


Figure 37: Array visualisation for SchS patient 2.

With a specific focus on subarray 22, Figure 37A denotes the anti-GST staining showing protein locations within the subarray; Figure 37B portrays anti-IgM staining showing strong reactivity with DPP10 which is absent in 37C - the negative control array incubated with secondary antibodies only.

Target	Gene name	Functionality	Location (s)	Sample-control	Sample/control	z-score	i-score
FBXO2	F-box protein 2	Substrate of an E3 ubiquitin ligase complex	ER	9141	11.1	4.67	2.4
DPP10	Dipeptidyl-peptidase like 10	Potassium channel regulator	PM, GA	4852	37.2	4.21	5.0
ATF1	Activating transcription factor-1	TF- regulating cell growth and survival genes	Nucleus	4192	27.2	4.10	3.4
CREM	cAMP responsive element modulator	TF binding to cAMP responsive element	Nucleus	3902	37.1	4.05	2.7
TLK1	Tousled-like kinase 1	Serine-threonine kinase involved in chromatin regulation assembly	Nucleus	3532	13.5	3.98	2.4
EDC4	Enhancer of mRNA decapping-4	mRNA decapping	Nucleus, cytosol	3311	14.1	3.93	1.6
NR6A1	Nuclear receptor subfamily 6 group A, member 1	Hormone receptor – involved in neurogenesis and germ cell development	Nucleus	3305	35.4	3.93	3.5
SSH3	Slingshot protein phosphatase-3	Protein phosphatase – regulator of actin filament dynamics	Nucleus, cytoskeleton	3203	7.5	3.91	0.9
ZNF384	Zinc finger protein-384	TF – binds and regulates promoters of extracellular matrix genes	Nucleus	2982	22.9	3.85	2.4
LHX5	LIM homeobox-5	Regulator of neuronal differentiation and migration during development of the CNS	Nucleus	2962	20.0	3.85	6.2
MLX	MLX, MAX dimerisation protein	TF - Involved in transcriptional regulation – cellular proliferation and differentiation	Nucleus	2904	8.0	3.83	0.7
THRA	Thyroid hormone receptor-alpha	Hormone receptor for the thyroid hormone	Nucleus, cytosol	2833	27.7	3.82	3.6
MAX	MYC-associated factor X	Transcriptional regulator forming a complex with MYC, an oncogenic associated TF	Nucleus, cytosol	2675	34.4	3.78	2.7
NR2E1	Nuclear receptor sub-family 2, group E, member 1	Receptor involved in retinal development	Nucleus	2566	12.6	3.75	7.4
ATF7	Activating transcription factor-7	TF – binds the cAMP responsive element	Nucleus	2588	7.8	3.75	0.7
BHLHE22	Basic helix-loop-helix family member e22	TF – regulates cell fate determination, proliferation and differentiation	Nucleus	2486	45.4	3.72	5.0
Hep B Protein X*	Hepatitis B Protein X	Viral protein involved with transcription, signal transduction, cell cycle progress and chromosomal instability – within the host	Nucleus, cytosol	2421	18.0	3.7	n/a
MITF**	Melanogenesis associated transcription factor	TF- regulates genes involved in cell differentiation, proliferation and survival	Nucleus	2274	23.3	3.66	1.7
H2AFY	H2A histone family member Y	One of the proteins responsible for compacting the nucleosome structure of chromosomes	Nucleus	2256	9.1	3.65	1.7
PARP11	Poly(ADP-ribose) polymerase family-11	Involved in protein PTM by addition of ADP-ribose moieties	Nucleus, cytosol	2221	4.5	3.64	1.8

Table 11: Top 20 hits from the protein microarray for sample SchS-2.

The target, gene name, protein function & primary locations, sample fluorescence intensities, alongside the z-scores and i-scores are presented within the table. *Protein without a GST tag **Known autoantigen

cAMP: Cyclic adenosine monophosphate; CNS: Central nervous system; ER: Endoplasmic reticulum; GA: Golgi apparatus; PM: Plasma membrane; TF: Transcription factor; PTM: Post-translational modification

Location

Eighteen out of 20 proteins are reported to be nuclear, and also can be located within the cytosol (5); cytoskeleton (1), PM (1) & GA (1), and another within the ER. This sample shares nine targets with WM-2: FBXO2, CREM, EDC4, NR6A1, ZNF384, LHX5, THRA, NR2E1 and ATF7. Another five proteins hits are shared amongst this sample, SchS-23 and WM-2: DPP10, ATF1, TLK1, SSH3, MLX; with H2AFY unique to this sample and SchS-23.

Function

Even though FBXO2 was the top interactor in this sample, this protein is noted to retain strong binding capacities on the array, and therefore is regarded with caution. Nevertheless, this ubiquitinating protein was the second top hit for WM-2 with a very similar z and i-score. The potassium channel regulator DPP10 (indicated in Figure 37) was the second top hit – was also found significant in SchS-23 and WM-2. Interestingly, TLK1 was the top interactor in WM-2 and also was ranked 16 in sample SchS-23. This protein belongs to a family of nuclear serine/threonine kinases is predicted to play a role in chromatin assembly and remodelling. Another chromatin associated hit was H2AFY. Although ranked towards the bottom of the shown data, this transcriptional repressor was the top antigen in SchS-23 and signifies the only top hit seen in the SchS samples. Out of the other nuclear located proteins, seven were transcription factors: ATF1, CREM, ZNF384, MLX, ATF7, BHLHE22 and MITF. Of note, MITF is a known autoantigen associated with the autoimmune condition, Vitiligo. Proteins MAX, BHLHE22, Hep B Protein X, MITF and PARP11 were unique to this sample. Particularly, interaction with the Hep B protein may represent a mounted response to recent infection or vaccination. NR6A1, NR2E1 and THRA were three receptors found in this dataset, located in the nucleus with ligand binding resulting in cellular growth and development. The latter three proteins also interacted with WM-2. Other top interactors included an mRNA degradation protein, EDC4; the neuronal cell regulator LHX5, and the protein phosphatase, SSH3.

Fluorescence, z-score + i-score

This sample had weaker fluorescence intensities than SchS-31, but similar to those values found in SchS-23 and WM-1 and stronger than WM-2 and NLRP3-AID-7. The i-scores ranged between 0.7 to 5 with the z-scores all above 3.64.

4.3.2.2 Sample SchS- 23

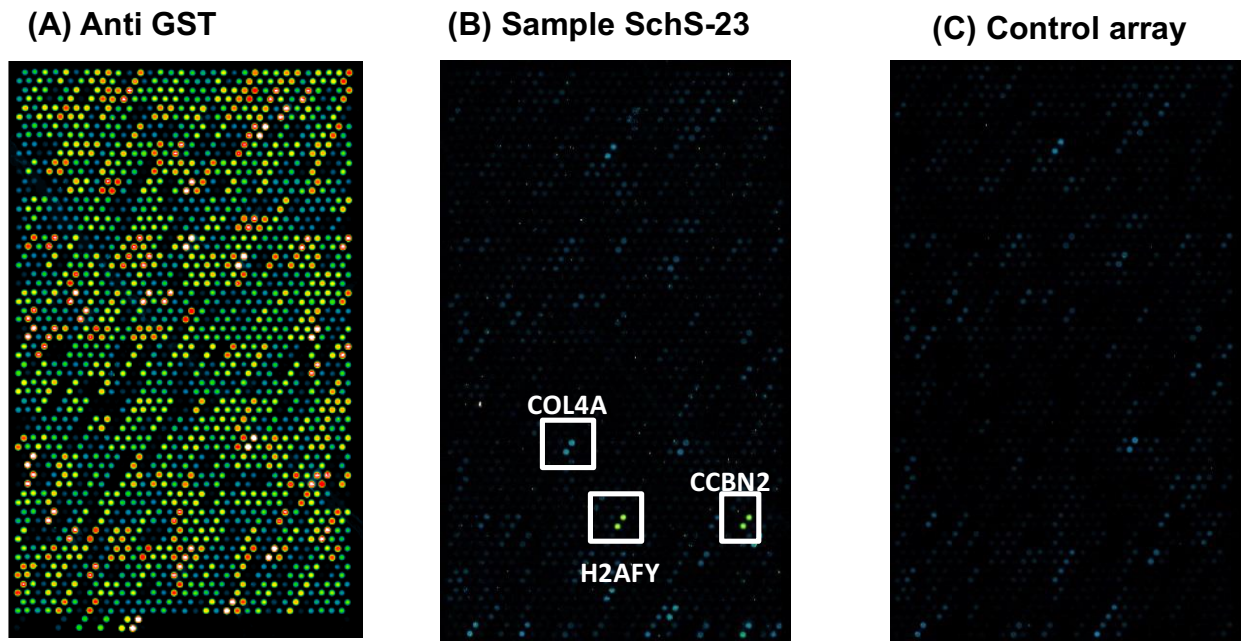


Figure 38: Array visualisation for SchS patient 23.

With a specific focus on subarray 11 for illustrative purposes, Figure 38A represents anti-GST staining showing protein locations within the subarray. Figure 38B portrays anti-IgM staining showing strong reactivity with COL4A, H2AFY & CCBN2- which are absent in 38C - the negative control array incubated with secondary antibodies only.

Target	Gene name	Functionality	Location	Sample-control	Sample/control	z-score	i-score
H2AFY	H2A histone family Y	One of the proteins responsible for compacting the nucleosome structure of chromosomes	Nucleus	10208	37.7	4.62	9.8
GCLC	Glutamate-cysteine ligase catalytic subunit	Rate-limiting enzyme of glutathione synthesis	Nucleus, cytosol, mitochondrion	9883	7.0	4.59	1.5
FAM84A	Family with sequence similarity 84, member A	Involved in cell migration and wound healing	Nucleus, cytosol, perioxosome	9524	4.6	4.57	1.5
CCNB2	Cyclin B2	Cell cycle control at G2/mitosis transition	Nucleus, cytosol, cytoskeleton	7832	28.2	4.42	6.4
GALK2	Galactokinase 2	Galactose phosphorylation activity	Nucleus, cytosol, GA	7392	12.3	4.37	1.7
MAF1	MAF1 homolog, negative regulator of RNA polymerase-III	Transcriptional repressor of RNA polymerase-III	Nucleus, cytosol	5526	5.8	4.15	0.9
SMOX	Spermidine Oxidase	Spermidine forming activity	Nucleus, cytosol	4830	12	4.05	1.4
PLEKH-O2	Pleckstrin homology domain containing O2	Potential regulator of macrophage survival	Cytosol	4039	17.9	3.92	2.2
TFG	TRK-fused gene	Involved in ER functioning and its associated microtubules	Cytosol, ER	3676	3.9	3.84	0.7
ZMYM3	Zinc finger MYM type containing-3	Component of histone deacetylase-containing complexes	Nucleus	3216	6.1	3.74	0.6
COG3	Component of oligomeric golgi complex-3	Forms part of the conserved oligomeric golgi complex-3 involved in normal GA functioning	GA, PM	3014	6.0	3.69	0.8
ATF1	Activating transcription factor 1	TF- regulating cell growth and survival genes	Nucleus	2840	18.8	3.65	2.3
GMPPA	GDP-mannose pyrophosphorylase A	Enzyme involved in the formation of GDP-mannose	Nucleus	2792	4.8	3.64	0.8
COL4A5	Collagen type IV alpha 5 chain	Forms part of type IV collagen, a structural component of basement membranes	ER	2820	17.4	3.64	4.9
MLX	MLX, MAX dimerisation protein	TF - Involved in transcriptional regulation – cellular proliferation and differentiation	Nucleus	2770	7.7	3.63	0.7
TLK1	Tousled-like kinase 1	Serine-threonine kinase involved in chromatin regulation assembly	Nucleus	2760	8.0	3.63	2.0
DPP10	Dipeptidyl peptidase like 10	Potassium channel regulator	PM, GA	2655	20.8	3.59	3.0
BCAR1	Breast cancer anti-oestrogen resistance protein 1	Involved in tyrosine kinase based signalling, role in cell adhesion and migration	Cytosol, cytoskeleton	2526	5.7	3.56	0.7
SSH3	Slingshot protein phosphatase 3	Protein phosphatase – regulator of actin filament dynamics	Nucleus, cytoskeleton	2507	6.1	3.55	0.6
GORAS-P2	Golgi reassembly stacking protein 2	Involved in assembly and membrane stacking of the GA	GA	2320	4.9	3.49	0.4

Table 12: Top 20 hits from the protein microarray for SchS patient 23.

The target, gene name, protein function & primary locations, sample fluorescence intensities, alongside the z-scores and i-scores are presented within the table. ER: Endoplasmic reticulum; GA: Golgi apparatus; PM: Plasma membrane; TF: Transcription factor

Location

Thirteen out of the top 20 interactors can be found within the nucleus. Interestingly, four proteins can also be found in the GA, indicating roles pertaining to protein modifications and secretion. Other locations for these hits were cytosolic (9), cytoskeleton (3), PM (2), and/or ER (2). This sample shares five top hits with both SchS-2 and WM-2 and solely H2AFY was shared with SchS-2.

Function

SchS-23 showed strongest reactivity with H2AFY, also interacting with SchS-2 IgM found as the 19th hit, though interestingly this protein was not within the top 20 of the other samples. This reaction was closely followed by the glutathione synthesis rate limiting enzyme, GCLC. The cell migration and wound healing associated protein, FAM84A, was the third hit within this sample. Though this has been noted by CPA to reoccur numerous times with other arrays, FAM84A was not witnessed with the other five samples and is therefore unique to SchS-23. Located in the cytosol, PLEKH-O2 is a potential regulator of macrophage survival and is an interesting hit given that SchS is an autoinflammatory disease with macrophages/monocytes known to be cells mediating inflammation. Other hits include the transcriptional regulators, MAF1, ZMYM3, and TLK1. The latter protein was also seen as the top hit in WM-2, but was the fifth hit in SchS-2. A further two TF's identified were ATF-1 and MLX; hits also seen in SchS-2 and WM-2. DPP10 and SSH3 were also seen in samples SchS-2 and WM-2 with roles in potassium channel function and actin regulation respectively. Proteins located in the ER included COL4A5, forming parts of the basement membrane of a cell and TFG, with roles in functioning of the ER and its associated microtubules. CCBN2 and BCAR1 were other proteins also functioning within the cytoskeleton. COG3 AND GORAS-P2 are involved in the regulation and functioning of the GA, whereas GALK2 is simply found here known to be a phosphorylating enzyme of galactose. Other nuclear located proteins included the enzymes spermidine oxidase, SMOX and GMPPA – involved in the generation of GDP mannose.

Fluorescence activity z-score + i-score

In comparison to the other five samples, the fluorescence intensities were similar to those found in SchS-2 and WM-1, higher than WM-2 and NLRP3-AID-7 but much lower than those found in SchS-31. The i-scores ranged between 0.7 and 9.8, with the z-scores all above 3.49.

4.3.2.3 Sample SchS – 31

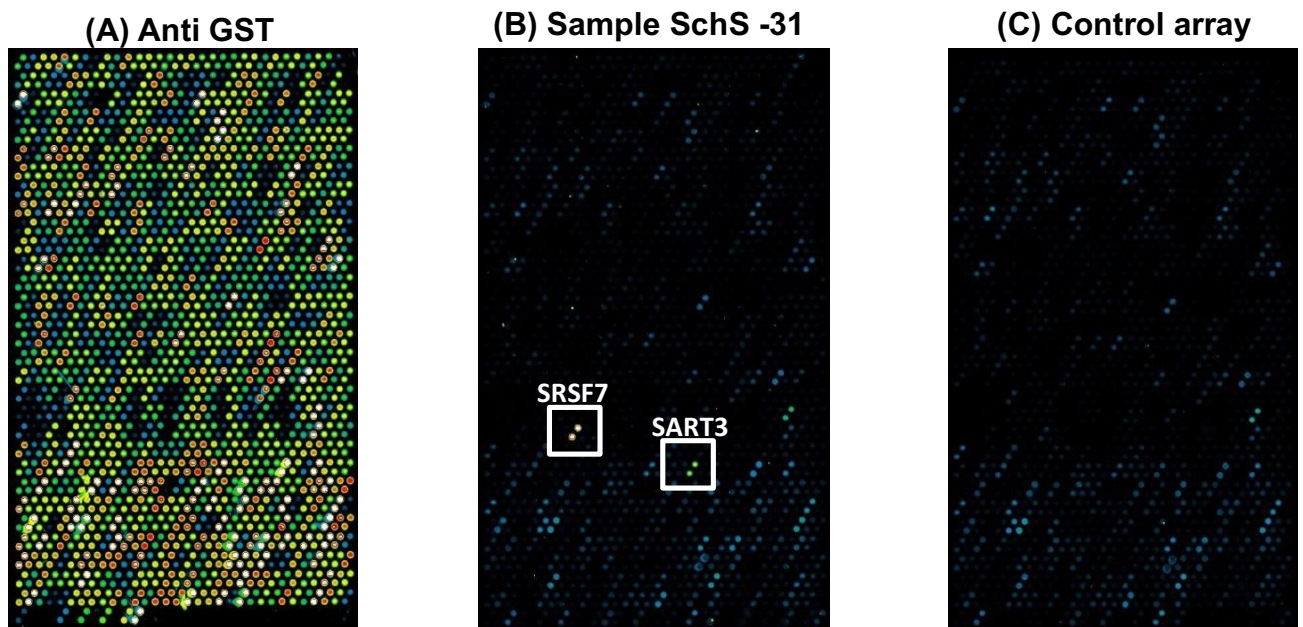


Figure 39: Array visualisation for SchS-31.

With a specific focus on subarray 7, Figure 39A represents the anti-GST staining showing protein locations within the subarray. Figure 39B shows the anti-IgM staining illustrating strong reactivity with SRSF7 and SART3 – which is absent in 39C - the negative control array incubated with secondary antibodies only.

Target	Gene name	Functionality	Cellular location(s)	Sample-control	Sample/control	z-score	i-score
SRSF7	Serine and arginine rich splicing factor-7	RNA binding and splicing	Nucleus, cytosol	64758	91.2	5.99	29.4
UBL7	Ubiquitin-like 7	Regulation of bone marrow stem cells function and/or differentiation	Nucleus, cytosol	64303	55.5	5.99	9.8
CNKSR1	Connector enhancer of kinase suppressor of Ras 1	Adaptor protein and/or regulator of Ras signalling pathways	Nucleus, cytosol, PM	38806	69.2	5.62	8.4
OGFR	Opioid growth factor receptor	Growth regulator	Nucleus, cytosol	35541	121.1	5.55	7.4
PNPO	Pyridoxamine 5'-phosphate oxidase	Oxidoreductase activity	Nucleus, cytosol, mitochondrion	30337	22.6	5.44	5.7
OXR1	Oxidation resistance-1	Oxidoreductase activity	Nucleus, cytosol, mitochondrion	18609	31.3	5.07	3.0
DAXX	Death domain associated protein	Apoptosis modulator/transcriptional repressor	Nucleus, cytosol	15758	37.1	4.95	4.1
PDZD3	PDZ domain containing-3	Protein C terminus binding/ guanylate cyclase inhibitor activity	Nucleus, PM	15062	12.3	4.92	3.4
RHBDF1	Rhomboid 5, homolog-1	Regulates secretion of eGFR associated ligands	ER, GA	13474	73.4	4.84	10
CYB5R3	Cytochrome B5 reductase-3	Fatty acid regulator, cholesterol biosynthesis, methemoglobin reduction	Mitochondrion, cytosol, ER	10288	6.8	4.64	1.6
SMARCC1	SWI/SNF related, matrix associated, actin dependent regulator of chromatin subfamily c, member 1	Transcription activation/repression of select genes by chromatin remodelling	Nucleus	9358	10.8	4.56	1.4
TRIM16	Tripartite motif containing-16	Tumour suppressor, nucleic acid binding, NACHT domain binding	Nucleus, cytosol, PM	8825	5.8	4.52	1.4
TRAPPC12	Trafficking protein particle complex-12	Component of TRAPP complex – ER to GA protein trafficking	Nucleus, cytosol	5154	70.6	4.12	4.4
CNNM1	Cyclin and CBS domain divalent metal cation transport mediator-1	Copper/metal binding activity	PM	4906	5.1	4.09	0.8
FAM53C	Family with sequence similarity 53, member C	Bind to transcriptional regulators modulating cellular proliferation	Nucleus, cytosol	4580	4.9	4.04	1.0
ZFP36L2	ZFP36 ring finger protein like-2	TF – regulates the response to growth factors	Nucleus	4163	17	3.96	3.2
SNX4	Sorting nexin-4	Involved in several stages of intracellular trafficking, EGFR binding	PM, cytoskeleton, endosome	3959	6.9	3.93	0.7
FAM131B	Family with sequence similarity 131 member B	Involved in oncogenic MAPK signalling, HIV life cycle	Nucleus, cytosol	3879	3.5	3.91	0.6
SART3	Squamous cell carcinoma antigen recognised by T-cells 3	RNA-binding nuclear protein, regulation of mRNA splicing	Nucleus	3764	3.8	3.89	0.6
CREB3L1	cAMP responsive element binding protein 3 like-1	TF – involved in the unfolded protein response	Nucleus, ER	3121	20.3	3.75	2.0

Table 13: Top 20 hits from the protein microarray for SchS patient 31.

The target, gene name, protein function & primary locations, sample fluorescence intensities, alongside the z-scores and i-scores are presented within the table.

EGFR: Epidermal growth factor receptor; ER: Endoplasmic reticulum; GA: Golgi apparatus; MAPK: mitogen-activated protein kinases; PM: Plasma membrane; TF: Transcription factor

Location

All hits shown in this table were unique to this sample. Eleven out of 20 top interactors are both nuclear and cytosolic, with two of these also found within the mitochondrion. Other proteins reside within the PM, cytoskeleton, ER, endosome and/or GA.

Function

The strongest hit was SRSF7, an RNA binding and splicing molecule forming part of the spliceosome with a nuclear location. Another splicing associated protein identified was SART3, though ranked towards the end of the top 20 hits. Coming second, UBL7 also has nuclear location and has been noted to be involved with bone-marrow stem cell differentiation. The third top hit was the adaptor CNKSR1, known to be involved with Ras signalling pathways. Coming fourth, OGFR encodes a growth factor receptor, and interestingly, two EGFR signalling related proteins were also identified: RHBDF1 and SNX4, playing roles in EGFR ligand signalling and EGFR binding respectively. Mainly situated in the mitochondria, PNPO and OXR1 both exhibit oxidoreductase activity, with the enzyme CYB5R3 being regulator of fatty acids and cholesterol biosynthesis. Where DAXX is noted to be a transcriptional repressor only, SMARCC1 is both a transcriptional activator and repressor acting through chromatin remodelling. FAM53C has been documented to bind to transcriptional regulators, modulating cellular proliferation. PDZD3 binds proteins at their C-terminal, with additional guanylate cyclase inhibitor activity. TRIM16, binding to the evolutionary conserved NACHT domains is a notable hit, given the role of NLRP3 in SchS. TRAPPC12 is an integral component of the TRAPP complex, the latter responsible for trafficking proteins from the ER to the GA. CNM1 was an interesting finding, known to have copper binding activity. FP36L2 and CREB3L1 were two TF's amongst the top hits, with the former regulating the response to growth factors and the latter transcribing genes associated with the unfolded protein response. FAM131B is known to play a role in oncogenic MAPK signalling.

Fluorescence, z-score + i-score

This sample had the highest sample intensities in comparison to the other five samples and therefore strongest interactions. The i-scores ranged between 0.6 and 29.4, with the highest score pertaining to the top hit (SRSF7) within this sample. Not only is this elevated value obtained reflective of the strong protein interaction, but this can also be attributed to the slightly weaker anti-GST staining obtained with this array spot, thus affecting the overall i-score calculation.

4.3.2.4 Sample WM-1

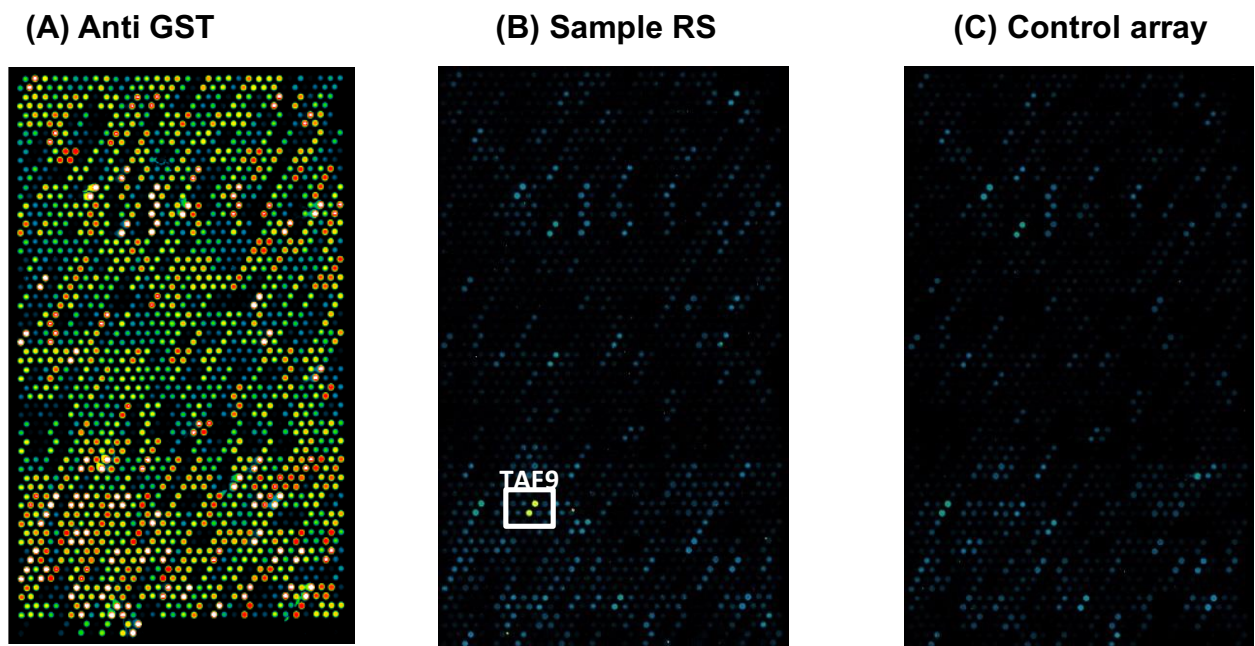


Figure 40: Array visualisation for WM-1.

With a specific focus on subarray 8, Figure 44A illustrates anti-GST staining showing protein locations within the subarray. Figure 44B is the anti-IgM staining showing strong reactivity towards TAF9 – which is absent in 44C - the negative control array incubated with secondary antibodies only.

Target	Gene name	Functionality	Location(s)	Sample – control	Sample/ control	z-score	i-score
TAF9	TATA-box binding protein associated factor 9	Transcriptional activation and repression	Nucleus	11128	8.4	4.04	4.1
FAM175B	Family with sequence similarity 175, member B	Protein metabolism, deubiquinating activity	Nucleus, cytosol	10558	10.8	4.01	2.5
TLL2	Tubulin tyrosine ligase like 2	Ligase activity – forms polyglutamate side chains on tubulin	Nucleus, ER, mitochondrion	10188	10.1	4.01	2.5
DHRS4	Dehydrogenase/reductase 4	Signalling receptor binding, oxidoreductase activity	Nucleus, cytosol, mitochondrion, peroxisome, ER	6958	6	3.69	1.8
MRPL1	Mitochondrial ribosomal protein L1	Structural component of mitochondrial ribosomes	Mitochondrion	6828	8.3	3.68	2.3
EXOC3	Exocyst complex component 3	Component of the exocyst complex – docks exocytic vesicles on the PM	Cytosol, GA, PM	5972	5.8	3.58	2.0
GAPDHS	Glyceraldehyde-3-phosphate dehydrogenase, spermatogenic	Involved in carbohydrate metabolism during spermatogenesis	Cytosol	4546	5.1	3.38	1.3
TMPRSS12	Transmembrane protease, serine 12	Serine type endopeptidase activity	PM	4346	10.8	3.35	4.8
RAD51	RAD51 recombinase	Assists in the repair of double-stranded DNA breaks	Nucleus, mitochondrion	4230	7.2	3.32	4.9
TOLLIP	Toll-interacting protein	IL-1R trafficking, ubiquitin binding, interacts with TLR signaling cascade components	Cytosol, lysosome, PM	3880	8.2	3.26	2.8
MTPAP	Mitochondrial poly(A) polymerase	Synthesises the 3' poly(A) tail of mitochondrial transcripts, involved in mRNA degradation	Mitochondrion, cytosol	3832	8.5	3.25	5.3
TPMT	Thiopurine S-methyltransferase	Catalyses S-methylation of thiopurine drugs	Cytosol	3223	6.1	3.12	1.1
NXF2	Nuclear RNA export factor 2	Export of mRNA and association with the nuclear envelope	Nucleus, cytosol	2920	10	3.05	6.3
RGS18	Regulator of G protein signalling 18	Attenuates signaling of G proteins	Cytosol, PM	2760	6.1	3.01	1.3
MIC13	Micos complex subunit 13	Component of MICOS complex – within the inner mitochondrial membrane	Nucleus, mitochondrion	2772	5.3	3.01	1.6
C17orf64	Chromosome 17 open reading frame 64	Uncharacterised	/	2740	7.6	3.00	1.9
VGLL4	Vestigial like family member 4	Co-activator of transcription-enhancer factor	Nucleus	2712	4.1	2.99	0.9
NDOR1	NADPH dependent diflavin oxidoreductase 1	NADPH reductase – oxidoreductase activity	Nucleus, cytosol, cytoskeleton	2675	3.0	2.98	0.4
AGTR1	Angiotensin II receptor type 1	Receptor for the vasopressor hormone, angiotensin II	PM	2580	16.7	2.95	7.4
USP2	Ubiquitin specific peptidase 2	Enzyme required for TNF- induced NF-κB signalling	Nucleus, cytosol	2515	120.8	2.94	143.7

Table 14: Top 20 hits from the protein microarray for sample WM-1.

The target, gene name, protein function & primary locations, sample fluorescence intensities, alongside the z-scores and i-scores are presented within the table. ER: Endoplasmic reticulum; GA: Golgi apparatus; PM: Plasma membrane.

Location

All interactions within the table are unique to this sample with nine out of the top 20 interactors reported to be located within the nucleus, and six also mitochondrial associated. The remaining proteins reside within the cytosol, cytoskeleton, ER, GA and/or PM, with two reported to also be found within the lysosome and peroxisome.

Function

Notably, the two WM patients did not share any of the top proteins found on the array. TAF9 presented as the chief hit in this dataset, a transcriptional activator and repressor, reported to bind and potentially activate NF- κ B and interestingly, the IL-1R and TLR interactor, TOLLIP was amongst the top proteins. The latter protein plays an important adaptive role in AI disease signalling cascades associated with MYD88. Both FAM175B (2nd top hit) and USP2 demonstrate deubiquitinating activity with the third interactor being TTLL2, an enzyme with ligase activity related to tubulin. Other enzymes include DHRS4 and NDOR1, exhibiting oxidoreductase activity. Associated with mitochondria, MRPL1 is a structural component of mitochondrial ribosomes, whereas MIC13 forms part of the MICOS complex located within the inner mitochondrial membrane. MTPAP primarily functions to generate the 3' end poly (A) tail of mitochondrial transcripts, but can also be involved with mRNA degradation. The four PM located proteins were (1) EXOC3 – involved in exocyst vesicle docking; (2) TMPRSS12 – with serine type endopeptidase activity; (3) RGS18 – halting G-protein signalling and (4) AGTR1 – the angiotensin II receptor. Unusually, TPMT is an enzyme responsible for the breaking down of thiopurine-containing drugs. An example of the latter drug is methotrexate, a chemotherapeutic which can be prescribed for WM.

Although TFs are present in the other five samples, none were found within the top 20 of WM-1, although TAF9 and VGLL4 are known to play roles in transcriptional activation. Other hits included the DNA repair enzyme – RAD51; GAPDHS, involved in spermatogenesis metabolism, and NXF2 involved in mRNA export. C17orf64 was within the top 20 but is a protein yet to be characterised.

Fluorescence, i-score and z-score

This sample demonstrated fluorescence activity comparable to SchS-2 and SchS-23. Though higher than the other WM sample and NLRP3-AID-7, this sample showed a reduced intensity in comparison to SchS-31. The i-scores varied between 0.4 to an elevated 143.7. Though the latter value can be regarded as another indicator of strong protein-protein binding, this skewed value is likely due to the extremely weak GST staining intensity in comparison to the average intensity found within these samples.

4.3.2.5 Sample WM-2

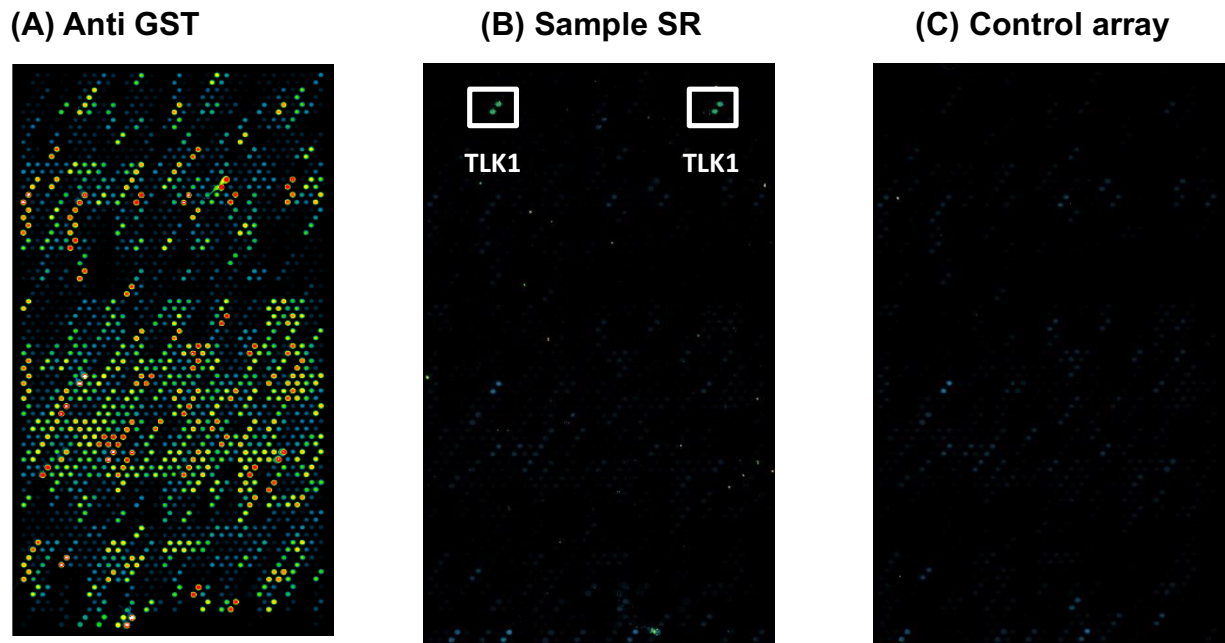


Figure 41: Array visualisation for WM-2.

With a specific focus on subarray 24, Figure 45A is representative of anti-GST staining showing protein locations within the subarray. Figure 45B indicates anti-IgM staining showing strong reactivity towards TLK1 (2 different clones) – which is absent in 45C - the negative control array incubated with secondary antibodies only.

Target	Gene name	Functionality	Location(s)	Sample – control	Sample/c control	z-score	i-score
TLK1	Tousled like kinase-1	Serine-threonine kinase involved in chromatin regulation assembly	Nucleus	3652	14	4.59	2.8
FBXO2	F-box protein 2	Substrate of an E3 ubiquitin ligase complex	ER	3339	4.7	4.53	0.9
ATF1	Activating transcription factor-1	TF- regulating cell growth and survival genes	Nucleus	2376	15.8	4.26	1.7
DPP10	Dipeptidyl peptidase like 10	Potassium channel regulator	PM, GA	2194	17.4	4.20	2.2
PNMA1	PNMA family member-1	Neuronal specific protein	Nucleus	1730	4.4	4.01	0.7
ZNF384	Zinc finger protein-384	TF – binds and regulates promoters of extracellular matrix genes	Nucleus	1454	11.7	3.87	1.3
NR6A1	Nuclear receptor subfamily 6 group A member 1	Hormone receptor – involved in neurogenesis and germ cell development	Nucleus	1410	17.6	3.85	4.0
MLX	MLX, MAX dimerisation protein	TF - Involved in transcriptional regulation – cellular proliferation and differentiation	Nucleus	1388	4.3	3.84	0.4
SSH3	Slingshot protein phosphatase-3	Protein phosphatase – regulator of actin filament dynamics	Nucleus, cytoskeleton	1395	3.8	3.84	0.4
EDC4	Enhancer of mRNA decapping-4	mRNA decapping	Nucleus, cytosol	1359	6.4	3.82	0.7
THRA	Thyroid hormone receptor alpha	Hormone receptor for the thyroid hormone	Nucleus, cytosol	1318	13.4	3.79	2.0
LHX5	LIM homeobox 5	Regulator of neuronal differentiation and migration during development of the CNS	Nucleus	1244	9.0	3.75	2.2
NR2E1	Nuclear receptor subfamily 2, group E, member 1	Receptor involved in retinal development	Nucleus	1158	6.2	3.70	4.4
Onecut1	One cut homeobox-1	Transcriptional activator, particularly of liver-associated genes	Nucleus	1158	26.2	3.70	3.6
ATF7	Activating transcription factor-7	TF – binds the cAMP responsive element	Nucleus	1127	3.9	3.67	0.3
BARX1	BARX homeobox -1	TF – craniofacial development and stomach organogenesis	Nucleus	1078	2.1	3.64	0.3
CREM	cAMP responsive element modulator	TF binding to cAMP responsive element	Nucleus	1050	10.7	3.62	0.8
NOP56	NOP56 ribonucleoprotein	Involved with the initial 60S ribosomal subunit stage synthesis and with small nucleolar RNA synthesis	Nucleus	1004	11	3.58	1.6
CREB1	cAMP responsive element binding protein-1	Binds the cAMP response element, stimulating transcription	Nucleus	979	15.4	3.57	1.5
SOX8	SRY-box 8	TF – embryonic development and cell fate determination	Nucleus	952	7.9	3.54	0.6

Table 15: Top 20 hits from the protein microarray for sample WM-2.

The target, gene name, protein function & primary locations, sample fluorescence intensities, alongside the z-scores and i-scores are presented within the table. cAMP: Cyclic adenosine monophosphate; ER: Endoplasmic reticulum; GA: Golgi apparatus; PM: Plasma membrane; TF: Transcription factor

Location

Eighteen out of the 20 hits are nuclear, with two of these proteins also found within the cytosol. The other two interactors were located within the ER (FBXO2), alongside DPP10 located both in the GA and PM. This sample shares nine hits with SchS-2 and a further five hits with both SchS-2 and WM-2.

Function

The basic functions of the five overlapping proteins seen in this dataset with SchS-2 and SchS-23 have been outlined in the abovementioned sections (ATF1, MLX, TLK1, DPP10 and SSH3). These proteins were found within the top 10 hits of this sample. WM-2 IgM uniquely bound proteins associated with organ development. Two of these were the transcription factors BARX1 and SOX8; the transcriptional activators oncut1 and CREB1; alongside the RNA synthesis protein NOP56 and the neuronal specific protein, PNMA1.

Fluorescence, i-score and z-score

This sample exhibited reduced fluorescence intensities when compared to SchS-2, 23, 31 and WM-1, but comparable to those values sought in NLRP3-AID-7. Nevertheless, the i-scores were in the range of 0.4 to 4.4 with the z-scores above 3.54, confirming the accuracy of the top interactions documented.

4.3.2.6 Sample NLRP3-AID - 7

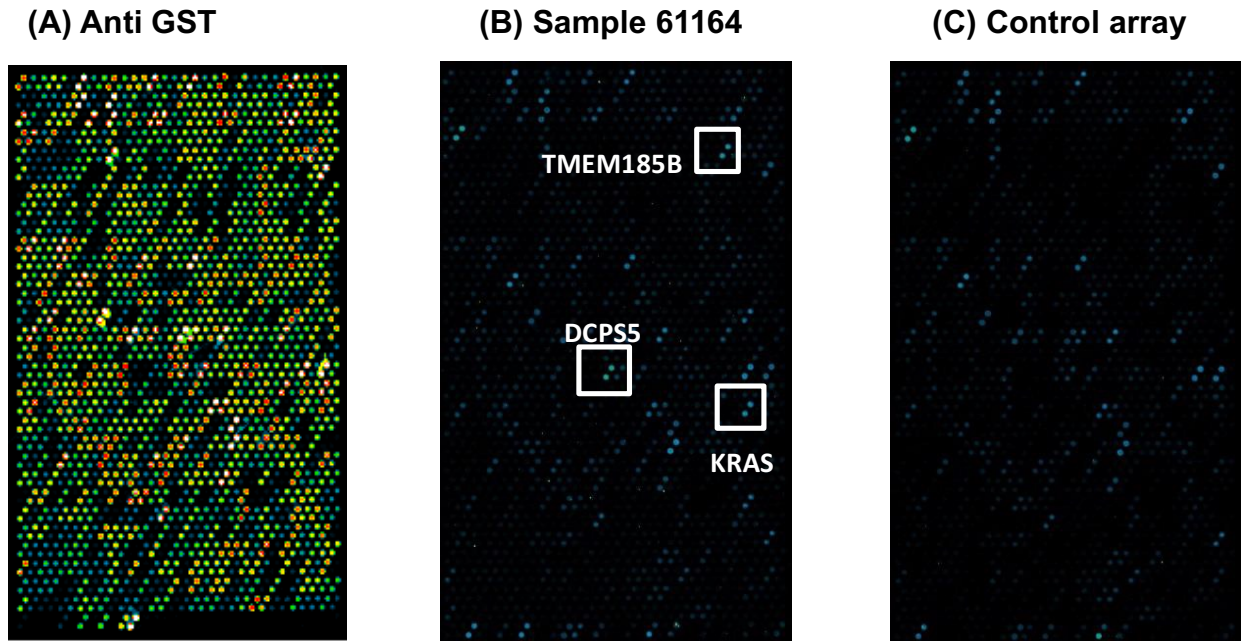


Figure 42: Array visualisation for NLRP3-AID patient 7.

With a specific focus on subarray 15, Figure 46A represents anti-GST staining showing protein locations within the subarray. Figure 46B indicates anti-IgM staining showing strong reactivity with TMEM185B, DCPS5 & KRAS – which is absent in 46C - the negative control array incubated with secondary antibodies only.

Target	Gene name	Functionality	Location(s)	Sample-control	Sample/control	z-score	i-score
DCPS	Decapping enzyme, scavenger	mRNA decapping enzyme	Nucleus, cytosol, mitochondrion	3062	5.8	4.16	0.8
DDIAS	DNA-damage induced apoptosis suppressor	Anti-apoptotic protein involved in DNA repair/cell cycle networks	Nucleus	2767	3.8	4.06	0.5
GTF3C3	General transcription factor IIIC subunit-3	TF - Recruitment of RNA polymerase III	Nucleus	2706	4.2	4.04	0.4
NINJ1	Ninjurin-1	Cell adhesion protein with axonal growth roles	PM	2343	3.2	3.89	1.4
KRAS	KRAS proto-oncogene, GTPase	GTPase activity, regulation of cell proliferation, silencing of tumour suppressing genes	Cytosol, PM	1996	7.7	3.73	1.2
TMEM185B	Transmembrane protein 185B	Unknown	PM	1946	6.2	3.70	1.3
RHOD	Ras homolog family member D	Involved in endosome dynamics and actin cytoskeleton reorganisation	Cytosol, endosome, PM	1907	13.1	3.68	1.1
TMEM243	Transmembrane protein-243	Unknown	Perioxosome, PM	1698	4.5	3.56	0.6
AQP5	Aquaporin 5	Water channel	PM	1580	4.9	3.49	1.1
RND2	Rho family GTPase-2	Actin cytoskeleton organisation, specifically in neuronal and hepatic networks	Cytosol, cytoskeleton	1449	4.2	3.40	0.7
PMAIP1	PMA induced protein-1	Promotes activation of caspases and apoptosis	Nucleus, cytosol, mitochondrion	1408	3.8	3.37	0.5
POTEB	POTE Ankyrin domain family member B	Intracellular signalling and protein-protein interaction	Cytosol, PM*	1406	5.7	3.37	1.7
RHOG	Ras homolog family member G	Actin cytoskeleton arrangement, cell migration	Cytosol, ER, PM	1261	3.2	3.26	0.3
PRRG2	Proline rich and GLA domain-2	Transmembrane protein, involved in calcium binding	PM	1249	3.9	3.25	1.0
RND1	Rho family GTPase-1	Actin cytoskeleton arrangement	Cytosol, cytoskeleton, PM	1173	3.2	3.19	0.6
EDIL3	EGF-like repeats and discoidin domains-3	Integrin ligand – mediates endothelial cell adhesion	PM	1172	3.6	3.18	0.9
SFT2D2	SFT2 domain containing-2	Involved with the fusion of endocytic transport vesicles to the GA	Endosome, GA	1162	3.3	3.18	0.7
ING3	Inhibitor of growth family member-3	Tumour suppressor – inhibits cell growth and induces apoptosis	Nucleus, cytosol	1083	5.5	3.11	0.5
ACP6	Acid phosphatase 6, lysophosphatidic	Hydrolyses lysophosphatidic acid	Mitochondrion	1078	2.8	3.1	0.4
ORAI3	ORAI calcium release activated calcium modulator-3	Calcium channel regulator	Cytosol, PM	1062	3	3.08	0.5

Table 16: Top 20 hits from the protein microarray for sample NLRP3-AID 7.

The target, gene name, protein function & primary locations, sample fluorescence intensities, alongside the z-scores and i-scores are presented within the table. *likely to be based on function – not confirmed.

ER: Endoplasmic reticulum; GA: Golgi apparatus; PM: Plasma membrane; TF: Transcription factor

Location

All hits were exclusive to this sample. Five out of 20 protein hits were reported to be nuclear, with the majority located within the cytosol or components within the cytoplasm. Interestingly, three proteins are located within the mitochondrion, but a majority reside within the cytosol/and or PM. These results are in contrast to B2, whereby 90% of the top 20 interactors were primarily located in the nucleus.

Function

The top hit in this sample was DCPS, an enzyme necessary for the complete degradation of mRNA, closely followed by DDIAS - an anti-apoptotic protein involved in DNA repair and cell cycle networks. The latter interaction is contrasted by ING3 and PMAIP1 findings, both having roles in the induction of apoptosis. GTF3C3 was the only TF associated protein within this set of interactors. This is in contrast to the other five samples, where at least over 80% were TF's. The fourth top protein was NINJ1, understood to be a cell adhesion molecule. Interestingly, EDIL3, another significant hit, has a similar role and is known as an integrin ligand. There are several recurrent hits on families of GTPases or GTP binding proteins: KRAS, RHOD, RND2, RHOG, RND1, (in order of significant interactions), suggesting linkage to signal transduction and cell signalling. Intriguingly, ORAI3 and PRRG2 are play roles in regulating calcium binding and transport. Among the other principle interactions were AQP5 – a water channel, POTEB – playing a role within intracellular signalling, SFT2D2 – involved in vesicle transport to the GA and ACP6, an enzyme known to hydrolyse lysophosphatidic acid. Two of the identified transmembrane proteins, TMEM185B and TMEM243, have unknown protein function.

Fluorescence, z-score + i-score

The serum IgM obtained from this sample demonstrated the lowest fluorescent intensities in evaluation with the other five samples tested. This is an unsurprising observation given that NLRP3-AID is not an IgM-associated disorder and therefore the low affinity of IgM can also be reflected in these antigen binding reduced fluorescent values. Nonetheless, the i-score values were between 0.3 to 1.7, the z-score values obtained for each interaction all above 3.08 and with the three top interactors all having z-scores above 4.0, indicating the high likelihood of IgM-antigen interface.

4.3.3 Shared protein targets

The top 20 hits found within samples SchS-31, NLRP3-AID-7 and WM-1 are exclusive to each patient; whereas SchS-2, SchS-23 and WM-2 share common targets. Figure 47 provides an overview of shared protein targets with considerations of the hits for each sample reviewed individually in Section 4.3.2.

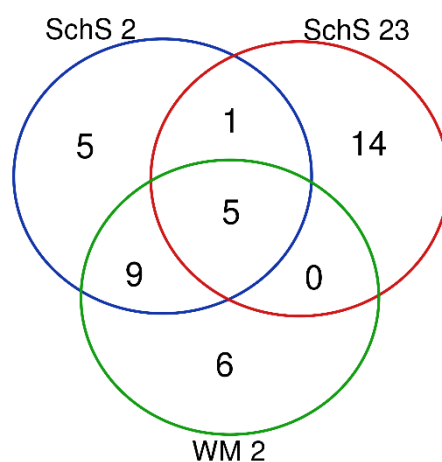


Figure 43: Overlapping IgM targets.

Three out of the six samples tested for IgM binding had shared hits and these results are further depicted as a Venn diagram above.

Nine antigenic targets were exclusively shared between WM-2 and SchS-2, one between SchS-2 and SchS-23, but none were unique to both WM-2 and SchS-23. ATF-1 (transcription factor), MLX (transcription), TLK-1 (chromatin assembly), DPP10 (peptidase) and SSH3 (protein phosphatase) are the five proteins which bound serum IgM from SchS-2, SchS-23 and WM-2. Whilst the overarching function of the aforementioned proteins could be broadly linked to cellular growth and pro-survival, their disparate functions and intracellular locations essentially indicate they don't belong to a specific pathway or collectively serve a combined purpose. Considerably, the observation of shared antigenic targets underscores the potential of related IgM properties amongst SchS-2, SchS-23 and WM-2.

4.4 Discussion

The work described in this chapter isolated the IgM from individuals with SchS, NLRP3-AID, WM and HCs, in order to explore the idea that the IgM paraprotein produced by SchS patients differs to IgM generated by other control groups in view of its preferential binding capacity to a select group of proteins.

To summarise, the main outcomes and findings in this chapter were:

- i. Serum IgM was effectively isolated from two HCs, three SchS patients, two WM patients and one NLRP3-AID patient
- ii. SchS IgM appears to bind to mainly intracellular targets
- iii. Shared hits were seen between two SchS patients and one WM patient

4.4.1 IgM isolation from serum

In order to investigate the activity of the monoclonal component characteristic of SchS, purification of such antibodies from serum was therefore necessary. Employment of the FPLC based AKTA Pure system in union with IgM HiTrap™ column enabled antibody isolation. Despite high levels of the monoclonal component in the serum of SchS and WM patients, this was not reflected in the quantity of isolated protein in comparison to the other samples where paraproteinaemia is uncharacteristic. This observation could highlight ligand saturation within the column but also the fact that partial loss of material occurred during the washing steps. Nevertheless, the resulting antibody fractions obtained required approximately a 40 fold dilution for protein microarray application (Section 4.2.2).

The clonal population of B cells responsible for SchS paraproteinaemia is yet to be characterised, thus simply isolating the monoclonal component poses a challenge. It is therefore imperative to consider the fractions garnered through the described isolation methodology comprise of both the monoclonal component and generally produced IgM. Regardless, even a limited part of the clonal IgM repertoire directed at a specific antigen should theoretically be discernible on the protein microarray.

4.4.1.1 Protein microarray

All patient samples were suitable for HuProt™ analysis with no background observed and showed a moderate strength of microarray spot interaction as indicated by the z-scores and i-scores, with the exception of SchS-31 demonstrating strong binding. As shown in Figure 38, the proteins immobilised on the array were tagged with GST, thus anti-GST staining on each of the microarrays served as a positive control. The negative control was a seventh slide, incubated with both the anti-GST antibody and anti-IgM antibody, lacking isolated IgM.

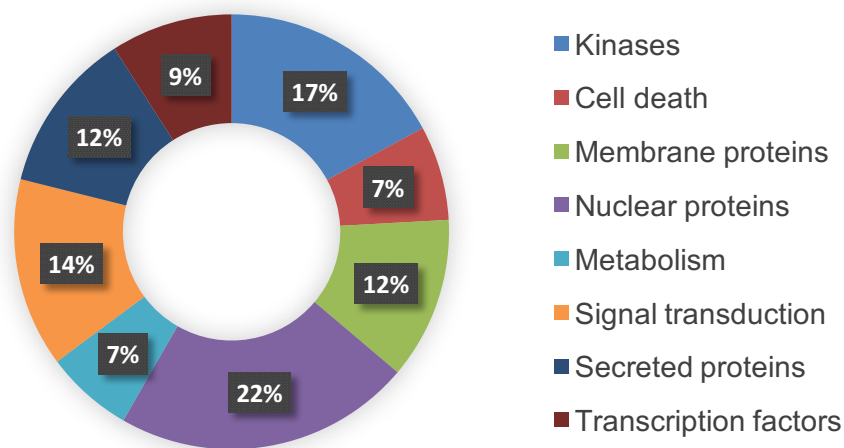


Figure 44: Percentage composition of proteins imprinted on the HuProt™ array slide.

The proteins comprised of kinases, cell death, membrane, nuclear, metabolism, transduction of signals, secretory and transcription factor categories.

WM patients together with the SchS patients found over 90% of their top 20 hits as nuclear, whereas NLRP3-AID-IgM was directed towards both nuclear and PM associated proteins. A significant proportion of these intracellular targets included transcription factors and transcriptional activators; regulators of chromatin and RNA related proteins. In contrast, extracellular antigens were largely absent with all samples. Given the inability of IgM to penetrate the cell, presence of these targets extracellularly is therefore assumed and therefore implies cellular release of contents into the milieu. Alternatively, the interactions noted could refer to the humoral immune response in generating a low affinity IgM with broad range specificity (298). Nevertheless, the shared targets seen within SchS-2, SchS-23 and WM-2 indicates that there is a similarity in the IgM binding properties and given the 15,700 proteins

probed, it is unlikely that these findings are merely coincidental. Whether SchS and WM share resemblance within their antibody repertoires is experimentally addressed in the following results chapter.

4.4.1.2 Autoimmune-related hits

The presence of a few proteins in this data that are also targeted by autoantibodies in several autoimmune conditions could indicate that the paraprotein generated in SchS and WM bears a predisposition to recognising self-proteins as antigenic targets. Given that autoinflammatory syndromes rarely present with paraproteinaemia, attempting to functionally characterise the overabundant IgM based on shared mechanisms is rather challenging. Nevertheless, there is a broader range of literature comprehensively describing autoantigens found in autoimmunity-related conditions. Therefore, the following section highlights microarray hits of particular interest found in this work that are known autoantigens in autoimmune disorders. Comparison of autoantibody targets generated in SLE for example, to those found in autoinflammatory and haematological diseases may underscore the shared characteristics of the clonal components produced and indicate the aspects triggering antibody production towards such proteins. Notably, the hits described were solely within SchS and were found unique to each sample (aside from H2AFY found in two samples).

The strongest interaction seen in the entire dataset was that observed between SchS-31 and SRSF7, an RNA binding and splicing molecule. This protein forms part of the nuclear 'spliceosome' with literature reporting this as an autoantigen in MS (191, 299). Around 30% of SLE patients demonstrate activity against several other spliceosome components (known as Sm antigens) (300, 301), with other research linking these interactions to kidney damage (302). HIV and antigenic components of EBV (EBNA-1 and EBNA-2) have shown strong capability of inducing autoantibody production against Sm antigens (303, 304), though this unlikely to be the scenario for patient SchS-31 given the absence of the latter viruses. Another RNA splicing molecule SART3, was another top hit in SchS-31. Interestingly, IgG auto-abs against other members of the SART family have been distinguished in atopic dermatitis (305), a condition linked to autoimmunity. Given the dermal manifestations of SchS (NUD),

Located within the nuclear envelope, the opioid growth factor receptor (OGFR) was the fourth hit in SchS-31. Clinically, blockade of the pathway through low doses of Naltrexone results in increased enkephalin levels of patients associated with an improvement in clinical symptoms such as fatigue and decreased motor activity. These observations are seen in several autoimmune diseases such as Crohn's (306), fibromyalgia (307), and Multiple Sclerosis (MS) (308, 309).

Both H2AFY and COL4A5 are known auto-antigens in SLE (310, 311). Whilst the histone H2AFY was the top interactor with SchS-23, COL4A5 reacted more weakly within this sample. SchS-2 also demonstrated interaction with H2AFY though to a lower intensity relative to SchS-23 and signifies the only shared hit amongst SchS. Anti-histone antibodies are directed to the transcriptionally inactive chromatin and are predominantly found in 95% of patients with drug induced SLE (312). The aforementioned antibodies can also be found in other autoimmune rheumatic diseases such as Scleroderma and RA and also discovered upon chronic EBV infection (313). The other notable hit was COL4A5, seen with SchS-23 only. This subunit forms the collagen IV protein (COL4), important for the cellular structure of basement membranes. Whilst denatured COL4 is a noted auto-antigen in RA, Scleroderma, and SLE (314, 315), this protein is the sole target protein implicated in the autoimmune Goodpasture's syndrome (GPS), manifesting in kidney and pulmonary damage (311). Whilst the latter occurrence is not documented in SchS, there have been various kidney complications such as glomerulonephritis and diffuse tubulointerstitial nephritis in five SchS patients (50, 54). The development of histone autoantibodies is linked to drug induced SLE and also polyoma virus infection (316), but the aetiology of COL4 autoantibodies remains obscure – likewise to the monoclonal component seen in SchS and WM.

Evidently, these observed autoimmune related hits are unique to the SchS samples but are also found in both common and rare autoimmune conditions. Based on these descriptions, previous exposure to viral proteins or environmental components bearing unknown motifs may predispose to a heightened immune response is a credible supposition to suggest. Subsequent misidentification of numerous self-peptides as foreign by the already precarious immune repertoire may render the generation of a monoclonal component with a wide-ranging antigen binding capacity.

4.4.1.3 Link to clonal entities and autoinflammatory manifestations

Papers have reported WM-IgM exhibiting anti heparin activity (317), and against mixed cryoglobulins with high titre rheumatoid factor (318). Other research has established a proportion of WM-IgM directed at polysaccharides, lipids and DNA (319), thus akin to SchS and from the results in this work, the WM monoclonal component does not preferentially bind a common antigen. Another study also looking into the immunological properties of the paraproteinaemia produced in both MGUS and MM also found no universal hits. Screening of 115 patient sera with cDNA libraries originating from human tissues, found one IgA monoclonal component bound to sperm specific cyclin 2, with another three patients IgG binding to either TPP2, IGFBP2 or porcine kinesin. Arguably and likewise to this study, isolation of the monoclonal component was not carried out and the total antibody repertoires

were exposed, thus the interactions noted may not represent the correct antigenic target. Nevertheless, the absence of a common antigen largely indicates that the monoclonal components derived from MGUS, MM, WM and SchS lack functional antigen binding properties (188, 319). Hence in view of the results presented in this chapter, the function of the IgM paraprotein remains unclear with regards to SchS pathobiology. This is in opposition to autoimmune diseases such as RA where generation of antibodies of IgM, IgG and IgA isotypes against citrullinated proteins contribute to bone destruction and are considered biomarkers of disease (320).

IgM was isolated from sera at one time point, with the biologically significant SchS monoclonal component isolated alongside other IgM present in the serum. The latter aspect is an imperative detail to consider with regards to target specificity as 15% of serum antibodies are IgM type, and the proportion of clonally derived IgM is unknown. Though intriguingly, the top 20 hits for each sample principally pertained to proteins located intracellularly and considering the relatively size of IgM (>900kDa), its infiltration into cells is highly unlikely. As SchS is an auto-inflammatory condition, intracellular protein contact with the monoclonal component could be achieved through pyroptosis. Although complete disease remission with IL-1 blockade is achieved in a majority of SchS patients, a persistent level of baseline inflammation still exists (i.e. significantly higher levels of ASC specks – Results Chapter 2). Thus, continual inflammasome activation substantiates the latter proposition and could further suggest that SchS IgM may not be biologically relevant in the disease mechanism – but instead, a by-product of pyroptosis.

Speculation as to whether the monoclonal component produced is a consequence of inflammation manifestations or formed as part of the disease presentation remains unknown. Even though SchS patients demonstrate chronic stimulation as evidenced through pro inflammatory manifestations, the broad range of interacting antigens renders the hypothesised 'pathogenic' role of SchS-IgM unlikely. Rather, an already biased IgH repertoire exposed to a broad spectrum of cell debris as a consequence of pyroptosis characterises a more fitting theory in view of the paraproteinaemia. Granted the remarkable response of anti-IL-1 therapy in SchS patients sustaining reduced autoinflammation, a degree of autonomous inflammation is likely to still exist (321), supporting IgM overproduction through presentation of non-specific antigens. Further speculation that an already hyper-inflammatory environment exposed to exogenous antigens (i.e. bacteria) not necessarily pathogenic, may also result in persistence of the monoclonal response. Although IgM levels and SchS disease activity do not immediately correlate, observations that the former levels increase by 1g/L may be attributed to the above speculations.

4.4.2 Chapter conclusions

The identification of IgM targets was achievable by taking advantage of FPLC techniques facilitating the isolation of IgM from serum samples and subsequent application onto a protein microarray. The predominance of nuclear located targets of SchS-IgM and WM as opposed to NLRP3-AID IgM is noteworthy. Access of the Ig to these intracellular proteins through autoinflammatory-mediated cell death (pyroptosis) is one plausible explanation considering the pivotal role of NLRP3, ASC specks and IL-1 in the pathogenesis behind SchS (Results Chapter 2). Furthermore, the levels of IgM witnessed in SchS patients remain the same as upon diagnosis or elevate over the course of disease, despite IL-1 inhibition. Though the blockade of IL-1 successfully abrogates the inflammatory symptoms phenotypically, the results of this thesis could lead to the hypothesis that baseline levels of inflammation caused by inflammasome activation in innate immunity related cells such as neutrophils, leading to pyroptosis stimulates the continual production of IgM from B cells. The absence of inflammatory symptoms in WM renders applicability of aforesaid supposition to WM questionable.

In view of these results and the fact that clonal evolution to haematological malignancy is an outcome in 20% of SchS patients, it is therefore reasonable to propose that the paraprotein seen in both conditions share inherent features that may arise from Ig recombination. The investigations presented in the following results chapter explores this theory through sequencing of the IgH region to probe for genomic evidence of a clonal B-cell population – as found in WM.

Chapter 5 IgH sequencing

5.1 Introduction

The aim of the work presented in this chapter is to genetically investigate the hypothesis that a clonal population of B cells secreting elevated titres of monoclonal IgM contribute to the inflammatory phenotype seen within SchS. Identification of a shared B cell clone between SchS patients could suggest that the manifesting paraproteinaemia may bear the same antigenic property. Through next-generation sequencing of the IgH region, this chapter more specifically assesses the CDR3 region and VH usage dynamics of 10 SchS patients.

As a consequence of the V(D)J rearrangement events B cells, a vast degree of diversity is generated within the hypervariable CDR3 region. In the context of Igs, CDR3 loops are critical for antigenic binding, with various research papers discussing and employing the length and composition of said region to assess B cell clonality. For example, Kriangkum *et al* analysed the CDR3 region of 198 CLL cases to identify 26 patients who demonstrated evidence more than the usual one CDR3 clone detected in CLL, and followed these clones over the course of three to nine years to determine the degree of B cell expansion (322). Another study utilised the number of unique CDR3 sequences to gauge clonal characteristics of liver disease (323). Accordingly, this work investigates the length distribution and composition of both entire CDR3 repertoire and expanded CDR3 clones per sample.

The production of an identical Ig rearrangement is very rare at a 10^{-9} probability, underscoring the diminished likelihood of this event occurring at random, further emphasises this is not by chance (324). The exposure of individuals to a common antigen results in the formation of stereotyped CDR3 aa sequences (i.e. identical shared sequences), highlighting the increased degree of similarity generated by different immune repertoires (325). Evidence that malignant cells found in LPDs do not survive autonomously or *ex-vivo* further propagates the notion that clonal expansions are largely dependent on endogenous or exogenous antigenic stimulation (324). Clinically, the therapeutic efficacy of B cell receptor associated kinase antagonists such as spleen tyrosine kinase and Bruton's tyrosine kinase, underscores the latter postulation through hindrance of B cell signalling (324).

Whilst the phenomenon of detecting stereotyped receptors is imperative to those evaluating vaccination responses (i.e. influenza – (326)), in the context of chronic B cell LPDs, numerous studies show homologous heavy chain CDR3 aa sequences accounting for nearly 30% of CLL cohorts. Strongly inferring the role of antigen selection in the shaping of the expressed B cell repertoire, such antigens are postulated to be self or exogenous (327, 328).

The study of VDJ gene usage has been of tremendous interest, given the possibility that immune repertoires from certain lymphoproliferative conditions exhibit properties suggestive of presence of a clonal B cell population (329). Such characteristics include preference towards the usage of certain V, D and J gene families, usage of a particular one of these gene segments and/or specific V-J combinations perhaps utilised to higher degrees. In conditions where the pathogenic role of the monoclonal Ig is questionable, comparison of V gene usage may be helpful for documenting common antibody reactivity, as highlighted by Fermand *et al* (330).

5.1.1 Properties of the IgH region

The adaptive immune system yields a significant breadth of diversity by the generation of antigen-specific T-cell receptors and immunoglobulins (Igs). The diversity of an antibody is generated by recombination events between one of each of the following: 44 VH gene segments; 27 DH gene segments and 6 JH gene segments – ultimately coding for the CDR3 region of the Ig heavy chain region (IgH) responsible for antigen binding (Fab) (Figures 42 and 43). Removal or addition of non-templated and palindromic nucleotides within junctional regions in the recombination process, followed by further changes resulting from somatic hypermutation later in antibody development, increases the diversity within the antigen binding areas (331). For light chain production (IgL), the combinatorial process is identical except for the absence of light chain D gene segments. IgL is either of kappa or lambda subtype constructed from one V gene (out of 30-36 V genes) and one J gene (out of 4-5 J genes). Thus, the greater diversity of the IgH region allows for more detailed analyses (V, D and J genes) as opposed to IgL (V and J genes only). Due to the aforementioned process of somatic recombination and hypermutation, an estimated 10^{13} unique antibodies can be generated by an individual (329, 332).

Segment	Heavy chain	Light chain	
		K	λ
Variable (V)	38-46	31-36	29-33
Diversity (D)	27	0	0
Joining (J)	6	5	4-5

Table 17: Combinatorial diversity.

Antibody diversity is attributed to the different combinations of gene segments of both the heavy and light chain variable regions. Numbers of V, D and J gene segments are shown for each antigen receptor locus. Due to genetic polymorphism the numbers vary from individual to individual (333).

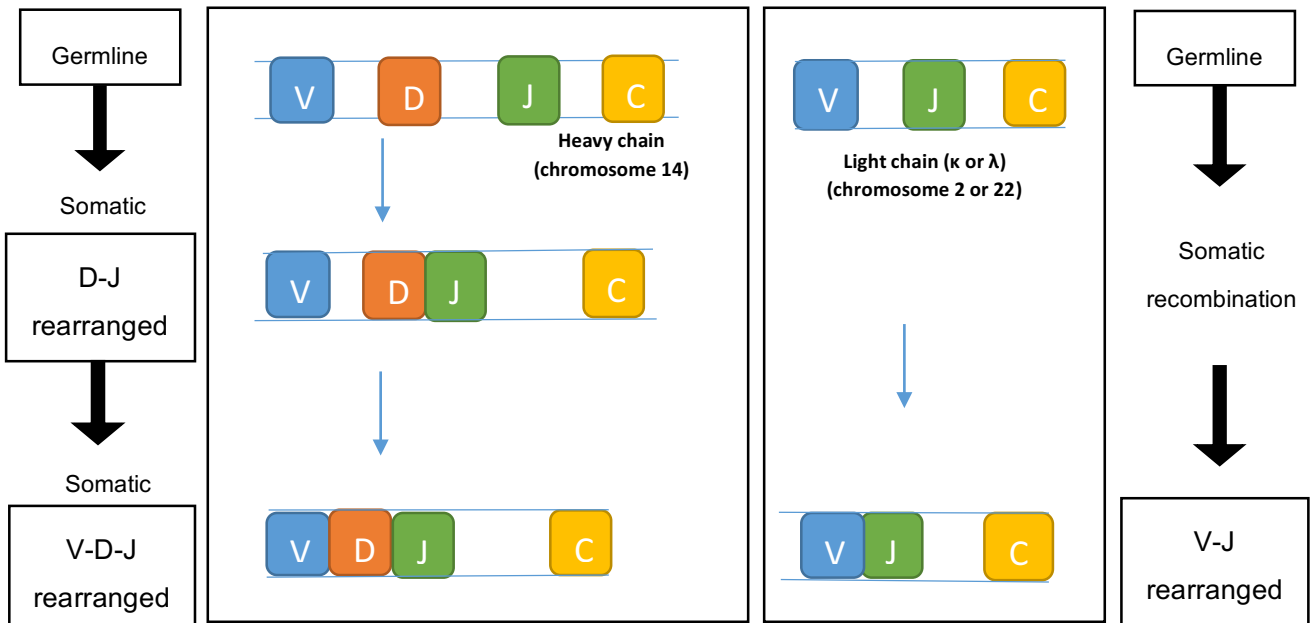


Figure 45: Overview of VDJ recombination.

The IgH locus is located on chromosome 14, and rearrangement of genes at this position initially starts with D-J recombination alongside the constant region, followed by V-DJ recombination. The IgL variable chain can either be of κ or λ subtype, with these loci positioned on chromosomes 2 and 22 respectively. Somatic recombination results in the formation of V-J rearranged DNA. Figure 45 adapted and recreated using references (332) and (333).

The diverse B-cell populations of healthy individuals permits the identification of broad ranges of foreign antigens, through the binding of B-cell receptors or secreted antibodies to antigenic epitopes. Following recognition, a strong, adaptive immune response is mounted, allowing the degradation and removal of the antigen. Within a B-cell, following successful VDJ (heavy chain) or VJ (light chain) recombination, the rearrangement machinery ceases to work and thus stops the potential production of a second functional heavy or light chain being generated from the alternate alleles. The latter phenomenon is known as allelic exclusion (334), and thus one B cell expresses one unique BCR (335).

Each B cell V(D)J rearrangement is unique, with an extremely low probability that the same sequence will be common to two unrelated cells (336). Hence, when identical sequences are detected, the clonal nature of the given population of B cells is demonstrated.

5.1.1.1 Complementarity-Determining and Framework regions

Complementarity determining regions (CDRs) form part of the antibody recognising and binding antigens in a cooperative manner (337). CDR1 and CDR2 are encoded by germline V segments for both heavy and light chains, but can be altered by somatic mutation. Contrastingly, CDR3 regions are created during V(D)J recombination and can also be subject to further somatic hypermutation (337, 338). The structural location of CDRs was initially resolved through the work of Chothia and Lesk (339, 340), with their findings further demonstrating that CDRs maintain limited sets of conformations due to particular aa residues at certain positions within the CDRs and their flanking framework regions (FRs). The four FRs are primarily known as the scaffolding beta-sheet peptides holding the CDRs in position, though demonstration that amino acid (aa) residues for antigenic contact can be located within the conserved FRs highlights the role this region plays for antibody affinity (341). Between the V-D and D-J gene segments (largely encoding CDR3), diversity is further achieved by the addition of palindromic and random nucleotides, or exonuclease mediated loss of nucleotides (342).

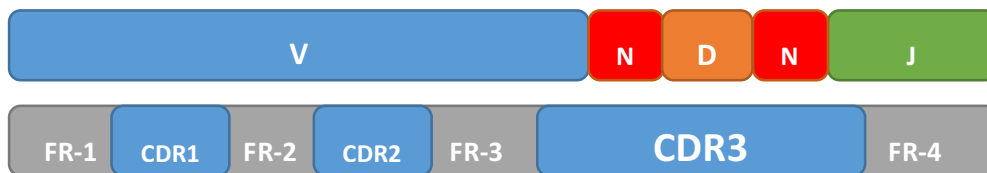


Figure 46: Generation of the antigen binding section an antibody from the IgH locus.

CDR1 and CDR2 are encoded by germline V gene segments, whereas CDR3 is encoded by the latter part of the V gene, the entire D gene and the former part of the J gene via somatic recombination. There are four framework regions (FR-1, FR-2, FR-3 and FR-4), mainly acting as a scaffold for the CDRs within an antibody. Diversity of the antigen receptor loci is further increased by the addition of non-templated nucleotides (N) between the junctional regions of the V, D and J genes. Figure 46 adapted and reconstructed using information from (343).

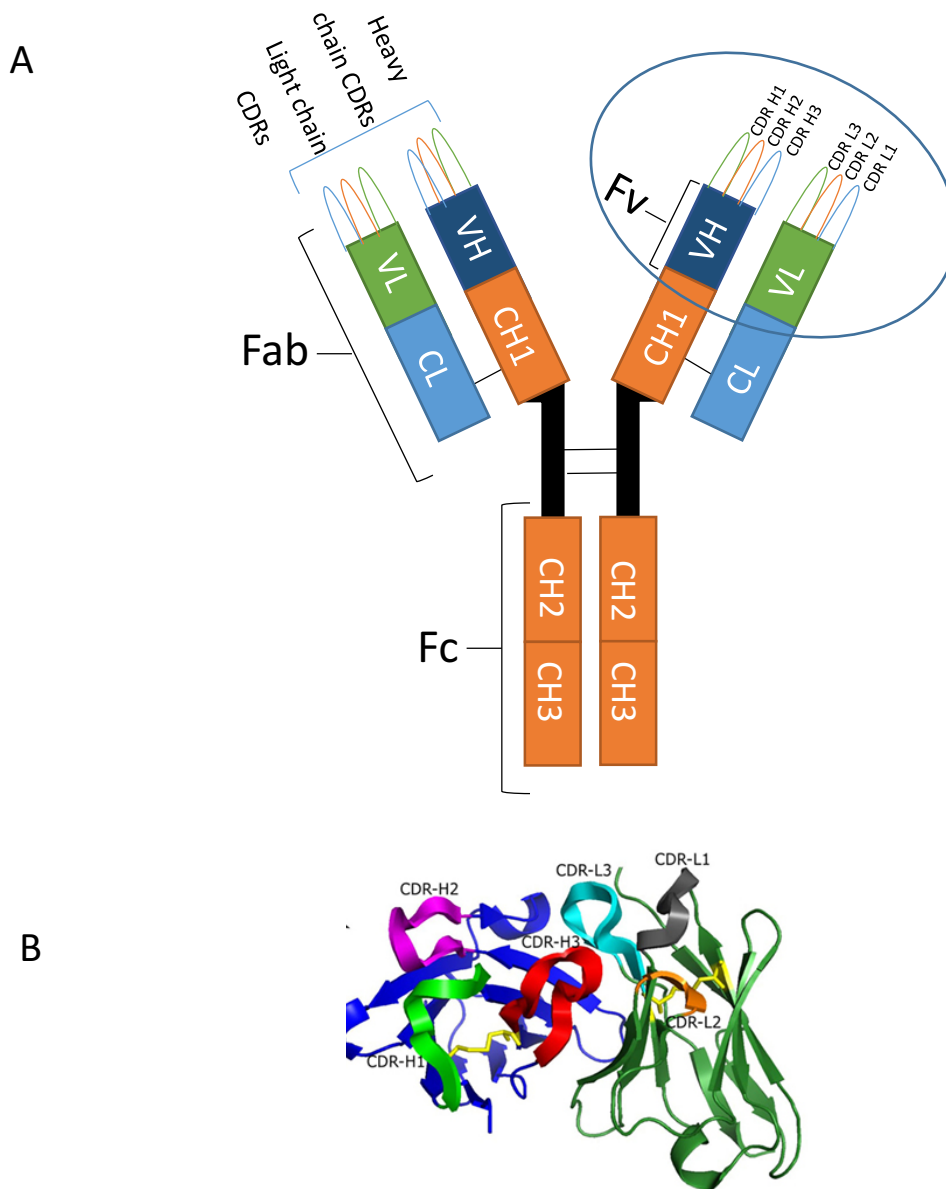


Figure 47: Basic structure of an antibody

(A) Antibodies comprise of two identical heavy chains and two identical light chains. The heavy and light chains are linked together by disulphide bond. There are two variable domains in the F(ab) region, VH and VL), responsible for antigen binding. The constant domains (CH1 – heavy chain) and (CL – light chain) are also within the Fab region. CH2 and CH3 make up the Fc region which act as mediators for the antibody activity.

(B) Each variable domain consists of 3 CDR regions (CDR1, CDR2, CDR3), thus each antibody consists of 12 hypervariable loops. The variable domains are folded in a way uniting the CDR hypervariable loops to form an antigen-binding site. Four conserved framework regions (FRs) flank these CDR regions. The heavy domains and light domains are linked together by a disulphide bond. Figure 47 created using the information from reference (344).

5.1.1.2 CDR3

Among the CDRs, the heavy chain CDR3 is recognised as the region bearing most variability, due to the fusion of V, (D) and J gene segments. Bagnara *et al* defined the heavy chain CDR3 to be the 'nucleotide region comprised between the invariant cysteine residue at the end of all VH genes and the invariant tryptophan from all JH segments (298). Given the absence of the diversity set of genes in the light chain loci, heavy chain CDR3 is regarded as the most diverse. Though the other 5 CDRs demonstrate a supportive role by increasing the affinity of antigen binding (337). Where CDR3 hypervariable loops characterise the 'highly antigen specific recognition core', it has been hypothesised that the other CDRs bind 'opportunistically' (345). The structural and central location of the CDR3 within the antigen binding region of the antibody not only enables contact with the antigen, but also permits the interface between CDR1, CDR2 and FRs from both the heavy and light chains (346).

In spite of the extensive variability within CDR3, analysing its aa sequences provides clues to the extent of constraint on this structure due to the aforementioned process of recombination (347). Typically, CDR3 length follows a Gaussian distribution, with skewed profiles indicative of lymphocyte selection and conceivably, clonal expansion (348). Commonly, aa's forming a large proportion of the CDR3 region tend to be neutral or leaning towards hydrophilicity (347). Alterations in the length and composition of CDR3 consequently changes the charge, hydrophobicity and shape of the site where the antigen binds - thus affecting potential antibody-antigen interaction and binding (349).

Features of CDR3 were initially determined from electrophoresis, Sanger sequencing and spectratyping until the emergence of NGS in the mid 2000's. Since then, vast amounts of data has been published in regards to CDR3 characteristics within a variety of B-cell malignancies such as Chronic Lymphocytic Leukaemia (CLL) (350) and Burkitt's lymphoma (351), and also conditions where the pathology of antibody under or overproduction is largely unknown such as IgM-MGUS (352).

5.1.1.3 V(D)J recombination/usage

V(D)J recombination (Figure 45) has been studied in-depth owing to the concept that skewed immune repertoires are attributed the increased usage of particular V(D)J gene families, or even certain V, D or J gene segments (353). Preferential uses of specific gene segments may result in a restricted immune repertoire, as potential specificities to antigens are reduced thereby constricting diversity (354). Two main factors have hindered the extensive efforts to define the human repertoire over the past couple of decades since the initial sequencing of the Ig genes in the 1980's (355). (A) The vast diversity of the antibody repertoire itself; and (B) the fact that the repertoire of each individual is ever changing and dynamic - in response to both intrinsic factors (e.g. ageing) and extrinsic factors (e.g. infection) (353).

Antigen exposure largely shapes the immune repertoire of an individual, though repeated interaction can result in preferential recombinations and employment of V(D)J families/gene segments due to B cell selection. Generally, exposure to a wide-range of antigenic challenges usually forms an extensive repertoire in preparation for future contact with previously encountered antigens in a more efficient and rapid response than the prior interaction (356). Though V(D)J recombination and its associated processes such as somatic hypermutation and class switching yields large amounts of antibody specificities, certain factors indicate that this process is not entirely random. For example, in early years of life, V-region gene segments and other diversifier use is limited (357) - reflecting the underdeveloped immune system. The study by Hong *et al* found that neonates particularly used the IgHV3 sub-family in contrast to healthy adults preferentially using IgHV4 (353). Even within different types of B cells, usage differences have been demonstrated. In three healthy controls, Wu *et al* showed an increased usage of IgHV3 sub-family and decreased usage of IgHV1 sub-family in IgM memory cells, with these findings not mirrored in switched memory cells (356). With regards to clonal diseases such as WM and IgM-MGUS, research has shown that the IgHV3-23 segment are preferentially used at 24% (out of all V gene segments), whereas the same segment was used at 12% in healthy controls (358). Thus, analysis of V(D)J recombination and gene segment usage can be used deduce common patterns seen within a given condition, providing clues to the diversity and clonality of the B-cell repertoire.

5.1.1.4 IgM

Generated during the primary immune response, IgM constitutes a major antibody class persisting in serum for 5 to 8 days (359). Monomeric IgM is initially attached to the surface of B cells and upon antigenic stimulation, the process of V(D)J recombination (outlined in Section 5.1.1.3) is initiated to generate the pentameric form of IgM. Highly effective against viruses, the latter type of IgM is a 900kDa multimeric antibody (Figure 48), generally having a low affinity and broad specificity perpetuating binding of this antibody to both self and foreign antigens (360). One IgM antibody consists of 60 CDRs given its pentameric structure (5 x 2 binding units), thus the high avidity of this Ig compensates for its low affinity. However, steric hindrance of the F(ab) regions means that the valence of IgM is actually 5, not 10 (361).

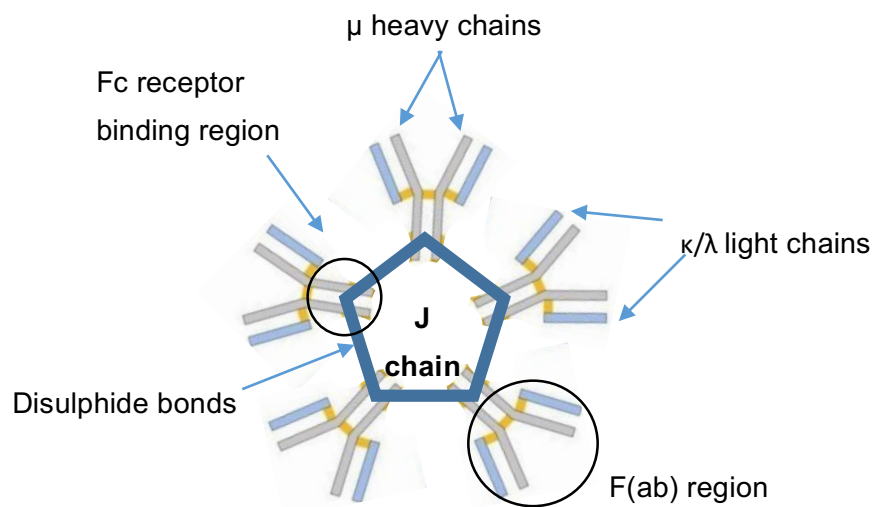


Figure 48: The structure of IgM.

IgM is made up of μ heavy chains and κ or λ light chains. The five monomers are held together by disulphide bonds and the joining (J) chain. The J chain is necessary for monomer polymerisation. Figure 48 recreated using information from reference (361).

Forming 10% of total Ig in humans and mostly found in extravascular spaces, the IgM pentamer is a potent activator of complement. It is known to activate the classical pathway by a singularly bound IgM, in contrast to where over a thousand IgG antibodies are warranted to yield the equivalent (362). B cell receptors also recognise the inactive form of C3 – i.e. iC3b, C3d or C3dg, and thus the IgM-antigenic complex alongside the activated component of complement (C3), markedly augments the B-cell response (359). Interestingly, recent research demonstrates that IgM defective of complement activating properties can still yield a humoral response through the Fc binding region. The IgM-antigenic complex also promotes the survival and activation of B cells through crosslinking of the B-cell receptor and Fc receptors on B cells.

Healthy individuals have IgM levels within the range of 0.2-2.8mg/ml, whereas the SchS patients included in this work demonstrate levels above 3mg/ml (range: between 3 and 8mg/ml), except for patient 15 at 1mg/ml. It has been noted that within SchS, these IgM levels either remain stable or demonstrate an incline of 0.5 to 1mg/ml per year (26). Several lipid antigens such as phosphorylcholine and malondialdehyde are known autoantigens recognised by subsets of naturally occurring IgM (363). More specifically, IgM generated by the autoimmune condition SLE, has a tendency to target nuclear antigens (364), with the aforementioned disease largely associated with inflammation leading to permanent tissue damage (365). The possibility that the monoclonal component of SchS bears a specific physiological role is borne from the fact that over 90% of SchS patients demonstrate monoclonal IgM_k - seen in 7 out of 10 SchS patients included in this work (Table 20). A previous study indicated that IgM skin deposits were responsible for the pathophysiology of the rash (197) otherwise, the role of IgM in SchS remains obscure.

5.1.2 Assessment of the immune repertoire

Recent technical advances have enabled the detailed assessment of T and B-cell repertoires. In depth sequencing of the immune repertoire serves several purposes including disease monitoring (i.e. minimal residual disease (MRD), therapeutic antibody development, and vaccine design (366)).

5.1.2.1 NGS

The past two decades have seen the heightened development of PCR based analysis of Ig as the gold standard for molecular clonality testing, primarily built upon the work of the Euroclonality/BIOMED-2 consortium published in 2003 (367). These standardised multiplex PCR assays for all Ig/TCR receptor targets, with overrepresentation of particular V-J/D-J sequences detected by gel or capillary electrophoresis. With millions of reads, NGS permits the depth of sequencing to be significantly greater than the amount of B cells within a sample, “allowing comprehensive snapshots of repertoire diversity”(344). These high-throughput platforms have taken the examination of immune repertoires beyond the question of clonality, but rather provide a comprehensive insight into the dynamics of the immune repertoire (e.g. CDR3 diversity & analysis and VDJ allele identification)(331). Sequencing gDNA allows the approximation of the number of B cells expressing a particular antibody (i.e. clonality), as the number of sequencing reads will be relative to the quantity of gDNA template input (368). Employing this concept, the objective of this section of work was to utilise NGS for comprehensive analysis of the IgH repertoire in SchS, specifically surveying IGHV gene family usage and CDR3 diversity.

5.1.2.2 Data analysis

Over the past 2 decades, bioinformatics tools have been developed for in-depth study of VDJ rearrangements and CDR3 aa sequences. Analysing up to 500,000 Ig or T cell receptor sequences, IMGT™ (ImMunoGeneTics)/HiVQuest identifies the closest V, D and J germline genes pertaining to an arrangement, analyses the presence of somatic mutations and changes in amino acids with a detailed examination of the junction additions and deletions (369). The resulting outputs are based on the following models: (A) classification based on nomenclature of the gene segments (370) and (B) enumeration – unique numbering of the genes/alleles (371-373).

5.1.2.3 The Role of B cells in SchS

Although the prevalence of TCR clones are greater within 'non-neoplastic diseases'(374), abnormal B-cell rearrangements are also found in autoimmune diseases such as Systemic Lupus Erythematosus (SLE) and Rheumatoid Arthritis (RA) (375), Cold Agglutinin Disease (CAD) (376) and are a conventional finding with ageing (377). SLE, RA and CAD present with autoantibodies mainly targeted at nuclear components, rheumatoid factors and the carbohydrate antigens on red blood cell surfaces respectively, with the former two diseases manifesting inflammatory consequences. Additionally, an IgM paraproteinaemia of unknown significance is a key diagnostic criterion (above levels of 60g/l) for the B-cell LPD, Waldenström's Macroglobulinaemia (290). The latter condition develops in 20% of SchS patients, whereas in SchS, the monoclonal gammopathy is of unknown implication.

Since IgM overproduction is a hallmark of SchS and taking the disease models of SLE, RA and CAD into consideration, it is plausible to consider that these high levels may contribute to the pathophysiology of the condition by binding of SchS IgM to an unknown molecule/antigen. Surveying the general metrics of repertoire skewing (as described in sections 5.1.1.2 and 5.1.1.3) is one approach to investigate if the auto-inflammation seen within this disease is perpetuated by the monoclonal component. Investigating the latter within 10 SchS patients will not only provide evidence pertaining to the usage of VDJ gene families and segments, but could also indicate if the SchS B-cell populations share similar antigen binding regions through CDR3 aa sequence evaluation. Moreover, a clonal population may be in a germline configuration indicating a response to a natural antigen, or alternatively, could be heavily mutated with SHM, suggesting a specific antigen response. As the generation of one heavy chain CDR3 aa sequence can be the product of alternative events, including different IgH gene segment recombination and the random insertion of non-templated and palindromic nucleotides at the junctional regions (378), these sequences are rarely shared inter-individually in health. However these shared sequences (also known as public repertoires or stereotyped sequences), can be seen in disease conditions (368). Out of many such examples, stereotyped CDR3 sequences were found in those individuals suffering from Dengue Fever (379). Highly suggestive of derivation from a parent B-cell, overrepresented CDR3 sequences can be considered as clones when they make up a certain percentage of the overall repertoire (e.g. 2.5% (331)). Indicative of B-cell repertoire skewing, large CDR3 clones can further be evident of bias towards the clonal expansion of a progeny derivative from a parent B-cell (clonality). Theoretically, a restricted IgH repertoire leading to the expansion of a sub-set of clonal cells could also be those IgM generating cells – hence the establishment of high IgM titres as seen in SchS. Thus, examination of the IgH region will overall address the previously unexplored notion that SchS is a clonal disease.

5.1.2.4 IgM related disorders

The idea that IgM clonal diseases harbour the MYD88 L265P mutation was further developed through research by Varettoni *et al* in 2013, who noted that those IgM-MGUS patients who had 'significantly higher levels of IgM' carried the MYD88 variant (183). The mutation in question is found in 50% to 80% of IgM-MGUS patients, 6% of patients with lymphomas such as Marginal Zone Lymphoma (MZL) and in 5% of chronic B-cell LPD (183, 290). As demonstrated in Results Chapter 2, approximately a third of SchS patients harbour the MYD88 L265P mutation. This novel finding was based on the hypothesis that since 20% of SchS patients go on to develop the IgM related WM, where over 90% of patients carry the aforementioned mutation, that this would be mirrored in SchS patients. However, in CAD, established monoclonal IgM binds to red blood cells activating the complement cascade, within peripheral blood circulation due to cooler temperatures (189) - but patients don't harbour the MYD88 L265P mutation. Sequencing of the VH regions determined that the IgHV4-34 gene segment encodes for the monoclonal cold agglutinin IgM molecule, indicative of particular aa sequences having an important role in antigen recognition (189). Given the pathophysiology of the latter, though the MYD88 mutation is not universally present in SchS patients, it is plausible that the IgM paraprotein may have a pathological effect in SchS. Together with the results of the previous chapter, the following research investigates the aforementioned concept through sequencing of SchS IgH regions in order to search for shared patterns (n=10). Therefore, the aims of this chapter are as follows:

A. Amplify the IgH region of 10 SchS patients for deep sequencing

B. Bioinformatics pipeline construction using the Galaxy, AR Galaxy and IMGT® open access platforms to examine the resulting sequences with specific regard to CDR3 properties and VDJ recombination

5.2 Methods

5.2.1 IgH NGS

This part of the project was conducted to evaluate if SchS demonstrates evidence of B cell clonality by analysis of the B cell repertoire followed by assessment of CDR3 region characteristics, within 10 SchS patients. The following work describes the NGS methodology used to review the landscape of the B cell repertoire in SchS. Formal power calculations to determine sample size were not carried out due to the rarity of SchS and the limited availability of starting sample material.

5.2.1.1 PCR and agarose-gel electrophoresis

The Leader sequence and JH consensus primers (367, 380) listed within section 7.2.1, appendix were used to amplify the IgH region of B cells via PCR, using a minimum of 200ng of gDNA from PB (DNA extraction method described in 2.2.5). Figure 49 below demonstrates the amplification strategy employed within this section of work.

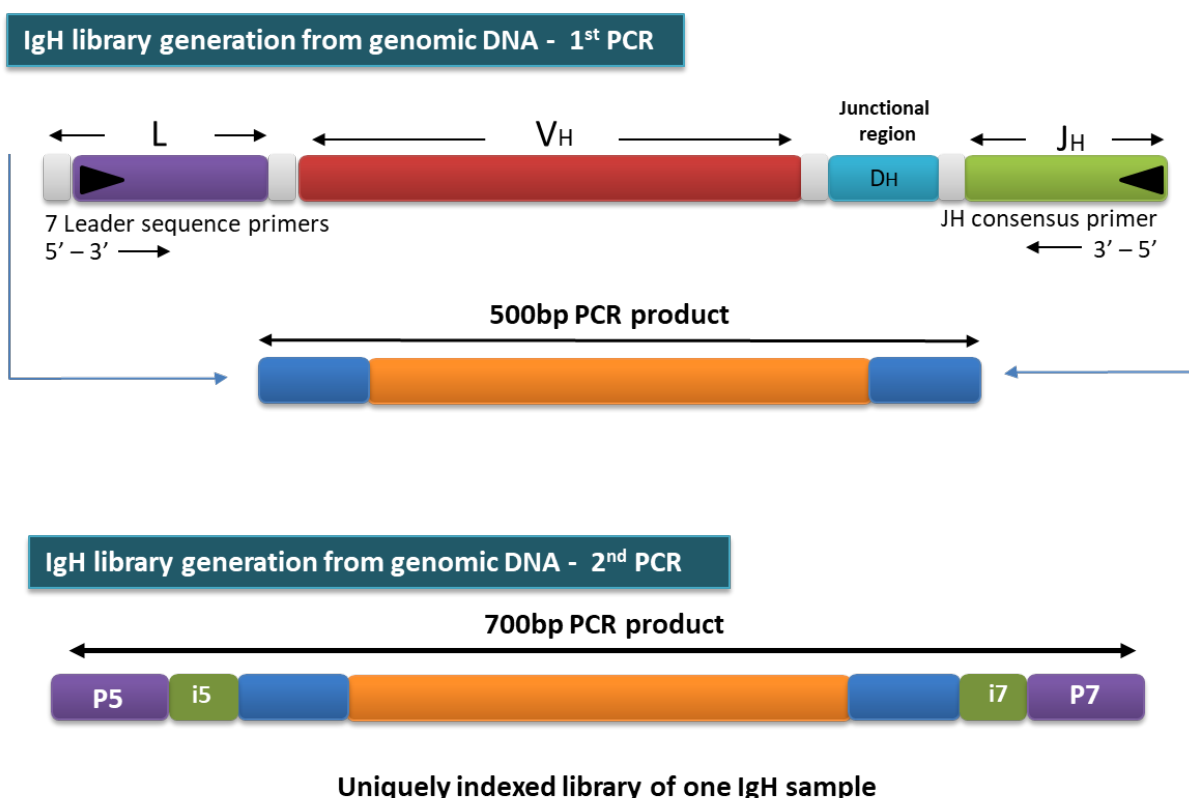


Figure 49: Amplification of the IgH region

Figure 49 is a schematic diagram of the gDNA IgH amplification from the peptide leader region across to the JH regions, with their approximate positions. The 7 leader sequence and 1 JH

consensus primers are indicated with their appropriate orientations. The forward primers initiate amplification from the first, untranslated exon and are regarded as superior to the commonly used BIOMED-2 primers (367). The latter primers bind to the Framework-1 (FR-1) region of the VH segment, which is commonly subject to somatic hypermutation and thus loss of binding can occur (381). The sequence ends of the 500bp product (indicated in blue) are recognised by the Nextera indexing primers used in the second round of PCR.

5.2.1.1.1 Primary PCR

The initial PCR amplified the IgH region as illustrated in Figure 49, using 200ng of gDNA as a starting template and 10µl of Phusion Flash High-Fidelity Master Mix (Thermo-Fisher Scientific, UK), per sample. The primers, with adapter sequences recognised by the Nextera indexing primers (section 7.2.1, Appendix), were diluted down 10µM working stocks to a final 1µM concentration. 0.29µl of an equimolar stock of the 7 leader primers was added to the final PCR reaction. 0.40µl from a 10µM stock of JH primer was added, with the total reaction made up to 20µl with DNase-free water. Thermocycling conditions were as follows for 35 cycles: denaturation at 98°C for 10 seconds; annealing at 65°C for 5 seconds and elongation at 72°C for 30 seconds. Following PCR amplification, 0.8µl of Midori Green Direct, (Nippon Genetics, Duren, Germany), was added to each PCR reaction to enable visualisation on the agarose gel. The gel was visualised using the blue light GelDoc system and Quantity-One analysis software (BioRad, USA). Alongside a 100bp ladder (NEB, UK), all the PCR products were run on a 2% agarose gel for 30 minutes at 90V. Bands corresponding to a region around 500bp were cut out and the DNA purified using the Zymoclean Gel DNA recovery kit (Zymo Research, USA). Further details of the latter technique are outlined in Results Chapter 2, Section 2.2.

5.2.1.1.2 Second round PCR

The aim of the second round PCR was to incorporate the multiplex indices and Illumina sequence tags onto the 5' end and 3' ends of the PCR products, in order for sample pooling and NGS. PCR with the following primers below adds the P5 and P7 termini that bind to the flowcell on the Illumina sequencer:

- (1) 5' AATGATACGGCGACCACCGAGATCTACAC[i5]TCGTCCGGCAGCGTC 3'
- (2) 5' CAAGCAGAAGACGGCATAACGAGAT[i7]GTCTCGTGGGCTCGG 3'

This step also adds the dual 8bp tags denoted by 'i5' and 'i7'. The PCR mix consisted of 8µl of purified DNA from 1.2.1.2, 10µl of Phusion Flash (ThermoFisher, UK), and 1µl of each

indexing primer as stated. The limited cycle PCR conditions were as follows: Initial denaturation at 95°C for 10 minutes, followed by denaturation at 95°C for 30 seconds, annealing at 60°C for 30 seconds and extension at 72°C at 45 seconds for 10 cycles. A final extension step was carried out at 72°C for 10 minutes. Agarose-gel electrophoresis, gel visualisation and purification were carried out as outlined in section 2.2.6.

5.2.1.2 Quality control

The concentrations of the final individual libraries were determined by pico-green fluorescence using the Quant-iT™ dsDNA Assay Kit (Invitrogen, USA) with the size of the final amplicons (~700bp) and purity determined using the Agilent 2200 TapeStation system (Agilent Technologies, UK). The aforementioned methodologies are discussed in depth within Results Chapter 2 (Section 2.2.6.5). Equal quantities of uniquely tagged PCR products were mixed, generating a multiplexed pool of uniquely indexed samples.

5.2.1.3 Sequencing run

Sequencing was carried out by the NGS facility within the Leeds Institute of Medical Research at St James's Hospital. NGS was performed on an Illumina MiSeq sequencing instrument (Illumina, UK), with a 600 cycle (2 x 300bp) paired-end run, according to the manufacturer's instructions. MiSeq reporter software demultiplexed the samples with FastQ (.fastq) files as the final output.

5.2.1.4 Data analysis and Bioinformatics

The sequencing reads generated by MiSeq were demultiplexed based on their unique adaptor, resulting in fastq files generated for the 10 samples. The resulting data were subject to downstream processing, analysis and visualisation as outlined in Figure 50. The following NGS platforms are open access web-based programs and used sequentially in this work: www.usegalaxy.org; www.imgt.org; and www.bioinf-galaxian.erasmusmc.nl/argalaxy. Figure 54 portrays how these bioinformatics tools are utilised, starting from the Illumina MiSeq generated fastq file (Galaxy), to the generation of CSV files for use with Microsoft Excel (IMGT HiVQuest), and finally to the downloadable graphs and plots generated by AR Galaxy pertaining to VDJ and CDR3 properties.

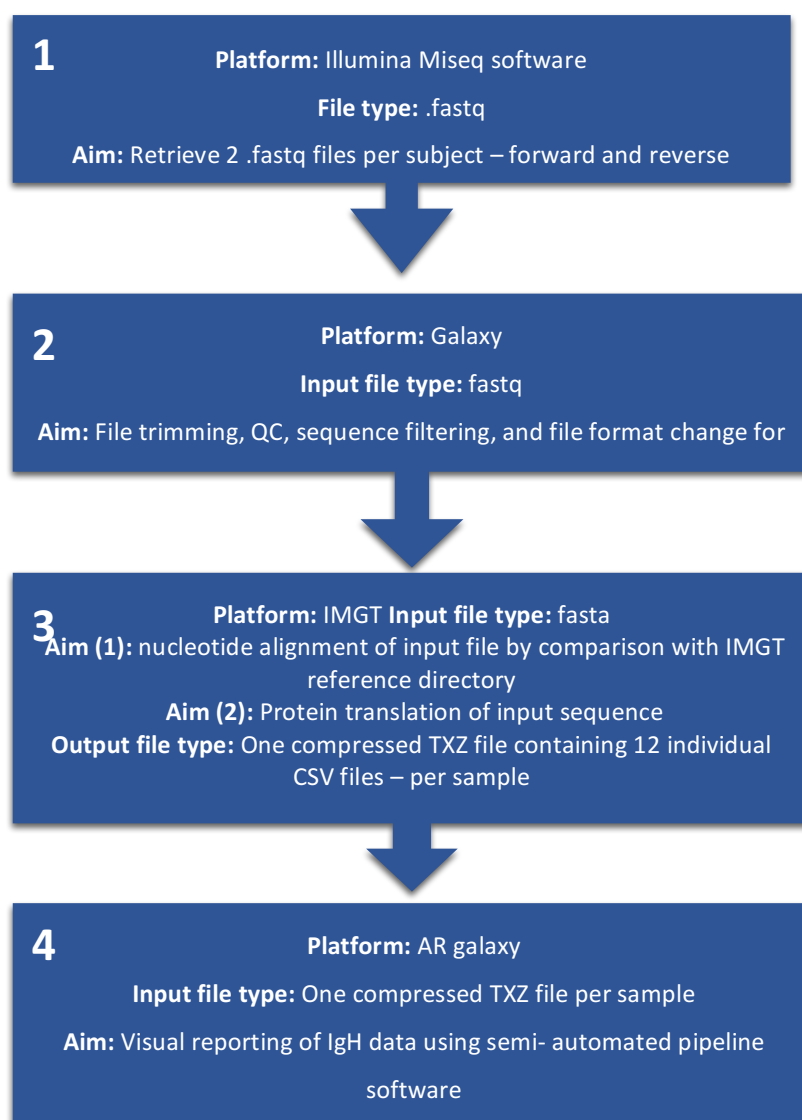


Figure 50: Workflow for processing IgH data.

Figure 50 provides an overview of the four stages required to process the IgH data obtained from the MiSeq sequencing platform. The first stage retrieves fastq files from the sequencing platform. The second stage requires the transfer of these fastq files to the Galaxy open access database for the following actions: (I) file trimming, (II) QC, (III) filtering and (IV) fastq to fasta file conversion and (V) fasta file modifications. The third stage necessitates the upload of the fasta file from stage two onto the IMGT database – resulting in the alignment and translation of the input sequences. The output from this stage are 12 CSV files per sample. The compressed TXZ file from (3) is the starting file for implementation of the Immune Repertoire pipeline on the Antigen Receptor (AR) Galaxy platform. The aim of this last step is to generate visual descriptions of the data in the form of graphs, reporting the properties of VDJ and CDR3.

5.2.1.4.1 Galaxy

All 10 SchS fastq files were subject to strict filtering criteria in order to exclude sequences that did not pass the stringent quality control filters, and thus were irrelevant for further downstream exploration. Firstly, the employment of the 'FastQC' tool provided basic statistics such as GC content, adaptor content and sequence lengths. The single output files contained the filtered reads only. Subsequently, the 'Trimmomatic Crop' tool was utilised to define the number of bases to keep at the start of the read, determined by the quality of the sequences. The 'Filter by Quality' tool narrowed the sequences down by application of a Phred Quality Score of 20 and a base call accuracy of 99%, ensuring the removal of sequences due to sequencing artefacts. The 'FASTQ to FASTA' step converted the resulting Galaxy 'FASTQ' file to a 'FASTA' file suitable for use with the IMGT platform after using fastwidth (removes artificial nucleotide line breaks).

5.2.1.4.2 IMGT HighV-Quest

The output FASTA files from the previous step consisting of IgH sequences from 10 SchS patients were uploaded onto the IMGT HighV-Quest platform - for assignment of the germline V, D and J segments and CDR3 region identification (382). User-defined parameters included selection of the locus (IgH) and the species (Homo sapiens). Processing took up to 72 hours and the 12 output CSV files were archived into one TXZ file, per sample. These resulting TXZ files were extracted using the Windows default archive tool (7-zip) and subsequently opened with Microsoft Excel for visualisation of the assigned data.

5.2.1.4.3 AR Galaxy

Antigen Receptor (AR) Galaxy extracts information from the IMGT Archive created with HighV-Quest (383). The TXZ files were uploaded onto the AR galaxy platform for processing through the 'Immune Repertoire Pipeline'. Multiple filtering stages were employed to eliminate sequencing reads where the rearrangement was non-functional, or a rearrangement was not found. The first stage of the pipeline only considered the best matched V, D and J gene, as assigned by IMGT/HighV-Quest. Secondly, reads pertaining to 'no-results' from IMGT/HighV-Quest were removed. Thirdly, the 'clonal type definition' filter was applied to remove duplicate rearrangements. The output of this pipeline initially showed the total number of sequences and the productive/unproductive sequences (Table 18). Other files from this analysis included CDR3 length distribution and V, D and J gene usage, for each individual sample.

5.3 Results

In this chapter I sequenced the heavy chain region (IgH) of 10 SchS patients. Clonal expansion of lymphocytes is a defining element of the immune response (384), but work involving SchS patients has not experimentally explored the notion that SchS may be a clonally-derived B cell disorder. Given that IgM paraproteinaemia is fundamental to a SchS diagnosis, exploring the landscape of the IgH repertoire by examining CDR3 characteristics and VDJ gene usage provides detail on this concept.

5.3.1 PCR and agarose gel-electrophoresis

The aim of the primary PCR was to amplify the IgH segment using the Leader sequence and JH primers under the conditions listed in Table 26, appendix. Use of Leader sequence primers enabled amplification of the entire rearranged IgHV-IgHD-IgHJ genetic sequence. BIOMED-2 primers are more prone to fail to amplify the whole IG gene, harbouring the possibility of failure to amplify some rearrangements (381).

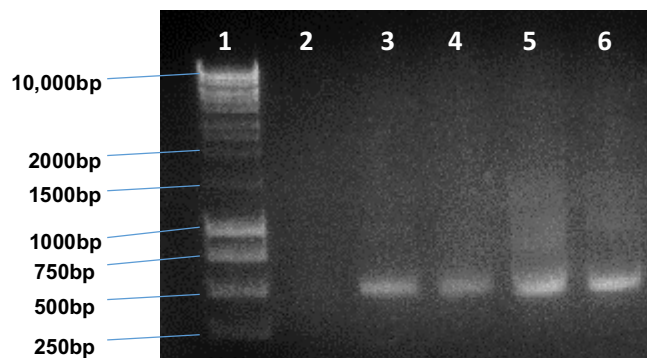


Figure 51: Representative gel doc image of the first round of IgH PCR.

Lane 1 corresponds to the 10KB ladder used. Lane 2 contained primers only, Lane 3-6 contained SchS gDNA samples. Bands corresponding to around 500bp (range 450bp – 500bp) were cut out and subject to gel digestion and purification as described in section 2.2, for the second round of PCR.

The aim of the second PCR was to add the NEXTERA indices and Illumina sequencing tags via thermocycling onto the products generated from the primary PCR.

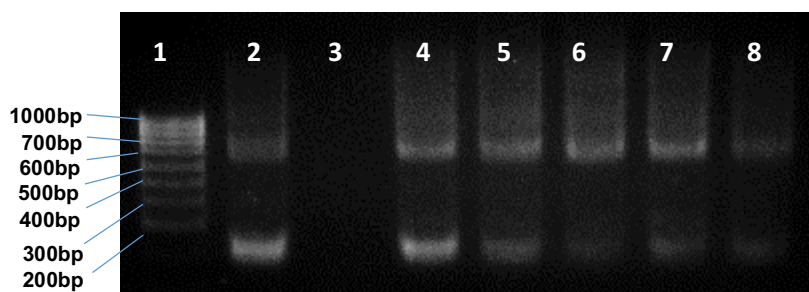


Figure 52: Representative PCR image denoting the second round of indexing.

Lane 1 corresponds to the 1kb ladder used, lanes 2, 4-8 show the successfully indexed DNA, with lane 3 being a negative control (primers and water only). Bands corresponding to around 700bp were cut out and subject to another round of gel digestion and subsequent QC (as described in 2.2.8) prior to mixing to generate the sequencing library for the MiSeq run. The NEXTERA dual indexing principle utilises 2 indices of 8 base pairs in length. This strategy is employed by addition of a unique index 1 (i7) and a unique index 2 (i5) to each end of a sample (Fig 53). More compatible barcodes are listed within the manufacturer instructions.

5.3.2 Quality control of the libraries

Prior to pooling the samples for MiSeq loading, two QC steps were carried out in order to quantitate and assess the purity of the indexed libraries: (1) TapeStation analysis to determine the size of the libraries, followed by (2) Quant-iT™ assay to assess the concentration of each sample.

5.3.2.1 TapeStation

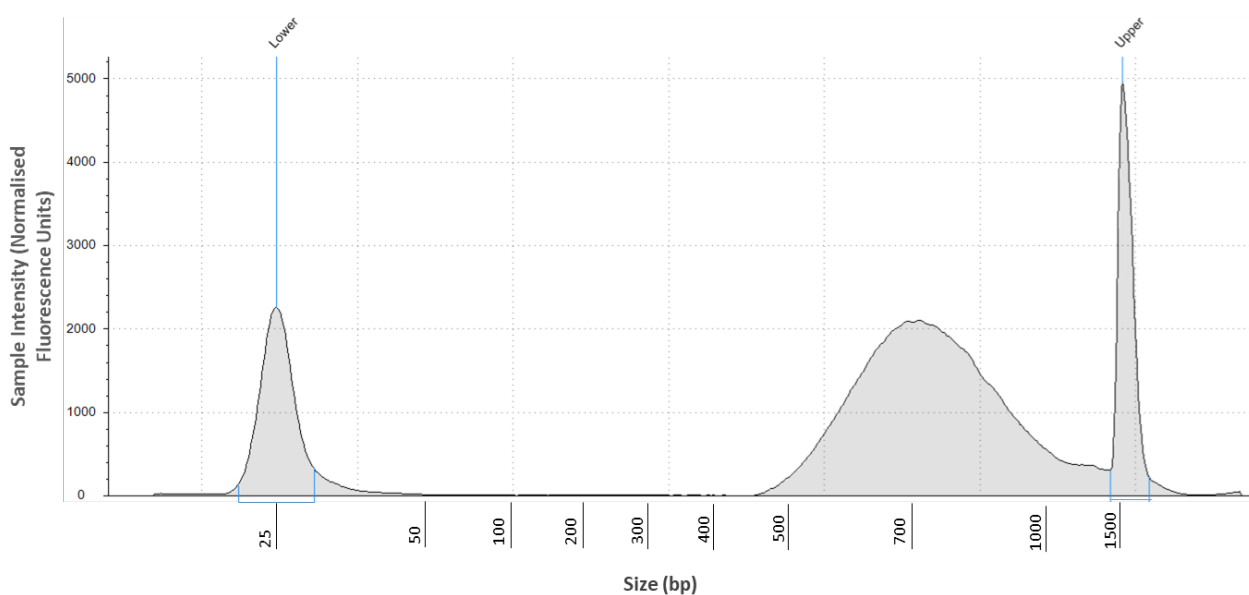


Figure 53: Representative bioanalyser trace.

Figure 53 is a representative bioanalyser trace demonstrating the average size and distribution of the indexed library constructed from the steps described for sample 12. The trace was acquired using the Agilent DH1000 DNA screen tape assay in conjunction with Agilent 2200 TapeStation system (Agilent Technologies, UK). Figure 53 shows the size fragment distribution of the indexed library for sample 12. The X axis refers to the size in base pairs of the DNA library, with the Sample Intensity (normalised fluorescence units) on the Y axis. The lower marker (left peak) and the upper marker (rightmost peak) correspond to the size markers of 25bp and 1500bp respectively. The average size of the library was 700bp, thus this broad peak is expected to cover the range of VDJ rearrangements. Given the average size of the amplified VDJ rearrangement in the 1st round of PCR was 500bp, combined with adaptor ligation in the 2nd round of PCR, the average size of the assembled library would fall within the broad peak as seen in the figure, thus covering the array of DNA rearrangements. The absence of other peaks (i.e. primer dimer at 50bp) within the sample, indicates there are no other artefacts which would interfere with the sequencing of the library.

5.3.2.2 Quant-iT™ PicoGreen assay

The purpose of carrying out Quant-iT™ assay was to accurately assess the amount of the DNA library per sample, in order to ultimately pool together the samples for sequencing in equimolar amounts.

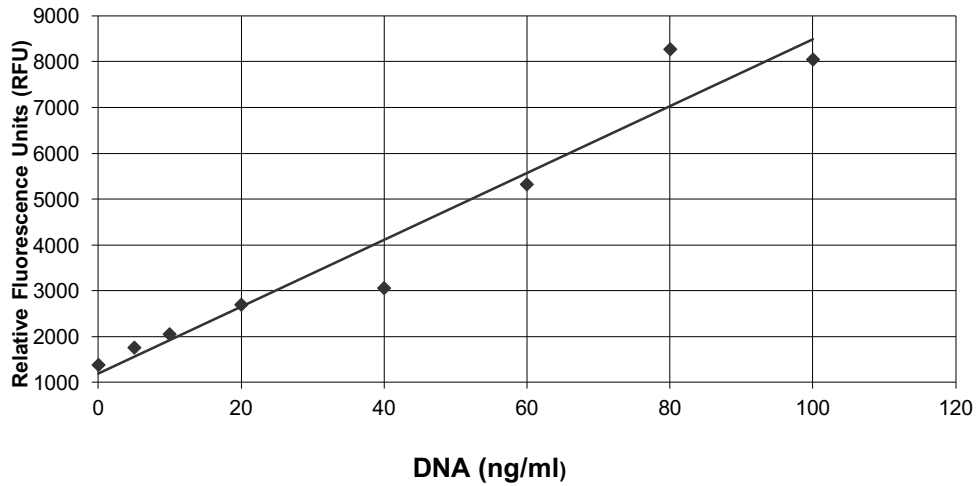


Figure 54: The 8 point standard curve obtained with the PicoGreen assay.

The X-axis demonstrates the concentration of DNA in ng/ml (0-100ng/ml) with relative fluorescence units on the Y-axis (arbitrary). The samples were excited at 480nm with the fluorescence emission intensity measured at 520nm. Per DNA library, equimolar amounts of each sample were pooled to generate a combined library with equal amounts of DNA for sequencing to prevent disproportionate sequencing of each of the 10 samples.

5.3.3 Sequencing and quality scores

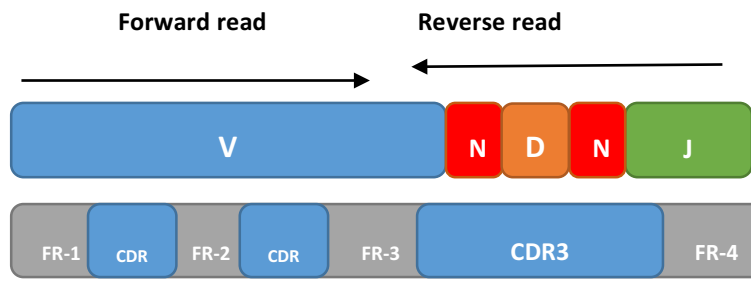


Figure 55: Schematic showing the sequencing coverage of the VDJ region carried out.

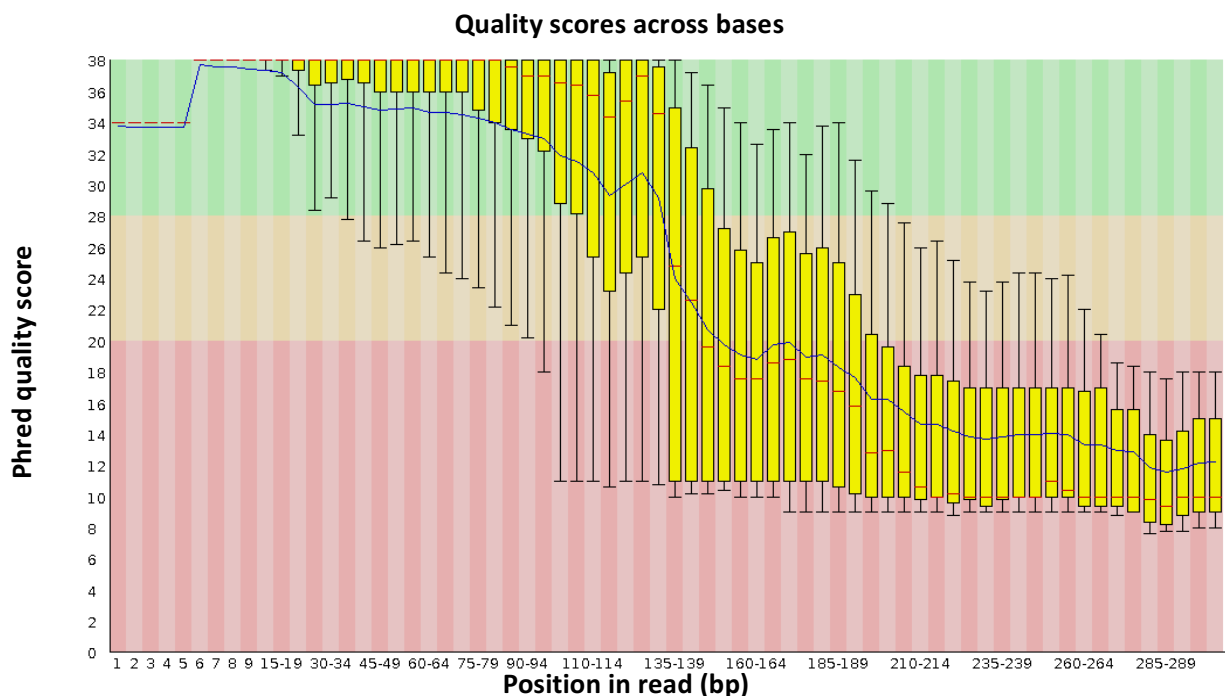


Figure 56: Galaxy quality score boxplots.

Figure 56 demonstrates the box plots for the sequencing quality score as generated by Galaxy for sample 12. The yellow boxes represent the 25th to 75th percentiles, with the upper and lower whiskers demonstrating the 10th and 90th percentiles respectively.

The Y-axis refers to the Phred quality scores, with the X-axis showing the results in relation to the position in the read (1-300bp). A Phred quality score of 20 implies the probability of an incorrect base call is 1 in 100, with a 99% base call accuracy. An increased Phred score of 30 implies that the probability of an incorrect base call is 1 in 1000, and a 99.99% base call accuracy. Although there is an apparent dip in quality (Phred scores from below 20), and these sequences were filtered out from the dataset.

5.3.4 Repertoire diversity

Initially, 5,185,201 raw sequences were obtained, with application of stringent filtering (as described in 5.3.4) cutting this initial value down to 2,860,786 sequences. These sequences were then split into productive and unproductive as outlined in the table below.

Sample ID	Total sequences	Productive	Productive (%)	Unproductive	Unproductive (%)
SchS – 12	156142	133271	85	22871	15
SchS – 14	172577	145525	84	27052	16
SchS – 15	153256	131436	86	21820	14
SchS – 16	169726	146656	86	23070	14
SchS – 18	419474	328040	78	91434	22
SchS – 20	270400	212452	79	57948	21
SchS – 21	250427	216294	86	34133	14
SchS – 22	619601	568651	92	50950	8
SchS – 24	564216	415622	74	148594	26
SchS – 25	84967	71806	85	13161	15

Table 18: Initial sequencing counts as computed by IMG.T.

Sample ID, the number of total sequences, productive sequences and unproductive sequences are stated in Table 18. Total sequences refers to the sum of productive sequences and unproductive sequences. Productive sequences refers to the rearranged Igs with the coding region having an open-reading frame, no stop codon and no defect in the initiating codons, splicing sites, and comprises an in-frame Junction. Unproductive sequences can be characterised by an out-of-frame junction, and/or the presence of stop codons, frameshift mutations within splicing sites or regulatory elements. These unproductive rearrangements originate from B-cell DNA that underwent a productive rearrangement on their second allele, therefore, these sequences have not been chosen and allow the study of VDJ recombination without selection influence (383). Only productive, and thus functional sequences were carried downstream for further analysis.

The high percentage of productive sequences (ranging from 74% to 92%) in comparison to healthy controls and other diseases may indicate that a proportion of IgH DNA is rearranged for a second time – an infrequent occurrence though found in autoimmune disease (385) and noted in CLL (292). Ijspeert *et al* found that out of the total sequences per individual, healthy

controls had an average productive percentage of 70% (n=10), whereas 18 patients with common variable immune deficiency (CVID) showed an average 64% productive percentage (386). Given the aforementioned suggestion that a pool of proliferating clonal B cells generating Igs could be the cause of high productive sequence percentages seen in this data, the proposal that SchS patients demonstrate oligoclonality in a polyclonal background is a proposal further investigated in subsequent analyses.

5.3.5 CDR3 characteristics

The CDR3 region is formed as a result of VDJ recombination and is the interface by which most antibodies and antigenic epitopes interact. Given that antibody specificity is largely determined by the heavy chain site of recombination which is CDR3, analysing the characteristics of this region within 10 SchS patients may indicate whether the B-cell repertoire is of a clonal nature. Although there is high sequence variability within this region, through studying the length, composition, and frequency of CDR3 clones, it is possible to gauge the degree of repertoire skewing (387). Self-antigens bearing structural motifs that are recognised by a particular CDR3 sequences could explain the occurrence of CDR3 clones within a sample (344).

5.3.5.1 CDR3 clone definition

In this work, a clone refers to a unique CDR3 aa sequence generated by the Ig heavy chain locus, irrespective of V or J gene usage. The presence of a clone in this work is defined as an aa sequence making up 2% or over of the total productive reads per sample, based on previous experimental design. Where the research on RA by Tak *et al* referred to a CDR3 clone comprising of over 5% of the total CDR3 sequences (388), work on the plasma cell repertoire (389) and autoimmune liver disease (323) pertained to CDR3 sequences as clones over 1% or over 0.1% respectively.

5.3.5.2 Frequency of CDR3 clones

As stated by Tan *et al* in 2016 (323), the precise number of B cells expressing each CDR3 cannot be precisely clarified – denoting one of the few limitations of implementing this NGS technique of B-cell repertoire sequencing. However it is possible to estimate the number of cells, and in turn, lymphocyte frequency, based on the quantity of gDNA isolated from whole blood. Whilst the B-cell count was unknown for the 10 SchS patients in this work, estimation of the cell number allowed for subsequent CDR3 clonal frequency analysis. The over-

abundance of certain CDR3 sequences in samples can be an indicator of a clonal population of B cells and hence the following calculations provide approximate number of sequencing reads, alongside a B cell count. The 2 estimates detailed below are based on the postulation that the gDNA starting sample has a 10% B cell population, or a 1% B cell population. Given these assumptions, these results are not absolute, but rather provide a general insight into the measure of clonality within 10 SchS patients. Presuming no gDNA amplification and library preparation bias, the number of sequencing reads pertaining to a certain CDR3 aa sequence should be 'directly proportional to the number of clonal lymphocytes bearing a certain receptor' (333). Taking into account the addition of non-templated nucleotides and exonuclease activity at junctional regions, the likelihood of two clonally un-related cells producing the same CDR3 aa sequence has been estimated at 1%, (325). Thus, CDR3 sequence analysis can be an additional indicator of recombination and usage patterns of V, D and J genes.

The aforementioned lack of clinical data available in this study hinders the accuracy of the analyses undertaken in this work. One method to address the hypothesised concept that SchS is a clonal disease is to explore the richness and diversity of CDR3 aa sequences within a sample. Analysing the proportional abundance of the top CDR3 aa sequences per sample (i.e. top 50 sequences versus top 10 sequences), assesses if the top clones remain represented at the same levels.

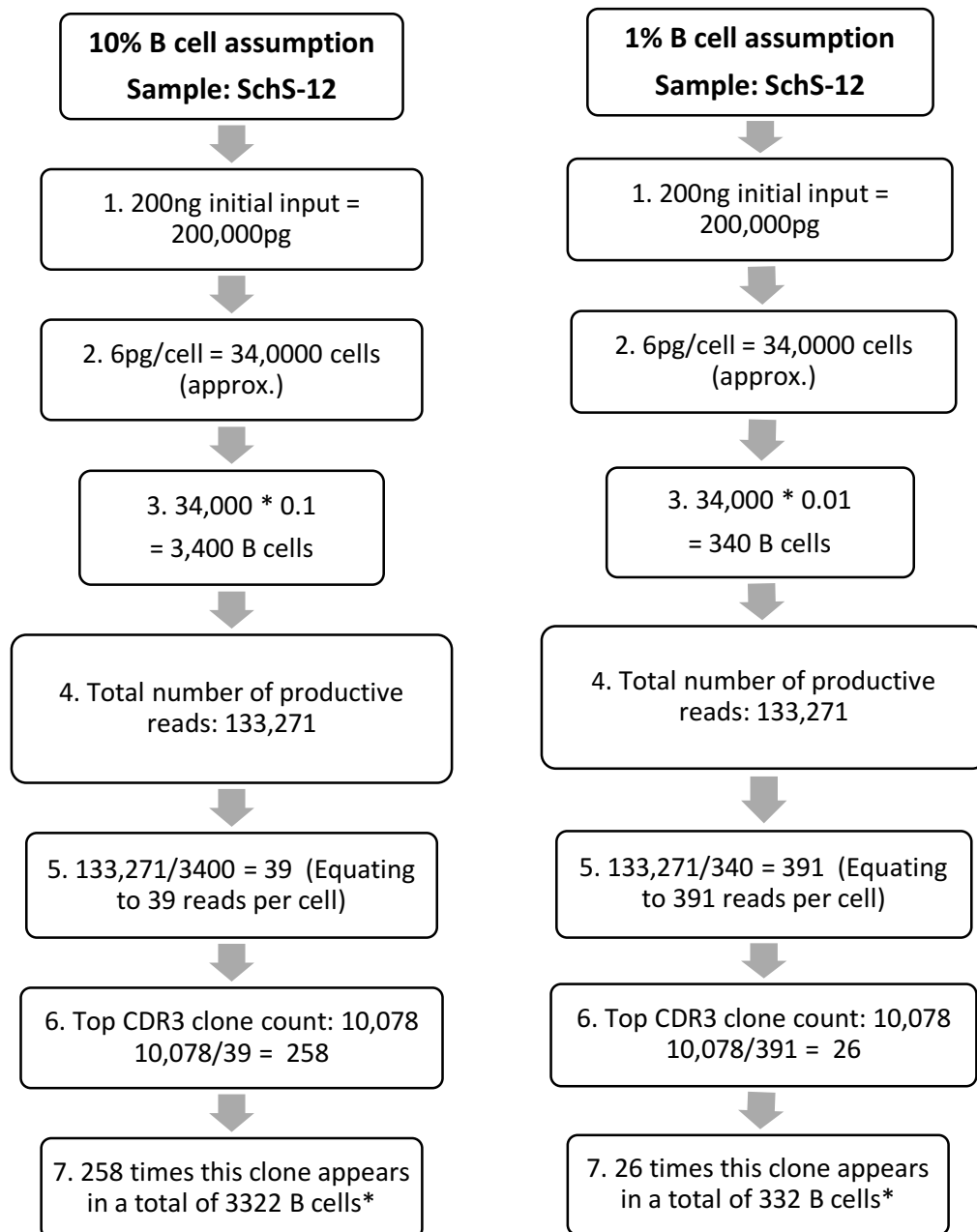


Figure 57: The calculated number of input cells and reads per B cell.

The theoretical number of B cells was estimated using the amount of gDNA with the assumption that 10%, or 1%, of the gDNA content comprised of B cells. This outlined estimation was applied to all 10 SchS patients (all calculations are listed in Section 7.4, appendix).

*The minor reduction in B cells was computed by the addition of all reads at a 1% assumption, however excluded those cells that had a read value of <1.

For each sample, the initial PCR reaction for IgH amplification had an initial 200ng input, equating to 200,000pg. 6pg of DNA is estimated to be in each human nucleated cell (390), therefore, dividing 200,000pg by 6pg provides an approximate number of all cells input into the PCR. The following step assumes either a 1% B-cell content or 10% B-cell content, by multiplying the approximate cell count by either 0.01 or 0.10 respectively, resulting in the number of B cells. Dividing the total number of productive reads by the approximate B-cell count equates to the number of reads per cell. Finally, taking the clone count and dividing that by the number of reads per cell provides a clone frequency per number of B cells. Figure 57 is demonstrative of these steps, with the calculations for each sample presented in Section 7.4, appendix.

Sample ID	No. of B cells (10% assumption)	Reads per B cell (10% assumption)	No. of B cells (1% assumption)	Reads per B cell (1% assumption)
SchS – 12	3322	39	328	390
SchS – 14	3281	43	328	428
SchS – 15	3215	39	321	387
SchS – 16	3270	43	327	431
SchS – 18	3279	96	328	964
SchS – 20	3361	63	336	625
SchS – 21	3380	64	338	636
SchS – 22	3225	167	325	1672
SchS – 24	3282	122	328	1222
SchS – 25	3149	25	315	211

Table 19: Inference of B-cell counts and reads.

Sample ID's, number of B cells and reads per B cells – based on a 10%, or 1% B cell assumption. This summary table was constructed using the figures as calculated in Figure 57.

On a 10% assumption, the number of B-cells for the 10 SchS samples vary from 3149 to 3380, with range of reads per B cell from 25 to 167. On a 1% assumption, the number of B-cells vary from 321 to 336 with the number of reads ranging from 211 to 1672. The purpose of calculating 2 different parameters was to demonstrate that despite the fluctuations in estimating the B-cells, this does not affect the proportions of the top CDR3 aa sequences (as demonstrated by Figure 57).

5.3.5.3 Patient details

Patient Number	Sex	Age at symptom onset	Paraprotein	IgMk para-protein levels (g/l)	Response to IL-1 inhibition	Bone marrow histology	Genes/Variants identified by MDS panel	MYD88 mutational status	NLRP3 mutational status	X inactivation result (if applicable)
12	male	36.8	IgMk	3	Partial	No overt LPL				-
14	male	43.9	IgGλ	N/A	complete	15% plasma cell				-
15	female	44.8	IgMk	1	complete	No overt LPL				random
16	female	49.6	IgMk	4	complete	not done				random
18	male	52.8	IgMλ (IF)	N/A	complete	No overt LPL				-
20	male	58.1	IgMk	3	complete	LPL	STAG-2 c.559C>T p.Gln187* Predicted: pathogenic VAF: 0.081			-
21	male	59.6	IgMλ	7	died before treatment	No overt LPL				-
22	male	61.7	IgMk	5	complete	No overt LPL				-
24	female	68.4	IgMk	8	complete	No overt LPL				random
25	male	78.9	IgMk	7	complete	No overt LPL		L265P		-

Table 20: SchS patients included for the IgH research.

Clinical data and previous findings pertaining to the SchS patients included in this chapter are outlined above. Patient number, sex, age at symptom onset, CRP levels, paraprotein type and level, response to IL-1 inhibition, bone marrow histology and findings from the previous two results chapters are included in this table.

IF: Immunofluorescence VAF: Variant allele frequency LPL: lymphoproliferative lymphoma

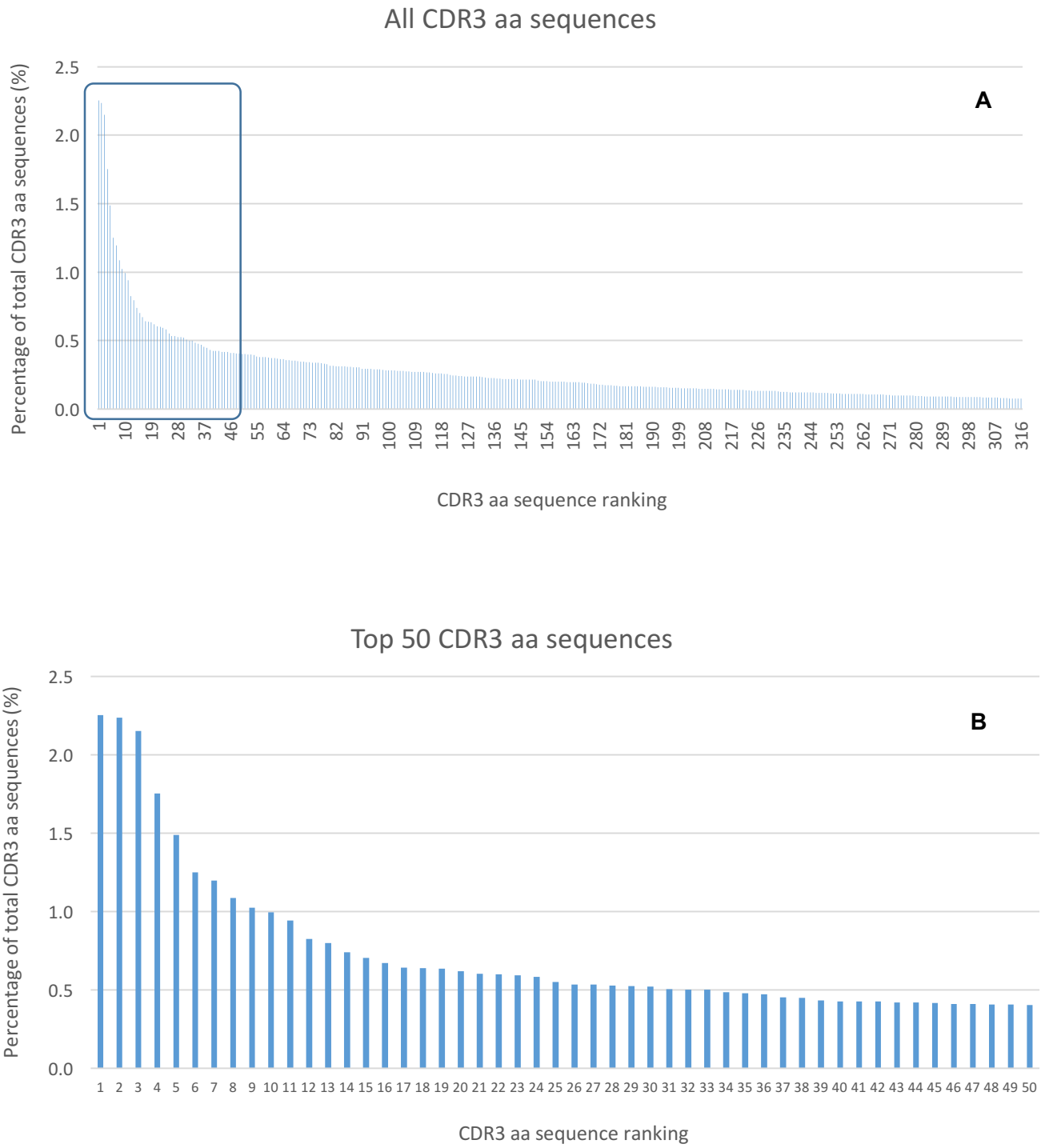


Figure 58: Ranking of unique CDR3 aa sequences.

Figure 58 shows the ranking of decreasing frequency for sample SchS – 21. Panel A represents all CDR3 sequences, with panel B showing the ranking of the top 50 CDR3 sequences.

5.3.5.4 Summary of results

Sample ID	CDR3 clone sequence	% of total repertoire	VH family	DH family	JH family	V-region germline sequence identity (%)	Length (aa)	GRAVY score
12	CAREVVGGYGMDVW	8	VH3 74	DH3 16	JH6	100	15	0.17
	CARDHGGYFDYW	6	VH3 53	DH4 23	JH4	99	12	-0.99
	CTRPNNYYMVDVW	6	VH3 73		JH6	100	13	-0.86
	CARDGGGYNFYFDYW	5	VH3 11	DH2 15	JH4	100	14	-0.99
	CARAVAGTTDYW	5	VH3 43	DH6 19	JH4	99	12	0.00
	CATQLEHDAFDIW	5	VH3 66	DH1 1	JH3	100	13	-0.12
	CAREATGGYSYGPGGYW	4	VH3 11	DH5 18	JH4	100	17	-0.69
	CARGSEGCFDYW	4	VH3 64	DH7 27	JH4	99	12	-0.48
	CARDRVQHQPFGNYYYYYGMVDVW	4	VH6 1	DH6 19	JH6	100	23	-0.96
	CARDQSSGWYFYFDYW	4	VH3 20	DH6 19	JH4	100	15	-1.04
	CAKVLRRDGGALAYW	4	VH3 30	DH2 21	JH4	100	15	0.02
	CASPDSSGYYYW	3	VH3 74	DH3 22	JH4	100	12	-0.70
	CARDRQQLTYW	3	VH3 11	DH6 13	JH4	100	11	-1.30
	CARDSSGFYYYYYGMVDVW	3	VH3 74	DH6 19	JH6	100	18	-0.45
	CARVEMSVAAEDYW	3	VH3 73	DH2 15	JH4	96	14	0.02
CARDFDRWAPSEYFQHW	2	VH3 11	DH3 9	JH4	98	17	-1.12	
CASPRAFQDYW	2	VH3 48	DH1 26	JH4	99	10	-0.37	
14	CARLDRPGIAGVAGQDQW	7	VH3 11	DH6 19	JH4	95	17	-0.35
	CARDFYGDYDYW	6	VH3 11	DH3 31	JH4	98	12	-1.09
	CAKSRRDPQLDYW	6	VH3 30	DH5 24	JH4	100	13	-1.53
	CARDSTTVTTTTYYGMDVW	4	VH3 11	DH4 11	JH6	100	19	-0.40
	CARGGGSYLHYYYYYGMVDVW	4	VH3 33	DH1 26	JH6	95	20	-0.41
	CAGTTVTTSYW	4	VH3 30	DH4 17	JH4	95	11	-0.21
	CARRYFDLW	4	VH3 74		JH2	100	9	-0.42
	CAKGRGYGSSSLDYW	4	VH3 30	DH3 10	JH4	100	16	-0.71
	CARGGAAASDPFDYW	4	VH3 11	DH6 13	JH4	99	15	-0.29
	CARVQQWLVSQYFDLW	4	VH3 20	DH6 19	JH2	94	16	-0.24

	CARDRCSGGSCLFYYYYGMDVW	3	VH3 30	DH2 15	JH6	96	21	-0.07
	CARDWGTSSWRWFDSW	3	VH3 11	DH6 13	JH5	100	16	-1.00
	CASIQDCSGGRCRDYW	3	VH3 48	DH2 15	JH4	100	16	-0.64
	CARERATTVVTPAFDYW	3	VH3 30	DH4 23	JH4	100	17	-0.16
	CAKDVLDTVAGTVDYW	3	VH3 23	DH6 19	JH4	92	17	0.50
	CARDSIYSSGWGMFDYW	3	VH3 11	DH6 19	JH4	100	17	-0.33
	CARDTPYYDFWSGYGGFYGMDVW	3	VH3 53	DH3 3	JH6	100	23	-0.47
	CARECGYSYGCFDYW	3	VH3 30	DH5 18	JH4	100	15	-0.39
	CARDRGALNDFDIW	2	VH3 74	DH5 18	JH4	93	14	-0.51
	CARVRGGCIRGGCHSDYW	2	VH3 30	DH3 10	JH4	81	18	-0.38
	CARATLGSDAFDIW	2	VH3 74	DH3 16	JH3	100	14	0.34
	CAKDQTYDFGLVDYW	2	VH3 48	DH3 3	JH4	96	16	-0.54
15	CARETAGTGAFDYW	3	VH6 1	DH6 13	JH4	99	14	-0.37
	CARARLAYCGGDCHYYFDYW	3	VH3 11	DH2 21	JH4	98	20	-0.33
	CARGFGAYLLDYW	3	VH6 1	DH3 10	JH4	99	13	0.32
	CARAADYYMDVW	2	VH3 30	DH4 17	JH6	99	12	-0.08
	CAKAGETYGLGWYYDSW	2	VH3 30	DH5 18	JH4	84	18	-0.59
16	CARASALLARALDYW	9	VH3 74	DH1 14	JH4	97	15	0.49
	CAKPGYNSGWYPGYYYAMDVW	5	VH3 11	DH6 19	JH6	98	21	-0.58
	CARENWNDPLEDYW	5	VH3 11	DH1 1	JH4	96	14	-1.58
	CAKGHAFEIW	4	VH6 1	DH5 12	JH3	98	10	0.15
	CARAGDIVVPAARDYYYYGMDVW	4	VH3 30	DH2 2	JH6	100	24	0.20
	CANQLEGHNYGLDVW	4	VH3 11	DH5 24	JH6	92	15	-0.51
	CARVEGYSSWTIYYYYGMDVW	4	VH3 74	DH6 13	JH6	98	23	-0.26
	CARDFGGIAAAGRFGMDVW	4	VH3 30	DH6 13	JH6	100	19	0.39
	CASFRAVMGSPNW	4	VH3 74	DH5 18	JH5	100	13	0.19
	CARESSSSWPYYFDYW	4	VH3 11	DH6 13	JH4	100	16	-0.93
	CARDGLLSGYYYYGMDVW	3	VH3 30	DH3 9	JH6	100	19	-0.15
	CARDAKTTVTTPHFDYW	3	VH3 30	DH4 11	JH4	100	18	-0.74
	CGFSTRVWGIARRLYYGMDVW	3	VH3 11	DH6 6	JH6	100	22	0.15
	CAKDRAAAAGYYYYGMDVW	3	VH3 30	DH6 13	JH6	100	19	-0.25
	CATHGNANAFDIW	2	VH3 30	DH4 11	JH3	100	13	-0.04

	CARERADFWSGYYAAGYYYGMDVW	2	VH3 30	DH3 3	JH6	100	24	-0.47
	CARESPSAYYSGTYYYGMDVW	2	VH3 11	DH1 26	JH6	100	21	-0.58
	CARDRYSSSWYGGDDYW	2	VH3 11	DH6 13	JH4	98	17	-1.42
	CARDLLSSVGRFDPW	2	VH3 11	DH3 10	JH5	99	15	-0.10
	CTRDPRLSIPSFDDW	2	VH3 48	DH2 21	JH4	93	15	-0.82
	CVKDSSSWSHYYYYGMDVW	2	VH3 64	DH6 13	JH6	100	20	0.66
18	CARVLVRGALDYW	4	VH6 1	DH3 10	JH4	100	13	0.54
	CGRDGRDGGYGMDVW	3	VH6 1	DH1 26	JH6	98	15	-1.00
20	CATGKWNYEENYW	23	VH3 74	DH1 7	JH4	97	13	-1.47
	CARDNGRYAVDYC	19	VH3 11	DH6 19	JH4	92	13	-0.75
	CARGRGGWSGALDDW	9	VH3 11	DH6 19	JH4	96	15	-0.69
	CARDKWELQTSLLPDYW	9	VH3 30	DH1 26	JH4	100	17	-0.76
	CARHINWGWDSW	8	VH3 11	DH1 26	JH5	93	12	-0.82
	CARAIGAYEGLDIR	6	VH3 11	DH2 8	JH3	85	14	0.19
	CAKDIAPATTKTTYGMDVW	6	VH3 43	DH6 25	JH6	97	19	-0.17
	CARGSGGNSDSPLDYW	5	VH3 11	DH2 15	JH4	88	16	-0.89
	CARGRYGGGNAYSGTDSW	3	VH4 30	DH2 21	JH4	92	18	-0.98
21	CARATVTLDYYYGMDVW	2	VH6 1	DH1 1	JH6	100	18	0.04
	CARDRVSLAIFDYW	2	VH6 1	DH2 2	JH4	97	14	0.17
	CARVTFGEFDPW	2	VH6 2	DH3 10	JH5	100	12	-0.08
22	CARGYSSSGGTNWFDPW	14	VH6 1	DH6 13	JH5	100	17	-0.79
	CASDVSMSES	4	VH3 74	DH1 26	JH4	95	11	-0.06
	CAKAGETYGLGWYYYDSW	4	VH3 30	DH5-18	JH4	84	18	-0.59
	CARRVGLPGGGMDVW	4	VH6 1	DH3 16	JH6	99	15	0.12
	CTSLHSVSSVYW	3	VH3 74	DH3 9	JH4	99	12	0.45
	CARDRDGYSHYFDYW	3	VH3 30	DH5 24	JH4	100	15	-1.44
	CVRDGWELPRNYYYMDVW	3	VH3 64	DH1 26	JH6	97	19	-0.81
	CASPPYGDYDYW	2	VH3 30	DH4 17	JH4	98	12	-0.99
	CARDGWYSSSWYDGTDFDYW	2	VH3 30	DH6 13	JH4	100	20	-0.73

	CARALGWMSSSWQMGYW	2	VH3 30	DH6 13	JH4	100	17	-0.09
	CVKNSGPGWRFPDW	2	VH3 30	DH5 12	JH5	93	14	-0.89
	CARDRASAGEYW	2	VH3 74	DH6 13	JH4	95	12	-0.96
24	CAREGCGGDCYDFDYW	29	VH3 11	DH2 21	JH4	99	16	-0.69
	CARDHSGSSYGWAFW	15	VH3 11	DH1 26	JH4	93	15	-0.57
	CVRGEYSYDYGKGNLDYW	11	VH3 74	DH5 12	JH4	92	18	-1.06
	CARRGSIWGVSSSGPRHFFDYW	10	VH3 64	DH6 6	JH4	90	22	-0.48
	CAREIVAAGTLSSDYW	7	VH3 23	DH6 13	JH4	96	16	0.25
	CAKDTLPYGDFFDYW	7	VH3 30	DH4 17	JH4	96	15	-0.46
	CARDRPNSSYDMDYW	7	VH3 30	DH5 12	JH4	95	15	-1.54
	CAPTHSSGWAYFDYW	4	VH2 5	DH6 19	JH4	99	15	-0.43
	CARHGGWIPHSFYGMDIW	3	VH4 39	DH4 23	JH6	83	18	-0.17
25	CARAPVRANWFPDW	19	VH6 1	DH1 1	JH4	100	14	-0.44
	CSREHSEGSAPIWGLDYW	9	VH6 1	DH5 18	JH4	86	18	-0.75
	CARDSWFGERVLFVDIW	8	VH6 1	DH3 10	JH3	77	17	0.24
	CAREGRKRGYFDYW	4	VH3 23	DH5 24	JH4	100	14	-1.54
	CARHFSGLPDYFDYW	3	VH5 51	DH1 26	JH4	99	16	-0.50
	CARDSSGSSWRWFPDW	3	VH4 31	DH6 13	JH5	100	16	-1.05
	CARQLGYGMDVW	3	VH5 10	DH5 24	JH6	99	12	-0.03
	CVREVGATWDLGHW	2	VH3 13	DH1 26	JH6	95	14	-0.10
	CARSSGSGSYKYGMVDVW	2	VH4 30	DH3 10	JH6	82	18	-0.59
	CARRSYGDYSYDW	2	VH6 1	DH2 2	JH4	96	13	-1.42
	CARNKQHHYLIFDYW	2	VH4 30	DH2 2	JH4	100	15	-0.89
	CARLFSSAWYEDFDYW	2	VH4 39	DH2 2	JH4	86	16	-0.34
	CALSGSYLDYFDYW	2	VH5 51	DH1 26	JH4	99	14	-0.06

Table 21: CDR3 clones derived from the IgH sequencing data.

Sample ID, CDR3 clone sequence, percentage of the total CDR3 aa repertoire these clones make up, V, D and J gene usage, V-region germline sequence identity, aa length and the GRAVY scores are included within this table.

The maximally expanded clone amongst all samples was seen within SchS-24, making up nearly a third of its total CDR3 repertoire. This was closely followed by the topmost clone in SchS-20 at 23%, SchS-25 at 19% and SchS-22 at 14. Samples 12, 14 and 16 harboured their most abundant clone between 7% and 9%, lower than the aforementioned samples but higher than those of samples 15, 18 and 22. The latter samples demonstrated the lowest degree of clonal expansion and frequency amongst the SchS patients assessed.

Seventy-eight percent of CDR3 sequences making up 2% or over of the total CDR3 aa repertoire largely utilised the VH3 family, with JH4 and JH6 being the common J families amongst these sequences. DH1 to DH6 were the most utilised D families. Based on published CLL analyses, deviance of less than 2% from germline indicates that these sequences are unlikely to be mutated (391), with the latter being true for the top clone in eight out of ten SchS samples. For top clone in samples 14 and 20, the percentage variance from germline was 5% and 3% respectively, indicating possible hypermutation.

The clone length varied from 9 aa (sample 14) to 24 aa (sample 16), with the median value being 15 aa, comparable to healthy individuals (298, 367). The median values all CDR3 aa sequences seen in these SchS patients were in the range of 13 to 15 aa (Figure 61). The grand average of hydrophobicity index (GRAVY) value represents the hydrophobicity of a given peptide. This formula calculates the sum of the hydrophobicity values of each aa in a sequence divided by the sequence length (based on the values provided by Kyte and Doolittle) (392). Positive GRAVY scores indicate the hydrophobic nature of the peptide whereas negative scores denote hydrophilicity. Though the values obtained for the clones in this SchS data set were in the range of -1.54 and +0.66, 81% demonstrated a negative score indicating that the clones seen in this set of SchS are largely hydrophilic.

5.3.5.5 CDR3 clone composition

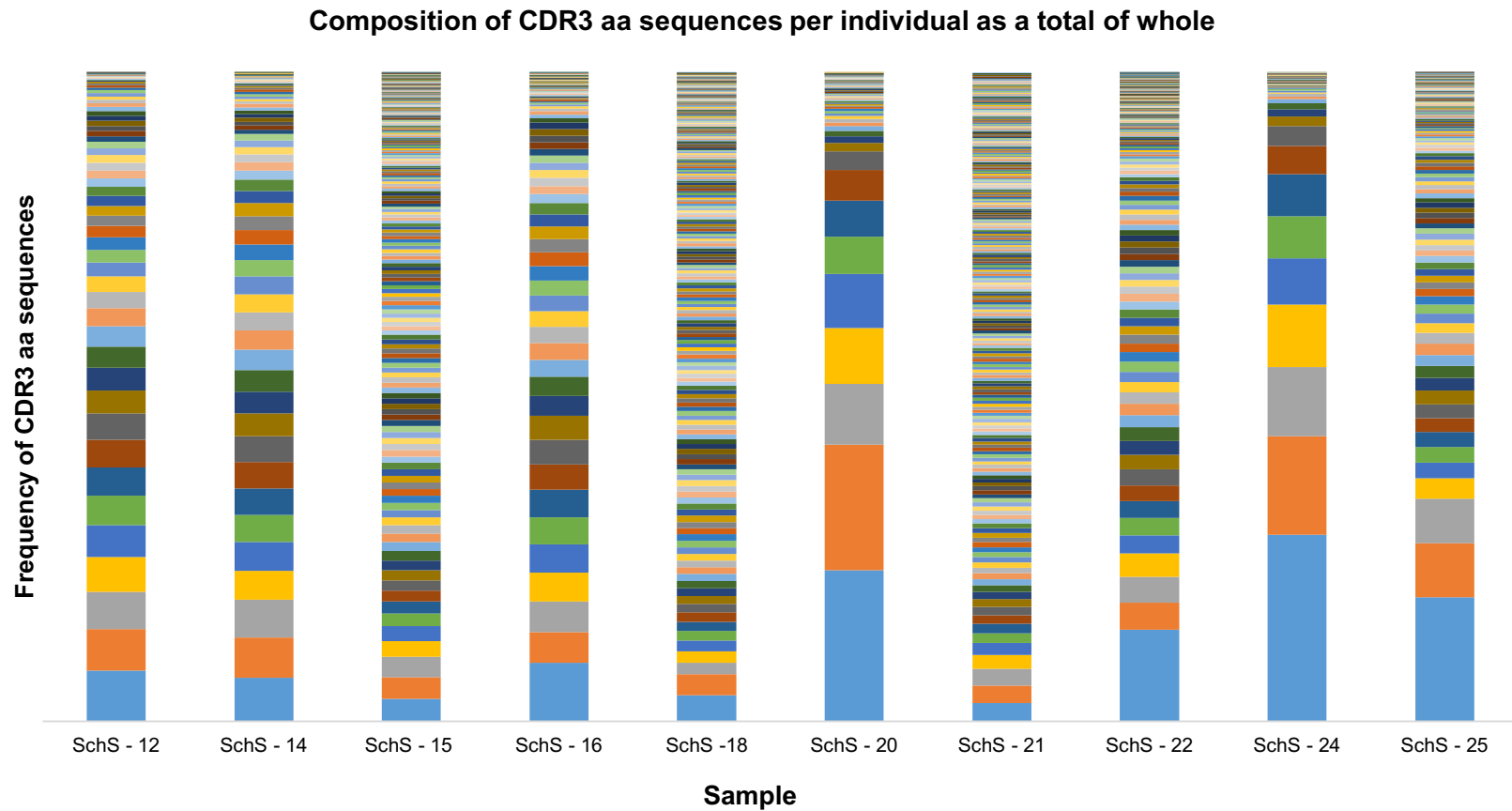


Figure 59 portrays the frequency distribution of all CDR3 aa sequences identified per SchS patient (n=10). One bar is representative of one sample. Each colour is representative of a unique CDR3 found within that sample, with bar thickness pertaining to the frequency of that CDR3 aa sequence.

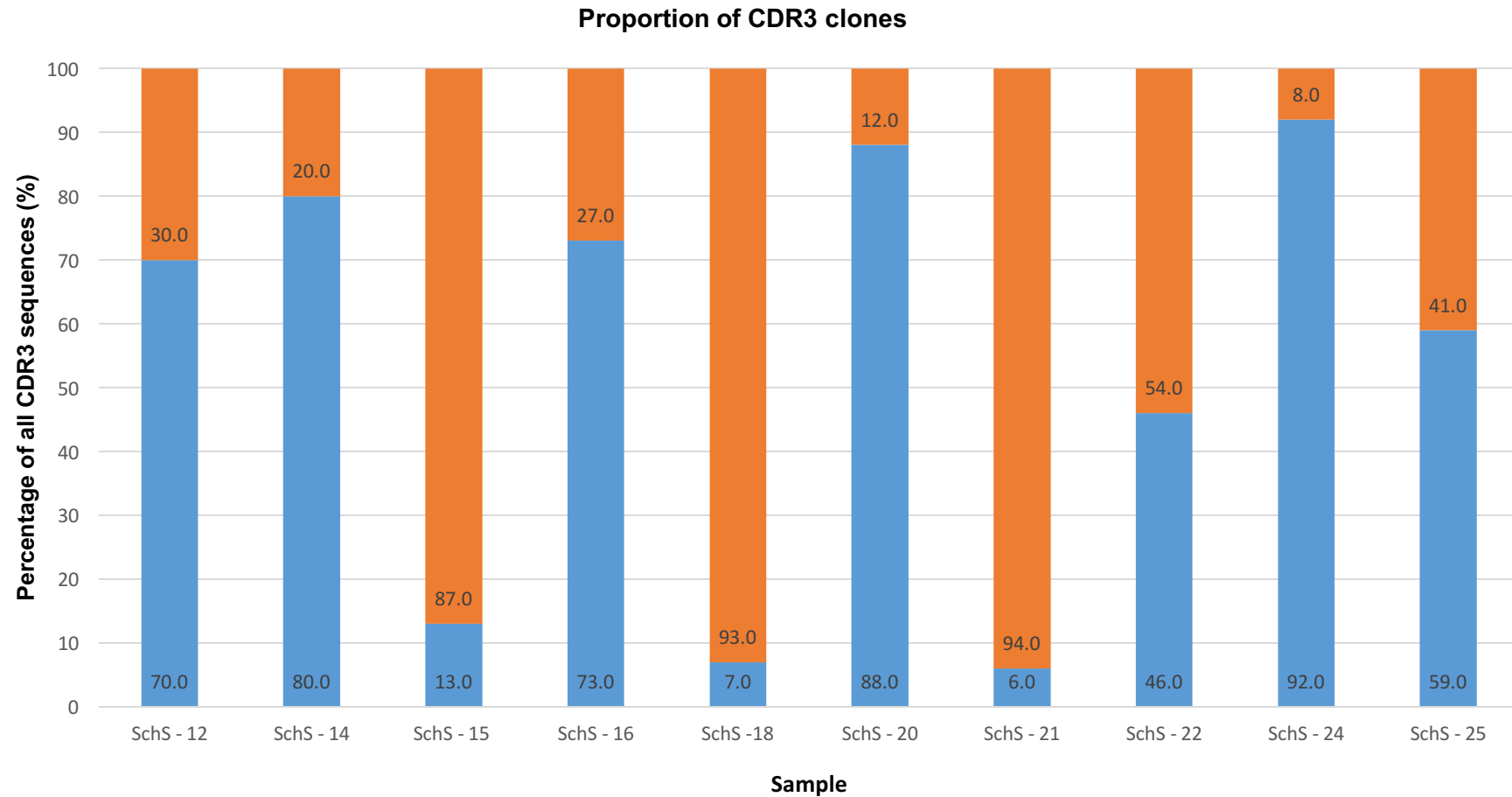


Figure 60: CDR3 clones as a proportion of all CDR3 aa sequences.

The cumulative prevalence of CDR3 aa sequences that appear at a level of 2% or over (regarded as a clone) within each SchS sample (blue), versus those sequences that appear at percentages less than 2% (orange), are shown in Figure 60.

Table 20 indicates the clinical and laboratory findings of the SchS patients included in this body of work. All SchS patients demonstrated evidence of a monoclonal component and NUD (latter detail not indicated in Table 20). The age of symptom onset ranged between 36.8 and 78.9 years, with the eldest patient harbouring the MYD88 L265P as detected by ASO-PCR. None of the patients demonstrated evidence of *NLRP3* mutations, nor did the female SchS patients show XCI as determined by the *HUMARA* assay. Patient 20 was the only patient out of the SchS cohort (n=30, Results Chapter 2), who had a mutation in the MDS-related 28 gene panel (stop-gain mutation in *STAG2*).

From the data shown in Figures 59 and 60 (based on a 10% gDNA B cell content), each SchS sample is indicative of CDR3 aa sequence expansion, though to varying degrees. Likewise, it is possible to categorise these samples into four groups based on these figures. Group one comprises of SchS patients 12, 14 and 16; group two comprises of 15, 18 and 21; group three consists of 20 and 24, with the last group containing 22 and 25. Imperatively, no public sequences were found in this dataset and therefore the aa sequences referred to are unique to each participant.

The most frequent CDR3 clone for each sample in group one exist within the range of 220 to 291 times, with the second most common appearing between 182 to 212 times. For samples 12, 14 and 16, those aa sequences regarded as a 'clone' (Section 5.3.5) cumulatively makeup 70%, 80% and 73% of the total CDR3 aa sequences respectively. Thus, deducing that 20%-30% of these sequences are not 'clones' indicates the existence of considerably sized CDR3 aa sequences amongst a polyclonal background. Interestingly, the detected monoclonal components of samples 12 and 16 are IgM κ , but that of sample 14 is IgG λ . The latter is documented to have a 15% plasma cell bone marrow infiltration, not seen in the other two samples in this group. However, in view of clonality, long term follow up would assess whether this disparity has an effect on clone size and frequency.

Amongst group two, the proportion of CDR3 aa sequences pertaining to a clone are less than 14% in each sample, with the most expanded sequence falling within the range of 76 to 127 times. Hence, in comparison to groups one, three and four, the clonal population is markedly lower. Unusually, SchS patient 15 had levels of IgM κ falling within the 'normal' range at 1g/l, which could be explanatory of the decreased clonality seen. Interestingly, the other two samples in this grouping had the monoclonal IgM of the lambda subtype. Literature indicates that 90% of SchS cases have been associated with a kappa light chain (26), therefore, the possible degree to which persistence of IgM λ has a bearing over clonal expansion, remains to be investigated through long term monitoring of these CDR3 clones.

Patients 20 and 24 establish CDR3 clones amounting to 88% and 93% of their total repertoires respectively. The relatively higher frequency of the unique CDR3 sequences making up their B cell repertoire suggests the existence of a subset of clonally expanded B-cells. The LPL and MDS-associated mutation documented in patient 20 is likely to influence clonal expansion and predisposition to a proinflammatory environment respectively. Inference that this increased degree of clonality is not entirely causative by the LPL or the *STAG2* mutation, is on the basis that SchS 24 didn't demonstrate these findings, yet showed a larger proportion of CDR3 clones.

SchS patients 22 and 25 can be placed into group four with their clones corresponding to 45% and 65% of their total sequences respectively. The top clone for each sample appeared between 452 and 638 times. Interestingly, patient 25 harbours the L265P mutation and the latter pathogenic variant is a predisposition to an altered proinflammatory microenvironment and increased NF- κ B signalling (393), possibly leading to the expansion of a subset of B cells producing the monoclonal component. However, the absence of this mutation in the other SchS patients also demonstrating clonal expansion indicates that this mutation is not entirely causative of such clonal events.

Although patient 12 had a partial response to treatment established a degree of clonality, those patients who were deemed 'most clonal' (i.e. groups three and four) established a successful response. Though the treatment outcome may be influential upon B-cell expansion, a clear association between IL-1 blockade and a clonal reaction can be ruled out.

The arrangement of these samples into four distinct groups based on the abundance of CDR3 clones per individual, perhaps indicates that SchS is a condition progressing into a more clonal disease over time, with a subset of patients likely to develop WM as a consequence of such expansion. Evidently, age plays a role in SchS, as those patients demonstrating the most clonal proliferation, were amongst the eldest in this cohort.

Regardless of a 10% or 1% B-cell DNA content, the CDR3 aa sequences remain represented at the same levels. For example, the first ranked sequence in both assumptions makes up 19% of the total CDR3 repertoire. In view of the top 10 CDR3 sequences, although the percentages remain the same, removal of the tail end leaves those aa sequences that pertain to a clone (making up over 2% of the CDR3 repertoire). Although this panel described refers to patient 25, this is also the case for the other nine patients included in this study.

5.3.5.6 CDR3 length

As the length of the CDR3 region of the Ig gene bears great influence over antigen specificity, the following section examines the length of this region from the resulting sequencing data. Analysis of CDR3 length variation may reveal certain trends in view of the hypothesis that SchS is a B-cell clonal disease, sharing IgH characteristics amongst 10 SchS patients.

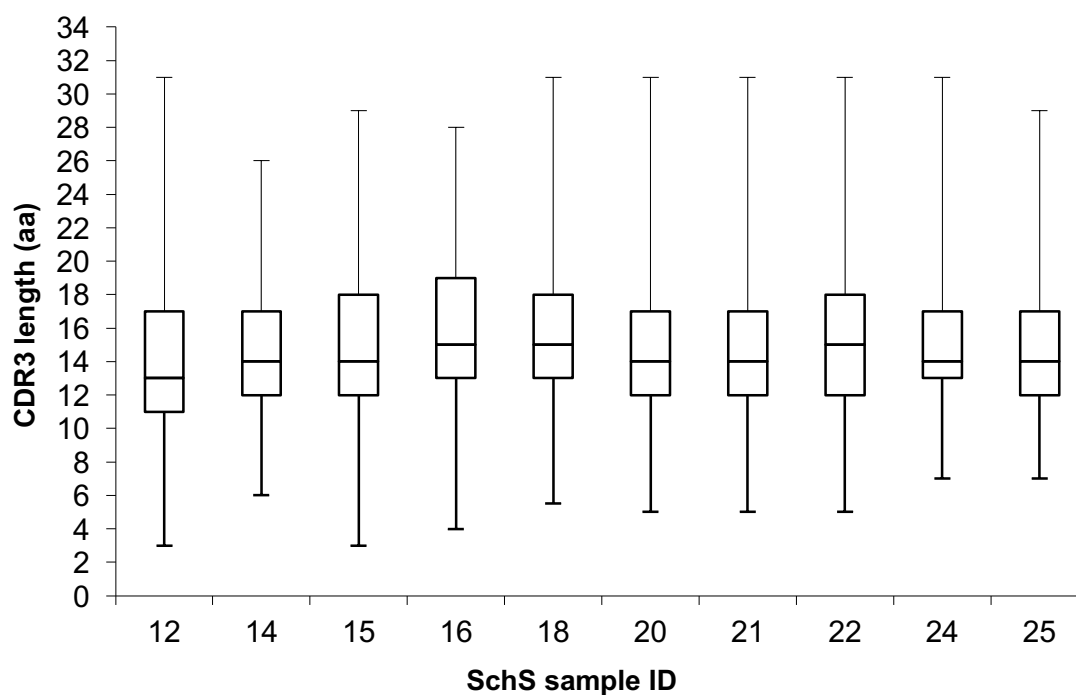
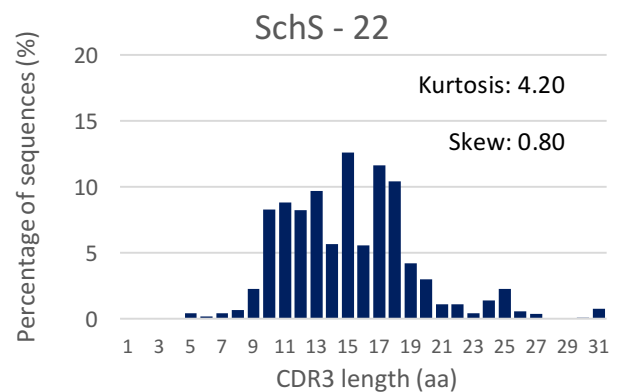
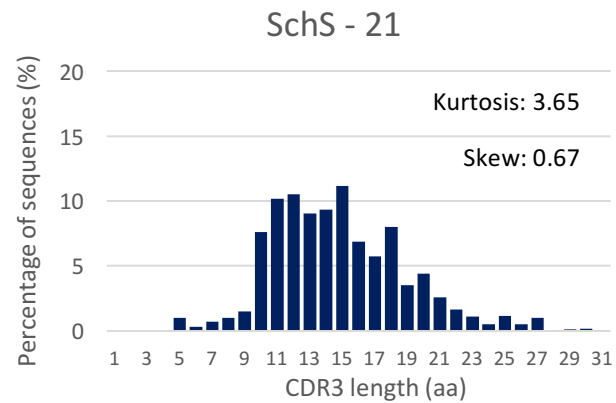
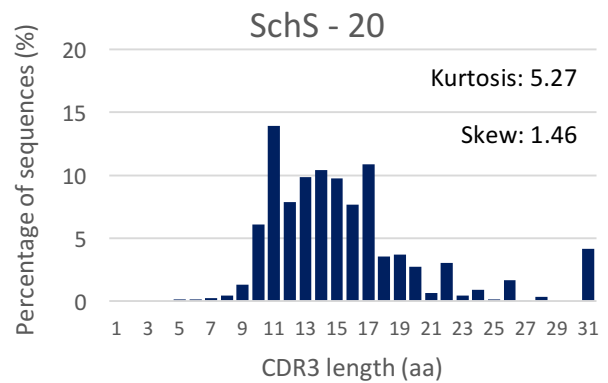
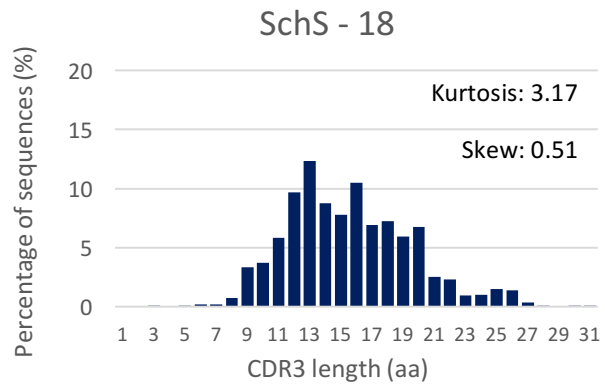
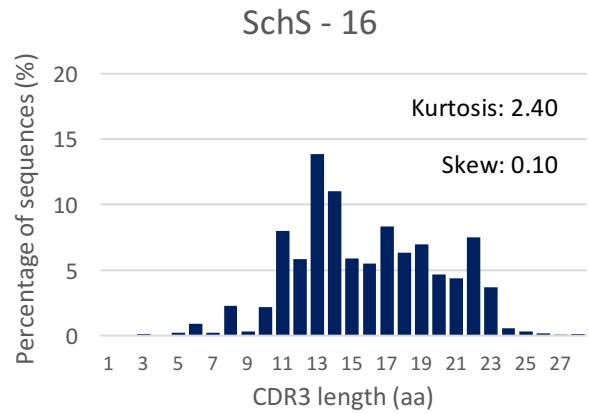
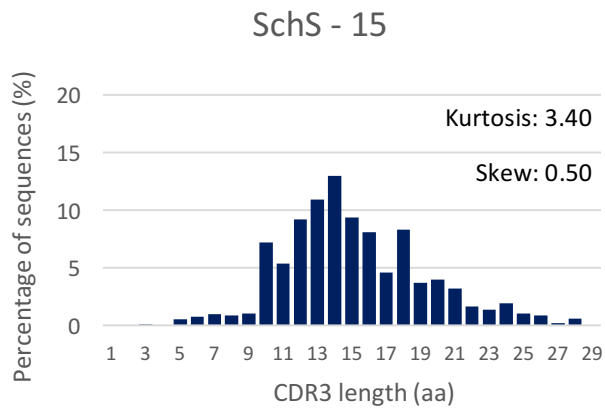
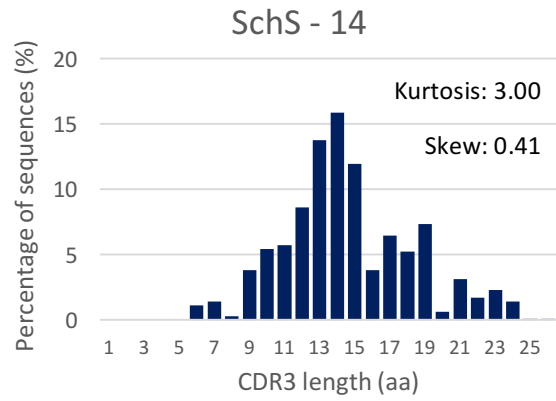
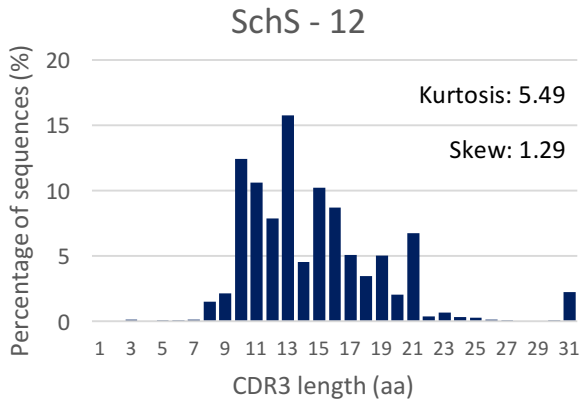


Figure 61: Box and whisker plots comparing CDR3 lengths across 10 SchS patients.

Figure 61 compares the CDR3 length data obtained from the 10 SchS patients included in this work. The whiskers denote the ranges, with the interquartile and median values indicated by the boxes. The median CDR3 lengths across all 10 SchS patients were either 13, 14 or 15 aa, with range between 3 and 31 aa. A large amount of data demonstrates that the majority 'healthy' CDR3 lengths are amongst 8 to 18 aa with median values of 15.5 to 16 aa (298, 353), one to two aa longer than the median values found within SchS patients.



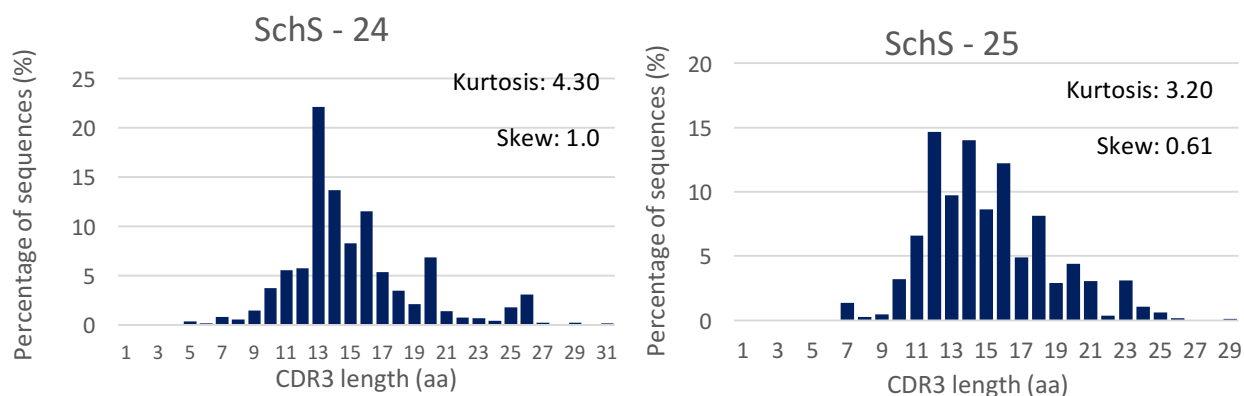


Figure 62: CDR3 length distribution.

Bar graphs demonstrating the distribution of the CDR3 length in amino acids between all sequences from 10 SchS patients. Each peak corresponds to a CDR3 length, comprising of multiple sequences.

The graphs in Figure 62 demonstrate the CDR3 lengths used within a sample, plotted as a percentage of total CDR3 aa sequences. Visualisation of length distribution is also possible with this figure and all 10 SchS samples generally follow a Gaussian distribution. SchS 12 had a median length of 13 and 95% of the CDR3 sequences varied between 8 to 21 aa's. The most commonly seen length was 13 aa, making up 15% of the total sequences. SchS 14 showed a median length of 14 with 99% of CDR3 sequences falling between the range of 6 to 24 aa's. The predominantly used length was determined to be 14 aa at a 16% frequency. Analogous to SchS-14, 14 aa was the commonly employed length in sample 15, but with a reduced fraction of these sequences at 13%. Fourteen aa was its median length and 94% of CDR3 sequences fell between 9 to 25 aa's. Sample 16 had 97% of its CDR3 sequence lengths encompassed within 8 to 23 aa's and the most prevalent length of 13 aa formulating 14% of the total sequences. The median for this sample was 15, with sample 18 showing the same. The latter sample encompassed 99% of its lengths between 9 and 26 aa's, with the most commonly used length of 13 aa pertaining to a 12% value of total. In contrast to the previous sample, 11 aa was the most frequently used length in SchS 20 at a 14% value, despite having 93% of its lengths between the same range as SchS 18. The median length for SchS 20 was 14. Similarly, sample 21 presented a median length of 14 aa, with the most frequently used length at 15 aa making up 11% of the total CDR3 sequences. Nearly 100% of CDR3 lengths found within SchS 21 were included within the range of 5 to 27 aa's. Identical to sample 21, sample 22 demonstrated 15 aa as the most prevalent length, but this pertained to a slightly elevated value of 13% of total CDR3 sequences. The range of aa was between 9 and 25,

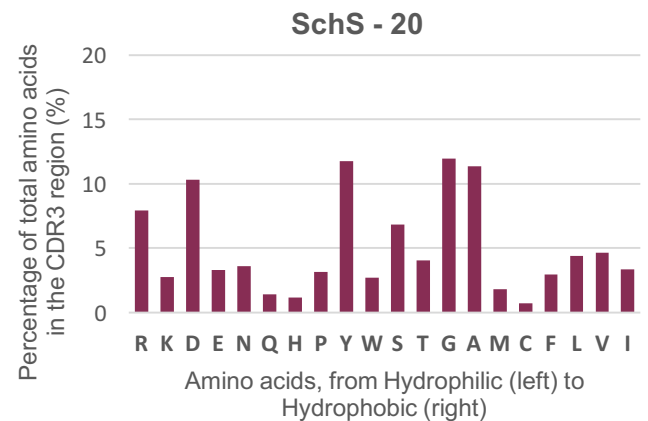
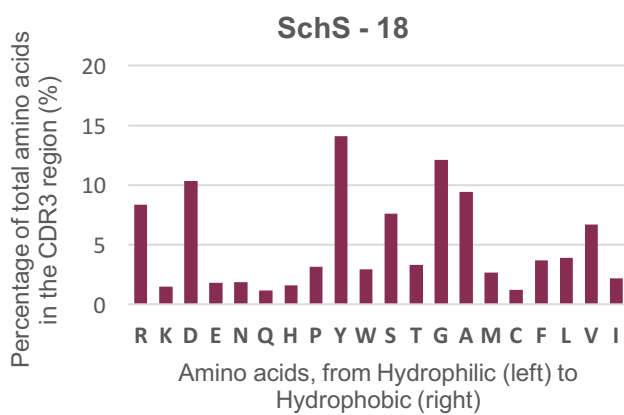
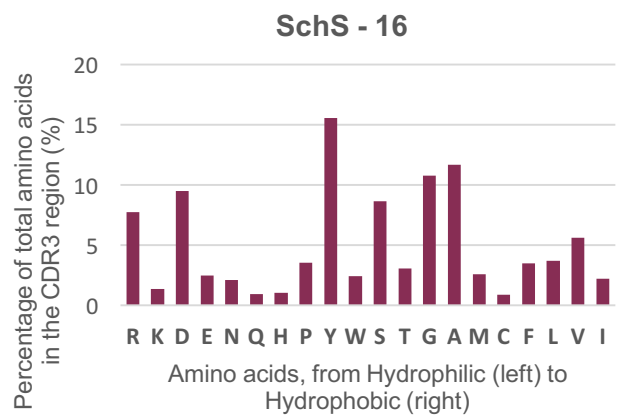
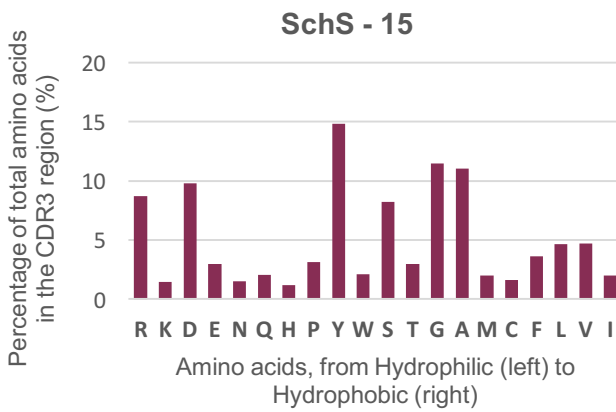
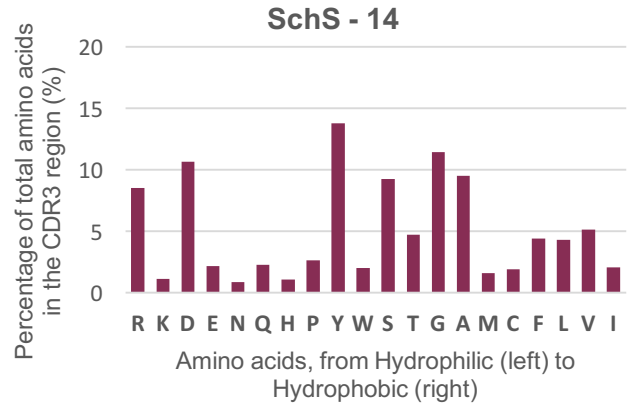
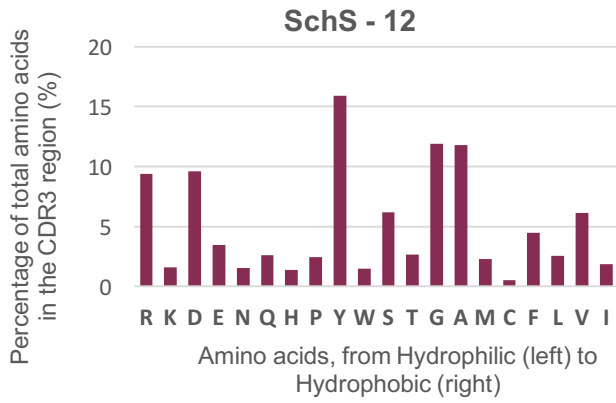
covering 96% of total sequences, accompanied by a median of 15. Comprising over a fifth of total sequences, 13 aa was the most common CDR3 length in sample 24. The median was 14 aa and 97% of sequences within this sample sat in the range between 9 and 26 aa. Lastly, sample 25 had a range of 7 to 24 aa, which encompassed 90% of the total CDR3 lengths found. Closely, 12 aa and 14 aa were the most prevalent lengths within this sample, making up 14.7% and 14% of the total frequency respectively. This sample had 14 aa median. Notably, samples 12, 20 and 22 demonstrated a 2%, 4% and 1% length at 31 aa's respectively, the largest length seen within this dataset with a percentage usage of 1% or over. Likewise, the shortest length of 5aa was seen within SchS 21, exhibiting a 1% frequency of total CDR3 samples.

In addition, the skewness and kurtosis of the data were calculated to assess whether the CDR3 lengths conformed to a normal distribution. Where skewness measured the CDR3 length distribution symmetry above and below the mean, kurtosis measured the events in the central part of CDR3 distribution in comparison to that in the tails of the data. Kurtosis therefore defines the height and peakedness of the central data, relative to a standard Gaussian distribution (348, 394). The following inferences have been made on the basis that values obtained between -1 to +1 for skewness and between -2 and +2 for kurtosis indicates a symmetric and univariate distribution (395). With regards to skewing, samples 12 and 20 are above 1 and thus highly skewed. Interestingly, sample 20 demonstrates one of the highest levels of clonal expansion in comparison to a majority of the other samples, whereas sample 12 shows evidence of such expansion but to a lesser degree. Samples 18, 21, 22, 24 and 25 have a moderately skewed distribution, although sample 21 can be considered as the sample exhibiting the least evidence of clonal expansion. Showing values between -0.5 and +0.5, samples 14, 15 and 16 can be considered as approximately symmetric, but show a degree of clonality. Overall, the lack of equivalence for length of distribution as denoted by the skewness of the data for seven out of 10 samples and the fact that all 10 samples demonstrated kurtosis values above 2 suggests that the CDR3 lengths do not generally follow a Gaussian distribution.

The median lengths for the clones (Table 21), remained in the region of 14 aa to 16 aa for each sample aside from sample 16, whose median clone length was 19 aa. In view of the kurtosis seen for each sample, this essentially indicates that the clones are not located in the tails of the data and are encompassed largely within the central part of CDR3 distribution.

5.3.5.7 CDR3 aa composition

The CDR3 is highly diverse in composition and thus, correlations can be drawn between B cell diversity and CDR3's broad variability (348).



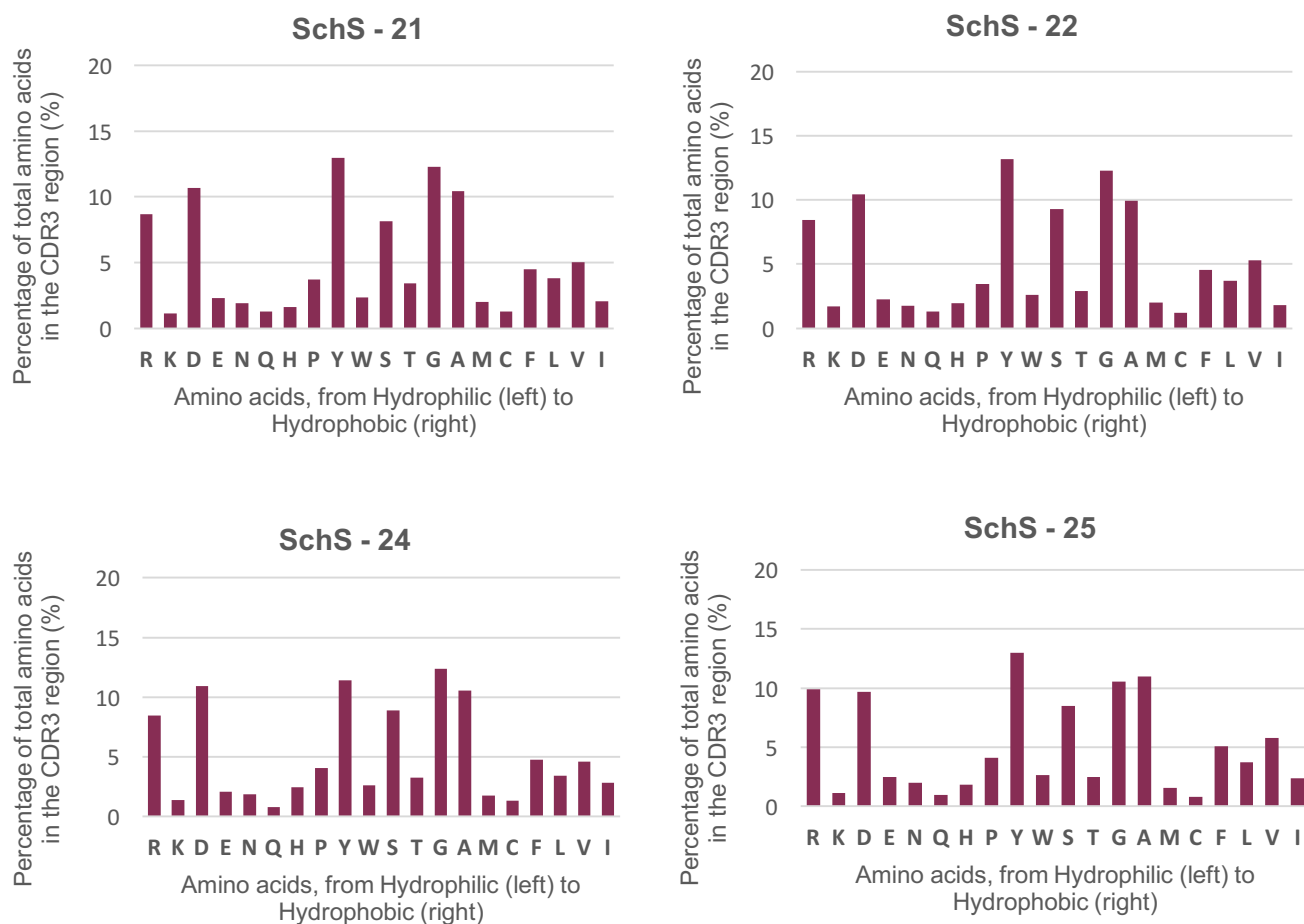


Figure 63: CDR3 composition in SchS patients.

Figure 63 comprises of bar graphs visualising how frequent each amino acid is used in the CDR3 of all sequences from 10 SchS patients. Percentages are plotted for each amino acid ranging from Hydrophilic to Hydrophobic, the order based on the Kyte & Doolittle scale of hydrophobicity (392).

Each graph shows the aa's on the X-axis – arranged by the Kyle Doolittle scale of hydrophobicity (392) – with the percentage of total aa's in the CDR3 region on the Y-axis. On the whole, each SchS sample had similar percentage compositions of aa's in their respective CDR3 regions, though minor fluctuations could be seen. The most commonly used aa's were tyrosine (Y), glycine (G), alanine (A), aspartic acid (D) and arginine (R) accompanied by the following ranges respectively: (Y) 11.4% - 15.9%; (G) 10.8% - 12.4%; (A) 9.5% - 11.8%; (D) 9.5% to 10.9% and (R) 7.8% to 9.9%. Cysteine (C), histidine (H), lysine (K), asparagine (N), methionine (M), glutamine (G) and tryptophan (W) were amongst the least employed aa's with all frequencies at 2% or below.

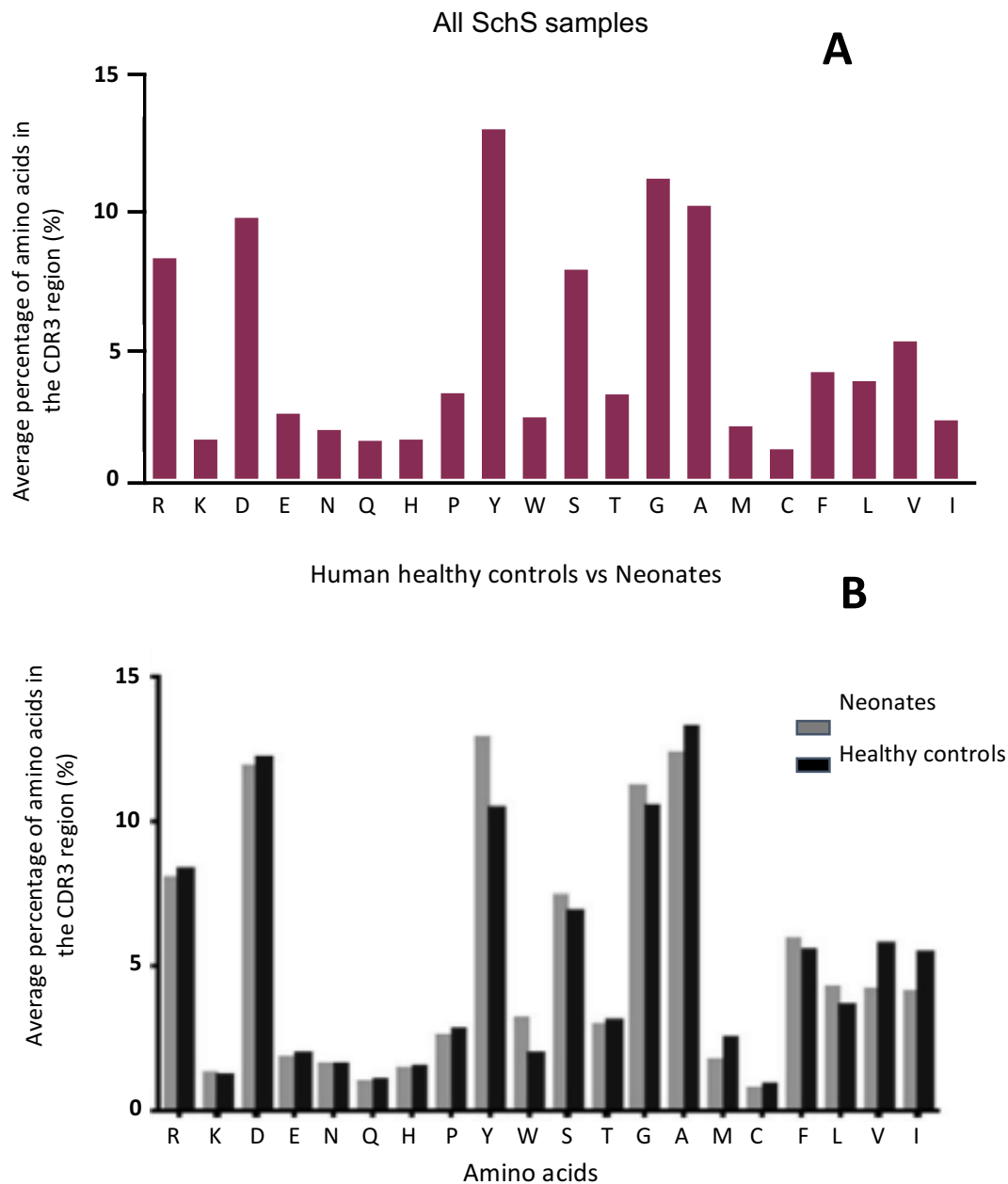


Figure 64: Comparison of 10 SchS CDR3 aa compositions.

Comparison of 10 SchS CDR3 aa composition 64A, with the compositions of 2 sets of data derived from literature. Figure 64B represents healthy controls (n=33) vs neonates (n=10).

Figure 64B has been included as an illustrative comparison for the CDR3 composition results obtained. Figure 64B corresponds to the work by Hong *et al* (353), in which the cord blood of 10 newborns and the peripheral blood of 33 healthy controls (average age of 44 years) was analysed using gDNA – analogous to the work presented in this section of work. Comparing Figure 64A and B, SchS patients and healthy controls both use top frequently occurring aa's in CDR3, arginine, lysine, tyrosine, glycine and alanine. Further, as shown in Table 21, a majority of the clones seen in the SchS data are largely hydrophilic, whereas more hydrophobic CDR3's are associated with autoreactivity (396, 397).

5.3.6 VDJ usage

The second parameter to study the entire immune repertoire of SchS patients in this work was the analysis of V-D-J gene segment combinations.

5.3.6.1 Frequency of VH, DH and JH gene usage (genes)

A widely used metric is the assessment of how frequently V gene segments are used, with the following data demonstrating the percentage of V gene segments utilised within the SchS cohort.

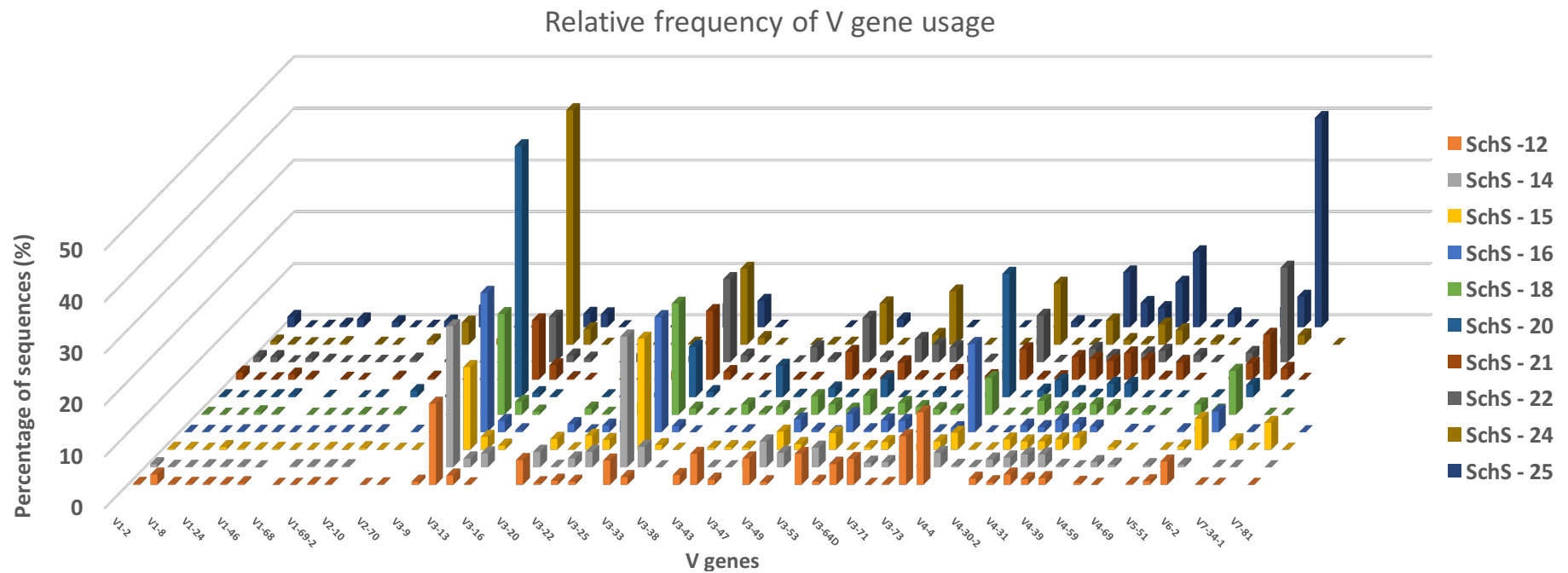


Figure 65: V gene usage in 10 SchS patients.

The bulk repertoire of total B cell DNA, demonstrating V gene usage amongst 10 SchS patients on the X axis, shown as a percentage on the Y axis.

Relative frequency of D gene usage

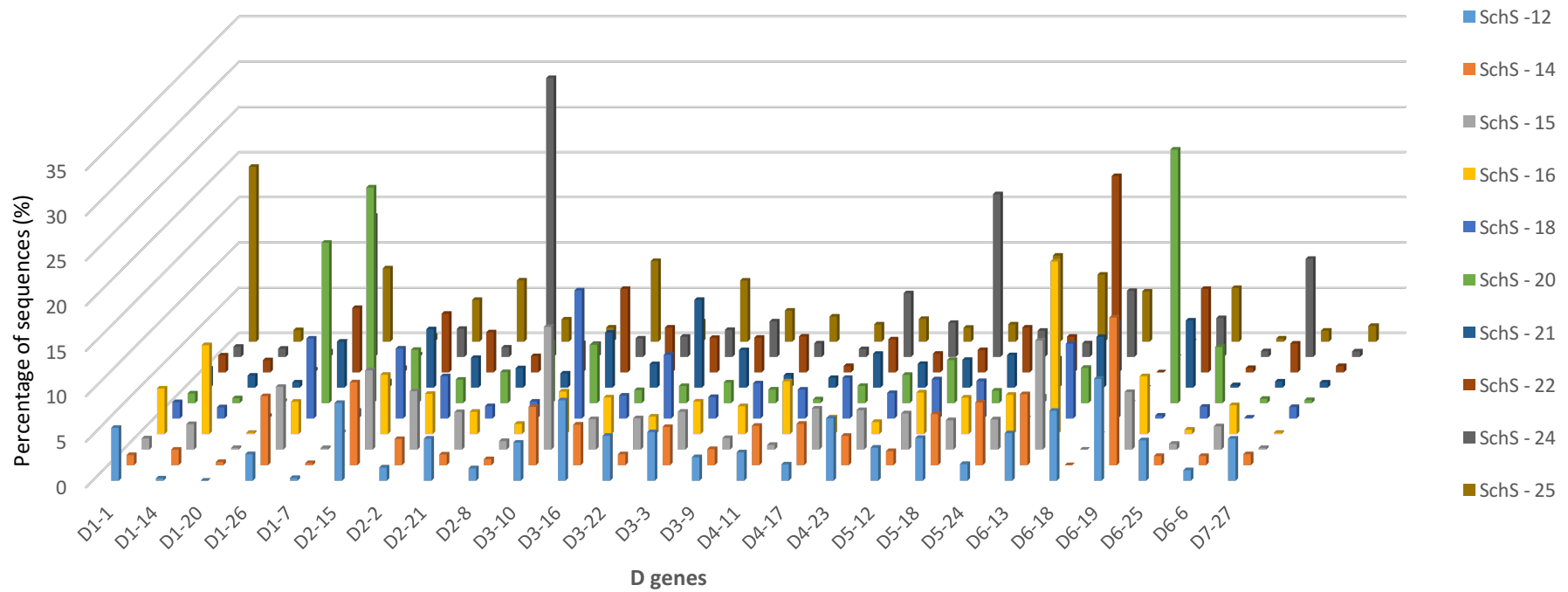


Figure 66: D gene usage in 10 SchS patients.

Figure 66 shows a bar chart showing specific D gene usage (X axis) as a percentage of total sequences (Y axis) for 10 SchS patients.

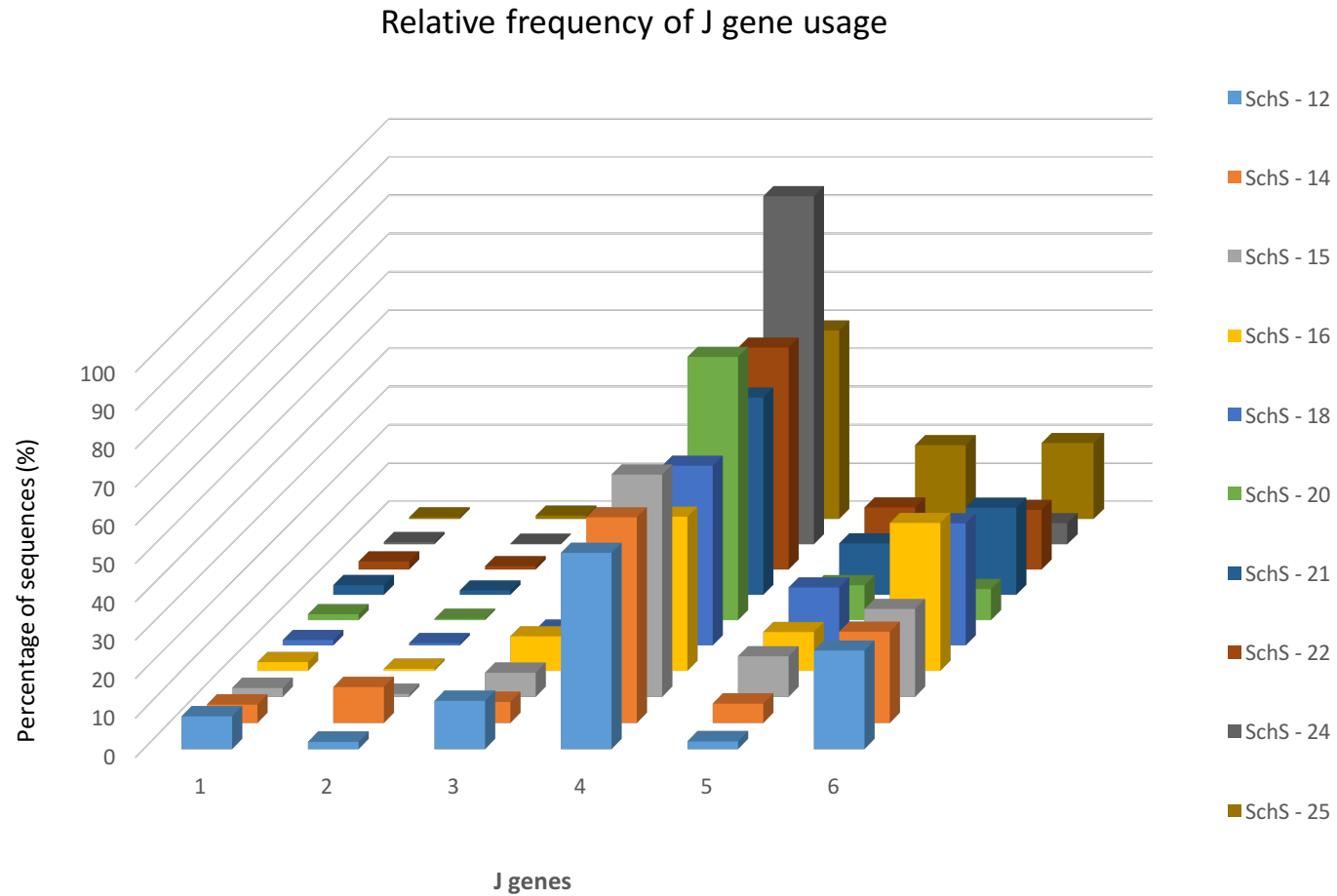
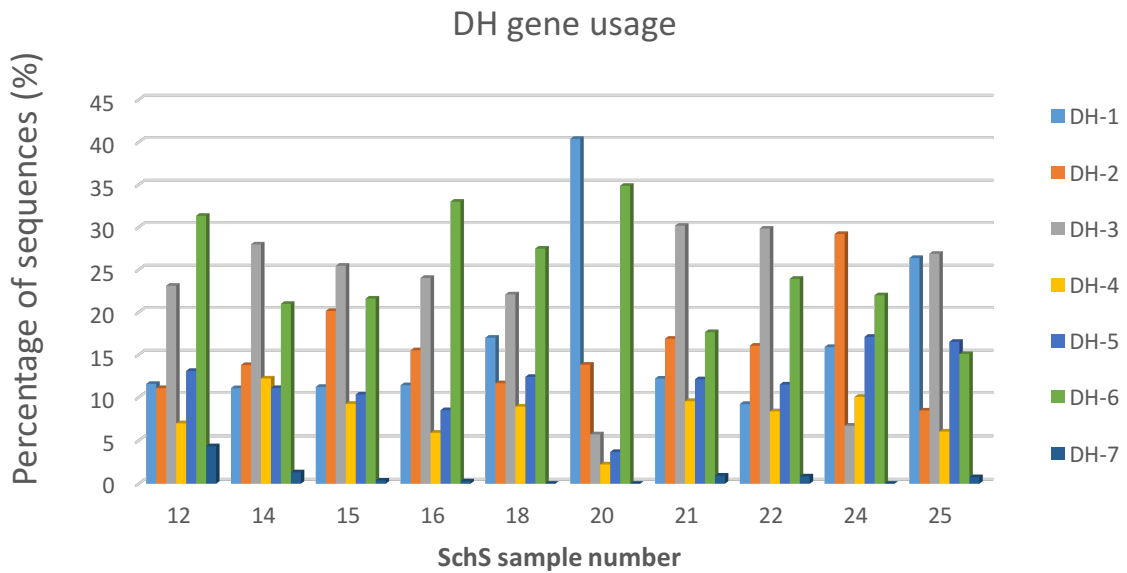
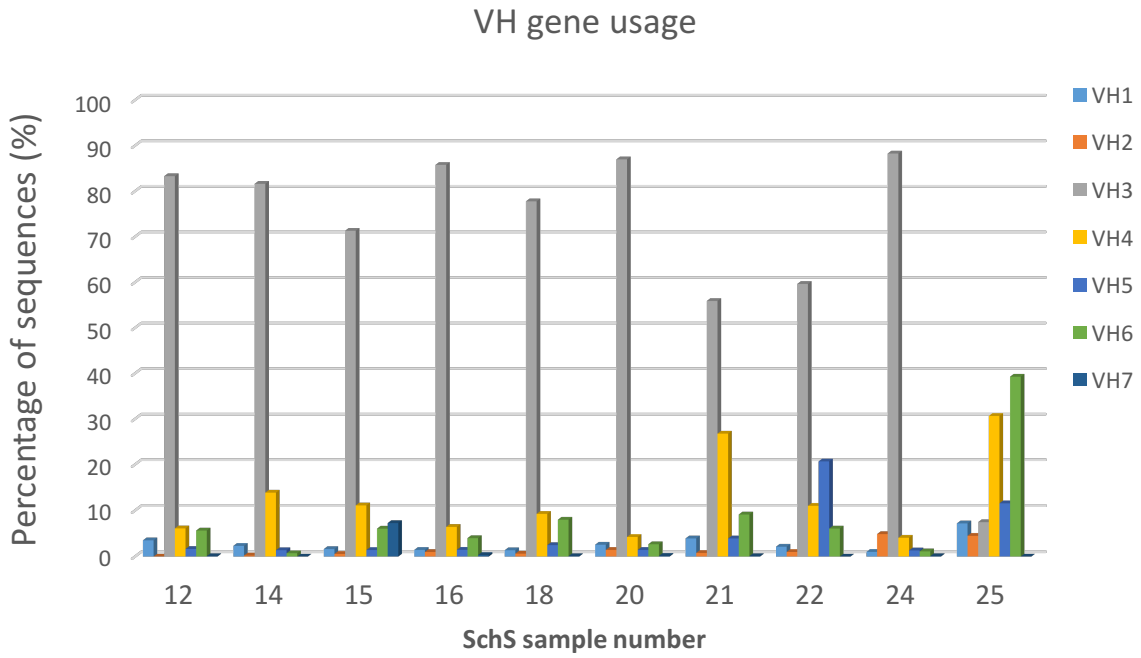


Figure 67: J gene usage in 10 SchS patients.

Figure 67 shows a bar chart alluding to specific J gene usage (X axis) as a percentage of total sequences (Y axis) for 10 SchS patients.

5.3.6.2 Distribution of V, D and J gene usage (families)



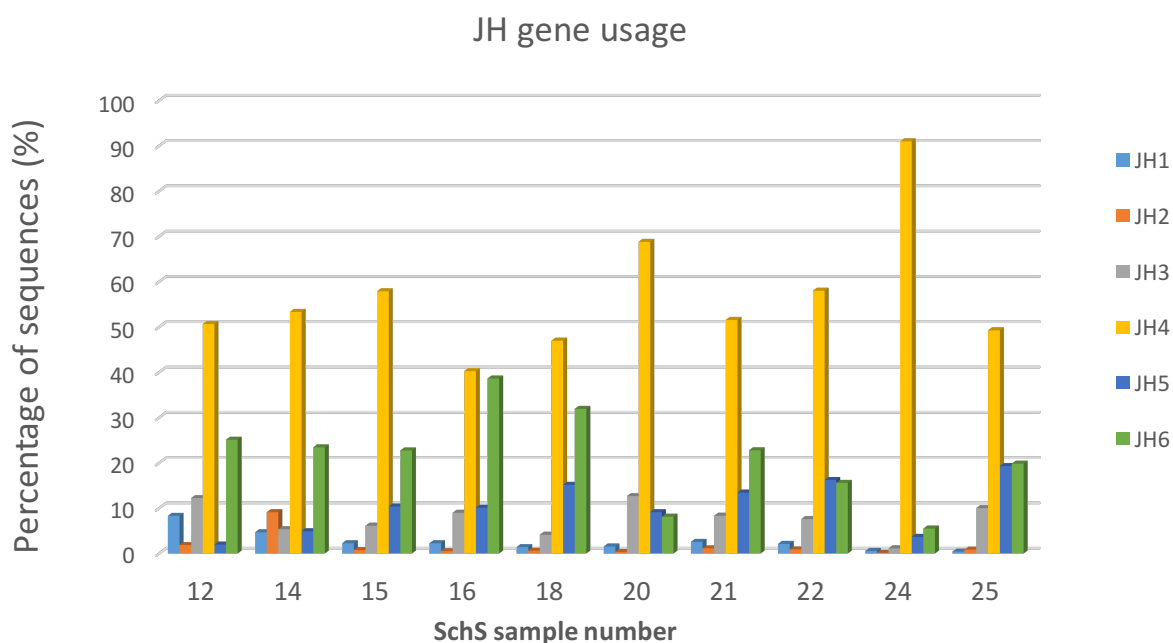


Figure 68: VH, DH and JH gene usage.

Figure 68 shows bar charts summarising VH, DH and JH gene usage in the SchS cohort. The percentage of sequences are on the Y axis with the sample number on the X axis. VH, DH and JH usages are shown as the percentage of sequences on the Y axis.

The IgHV, IgHD and IgHJ genes are grouped into major families based upon the homology of their nucleotide sequences. Dependent upon the haplotype of an individual, the IgHV locus comprises of over 50 functional genes and are grouped into 7 major families; the IgHD locus spans across 27 genes and grouped into 7 families; and the IgH locus consists of 6 genes and grouped into 6 families (398). The data presented in this section illustrates the usage bias that occurs to certain V/D/J genes and families within SchS patients, and comparing this to usage to other disease groups and healthy controls as stated in literature.

5.3.6.3 VH usage

Whilst encoding CDR1 and CDR2, the V gene family only contributes a few nucleotides to the CDR3 region. VH3 is the most used VH family in nine out of 10 SchS patients at an average of 75% and in contrast, sample 25 shows preference to VH6 at 40% usage of total sequences, closely followed by VH4 usage at 30%. More precisely, VH3-11, VH3-30, VH3-74 and VH6-1 are the most commonly employed VH gene segments in the data presented (Figure 65). In regards to the clones (Table 21), VH3-11, VH3-30, VH3-74, VH3-64 and VH3-23 were the maximally used VH3 genes with VH6-1 as the commonly used VH6 gene segment.

Samples 20, 22, 24 and in particular, sample 25, showed disparity with regards to VH gene segment patterns within their clones. The VH2 family was absent from the top CDR3 aa sequences of the other nine samples, although VH2-5 was exclusively used by sample 24 at 4%. The VH4 family was employed in the clones of SchS 20, 24 and 25, a finding not emulated in the other seven patients. Where the VH5 family usage in clones was exclusive to SchS 25, this sample also demonstrated VH6-1 usage at 36%, the highest VH6 family usage in the top clones of the samples, followed by sample 22 using VH6-1 at a cumulative 18%. The other patients utilised VH6 to a decreased percentage (i.e. top clones for SchS 18 and SchS 21 used VH6-1 at 7% and 6% respectively).

5.3.6.4 DH usage

Between the V, D and J genes families, the D gene family bears the greatest influence on CDR3 by the contribution of all nucleotides (391). In seven out of the 10 samples (SchS 12-18 and SchS 22) with a 25% usage each, DH3 and DH6 were the most frequently used gene families in the entire repertoire. Similar to VH findings, samples 20, 24 and 25 showed differential DH usage patterns in their repertoires. SchS 20 preferentially employed DH1 at 40%, sample 24 using DH2 at 29% and sample 25 used both DH1 and DH3 at 26% and 25% respectively. In view of the clones, these DH gene families were used to largely the same values.

5.3.6.5 JH usage

Encoding part of the last section of CDR3, J genes are also important contributors to the generation of antibody diversity (196). Each of the 10 SchS patients followed the same JH usage patterns in their repertoires with JH4 being the most frequent J gene followed by JH6. JH4 was the most used within the range of 40% to 90% and JH6 usage was within the range of 6% to 39%. These gene families were also recurrently used by the clones.

5.3.6.6 Comparison to WM and Healthy Controls

Interestingly, isolation of IgM from a WM patient and subsequent cloning of the variable region of the antibody (Figures 45, 46 and 47), showed preferential usage of VH3-30 (399), a segment used biasedly in this data at an average of 14.5% of all SchS patients. The former finding was further mirrored in the study by Petrikkos *et al*, demonstrating that 74% of the WM patients included in their research demonstrated preferential usage of the VH3 family, with distinctive usages of VH3-30 in 8% and VH3-74 in 17% of the patients (198). The authors also found VH3-23 particularly used in a quarter of the patients (averagely used at 2% in the entire repertoire of all SchS patients – but at 4% and 7% in SchS 24 and 25 respectively); however, VH3-74 was found used in all SchS patients' IgH repertoire at an average of 12.5%. Mirroring

the other WM findings, a largely VH3 restricted repertoire alongside preferential JH4 usage were the conclusions made by Kriangkum *et al* through repertoire analysis of 15 WM patients (400). Within the data sought through this chapter, JH4 was the most preferentially selected member of the JH family in all SchS samples at an average of 57%.

Bearing percentage similarities to SchS, a study sequencing the IgH region of monoclonal IgG antibodies derived from memory B cells from four healthy donors noted the heightened usage of the VH3 family at over 50% of the repertoires, followed by the VH4 family at around 25% (401). However, research by Hong *et al* (353) sequencing cDNA deduced that healthy individuals (n=33) used VH4 at 43% and VH3 at 25%, alongside neonates (n=10) using both these VH families at an average of 31%, both cohorts in stark contrast to nine out of the 10 SchS patients sequenced in this work where 75% was the average VH3 usage. The differences seen between the aforementioned papers maybe to do with the variation in sample size, or the fact that the latter study attempted to assess the entire IgH repertoire, as opposed to the former study where calculations were made based on secreted IgG antibodies only. Though comparably, Hong *et al* found the DH3, DH6, JH4 and JH6 the most frequently used gene segments, similar to the data found with these SchS patients (353).

5.3.7 V-J recombination

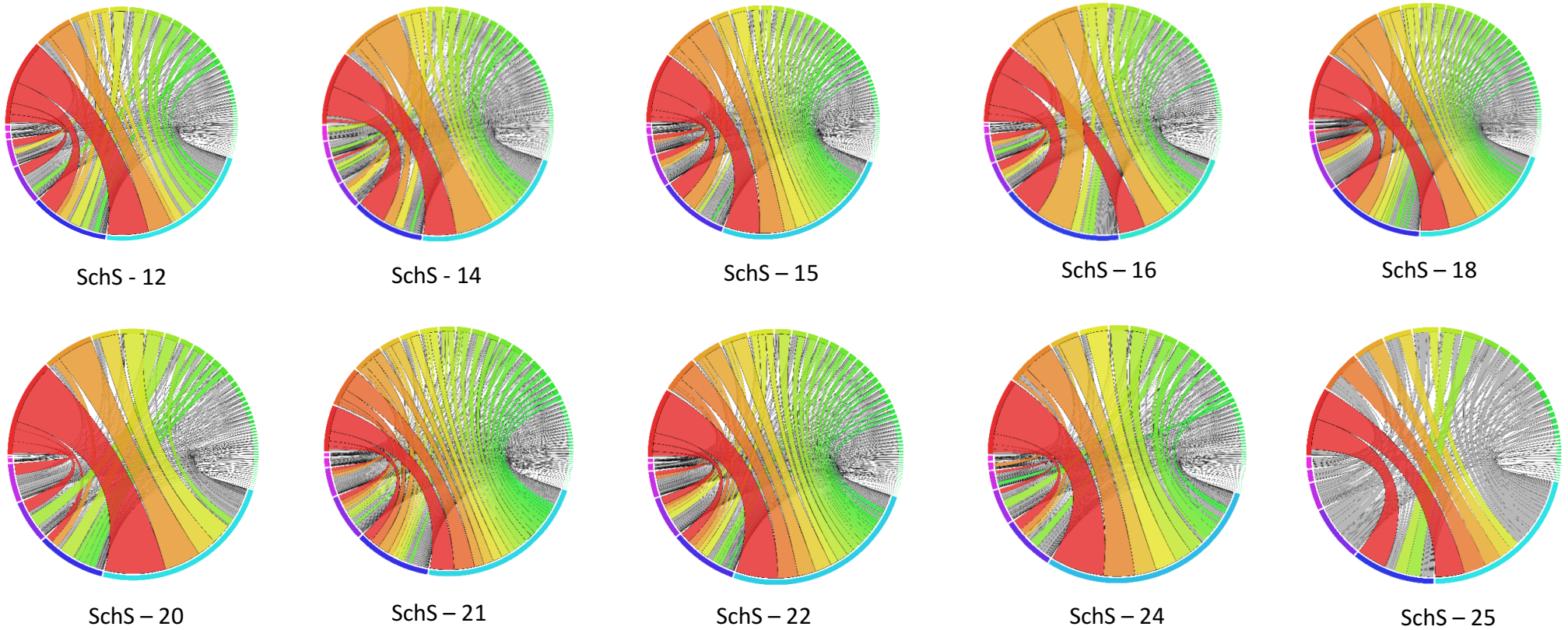


Figure 69: Representative circos plots of V-J recombination.

The plots shown in Figure 69 indicate the frequency at which a V-J combination is used. The colours indicate those V-J combinations pertaining to more than 1% of the total nucleotide sequences observed, whereas the grey lines correspond to combinations constituting less than 1%.

The circos plots in Figure 69 summarise the V to J combinations used in the rearranged Ig genes for IgH in 10 SchS gDNA samples. Rearrangement of a V gene with a J gene is shown by the presence of a ribbon. Each ribbon has a designated colour, each colour indicating a different member of the VH gene family participating in the recombination event. The greater the width of the ribbon, the higher the frequency of that particular VH gene combined with a certain JH gene. As alluded to in greater depth in Section 5.3.5.1, a 'clone' in this data was referred to as an identical CDR3 aa sequence using the same VH gene and JH segments forming 2% and above of the entire IgH repertoire sequenced. Therefore, additional V-J combinations resulting in CDR3 aa sequences not categorised as clones are also illustrated in the figures. These plots are a visual representation of the recombinations and easy to denote overrepresentation. Although the prevalence of certain V-J combinations are not entirely indicative of clonality (i.e. clonal populations of B cells), preferential usage of particular gene segments point towards a skewed IgH repertoire.

The light blue and navy blue arcs located within the bottom half of the circos plots denote the JH4 and JH6 families respectively (aside from sample 25, where the navy blue arc represents JH5). The VH family arcs within the top half of the plots are in clockwise order of most employed VH segment to the least. For each sample, the red and orange ribbons demonstrate the most frequent recombination within each patient. Samples 12, 14 and 16 preferentially pair the VH3/JH4 and JH6 families whereas samples 15, 18 and 21 have a preference to joining VH6/VH3 to JH4 and JH6. A substantial portion of the IgH repertoire in SchS 20, 22 and 24 is restricted to VH3/JH4 pairings, and in contrast to the other nine samples, sample 25 exhibits enhanced familial pairing of VH6/VH4 to the J4 and J5 genes. The sample grouping here is similar to that of those suggested in Section 5.3.5.5, where expansion of CDR3 aa sequences are described. The more clonal samples are those with a more restricted repertoire (i.e. samples 20, 22, 24 and 25) in contrast to the other SchS patients demonstrating more diverse CDR3 aa repertoires, varied IgH segment and heavy chain VJ recombination bias to a lesser extent.

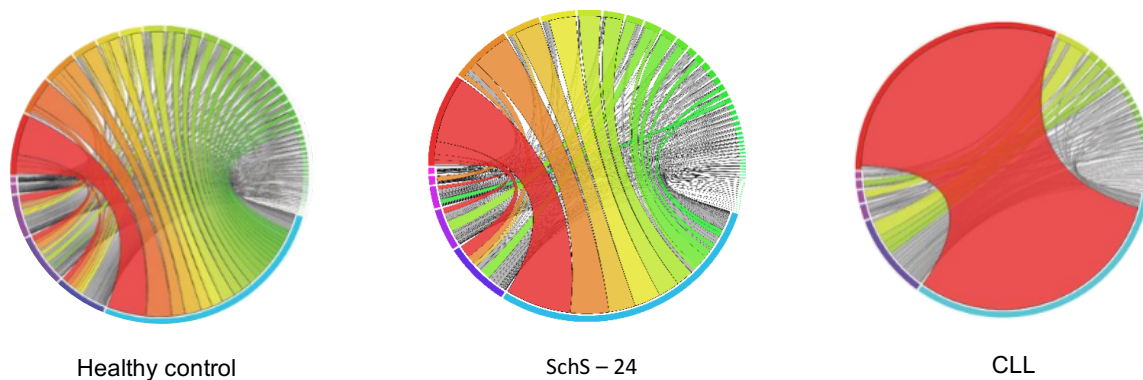


Figure 70: Circos plots of HC, SchS-24 and CLL.

HC and CLL plots were obtained from the work carried out by IJspeert *et al*, 2017 (383)

Figure 70 aims to visually compare HC and the clonal disease CLL circos plots with SchS. A diverse IgH repertoire is seen in the HC, in stark contrast to the CLL sample where clear overrepresentation of VH4-34 to JH6 is demonstrated - indicating clonal expansion of a particular B cell. Amongst the 10 SchS samples, SchS-24 can be considered as the one of the most clonal in terms of the increased frequency of CDR3 clones (Table 21). Comparison of this sample to HC and CLL illustrates a few disproportionately combined V-J genes (VH3-11 to JH4), but not to the extent of CLL and is more visually akin to the HC plot as compared to the CLL plot.

Similar to SchS, overrepresentations of the VH3 and JH4/JH6 genes in WM (400) and VH3 and JH3/JH4/JH5 families in IgM MGUS have been reported (402) - although V-J recombination has not been directly studied in the latter conditions. Subtle overrepresentations of VH4/JH4 in healthy individuals between the ages of 18 to 89 were observed in spleen derived gDNA samples; the same study also analysed lymph node derived gDNA, reporting a recombinational bias of the VH6 and JH6 families (403). Thus, in view of SchS where largely VH3/JH4 preferential combinations were seen, SchS bears more resemblance to WM and IgM MGUS in terms of pairings than to those documented in healthy individuals.

5.4 Discussion

The aim of this chapter was to utilise an NGS approach to sequence gDNA, for the purposes of investigating IgH gene usage alongside CDR3 characteristics, and comparing these metrics amongst 10 SchS patients.

To summarise, the main findings in this chapter were:

- i. Each SchS patient demonstrated evidence of intraclonality
- ii. Identical CDR3 aa sequences were not shared amongst the 10 SchS patients
- iii. The CDR3 aa lengths were found skewed for all patients, but the composition for these sequences were comparative to healthy individuals
- iv. For the complete and clonal repertoires VH3, VH6 and JH4 and JH6 were the most abundantly utilised genes
- v. A combinatorial bias was observed through the favoured rearrangements of VH3 and/or VH6, to the JH4 and/or JH6 gene segments in every sample, though to varying degrees

5.4.1 IgH

In this section of work, the humoral/adaptive response in the setting of an autoinflammatory condition was investigated, analysing three general metrics of B cell repertoire skewing: CDR3 length distribution, CDR3 aa composition and VH gene usage. Importantly, the approach of discriminating between different B cell populations was not employed; rather, gDNA representing pooled B cells derived from PB was used as the initial PCR template. Utilisation of gDNA provides two main benefits, with this sample type most frequently used in a clinical setting. Primarily, working with gDNA is robust, in that it is unlikely to be degraded in comparison to mRNA. When working with suboptimal samples (i.e. low viability/frozen EDTA samples), as was the case for some patients in this cohort, gDNA was a versatile starting material. Secondly, non-productive gene rearrangements can be investigated, “providing a potential second target to identify a clone in B cells with two heavy chain rearrangements” (195), though single cell analysis would be required. Additionally, the correction of differences is required when starting with RNA, due to varied quantities of transcript (325).

High yields of gDNA from B cells are imperative when trying to obtain comprehensive representation of the IgH repertoire, however this poses challenges when working with samples with limited numbers of lymphocytes (404). In heterogeneous conditions such as SchS, where the IgM paraprotein is likely originating from a small subset of clonally expanded B cells, it is important to consider that certain rearrangements may have not been detected due to potential absence of the initial template from gDNA (i.e. degradation). Henceforth, the

analyses presented in this section are representative of the B cell repertoire in 10 SchS patients with the comparisons made and conclusions derived from this data not absolute, but rather, comparative.

5.4.1.1 Repertoire Diversity

Until the advent of NGS in recent years, only limited B-cell receptor rearrangements (10-100) could be studied due to the use of traditional cloning and sequencing, simply providing a very restricted overview of diversity (386). At any given point, analysing the diversity of the repertoire by sequencing gDNA from whole blood provides a snapshot of only 2% of the total B-cell repertoire (368). It is imperative to know the B-cell count for a fully accurate assessment of the repertoire, as generally each B-cell is capable of solely one productive rearrangement for an Ig. Though with clonal populations, numerous B-cells with identical rearrangements are likely to be present. For example, with a starting sample comprising of 50,000 B-cells, discovering the same amount of different productive rearrangements is highly unlikely. However, taking into consideration PCR and sequencing error, more than 50,000 sequences will be produced in this scenario. Ideally, a precise B cell count would be obtained by either flow cytometry or qPCR assessing B cell markers (368). However, this was not possible in this work due to the type and availability of SchS samples.

Where the B-cell count was unknown, other studies used inference models to estimate the B-cell content and the maximum number of productive rearrangements (195, 353). In this work, inference of the number of B cells was based on the assumption that each cell contains 6pg of DNA and the total B-cell content of that gDNA was either 10% or 1%. Amongst all 10 SchS samples, the expanded clones remained represented at the same levels, supposing either a 10% B-cell assumption or a 1% content of B cell DNA (Figure 57). The research by Rosenfeld *et al* assumed the following parameters to deduce B cell-content and hence productive rearrangements: (1) each cell has 6.7pg of DNA; (2) one B cell harbours at least one heavy chain rearrangement; and (3) 1.4 VDJ rearrangements will occur per cell (195). Applying the latter two parameters stipulates that 71% sequences would be productive, with this value surpassed by SchS patients. The percentages of productive sequences were in the range of 74% to 92%, in line with the 75% productivity found in a patient with Follicular lymphoma, also bearing clonal B cell populations (405). Contrastingly in CLL, several studies have documented the decreased percentage of productive sequences (ranging from 21% to 40%) (406-408), and could be explained by the occurrence of oligoclonality through the abnormal expansion of one clone. The relatively higher percentage of productive sequences seen in SchS could indicate clonal expansion, to a much lesser degree than seen in CLL but comparable to other B-cell disorders.

5.4.1.1.1 Definition and frequency of CDR3 clones

The IMGT numbering system was used for CDR3 identification and annotation (382). In this work, a clone is defined as a unique CDR3 sequence appearing in more than 2% of the total CDR3 sequences per individual based on previous cut-off values by Tak *et al* (>2.5-5%) and Tan *et al* (>0.1%) (323, 388). Given the potential diversity of B-cell receptors generated by VDJ recombination (detailed in Section 5.1.1), the rare probability of converging upon the same IgH sequence renders each CDR3 aa sequence as a unique tag for a B-cell clone (409). Similar cut-off values have been used to define clonal populations in T cell analyses (0.1%-1%) (410). Arguably, the percentage limits drawn in literature for clone classifications is rather specific to each study and therefore classifying such clones could be deemed as subjective. However, portrayed via Figure 57 in this work, the CDR3 aa sequence composition generated from entire IgH repertoire at the nucleotide level is accurately representative of the proportional frequency of such CDR3 sequences per SchS patient.

5.4.1.1.2 CDR3 clone analyses

As demonstrated by both Figures 59 and 60, the increased abundance of specific CDR3 sequences demonstrates the level of cell clone expansion. The degree to which a healthy individual demonstrates clonality has been previously investigated. For example, Wang *et al* found that out of an average of 229,317 unique CDR3 aa sequences found for 6 HC's, only an average of 0.004% total sequences corresponded to clones (411). In contrast, each SchS patient demonstrated evidence of expanded CDR3 clones (7% to 93%) out of total CDR3 aa sequences. This stark variation in clone percentage amongst the 10 SchS patients underscore the variances seen with regards to the diversity of the IgH repertoire and resulting CDR3 sequences of this AI disease. Although may signify a recently mounted antigenic response, correlations between the reduction in diversity and other factors can be postulated. For example, samples 20 and 25 demonstrate pathogenic mutations in *STAG2* and *MYD88* respectively, a feature not present in the other eight patients. Likewise, samples 22 and 24, also demonstrating a narrower CDR3 repertoire are amongst the oldest three in this SchS group (Tables 20 and 21).

5.4.1.1.3 CDR3 length distribution

Within a diverse repertoire of B cells, it is expected that the length of CDR3 when plotted against percentage of sequences corresponding to that CDR3 loop, follows a 'discretised Gaussian distribution', typically composed of 8-10 different CDR3 lengths (325, 348).

Alternately, a skewed CDR3 distribution indicates overabundance of certain clones. The latter may be a consequence of abnormal VDJ recombination or demonstrative of a recently mounted response to an antigen (348). All 10 SchS samples do not follow a bell-shaped curve and bear increased numbers of CDR3 length classes (range of 11-14). Reflecting the entire repertoire, the median lengths of SchS patients were in the range of 13 aa to 15 aa, equivalent to the median length described in 123 patients with WM or IgM-MGUS (13 aa) but substantially shorter than that of CLL – 17 aa as portrayed by 7424 subjects (291). Median values obtained from healthy controls show CDR3 lengths at 15.5 aa to 16 aa (298, 353). Considering the clonal populations, the median lengths remained between 14 aa to 16 aa, with sample 16 bearing an overall longer length at 19 aa. The latter value is identical to CDR3 lengths established in clonal sequences of 68 CLL patients with VH4-39 overrepresentation (291) whereas VH was largely used in the clonal populations of SchS-16. Logically, longer CDR3 lengths (i.e. > 24 aa (412)) have an increased capacity of sequence variation with the potential to reach 'narrower antigenic pockets' (413), reflecting the role of innate immunity to broadly neutralise foreign antigens not previously encountered (412). Whereas decreased CDR3 lengths reflect previous antigenic exposure. For example, with SLE, shorter CDR3 length (averaging 14 aa) have been documented (396, 397), likely indicating the preponderance of the generated autoantibody reactivity to known antigens in this condition such as dsDNA (ref Shi short term again). In the data obtained with SchS patients, the inclination towards shorter median values in both clonal populations and the entire repertoire could be a consequence of selection bias those B cells producing longer CDR3 regions but also recurrent exposure to a particular epitope or group of peptides possessing canonical properties i.e. binding motifs. Though these speculations can be only precisely confirmed using through SchS-IgM analysis (i.e. exposure to a protein microarray), the trend in shorter CDR3 lengths proposes the likelihood of the SchS monoclonal component retaining binding partialities.

5.4.1.1.4 CDR3 composition

Augmented use of certain aa's in CDR regions have been suggested as a consequence of clonality. For example, increased frequency of arginine was suggested as the result of clonal B cell expansion in a study assessing anti-Cardiolipin antibodies (414). The CDR3 aa compositions of each SchS sample are akin to those percentages sought in healthy individuals (and thus CDR3 composition is less informative in regards to assessment of the adaptive response in comparison to length and hydrophobicity/hydrophilicity dynamics).

Observations that BM heavy chain CDR3 peptides are more hydrophobic in comparison to those found in PB (415), largely implies that selection against this feature occurs during central tolerance. Although not characteristic of SchS CDR3's, hydrophobic CDR3's have been

associated with autoreactivity in autoimmune conditions such as SLE (396, 397). In view of SchS, generation of the GRAVY scores for the clonal CDR3 sequences overall denoted a hydrophilic preponderance and is in accordance with the gDNA derived from PB, and not BM. Interestingly, Ademokun *et al* investigating the B-cell repertoire characteristics post pneumococcal vaccination demonstrated both young and old participants had significantly lower (hydrophilic) GRAVY scores in those CDR3 sequences deemed as clonal, as opposed to that of the entire repertoire (416). Following the aforementioned paper and in view of SchS – where the CDR3 clones are largely hydrophilic and the CDR3 lengths are in accordance with those associated with experienced repertoires, could suggest that an element of the SchS adaptive system is geared towards an antigenic response.

5.4.1.1.5 Stereotyped CDR3 sequences

In contrast to CLL but analogous to SchS, IgM-MGUS and WM demonstrated no evidence of stereotypy in cohort of 59 and 64 patients respectively (358). Thus, the lack of stereotypy amongst these patients and within SchS patients indicates the pathogenesis in these disorders are not B cell receptor mediated. Thus, whether the distinctive paraproteinaemia seen in the aforesaid conditions are essentially by-products of B cell expansion or are intentionally produced remains to be clarified. Such definitive answers can be sought through the isolation of the monoclonal component for investigation of its binding properties.

5.4.2 VH usage

The VH3 family was employed at an average of 75% in nine out of the 10 SchS patients, akin to the populations considered as clonal (76%, Table 21). Comprehensive research indicates the favoured use of both VH3 and VH4 in healthy individuals. Through sequencing IgH regions specific to the IgM derived heavy chains using cDNA (353), or gDNA derived from flow cytometry sorted B-cell populations (i.e. plasma cells) (417), VH4 was most favourably used family followed by VH3. Interestingly, the latter study noted a neonatal preferential bias of VH3. However, another recent study by Petrova *et al* noted around 60% of IgH sequences (IgM specific) analysed from 19 healthy controls utilised VH3 (418), the same as detected in WM (198, 419) and IgM MGUS (402). However, the difference sought between the latter B-cell malignancies and HC immune repertoires is the overrepresentation of certain gene segments, rendering a skewed immune profile. For example, while VH3 was used between the ranges of 42% - 66% in clonal populations of B cells derived from CLL and MBL, 77% of sequences were encoded by only 12 VH genes out of the possible 46 VH genes (420). Petrikos *et al* found all IgH sequences derived from BM derived gDNA of 34 WM patients utilising only 14 VH segments (198). Likewise, all the CDR3 clones found in SchS were encoded by 21 VH gene segments, less than half of the potential VH genes to utilise. Aside

from patient 25, VH3-11, VH3-30 and VH3-74 were the most used gene segments, both in the clonal and entire IgH repertoires. Primary Biliary Cholangitis, where the role of elevated serum IgM is elusive (analogous to SchS), has also shown a VH3 family preference (421).

Notably, autoimmune diseases such as SLE and RA demonstrate VH4-34 usage bias (422). Use of this region has documented to be integral to the formation of autoreactive antibodies, shown to recognise anti-DNA antibodies (423), the Fc portion of IgG (424) as well as commensal bacteria such as *Clostridium difficile* (425). The underrepresentation of VH4-34 in the germinal centre and memory B-cells from healthy subjects has been regarded as a conscious effort to hinder plasma cells from producing such auto-antibodies (426). With the cohort sequenced in this chapter, usage of this naïve B cell repertoire associated gene segment was not observed, generally supporting the notion that SchS is an autoinflammatory condition lacking autoantibody activity.

Although DH usage is more varied compared to the similar usage patterns observed in the VH and JH gene groups, seven out of 10 patients bear preference to using DH3 and DH6 at an average of 25% in their whole repertoires, also mirrored in their clonal populations. Where healthy individuals demonstrate favoured DH3 and DH6 usage, certain B-cell malignancies such as WM (n=22) and IgM-MGUS (n=5) both exhibit bias towards the DH1 and DH6 families (402). The latter findings were emulated in samples 20 and 25, with DH1 being the preferentially employed DH gene, whereas sample 24 exhibited highest preference towards DH2, different to the rest of the samples.

The data obtained from the entire repertoires show all patients demonstrating preferential JH4 gene family usage at a 57% average of all IgH sequences, essentially comparable to those values sought in plasma cells derived from a healthy control (50%) (417) and B-cell LPDs (range of 40% - 48%) (420).

5.4.2.1.1 VH-JH Recombinations

To obtain a more detailed insight into the combinatorial dynamics of SchS patients, V-J recombination was examined. Identification of specific gene recombinations within each patient underscores the observations in the previous work indicating that SchS bears preference to usage of certain gene segments. Nine out of 10 SchS samples demonstrated recombinations of VH3 to JH4, similar to the genes employed in WM and IgM MGUS. Although to varying degrees and not to the magnitude at which CLL presents, each SchS patient exhibits evidence of preferential recombination and such skewed patterns could be interpreted as oligoclonal expansions within a polyclonal background. Therefore, deciphering SchS as a

polyclonal B-cell disorder in amidst a fairly diverse environment is founded by clear overrepresentations of the aforementioned pairings (Section 5.3.7) in each SchS sample.

In this work, IgH sequences were considered to belong to the same clone if they shared V and J gene usage alongside identical CDR3 amino acid sequence at a level of 2% or over of the entire individual IgH repertoire. Therefore, it is imperative to note that although the clones are clearly represented in the circos plots, these figures also depict those recombinations not categorised as a clone in the analyses carried out in Section 5.3.5. Identical V-J recombinations can result in different CDR3 sequences, in part attributed to the employment of one of 27 DH region genes, and occurring at the VDJ junctional region – enzymatic addition of palindromic 'P' and random, non-templated 'N' nucleotides in conjunction with exonuclease activity (329).

5.4.2.1.2 MYD88 L265P and VH usage

SchS patient 25 presented with the MYD88 L265P mutation as deduced in Results Chapter 3, with the aforementioned pathogenic mutation diagnostic of the LPD, WM. The VH6-1 segment was mainly overrepresented in both the entire IgH repertoire and the clonal population in SchS-25 (Figures 65, 68 and 69, Table 21). Heightened use of VH6-1 has been linked to autoantibody production directed towards IL-18 in MS (427), and increased usage in autoimmune diseases such as Type I Diabetes and Idiopathic Thrombocytopenic Purpura (428) and is rarely employed in healthy individuals (417, 418). Another study assessing the IgH repertoire in healthy individuals using gDNA derived from BM and lymph nodes revealed preferential VH6-1/JH6 recombinations, mirrored in both young (<45 years) and older (>61 years) populations (403). Biased usage of VH3-30, VH3-74 and VH3-23 has been widely documented in WM (198, 419), with the latter gene segment used within a prevalent CDR3 clone making up 4% of the entire repertoire of sample 25. Though this was not the case for VH3-30 and VH3-74 in SchS-25, these genes were overrepresented other MYD88 mutation negative SchS patients, signifying traits of a related immune repertoire between SchS and WM, despite MYD88 status. Though the presence of the MYD88 L265P mutation alongside alternative VDJ segment usage in sample 25 emphasises the concept of biological variance seen amongst those positive and negative for the variant (198), similar patterns of VH usage amongst SchS patients negative for the mutation and WM patients positive for the mutation suggests VDJ gene segment biases are not entirely linked to the co-existence of the MYD88 L265P mutation. Increasing age is linked to the formation of a more restricted B-cell repertoire (403) and therefore could explain the disparity seen in terms of VDJ usage between this patient (78 years upon diagnosis) and the other SchS patients. Alternatively, recent response antigenic exposure could further corroborate the existence of a more skewed IgH repertoire. All samples demonstrate evidence of skewing

5.4.2.2 Perspectives

Present within each of the 10 analysed samples, the abundance of CDR3 clones, VDJ biased usage and distinct VJ recombinations, indicates that SchS has the bearings of a B cell clonal disorder. However, the degree of such clonal expansions vary immensely between the patients. For example, the clonal population in SchS-24 makes up 92% of its entire CDR3 aa repertoire, whereas the clonal population in SchS-21 comprises of only 6% of its CDR3 aa repertoire. Such findings make inter-disease clustering more challenging, and given that no public CDR3 aa sequences were discovered amongst these 10 SchS patients may suggest that clonal IgM may be produced as a consequence to non-specific antigenic stimulation within an autoinflammatory setting. However, these interpretations are in contrast with the evidence of combinatorial bias and relatively restricted VH, DH and JH gene usage sought in this work. Overrepresentation of VDJ gene segments indicates the existence of skewed IgH repertoire and could indicate that a certain division of the SchS IgH repertoire is directed at a particular group of antigens.

Since a majority B cells present in PB are in transit towards tissues, gDNA derived from the B cells here are likely to represent only a small subset of their repertoire in terms of both composition and phenotype. Chaudhary *et al* estimated that such select sequencing results in representation of only 2% of the entire B cell population (329). Therefore, the data gathered provides only a snapshot of the occurrences in SchS. Although these findings support the view that IgM dysregulation is likely due to an abnormal IgH setting, the research presented in this chapter could be further strengthened through the deep sequencing of B cell subsets in an effort to pinpoint the stage at which malignant transformation could be occurring. Though considerably, such experiments are dependent on sample availability and extensive resources.

5.4.2.3 Clinical perspectives

Given that a minority SchS patients are inclined to develop an LPD over the course of approximately eight years (range: four to 20 years) (21, 36), analysing degrees of clonal expansion presents an opportunity to identify those who are more likely to develop malignancy. Greater extents of clonal expansion and reduced diversity may predispose to WM on the basis of a narrower IgH repertoire. Identification of highly expanded CDR3 clones such as those documented in SchS 20, 22, 24 and 25, where the top clones are present at over 14% of the total CDR3 repertoires, warrant close monitoring to determine if these are causative of clonal evolution to WM. Halting the progression to WM or other LPDs would allow a prompt response with regards to appropriate treatment (i.e. B cell depletion) and preventative measures such as plasmapheresis to reduce the risk of associated complications such hyperviscosity syndrome (429).

Relating the data garnered from this chapter alongside the stated clinical findings (Table 20), out of the 10 patients investigated, SchS-20 is the most likely individual to develop WM. Upon SchS diagnosis, this patient demonstrated LPL in their bone marrow histology, a pathogenic STAG2 mutation (Results Chapter 3) and increased prevalence of CDR3 clones (88% of their CDR3 repertoire regarded as clonal, Figure 60). This postulation is further strengthened via data indicating that males are twice as likely to develop WM as opposed to females (429). Samples 22, 24 and 25 could also be hypothesised to potentially progress to a LPD, on the basis of increased age (61, 68 and 78 years upon diagnosis) and their degrees of clonal expansions as compared to the other six samples. Further determinations of those SchS patients likely to develop LPDs becomes trickier solely based on these datasets, although on comparison to the rest of the SchS patients, markedly reduced clonal expansions in samples 15, 18 and 21 and the lack evidence suggesting LPLs upon BM histology, renders evolution to malignancy less probable. Nevertheless, evolution of a clone from any samples would not be unexpected given the unknown pathogenesis of SchS itself.

5.4.2.4 Chapter conclusions

Using NGS technology and through bioinformatics analyses, the work in this chapter addresses the hypothesis that SchS is a clonal B cell disorder. The existence of a skewed CDR3 repertoire within each sample is highly suggestive of a clonal population of B cells. Though SchS exhibits abnormal CDR3 length distribution and preferential V, D and J segment usage and recombination, the absence of public CDR3 sequences could suggest that the monoclonal component produced by SchS is not directed at a sole antigen. The latter scenario is explored in the subsequent chapter through isolating the monoclonal component and exploring these SchS antibodies' binding preferences.

Taking the aforesaid perspectives into consideration, it is thus debatable as to whether SchS can be precisely defined as an oligoclonal or polyclonal disorder. Given the observation that 20% of SchS patients go onto develop lymphoproliferative disease, it is credible to suggest that the evidence of clonality seen in SchS maybe representative of various stages of pre-malignant transformation, co-existing with the 'normal' B cell repertoire. These pre-malignant B cell clones would then further require malignant transformation, an event that doesn't occur in all SchS patients. Whether the aforementioned event is due to a genetic event (i.e. somatic mutation) or caused by an epigenetic defect remains to be investigated. Nevertheless, as carried out in other LPDs such as CLL, monitoring the expanded CDR3 clones over a longitudinal course will deliberate if these expansions bear relevance in the progression to WM.

Chapter 6 Main Discussion

The data and observations described are discussed in this chapter, with regards to the implications of these novel findings pertaining to the basic understanding of SchS pathogenesis. The wide breadth of investigations carried out in this work with a relatively significant number of SchS patients have extensively addressed ideas and notions described in the literature. The work presented in thesis has addressed the hypotheses below, with the rationale explained in detail within Section 1.9, Introduction.

- SchS patients have mutations in the IL-1 β /IL-18 molecular processing platform known as the NLRP3 inflammasome.
- A proportion of SchS patients have the MYD88 L265P gain-of-function mutation.
- Oligoclonal Haematopoiesis (OH) is a feature of SchS, evident through the presence of additional 'passenger' mutations associated with myelodysplastic syndromes (MDS).
- Serum derived SchS IgM binds a common antigen.
- SchS bears characteristics of a clonal B cell disorder.

6.1 Main findings

- (1) NLRP3 activation-associated molecular markers (IL-18 and ASC specks) were found elevated in the serum of 19 SchS patients and whether *NLRP3* mutations were a feature of SchS in a larger cohort of patients (n=32), was the next line of enquiry. Deep sequencing of this gene revealed no somatic variants, excluding the idea that such mutations would be responsible for SchS pathology.
- (2) The suggestion that the L265P MYD88 mutation would be present in SchS patients was initially postulated by De Koning *et al* in 2014 (20), and prior to the publication of this work in this thesis - this concept was not experimentally addressed. Nine out of 30 SchS patients tested were positive for this pathogenic mutation, emulating the percentage of those patients who go onto develop WM (approximately a third).

- (3) The DNA from 30 SchS patients was subject to sequencing with a gene panel commonly used for the diagnosis of MDS using NGS. The results garnered from these explorations did not support the concept of CH in autoinflammatory disease, but rather underscored the incidence of age-related findings. An average of 1.3 somatic mutations are acquired per HSC every ten years, and the detection of HSC clones in those over 55 years is common (269). Considering the average age in the SchS and aNLRP3 patient cohorts was also 55 years, there is a high likelihood that these outcomes are a consequence of ageing, rather than a mechanism pertaining to development of auto inflammatory disease.
- (4) The results of the array for all IgM samples demonstrated preponderance to nuclear located proteins such as histones, transcriptional regulators and splicing factors, however a common antigen was not detected amongst the three SchS patients.
- (5) Biased V, D and J segment usage and recombination followed by abnormally skewed CDR3 lengths is suggestive that the landscape of the B cell repertoire in SchS is indeed inclined to produce abnormal Igs. These findings are further extended through the assessment of expanded CDR3 aa sequences, with each sample demonstrative of CDR3 clonal expansion, though to varying degrees.

6.2 Future Experiments

6.2.1 Precise assessment of IL-1 and related cytokines

As alluded to in the introduction section 1.2.7 and indeed demonstrated by the results in section 2.3, it is challenging to quantify levels of IL-1 β partly due to its short half-life (88). One way to address this issue is to assess the levels of IL-1Ra or indeed the soluble receptor form of IL-1R1 as an indirect marker of IL-1 β (90, 93). Whilst carrying out the aforementioned via several ELISAs would be one way to measure these markers in serum, qPCR would be a more precise method for several reasons. Assessment of transcript levels within myeloid cells

for example, would not only encompass those cytokines which largely remain endogenous – for example IL-1 α , but also quantify those cytokines which are challenging to detect in serum (i.e. IL-1 β). Other cytokines associated with SchS and autoinflammation (i.e. IL-18 and IL-18 binding protein) could also be detected this way. For both described ELISA and qPCR experiments, obtaining samples before, after and during a flare would indicate the levels of the cytokine at different disease intervals.

6.2.2 Screening for the MYD88 L265P mutation

The results of the MYD88 L265P ASO PCR revealed that a third of the SchS cohort have this mutation. Interpretation of this feature as a precursor to developing WM, is substantiated by similar percentages of SchS patients developing such LPL's. However, follow up of the *MYD88* positive subset of patients is necessary to validate this indication. Nevertheless, given the lengthy diagnosis period of SchS, averaging at five years, screening for this *MYD88* mutation will certainly aid clinicians where SchS is suspected. Additionally, the presence of alternate activating MYD88 mutations in SchS is imperative to consider. High throughput sequencing of RNA revealed 8% of 155 ABC-DLBCL patients had one of the following somatic mutations: V217F, S219C, M232T, S243N or T294P (184). Subsequently, Treon *et al* and Varettoni *et al* discovered three out of the latter MYD88 variants present in approximately 5% of WM cases, who were negative for the L265P mutation upon primary screening (430, 431). Four of the mutants reside within the evolutionarily conserved 'B-B loop' of the TIR domain (shown to be important in TLR4/IL-1 mediated signalling), whereas the T294P mutation alters the conserved 'box-3' region of the TIR domain, depicted to be also 'important in IL-1 signalling' (184). Given that such mutations are present in a relatively small proportion of patients with rare haematological malignancies, the proportion of SchS patients bearing these variants could be even lower. Even so, comprehensive analysis of the entire *MYD88* gene may further reveal novel variants in addition to the ones described in literature, accounting the proinflammatory role of this protein in the context of autoinflammatory disease.

6.2.3 The effect of IgM on SchS pathology

SchS-IgM exposure to pyroptotic debris as a consequence of autoinflammation, could create feedforward loop of recognising self-antigenic structures causing further immune stimulation. One way to investigate the aforementioned suppositions could be through mimicking an *in-vivo* pro-inflammatory environment through culturing SchS derived PBMCs and dosing in SchS-IgM. Assessing inflammation prior to and after IgM application by either quantifying

levels of proinflammatory cytokines (i.e. IL-6, IL-18) or via RT-PCR to determine if IgM application induces significant changes at the transcript level of inflammatory markers. Although not discriminatory in view of the binding preferences and the fact that IgM binds a wide range of epitopes, this approach would demonstrate the hypothesised, self-perpetuating inflammation. Certainly, anti-IL-1 treatment could break the supposed 'cycle' through reducing levels of IL-1, thus deregulating IL-6 and impeding further expansion of the B-cell clone. This is supported by the observation that IgM levels tend to remain steady during the course of disease in those SchS patients who do not develop LPDs (22, 26, 39).

6.2.4 Follow up of VDJ usage and CDR3 aa expansion

The clonal discrepancies seen among the SchS patients could be influenced by recent antigenic exposure or age-related immune decline, extensively reported in literature (329, 432, 433). Conversely, these findings may represent different stages of malignant transformation, with the aforesaid speculations necessitating longitudinal patient follow up. Through comparison of the data presented in Chapter 5 with analogous data sought in those who go on to develop LPD, would specifically reveal those VDJ gene segments preferentially used and show the expansion of particular CDR3 aa clones. Analysis of paired sample data, alongside IgH repertoire sequencing of sorted B-cells (i.e. naïve, memory, plasmablast, plasma), would precisely enable identification of the clonal origin of the malignantly transformed cells and hence implicate the cell type responsible for generation of the monoclonal gammopathy in SchS. For example, the IgM monoclonal component in MGUS has been identified to originate from CD20+ lymphoplasmacytic cells with the CD19+/CD20+ and CD25+ phenotype determined as the origin of WM (434, 435). Defining the same in SchS and subsequently quantifying BM infiltration of those particular cells is a supplementary means to monitor progression to LPDs. SchS patients showing a BM infiltration of >10% those cells, and/or demonstrate a mutation associated with haematological malignancy, are more susceptible to LPD development. This proposal is based on the follow up of five SchS patients who progressed to WM exhibiting over a 10% BM infiltrate of lymphocytes (436).

6.3 Strengths and Limitations of this PhD project

Access to a relatively large cohort of SchS patient samples formed the primary strength of this thesis, and in this regard all the investigations carried out are therefore 'novel'. Each of the results chapters contribute to elucidating the dysregulated pathogenesis and/or

pathophysiology, with a capacity to impact both the clinical and scientific aspects of this rare indication.

In a period where Whole Exome Sequencing and Whole Genome Sequencing are considered to be the 'gold standard' of genetic examinations, the cost, timing and applicability to this SchS cohort required deliberation. In view of the apparent heterogeneity of SchS, it is plausible to consider that screening the entire SchS exome or genome would demonstrate various mutations, a large proportion of which are unlikely to be SchS related. This body of work screened over 60 genes associated with autoinflammation, haematological malignancies and more specifically, MDS. Although extensive probing did not reveal a universal mutation, ruling out pathogenic variants within genes highly suspected of contributing to SchS pathogenesis is of great significance. For example, addressing the long standing stipulation that *NLRP3* mutations are causal of SchS, dismisses this notion in a relatively large group of patients and the focus of future genetic studies can be on other genes.

SchS patients in general have a low percentage of monotypic B cells present within the BM, and this is likely to be reflected through a lower amount of circulating B cell clones. On this supposition, MYD88 L265P 'mutation negative' patients, may in fact be positive for the mutation, but could not be picked up through gDNA analysis. Nevertheless, the presence of the latter mutation in a subset of SchS patients is a novel finding, and screening for this variant can certainly corroborate a suspected diagnosis.

The monoclonal component has not been the focus of previous SchS research to the extent and depth that this work has, despite many researchers theorising the generation and consequential effects of this Ig in SchS. The HuProt™ array targets 75% of the human protein coding genome, thus it is debateable as to whether the potential SchS target was in fact within the 25% of proteins not captured on this slide. Further, the assumption that the monoclonal component was in fact included within the isolation of total IgM cannot be ascertained, and thus the IgM isolated may not be fully representative of the SchS gammopathy. Nevertheless, the compelling evidence of skewed Ig repertoire sought through NGS of the IgH region, implies the presence of a monoclonal B-cell population. Highly expanded CDR3 aa sequences forming a substantial proportion of the total CDR3 repertoire was documented in each patient, though to different degrees. Although these findings may be suggestive of recent antigenic exposure or a feature of the ageing immune system, it is likely that the clonality detected is in part due to SchS combined with the transformation to haematological malignancy in a subset of these patients.

6.4 Conclusions

The work presented in this PhD thesis covered a broad range of well-regarded suppositions and theories based on previous experimental evidence and comparison to alike conditions in literature. The impact of these findings not only broadens the limited literature of this rare entity and but forms a point of reference for both clinicians and research scientists in the autoinflammatory disease field. Two publications were generated from this work thus far and each of the results chapters forms the foundation and further paves way for future research to be carried out. Continuing to establish both the genetic and molecular mechanisms causative of SchS as suggested will not only facilitate a streamlined diagnosis and but rapidly improve patient QoL, with the potential to halt LPD progression.

Chapter 7

Appendices

7.1 Primer sequences

7.1.1 Results Chapter 2 primer sequences

Gene	Primer name	Primer sequence 5'-3'	Product size (bp)	Exon Coverage
<i>NLRP3</i>	NLRP3 1F	ACCGAGACACGGTTTTGACA	3121	1,2
	NLRP3 1R	CACTATGTGCACTTGGCCACAA		
	NLRP3 2F	GCAGGTGGACAGCAGAAGTT	2725	3,4
	NLRP3 2R	TCAAACAGACAGTGGTGGCAT		
	NLRP3 3F	AGTGAGGACTGCCCTCTGAT	6918	5,6
	NLRP3 3R	TGCCTGACCAAAGTAACCCC		
	NLRP3 4F	AAGAAGTGGTGCTGAGGAGC	5594	7,8,9
	NLRP3 4R	ACAGTTAGAGTGAGGTAACGTTTT		

Table 22: Primer sequences for *NLRP3*.

Table 22 indicates the primer sequences used to generate PCR products for *NLRP3*. Primers were designed to cover the introns, exons, 5' UTR and 3' UTR, to encompass any mutations in regions not usually investigated. The product sizes varied from 2725 base pairs to 6918 base pairs.

7.1.2 IgH sequencing primers

Primer name	Primer sequence 5' - 3'
IGHLa	TCGTCGGCAGCGTCAGATGTGTATAAGAGACAGAACTCACCATGGACTGSAYYTGGAG
IGHL2	TCGTCCGGCAGCGTCAGATGTGTATAAGAGACAGATGGCAYACTTTGYTMCACRCTCC
IGHL3a	TCGTCGGCAGCGTCAGATGTGTATAAGAGACAGATGGARTTKGGGCTKWGCTGGGTTT
IGHL3b	TCGTCGGCAGCGTCAGATGTGTATAAGAGACAGGGCTGAGCTGGGTTTTCTTGTTGC
IGHL 4	TCGTCGGCAGCGTCAGATGTGTATAAGAGACAGCTGTGGTTCTTYCTBCTSCTGGTGG
IGHL 5	TCGTCGGCAGCGTCAGATGTGTATAAGAGACAGCCTCCTCCTRGCTRTTCTCCAAG
IGHL 6	TCGTCGGCAGCGTCAGATCTGTATAAGAGACAGCTGTCTCCTTCCTCATCTTCCTGCC
IGHJ	GTCTGTGGGCTCGGAGATGTGTATAAGAGACAGCTTACCTGAGGAGACGGTGACC

Table 23: List of primers used to amplify the IgH locus.

Wobble bases follows the IUB code: S=C/G, Y=C/T, M=A/C, R=A/G, K=G/T, W=A/T, B=C/G/T.

7.2 Results Chapter 3 primer sequences

7.2.1 ASO-PCR primer sequences for *MYD88*

Reverse primer: 5' AGG AGG CAG GGC AGA AGT A 3'

Forward primer (Wild Type): 5' GTG CCC ATC AGA AGC GCC T 3'

Forward primer (Mutant): 5' GTG CCC ATC AGA AGC GCC C 3'

7.2.2 List of MDS genes sequenced

Gene	Exons covered	Transcript Reference
<i>ASXL1</i>	12	NM_015338.5
<i>BCOR</i>	2-15	NM_001123385.1
<i>CALR</i>	9	NM_004343.3
<i>CBL</i>	8 & 9	NM_005188.2
<i>CSF3R</i>	14 & 17	NM_156039.3
<i>DNMT3-A</i>	2-23	NM_175629.2
<i>EZH2</i>	2-20	NM_004456.4
<i>FLT3</i>	20	NM_004119.2
<i>IDH1</i>	4	NM_005896.3
<i>IDH2</i>	4 & 5	NM_002168.3
<i>JAK2</i>	12 & 14	NM_004972.3
<i>cKIT</i>	8 & 17	NM_000222.2
<i>KRAS</i>	2 & 3	NM_004985.4
<i>MPL</i>	10	NM_005373.2
<i>NPM1</i>	12	NM_002520.6
<i>NRAS</i>	2 & 3	NM_002524.4
<i>RHOA</i>	2	NM_001664.3
<i>RUNX1</i>	4-8	NM_001754.4
<i>SETBP1</i>	4	NM_015559.2
<i>SF3B1</i>	12-16	NM_012433.2
<i>SRSF2</i>	1	NM_003016.4
<i>STAG-2</i>	3-35	NM_001042749.2
<i>STAT3</i>	21a & 23b	NM_139276.2
<i>TET-2</i>	3-11	NM_001127208.2
<i>TP53</i>	5-9	NM_000546.4
<i>U2AF1</i>	2 & 6	NM_006758.2
<i>WT1</i>	7 & 9	NM_024426.4
<i>ZRSR2</i>	2-11	NM_005089.3

Table 24: The panel of 28 MDS associated genes.

Table 24 indicates the MDS associated genes included within the targeted sequencing panel, alongside the exon coverage and reference sequences. This sequencing work was carried out at HMDS.

7.3 Genes sequenced as part of the UCL panel

Gene	Gene Description	Chromosomal location	Transcript reference
AP1S3	adaptor-related protein complex 1, sigma 3 subunit	2q36.3	NM_001039569
CARD14	caspase recruitment domain family, member 14	17q25	NM_024110
IL10	Interleukin 10	1q31-q32	NM_000572
IL10RA	Interleukin 10 receptor, alpha	11q23	NM_001558
IL10RB	Interleukin 10 receptor, beta	21q22.11	NM_000628
IL1RN	Interleukin 1 receptor antagonist	2q14.2	NM_173842
IL36RN	Interleukin 36 receptor antagonist	2q14	NM_173170
LPIN2	Lipin 2	18p	NM_014646
LYN	Tyrosine-Protein Kinase	8q13	NM_002350
MEFV	MEditerranean FeVer	16p13.3	NM_000243
MVK	Mevalonate Kinase	12q24	NM_000431
NLRC4	NLR family, CARD domain containing 4	2p22-p21	NM_021209
NLRP12	NLR pyrin domain containing protein 12	19q13.42	NM_144687
NLRP3	NLR pyrin domain containing protein 3	1q44	NM_001243133
NLRP6	NLR family, pyrin domain containing 6	11p15	NM_138329
NLRP7	NLR family, pyrin domain containing 7	19q13.42	NM_001127255
NOD2	Nucleotide-binding oligomerization domain 2	16q12	NM_022162
PLCG2	Phospholipase C, Gamma-2	16q24.1	NM_002661
POMP	proteasome maturation protein	13q12.13	NM_015932
PSMA3	proteasome (prosome, macropain) subunit, alpha type, 3	14q23	NM_002788
PSMB4	proteasome (prosome, macropain) subunit, beta type, 4	1q21	NM_002796
PSMB8	Proteasome Subunit, Beta-Type, 8	6p21.3	NM_148919
PSMB9	proteasome (prosome, macropain) subunit, beta type, 9	6p21.3	NM_002800
PSTPIP1	Proline-Serine-Threonine Phosphatase Interacting Protein 1	15q24-q25.1	NM_003978
PYCARD	PYD and CARD domain containing	16p11.2	NM_013258
RBCK1	Ranbp-Type and C3HC4-Type Zinc Finger-Containing 1	20p13	NM_031229

Table 25: Panel of 32 genes associated with monogenic autoinflammatory diseases.

This sequencing work was carried out at University College London for SchS patients 12-28 and 32 (Table 7, Results Chapter 2).

7.4 Calculation of the frequency of CDR3 clones

The following section details the CDR3 aa frequency calculations for the remaining 9 SchS patients corresponding to Section 5.3.5.

7.4.1 10% B-cell assumption within gDNA

Sample 14

Total number of productive reads: 145,525
200ng initial input = 200,000pg
6pg/cell = 34,000 cells (approx.)
$34,000 * 0.1$ (10% assumption) = 3,400 B cells
$145,525/3400 = 43$ (Equating to 43 reads per cell)
Top CDR3 clone count: 9,460 $9,460/43 = 220$
220 times this clone appears in a total of 3281 B cells*

Sample 15

Total number of productive reads: 131,436
200ng initial input = 200,000pg
6pg/cell = 34,000 cells (approx.)
$34,000 * 0.1$ (10% assumption) = 3,400 B cells
$131,436/3400 = 39$ (Equating to 39 reads per cell)
Top CDR3 clone count: 4,230 $4,230/39 = 108$
108 times this clone appears in a total of 3215 B cells*

Sample 16

Total number of productive reads: 146,656
200ng initial input = 200,000pg
6pg/cell = 34,000 cells (approx.)
$34,000 * 0.1$ (10% assumption) = 3,400 B cells
$146,656/3400 = 43$ (Equating to 43 reads per cell)
Top CDR3 clone count: 12,498 $12,498/43 = 291$
291 times this clone appears in a total of 3270 B cells*

Sample 18

Total number of productive reads: 382,040	
200ng initial input = 200,000pg	
6pg/cell = 34,000 cells (approx.)	
34,000 * 0.1 (10% assumption) = 3,400 B cells	
382,040/3400 = 96 (Equating to 96 reads per cell)	
Top CDR3 clone count: 12,236	12,236/96 = 258
127 times this clone appears in a total of 3279 B cells*	

Sample 20

Total number of productive reads: 133,271	
200ng initial input = 200,000pg	
6pg/cell = 34,000 cells (approx.)	
34,000 * 0.1 (10% assumption) = 3,400 B cells	
133,271/3400 = 39 (Equating to 39 reads per cell)	
Top CDR3 clone count: 10,078	10,078/39 = 258
258 times this clone appears in a total of 3322 B cells*	

Sample 21

Total number of productive reads: 212,452	
200ng initial input = 200,000pg	
6pg/cell = 34,000 cells (approx.)	
34,000 * 0.1 (10% assumption) = 3,400 B cells	
212,452/3400 = 62 (Equating to 62 reads per cell)	
Top CDR3 clone count: 48,205	48,205/62 = 778
778 times this clone appears in a total of 3361 B cells*	

Sample 22

Total number of productive reads: 568,651	
200ng initial input = 200,000pg	
6pg/cell = 34,000 cells (approx.)	
34,000 * 0.1 (10% assumption) = 3,400 B cells	
568,651/3400 = 167 (Equating to 167 reads per cell)	
Top CDR3 clone count: 75,453	75,453/167 = 452
452 times this clone appears in a total of 3225 B cells*	

Sample 24

Total number of productive reads: 415,622
200ng initial input = 200,000pg
6pg/cell = 34,000 cells (approx.)
$34,000 * 0.1$ (10% assumption) = 3,400 B cells
$415,622/3400 = 122$ (Equating to 122 reads per cell)
Top CDR3 clone count: 115,113 $115,113/122 = 944$
944 times this clone appears in a total of 3282 B cells*

Sample 25

Total number of productive reads: 71,806
200ng initial input = 200,000pg
6pg/cell = 34,000 cells (approx.)
$34,000 * 0.1$ (10% assumption) = 3,400 B cells
$71,806/3400 = 21$ (Equating to 21 reads per cell)
Top CDR3 clone count: 13,404 $13,404/21 = 638$
638 times this clone appears in a total of 3419 B cells*

The theoretical number of B cells was estimated using the total number of productive reads and the assumption that 10% of the gDNA content comprised of B cells. This outlined estimation was applied to all 10 SchS patients. The calculations pertaining to sample 12 are detailed within the main body of text (Section 5.3.5).

*The minor reduction in B cells was computed by the addition of all reads at a 1% assumption, however excluded those cells that had a read value of <1.

7.4.2 1% B-cell assumption in gDNA

Sample 14

Total number of productive reads: 145,525
200ng initial input = 200,000pg
6pg/cell = 34,000 cells (approx.)
$34,000 * 0.01$ (1% assumption) = 340 B cells
$145,525/340 = 428$ (Equating to 428 reads per cell)
Top CDR3 clone count: 9,460 $9,460/428 = 22$
22 times this clone appears in a total of 328 B cells*

Sample 15

Total number of productive reads: 131,436
200ng initial input = 200,000pg
6pg/cell = 34,000 cells (approx.)
$34,000 * 0.01$ (1% assumption) = 340 B cells
$131,436/340 = 387$ (Equating to 387 reads per cell)
Top CDR3 clone count: 4,230 $4,230/387 = 11$
11 times this clone appears in a total of 321 B cells*

Sample 16

Total number of productive reads: 146,656
200ng initial input = 200,000pg
6pg/cell = 34,000 cells (approx.)
$34,000 * 0.01$ (1% assumption) = 340 B cells
$146,656/340 = 431$ (Equating to 431 reads per cell)
Top CDR3 clone count: 12,498 $12,498/431 = 29$
29 times this clone appears in a total of 327 B cells*

Sample 18

Total number of productive reads: 328,040
200ng initial input = 200,000pg
6pg/cell = 34,000 cells (approx.)
$34,000 * 0.01$ (1% assumption) = 340 B cells
$328,040/340 = 964$ (Equating to 964 reads per cell)
Top CDR3 clone count: 12,236 $12,236/964 = 13$
13 times this clone appears in a total of 328 B cells*

Sample 20

Total number of productive reads: 212,452
200ng initial input = 200,000pg
6pg/cell = 34,000 cells (approx.)
$34,000 * 0.01$ (1% assumption) = 340 B cells
$212,452/340 = 625$ (Equating to 625 reads per cell)
Top CDR3 clone count: 48,205 $48,205/625 = 26$
77 times this clone appears in a total of 336 B cells*

Sample 21

Total number of productive reads: 216,294
200ng initial input = 200,000pg
6pg/cell = 34,000 cells (approx.)
$34,000 * 0.01$ (1% assumption) = 340 B cells
$216,294/340 = 636$ (Equating to 636 reads per cell)
Top CDR3 clone count: 4,873 $4,873/636 = 8$
8 times this clone appears in a total of 329 B cells*

Sample 22

Total number of productive reads: 568,651
200ng initial input = 200,000pg
6pg/cell = 34,000 cells (approx.)
$34,000 * 0.01$ (1% assumption) = 340 B cells
$568,651/340 = 1672$ (Equating to 1672 reads per cell)
Top CDR3 clone count: 75,453 $75,453/1672 = 26$
45 times this clone appears in a total of 325 B cells*

Sample 24

Total number of productive reads: 415,622
200ng initial input = 200,000pg
6pg/cell = 34,000 cells (approx.)
$34,000 * 0.01$ (1% assumption) = 340 B cells
$415,622/340 = 1222$ (Equating to 1222 reads per cell)
Top CDR3 clone count: 115,113 $115,113/1222 = 94$
94 times this clone appears in a total of 328 B cells*

Sample 25

Total number of productive reads: 71,806
200ng initial input = 200,000pg
6pg/cell = 34,000 cells (approx.)
$34,000 * 0.01$ (1% assumption) = 340 B cells
$71,806/340 = 211$ (Equating to 211 reads per cell)
Top CDR3 clone count: 13,404 $13,404/211 = 64$
Answer: 64 times this clone appears in a total of 344 B cells*

The theoretical number of B cells was estimated using the total number of productive reads and the assumption that 1% of the gDNA content comprised of B cells. This outlined estimation was applied to all 10 SchS patients. The calculations pertaining to sample 12 are detailed within the main body of text (Section 5.3.5).

*The minor reduction in B cells was computed by the addition of all reads at a 1% assumption, however excluded those cells that had a read value of <1.

References

1. McDermott MF, Aksentijevich I, Galon J, McDermott EM, Ogunkolade BW, Centola M, et al. Germline mutations in the extracellular domains of the 55 kDa TNF receptor, TNFR1, define a family of dominantly inherited autoinflammatory syndromes. *Cell*. 1999;97(1):133-44.
2. Pathak S, McDermott MF, Savic S. Autoinflammatory diseases: update on classification diagnosis and management. *J Clin Pathol*. 2017;70(1):1-8.
3. Consortium FF. A candidate gene for familial Mediterranean fever. *Nat Genet*. 1997;17(1):25-31.
4. Rigante D. The Broad-Ranging Panorama of Systemic Autoinflammatory Disorders with Specific Focus on Acute Painful Symptoms and Hematologic Manifestations in Children. *Mediterr J Hematol Infect Dis*. 2018;10(1).
5. Rigante D, Vitale A, Lucherini OM, Cantarini L. The hereditary autoinflammatory disorders uncovered. *Autoimmun Rev*. 2014;13(9):892-900.
6. Lawless D, Pathak S, Scambler TE, Ouboussad L, Anwar R, Savic S. A Case of Adult-Onset Still's Disease Caused by a Novel Splicing Mutation in TNFAIP3 Successfully Treated With Tocilizumab. *Front Immunol*. 2018;9:1527.
7. Berteau F, Rouviere B, Delluc A, Nau A, Le Berre R, Sarrabay G, et al. Autosomic dominant familial Behcet disease and haploinsufficiency A20: A review of the literature. *Autoimmun Rev*. 2018;17(8):809-15.
8. Li C, Zhang J, Li S, Han T, Kuang W, Zhou Y, et al. Gene mutations and clinical phenotypes in Chinese children with Blau syndrome. *Sci China Life Sci*. 2017;60(7):758-62.
9. Cowen EW, Goldbach-Mansky R. DIRA, DITRA, and New Insights Into Pathways of Skin Inflammation: What's in a Name? *Arch Dermatol*. 2012;148(3):381-4.
10. Liu Y, Jesus A, Marrero B, Yang D, Ramsey S, Sanchez GM, et al. Activated STING in a Vascular and Pulmonary Syndrome. *N Engl J Med*. 2014;371(6):507-18.
11. Rossi-Semerano L, Piram M, Chiaverini C, De Ricaud D, Smahi A, Kone-Paut I. First clinical description of an infant with interleukin-36-receptor antagonist deficiency successfully treated with anakinra. *Pediatrics*. 2013;132(4):e1043-7.
12. Badran YR, Dedeoglu F, Leyva Castillo JM, Bainter W, Ohsumi TK, Bousvaros A, et al. Human RELA haploinsufficiency results in autosomal-dominant chronic mucocutaneous ulceration. *J Exp Med*. 2017;214(7):1937-47.
13. Savic S, Dickie LJ, Battellino M, McDermott MF. Familial Mediterranean fever and related periodic fever syndromes/autoinflammatory diseases. *Curr Opin Rheumatol*. 2012;24(1):103-12.
14. Zhou Q, Aksentijevich I, Wood GM, Walts AD, Hoffmann P, Remmers EF, et al. Brief Report: Cryopyrin-Associated Periodic Syndrome Caused by a Myeloid-Restricted Somatic NLRP3 Mutation. *Arthritis Rheumatol*. 2015;67(9):2482-6.
15. Tanaka N, Izawa K, Saito MK, Sakuma M, Oshima K, Ohara O, et al. High incidence of NLRP3 somatic mosaicism in patients with chronic infantile neurologic, cutaneous, articular syndrome: results of an International Multicenter Collaborative Study. *Arthritis Rheum*. 2011;63(11):3625-32.
16. Rowczenio DM, Trojer H, Omoyinmi E, Arostegui JI, Arakelov G, Mensa-Vilaro A, et al. TNF Receptor Associated Periodic Syndrome associated with gonosomal mosaicism of a novel 24 nucleotide TNFRSF1A deletion. *Arthritis Rheumatol*. 2016.
17. Shinar Y, Tohami T, Livneh A, Schiby G, Hirshberg A, Nagar M, et al. Acquired familial Mediterranean fever associated with a somatic MEFV mutation in a patient with JAK2 associated post-polycythemia myelofibrosis. *Orphanet J Rare Dis*. 2015;10:86.
18. Saito M, Fujisawa A, Nishikomori R, Kambe N, Nakata-Hizume M, Yoshimoto M, et al. Somatic mosaicism of CIAS1 in a patient with chronic infantile neurologic, cutaneous, articular syndrome. *Arthritis Rheum*. 2005;52(11):3579-85.

19. de Koning HD, van Gijn ME, Stoffels M, Jongekrijg J, Zeeuwen PL, Elferink MG, et al. Myeloid lineage-restricted somatic mosaicism of NLRP3 mutations in patients with variant Schnitzler syndrome. *J Allergy Clin Immunol*. 2015;135(2):561-4.
20. de Koning HD. Schnitzler's syndrome: lessons from 281 cases. *Clin Transl Allergy*. 2014;4:41.
21. Sokumbi O, Drage LA, Peters MS. Clinical and histopathologic review of Schnitzler syndrome: the Mayo Clinic experience (1972-2011). *J Am Acad Dermatol*. 2012;67(6):1289-95.
22. Simon A, Asli B, Braun-Falco M, De Koning H, Ferman JP, Grattan C, et al. Schnitzler's syndrome: diagnosis, treatment, and follow-up. *Allergy*. 2013;68(5):562-8.
23. Dingli D, Camilleri M. Schnitzler syndrome: clinical features and histopathology. *Pathology and Laboratory Medicine International*. 2016;7:39-46.
24. Lipsker D, Veran Y, Grunenberger F, Cribier B, Heid E, Grosshans E. The Schnitzler syndrome. Four new cases and review of the literature. *Medicine (Baltimore)*. 2001;80(1):37-44.
25. Jain T, Offord CP, Kyle RA, Dingli D. Schnitzler syndrome: an under-diagnosed clinical entity. *Haematologica*. 2013;98(10):1581-5.
26. Lipsker D. The Schnitzler syndrome. *Orphanet J Rare Dis*. 2010;5:38.
27. Rowczenio DM, Trojer H, Russell T, Baginska A, Lane T, Stewart NM, et al. Clinical characteristics in subjects with NLRP3 V198M diagnosed at a single UK center and a review of the literature. *Arthritis Res Ther*. 2013;15(1):R30.
28. Schnitzler L. Lésion urticariennes chroniques permanents (érythème pétaloïde?) case clinique n. 46B. *Journée Dermatologique d'Angers*. 1972;46.
29. Schnitzler L, Schubert B, Boasson M, Gardais J, Tourmen A. Urticaire chronique, lésions osseuses, macroglobulinémie IgM: maladie de Waldenström ? 2ème présentation. *Bull Soc Fr Dermatol Syphil* 1. 1974;81:363.
30. Bashir M, Bettendorf B, Hariman R. A Rare but Fascinating Disorder: Case Collection of Patients with Schnitzler Syndrome. *Case Rep Rheumatol*. 2018;2018:7041576.
31. Kimura N, Takeshita H, Kai T, Inoue Y, Furue M. Schnitzler's syndrome: A female elderly case presenting intractable non-pruritic febrile urticarial rash. *Asian Pac J Allergy Immunol*. 2018.
32. Welsh B, Tate B. Schnitzler's syndrome: report of a case with progression to Waldenström's macroglobulinaemia. *Australas J Dermatol*. 1999;40(4):201-3.
33. de Koning HD, Bodar EJ, van der Meer JW, Simon A. Schnitzler syndrome: beyond the case reports: review and follow-up of 94 patients with an emphasis on prognosis and treatment. *Semin Arthritis Rheum*. 2007;37(3):137-48.
34. Gertz MA. Waldenström macroglobulinemia: 2013 update on diagnosis, risk stratification, and management. *Am J Hematol*. 2013;88(8):703-11.
35. Ngo ST, Steyn FJ, McCombe PA. Gender differences in autoimmune disease. *Front Neuroendocrinol*. 2014;35(3):347-69.
36. Gusdorf L, Asli B, Barbarot S, Neel A, Masseau A, Puechal X, et al. Schnitzler syndrome: validation and applicability of diagnostic criteria in real-life patients. *Allergy*. 2017;72(2):177-82.
37. Gellrich FF, Gunther C. Schnitzler syndrome. *Hautarzt*. 2019.
38. Hedrich CM, Gunther C, Aringer M. [Still's disease in children and adults]. *Z Rheumatol*. 2017;76(7):595-608.
39. Gusdorf L, Lipsker D. Schnitzler Syndrome: a Review. *Curr Rheumatol Rep*. 2017;19(8):46.
40. Krause K, Grattan CE, Bindslev-Jensen C, Gattorno M, Kallinich T, de Koning HD, et al. How not to miss autoinflammatory diseases masquerading as urticaria. *Allergy*. 2012;67(12):1465-74.
41. Kumar N, Surendran D, Bammigatti C. Angioedema as the presenting feature of systemic lupus erythematosus. *BMJ Case Rep*. 2018;2018.
42. Belani H, Gensler L, Bajpai U, Meinhardt E, Graf J, Pincus L, et al. Neutrophilic urticaria with systemic inflammation: a case series. *JAMA Dermatol*. 2013;149(4):453-8.
43. Neel A, Henry B, Barbarot S, Masseau A, Perrin F, Bernier C, et al. Long-term effectiveness and safety of interleukin-1 receptor antagonist (anakinra) in Schnitzler's syndrome: a French multicenter study. *Autoimmun Rev*. 2014;13(10):1035-41.

44. Gouveia AI, Micaelo M, Pierdomenico F, Freitas JP. Schnitzler Syndrome: A Dramatic Response to Anakinra. *Dermatol Ther (Heidelb)*. 2016;6(2):299-302.
45. Volz T, Wolbing F, Fischer J, Braun M, Maggosschitz I, Schaller M, et al. Dermal interleukin-1 expression and effective and long-lasting therapy with interleukin-1 receptor antagonist anakinra in Schnitzler syndrome. *Acta Derm Venereol*. 2012;92(4):393-4.
46. Kieffer C, Cribier B, Lipsker D. Neutrophilic urticarial dermatosis: a variant of neutrophilic urticaria strongly associated with systemic disease. Report of 9 new cases and review of the literature. *Medicine (Baltimore)*. 2009;88(1):23-31.
47. Lidar M, Livneh A. Familial Mediterranean fever: clinical, molecular and management advancements. *Neth J Med*. 2007;65(9):318-24.
48. Almeida de Jesus A, Goldbach-Mansky R. Monogenic autoinflammatory diseases: concept and clinical manifestations. *Clin Immunol*. 2013;147(3):155-74.
49. Seung OP, Sulaiman W. Adult-Onset Still's Disease: A Case Report. *Oman Med J*. 2011;26(5):e022.
50. O'Hare A, Olson JL, Connolly MK, Ward JW, Stein P, Wisnieski JJ, et al. Renal insufficiency with monoclonal gammopathy and urticarial vasculitis. *Am J Kidney Dis*. 2002;39(1):203-7.
51. Rossi L, Casucci F, Teutonico A, Libutti P, Lisi P, Lomonte C, et al. Membranoproliferative glomerulonephritis with relapsing episodes of acute kidney injury in the Schnitzler syndrome. *G Ital Nefrol*. 2019;36(3).
52. Westhoff TH, Zidek W, Uharek L, Steinhoff-Georgieva J, van der Giet M. Impairment of renal function in Schnitzler's syndrome. *J Nephrol*. 2006;19(5):660-3.
53. Iwafuchi Y, Morita T, Hata K, Nakamura A, Miyazaki S. Schnitzler syndrome complicated by membranous nephropathy. *Clin Nephrol*. 2012;78(6):497-500.
54. Basile C, Rossi L, Casucci F, Teutonico A, Libutti P, Lisi P, et al. Kidney involvement in the Schnitzler syndrome, a rare disease. *Clin Kidney J*. 2017;10(6):723-7.
55. de Koning H, Krause K. *Textbook of Autoinflammation*. Switzerland: Springer; 2019. 793 p.
56. Nashan D, Sunderkotter C, Bonsmann G, Luger T, Goerdts S. Chronic urticaria, arthralgia, raised erythrocyte sedimentation rate and IgG paraproteinaemia: a variant of Schnitzler's syndrome? *Br J Dermatol*. 1995;133(1):132-4.
57. Urbanski M, Holfeld K, Milne A, Abbas M. Schnitzler Syndrome Without a Monoclonal Gammopathy: A Case Report. *J Cutan Med Surg*. 2016;20(6):575-8.
58. Gladue H, Fox D, Lowe L, Kahlenberg JM. Schnitzler's Syndrome in the Absence of a Monoclonal Gammopathy. *Journal of Clinical and Cellular Immunology*. 2014;5(5).
59. Varella TC, Nishimura MY, Machado MC, de Moraes-Vasconcelos D, Rivitti EA. Schnitzler's syndrome without monoclonal gammopathy. *Acta Derm Venereol*. 2005;85(3):272-3.
60. Ahn MJ, Yu JE, Jeong J, Sim DW, Koh YI. A Case of Schnitzler's Syndrome without Monoclonal Gammopathy-Associated Chronic Urticaria Treated with Anakinra. *Yonsei Med J*. 2018;59(1):154-7.
61. Treudler R, Kauer F, Simon JC. Striking effect of the IL-1 receptor antagonist anakinra in chronic urticarial rash with polyclonal increase in IgA and IgG. *Acta Derm Venereol*. 2007;87(3):280-1.
62. Clinical Trials U. Schnitzler Syndrome: Clinical Study, Physiopathological and Search for Genetic Factors - Tabular View - [ClinicalTrials.gov](https://clinicaltrials.gov). 2009-2017.
63. Murota H, Shoda Y, Ishibashi T, Sugahara H, Matsumura I, Katayama I. Improvement of recurrent urticaria in a patient with Schnitzler syndrome associated with B-cell lymphoma with combination rituximab and radiotherapy. *J Am Acad Dermatol*. 2009;61(6):1070-5.
64. Jani P, Vissing MB, Ahmed S, Sluzevich JC, Aulakh S, Alegria V, et al. Ibrutinib for the Management of Schnitzler Syndrome: A Novel Therapy for a Rare Condition. *J Oncol Pract*. 2018;Jop1800050.
65. Rybojad M, Moraillon I, Cordoliani F, Lebbe C, Baccard M, Flageul B, et al. [Schnitzler syndrome with genetic C4 deficiency. 2 cases]. *Ann Dermatol Venereol*. 1993;120(11):783-5.

66. Terpos E, Asli B, Christoulas D, Brouet JC, Kastiris E, Rybojad M, et al. Increased angiogenesis and enhanced bone formation in patients with IgM monoclonal gammopathy and urticarial skin rash: new insight into the biology of Schnitzler syndrome. *Haematologica*. 2012;97(11):1699-703.
67. Saurat JH, Schifferli J, Steiger G, Dayer JM, Didierjean L. Anti-interleukin-1 alpha autoantibodies in humans: characterization, isotype distribution, and receptor-binding inhibition--higher frequency in Schnitzler's syndrome (urticaria and macroglobulinemia). *J Allergy Clin Immunol*. 1991;88(2):244-56.
68. de Koning HD, Bodar EJ, Simon A, van der Hilst JC, Netea MG, van der Meer JW. Beneficial response to anakinra and thalidomide in Schnitzler's syndrome. *Ann Rheum Dis*. 2006;65(4):542-4.
69. Morita A, Sakakibara S, Yokota M, Tsuji T. A case of urticarial vasculitis associated with macroglobulinemia (Schnitzler's syndrome). *J Dermatol*. 1995;22(1):32-5.
70. Puddu P, Cianchini G, Girardelli CR, Colonna L, Gatti S, de Pita O. Schnitzler's syndrome: report of a new case and a review of the literature. *Clin Exp Rheumatol*. 1997;15(1):91-5.
71. Goupille P, Pizzuti P, Diot E, Jattiot F, Guilmot JL, Valat JP. Schnitzler's syndrome (urticaria and macroglobulinemia) dramatically improved with corticosteroids. *Clin Exp Rheumatol*. 1995;13(1):95-8.
72. Modiano P, Barbaud A, Laveine E, Cabut S, Weber M, Schmutz J. Efficacité de la PUVAthérapie dans un syndrome de Schnitzler. *Nouv Dermatol*. 1995;14.
73. Famularo G, Barracchini A, Minisola G. Severe thrombophilia with antiphospholipid syndrome and hyperhomocysteinemia in a patient with Schnitzler's syndrome. *Clin Exp Rheumatol*. 2003;21(3):366-8.
74. Sperr WR, Natter S, Baghestanian M, Smolen J, Wolff K, Binder BR, et al. Autoantibody reactivity in a case of Schnitzler's syndrome: evidence for a Th1-like response and detection of IgG2 anti-FcepsilonR1alpha antibodies. *Int Arch Allergy Immunol*. 2000;122(4):279-86.
75. Sadig RR, Wakefield D, Fraser CL. The First Case Report of Schnitzler Syndrome Presenting with Eye Pain. *Ocul Immunol Inflamm*. 2019:1-3.
76. Bursztejn AC, Imperiale A, Lipsker D. Aortitis: A new feature of Schnitzler syndrome. *JAAD Case Rep*. 2017;3(5):454-6.
77. Lee KY, Grattan CE. Intracostal neuralgia as a previously undescribed symptom of Schnitzler's syndrome. *Br J Dermatol*. 2012;167(6):1392-3.
78. Larocca CA, McEvoy JW, Ellis CL, Junkins-Hopkins J, Kolb T, Baer AN, et al. Schnitzler's syndrome associated with pancreatitis: a disease of IL-1 dysregulation. *Clin Rheumatol*. 2012;31(1):169-74.
79. Dinarello CA. Interleukin-1 in the pathogenesis and treatment of inflammatory diseases. *Blood*. 2011;117(14):3720-32.
80. Asli B, Brouet JC, Fermanand JP. Spontaneous remission of Schnitzler syndrome. *Ann Allergy Asthma Immunol*. 2011;107(1):87-8.
81. Claes K, Bammens B, Delforge M, Evenepoel P, Kuypers D, Vanrenterghem Y. Another devastating complication of the Schnitzler syndrome: AA amyloidosis. *Br J Dermatol*. 2008;158(1):182-4.
82. Conlon NP, Hayden P, Barnes L, Doran M, O'Shea F, Feighery C. Schnitzler's syndrome; a case highlighting the complications of long-standing acquired autoinflammation. *Eur J Dermatol*. 2014;24(3):405-6.
83. Mittal N, Renaut P, Sharma R, Robbie M. Gastrointestinal amyloidosis associated with Schnitzler's syndrome. *Pathology*. 2013;45(4):424-6.
84. Lozano Gutierrez F, Aguirre Palacio A, Rivera Civico JM, Nevado Santo M. [The Schnitzler syndrome. A case report]. *Med Clin (Barc)*. 1999;112(4):158-9.
85. Rowczenio DM, Pathak S, Arostegui JI, Mensa-Vilaro A, Omoyinmi E, Brogan P, et al. Molecular genetic investigation, clinical features, and response to treatment in 21 patients with Schnitzler syndrome. *Blood*. 2018;131(9):974-81.

86. Braggio E, Philipsborn C, Novak A, Hodge L, Ansell S, Fonseca R. Molecular pathogenesis of Waldenstrom's macroglobulinemia. *Haematologica*. 2012;97(9):1281-90.
87. Dispenzieri A, Kyle RA, Lacy MQ, Rajkumar SV, Therneau TM, Larson DR, et al. POEMS syndrome: definitions and long-term outcome. *Blood*. 2003;101(7):2496-506.
88. de Koning HD, Schalkwijk J, Stoffels M, Jongekrijg J, Jacobs JF, Verwiel E, et al. The role of interleukin-1 beta in the pathophysiology of Schnitzler's syndrome. *Arthritis Res Ther*. 2015;17:187.
89. Migliorini P, Del Corso I, Tommasi C, Boraschi D. Free circulating interleukin-18 is increased in Schnitzler syndrome: a new autoinflammatory disease? *Eur Cytokine Netw*. 2009;20(3):108-11.
90. Italiani P, Puxeddu I, Napoletano S, Scala E, Melillo D, Manocchio S, et al. Circulating levels of IL-1 family cytokines and receptors in Alzheimer's disease: new markers of disease progression? *J Neuroinflammation*. 2018;15(1):342.
91. Dinarello CA. Overview of the IL-1 family in innate inflammation and acquired immunity. *Immunol Rev*. 2018;281(1):8-27.
92. Peters VA, Joesting JJ, Freund GG. IL-1 receptor 2 (IL-1R2) and its role in immune regulation. *Brain Behav Immun*. 2013;32:1-8.
93. Migliorini P, Italiani P, Pratesi F, Puxeddu I, Boraschi D. Cytokines and soluble receptors of the interleukin-1 family in Schnitzler syndrome. *Scand J Rheumatol*. 2019;48(3):235-8.
94. Szturcz P, Adam Z, Klabusay M, Fojtik Z, Kadanka Z, Stehlikova O, et al. Schnitzler syndrome: case report, the experience with glucocorticoid and anakinra (Kineret) therapies and monitoring of systemic cytokine response. *Vnitr Lek*. 2011;57(1):97-112.
95. Lust JA, Lacy MQ, Zeldenrust SR, Dispenzieri A, Gertz MA, Witzig TE, et al. Induction of a chronic disease state in patients with smoldering or indolent multiple myeloma by targeting interleukin 1{beta}-induced interleukin 6 production and the myeloma proliferative component. *Mayo Clin Proc*. 2009;84(2):114-22.
96. Krause K, Feist E, Fiene M, Kallinich T, Maurer M. Complete remission in 3 of 3 anti-IL-6-treated patients with Schnitzler syndrome. *J Allergy Clin Immunol*. 2012;129(3):848-50.
97. Gohar F, Orak B, Kallinich T, Jeske M, Lieber M, von Bernuth H, et al. Correlation of Secretory Activity of Neutrophils With Genotype in Patients With Familial Mediterranean Fever. *Arthritis Rheumatol*. 2016;68(12):3010-22.
98. Weiss ES, Girard-Guyonvarc'h C, Holzinger D, de Jesus AA, Tariq Z, Picarsic J, et al. Interleukin-18 diagnostically distinguishes and pathogenically promotes human and murine macrophage activation syndrome. *Blood*. 2018;131(13):1442-55.
99. Ryan JG, de Koning HD, Beck LA, Booty MG, Kastner DL, Simon A. IL-1 blockade in Schnitzler syndrome: ex vivo findings correlate with clinical remission. *J Allergy Clin Immunol*. 2008;121(1):260-2.
100. Aikawa NE, Silva CA, Bonfa E, Carvalho JF. Schnitzler's syndrome improvement after anti-TNF-alpha therapy. *Joint Bone Spine*. 2010;77(5):491.
101. Thonhofer R, Uitz E, Graninger W. Schnitzler's syndrome--exacerbation after anti-TNF treatment. *Rheumatology (Oxford)*. 2007;46(6):1041-2.
102. Heine G, Drozdenko G, Grun JR, Chang HD, Radbruch A, Worm M. Autocrine IL-10 promotes human B-cell differentiation into IgM- or IgG-secreting plasmablasts. *Eur J Immunol*. 2014;44(6):1615-21.
103. Armstrong L, Jordan N, Millar A. Interleukin 10 (IL-10) regulation of tumour necrosis factor alpha (TNF-alpha) from human alveolar macrophages and peripheral blood monocytes. *Thorax*. 1996;51(2):143-9.
104. Reinhardt RL, Liang HE, Bao K, Price AE, Mohrs M, Kelly BL, et al. A novel model for IFN-gamma-mediated autoinflammatory syndromes. *J Immunol*. 2015;194(5):2358-68.
105. Pollard KM, Cauvi DM, Toomey CB, Morris KV, Kono DH. Interferon-gamma and systemic autoimmunity. *Discov Med*. 2013;16(87):123-31.

106. Schaefer TM, Desouza K, Fahey JV, Beagley KW, Wira CR. Toll-like receptor (TLR) expression and TLR-mediated cytokine/chemokine production by human uterine epithelial cells. *Immunology*. 2004;112(3):428-36.
107. Wong H, Nowak J, Standage S, Oliveira F. *Pediatric Critical Care*. 4 ed: Elsevier; 2011.
108. Miossec P, Kolls JK. Targeting IL-17 and TH17 cells in chronic inflammation. *Nat Rev Drug Discov*. 2012;11(10):763-76.
109. Noster R, de Koning HD, Maier E, Prelog M, Lainka E, Zielinski CE. Dysregulation of proinflammatory versus anti-inflammatory human TH17 cell functionalities in the autoinflammatory Schnitzler syndrome. *J Allergy Clin Immunol*. 2016;138(4):1161-9.e6.
110. Villarreal RS, VandenBoom T, Gonzalez-Gonzalez FJ, Carter RG, Peters NT, Peters AT, et al. Schnitzler syndrome with IgG gammopathy and elevated IL-1beta and IL-17 in skin biopsy. *Ann Allergy Asthma Immunol*. 2018;120(1):99-101.
111. Gee K, Guzzo C, Che Mat NF, Ma W, Kumar A. The IL-12 family of cytokines in infection, inflammation and autoimmune disorders. *Inflamm Allergy Drug Targets*. 2009;8(1):40-52.
112. Hawkins PN, Lachmann HJ, McDermott MF. Interleukin-1-receptor antagonist in the Muckle-Wells syndrome. *N Engl J Med*. 348. United States 2003. p. 2583-4.
113. Hawkins PN, Lachmann HJ, Aganna E, McDermott MF. Spectrum of clinical features in Muckle-Wells syndrome and response to anakinra. *Arthritis Rheum*. 2004;50(2):607-12.
114. Hoffman HM, Rosengren S, Boyle DL, Cho JY, Nayar J, Mueller JL, et al. Prevention of cold-associated acute inflammation in familial cold autoinflammatory syndrome by interleukin-1 receptor antagonist. *Lancet*. 2004;364(9447):1779-85.
115. Martinez-Taboada VM, Fontalba A, Blanco R, Fernandez-Luna JL. Successful treatment of refractory Schnitzler syndrome with anakinra: comment on the article by Hawkins et al. *Arthritis Rheum*. 2005;52(7):2226-7.
116. Clinical Trials F. An exploratory, open-label, single centre, phase II, proof of concept study of gevokizumab treatment in patients with Schnitzler syndrome In: (I.R.I.S) IdRIS, editor. France 2013-2016. p. 5.
117. Rossi-Semerano L, Fautrel B, Wendling D, Hachulla E, Galeotti C, Semerano L, et al. Tolerance and efficacy of off-label anti-interleukin-1 treatments in France: a nationwide survey. *Orphanet J Rare Dis*. 2015;10:19.
118. Clinical Commissioning Policy: Anakinra to treat periodic fevers and autoinflammatory diseases (all ages) [press release]. NHS England 2018.
119. Leoni F, Fossati G, Lewis EC, Lee JK, Porro G, Pagani P, et al. The histone deacetylase inhibitor ITF2357 reduces production of pro-inflammatory cytokines in vitro and systemic inflammation in vivo. *Mol Med*. 2005;11(1-12):1-15.
120. McColl SR, Paquin R, Menard C, Beaulieu AD. Human neutrophils produce high levels of the interleukin 1 receptor antagonist in response to granulocyte/macrophage colony-stimulating factor and tumor necrosis factor alpha. *J Exp Med*. 1992;176(2):593-8.
121. Hageman DD, Okayama Y, D'Ambrosio C, Prussin C, Gilfillan AM, Metcalfe DD. Secretion of interleukin-1 receptor antagonist from human mast cells after immunoglobulin E-mediated activation and after segmental antigen challenge. *Am J Respir Cell Mol Biol*. 2001;25(6):685-91.
122. Gruaz-Chatellard D, Baumberger C, Saurat JH, Dayer JM. Interleukin 1 receptor antagonist in human epidermis and cultured keratinocytes. *FEBS Lett*. 1991;294(1-2):137-40.
123. Gabay C, Smith MF, Eidlen D, Arend WP. Interleukin 1 receptor antagonist (IL-1Ra) is an acute-phase protein. *J Clin Invest*. 1997;99(12):2930-40.
124. Daig R, Rogler G, Aschenbrenner E, Vogl D, Falk W, Gross V, et al. Human intestinal epithelial cells secrete interleukin-1 receptor antagonist and interleukin-8 but not interleukin-1 or interleukin-6. *Gut*. 2000;46(3):350-8.
125. Bachove I, Chang C. Anakinra and related drugs targeting interleukin-1 in the treatment of cryopyrin-associated periodic syndromes. *Open Access Rheumatol*. 2014;6:15-25.

126. Excellence N-TNIfHaC. Anakinra [CorporatePage]. UK: NICE; 2014 [updated 2014-08-05]. Available from: <https://bnf.nice.org.uk/drug/anakinra.html>.
127. Bresnihan B, Alvaro-Gracia JM, Cobby M, Doherty M, Domljan Z, Emery P, et al. Treatment of rheumatoid arthritis with recombinant human interleukin-1 receptor antagonist. *Arthritis Rheum*. 1998;41(12):2196-204.
128. Nuki G, Bresnihan B, Bear MB, McCabe D. Long-term safety and maintenance of clinical improvement following treatment with anakinra (recombinant human interleukin-1 receptor antagonist) in patients with rheumatoid arthritis: extension phase of a randomized, double-blind, placebo-controlled trial. *Arthritis Rheum*. 2002;46(11):2838-46.
129. Launay D, Dutoit-Lefevre V, Faure E, Robineau O, Hauspie C, Sobanski V, et al. Effect of in vitro and in vivo anakinra on cytokines production in Schnitzler syndrome. *PLoS One*. 2013;8(3):e59327.
130. Margerin F, Gottenberg JE, Lipsker D. Occurrence of Rheumatoid Arthritis in a Patient Treated with Anakinra for Schnitzler Syndrome: A Case Report. *J Rheumatol*. 2016;43(7):1447.
131. Saperia C, McAuley P, Raffagehlo J, Fazlul-Haque S, Sussman G. Clinical experiences with canakinumab as a treatment for autoinflammatory disorders. *Pediatric Rheumatology*. 2015;13(1):1-.
132. de Koning HD, Schalkwijk J, van der Meer JW, Simon A. Successful canakinumab treatment identifies IL-1beta as a pivotal mediator in Schnitzler syndrome. *J Allergy Clin Immunol*. 2011;128(6):1352-4.
133. Church LD, McDermott MF. Canakinumab: a human anti-IL-1beta monoclonal antibody for the treatment of cryopyrin-associated periodic syndromes. *Expert Rev Clin Immunol*. 2010;6(6):831-41.
134. Kuemmerle-Deschner JB, Hachulla E, Cartwright R, Hawkins PN, Tran TA, Bader-Meunier B, et al. Two-year results from an open-label, multicentre, phase III study evaluating the safety and efficacy of canakinumab in patients with cryopyrin-associated periodic syndrome across different severity phenotypes. *Ann Rheum Dis*. 2011;70(12):2095-102.
135. Lachmann HJ, Lowe P, Felix SD, Rordorf C, Leslie K, Madhoo S, et al. In vivo regulation of interleukin 1beta in patients with cryopyrin-associated periodic syndromes. *J Exp Med*. 2009;206(5):1029-36.
136. Lachmann HJ, Kone-Paut I, Kuemmerle-Deschner JB, Leslie KS, Hachulla E, Quartier P, et al. Use of canakinumab in the cryopyrin-associated periodic syndrome. *N Engl J Med*. 2009;360(23):2416-25.
137. De Benedetti F, Gattorno M, Anton J, Ben-Chetrit E, Frenkel J, Hoffman HM, et al. Canakinumab for the Treatment of Autoinflammatory Recurrent Fever Syndromes. *N Engl J Med*. 2018;378(20):1908-19.
138. Ridker PM, Everett BM, Thuren T, MacFadyen JG, Chang WH, Ballantyne C, et al. Antiinflammatory Therapy with Canakinumab for Atherosclerotic Disease. *N Engl J Med*. 2017;377(12):1119-31.
139. Krause K, Tsianakas A, Wagner N, Fischer J, Weller K, Metz M, et al. Efficacy and safety of canakinumab in Schnitzler syndrome: A multicenter randomized placebo-controlled study. *J Allergy Clin Immunol*. 2017;139(4):1311-20.
140. de Koning HD, Schalkwijk J, van der Ven-Jongekrijg J, Stoffels M, van der Meer JW, Simon A. Sustained efficacy of the monoclonal anti-interleukin-1 beta antibody canakinumab in a 9-month trial in Schnitzler's syndrome. *Ann Rheum Dis*. 2013;72(10):1634-8.
141. Salugina S, Gorodetskiy V, Fedorov E, Lopatina N. Schnitzler Syndrome in the Clinical Practice of a Rheumatologist. *Annals of the Rheumatic Diseases*. 2019;78.
142. Pesek R, Fox R. Successful treatment of Schnitzler syndrome with canakinumab. *Cutis*. 2014;94(3):E11-2.
143. Elmi AA, Wynne K, Cheng IL, Eleftheriou D, Lachmann HJ, Hawkins PN, et al. Retrospective case series describing the efficacy, safety and cost-effectiveness of a vial-sharing programme for

canakinumab treatment for paediatric patients with cryopyrin-associated periodic syndrome. *Pediatr Rheumatol Online J*. 2019;17(1):36.

144. So A, Dumusc A, Nasi S. The role of IL-1 in gout: from bench to bedside. *Rheumatology (Oxford)*. 2018;57(suppl_1):i12-i9.

145. Garg M, de Jesus AA, Chapelle D, Dancey P, Herzog R, Rivas-Chacon R, et al. Rilonacept maintains long-term inflammatory remission in patients with deficiency of the IL-1 receptor antagonist. *JCI Insight*. 2017;2(16).

146. White PC, Adhikari S, Grishman EK, Sumpter KM. A phase I study of anti-inflammatory therapy with rilonacept in adolescents and adults with type 1 diabetes mellitus. *Pediatr Diabetes*. 2018;19(4):788-93.

147. Krause K, Weller K, Stefaniak R, Wittkowski H, Altrichter S, Siebenhaar F, et al. Efficacy and safety of the interleukin-1 antagonist rilonacept in Schnitzler syndrome: an open-label study. *Allergy*. 2012;67(7):943-50.

148. Hashkes PJ, Spalding SJ, Hajj-Ali R, Giannini EH, Johnson A, Barron KS, et al. The effect of rilonacept versus placebo on health-related quality of life in patients with poorly controlled familial Mediterranean fever. *Biomed Res Int*. 2014;2014:854842.

149. Hoffman HM, Throne ML, Amar NJ, Sebai M, Kivitz AJ, Kavanaugh A, et al. Efficacy and safety of rilonacept (interleukin-1 Trap) in patients with cryopyrin-associated periodic syndromes: results from two sequential placebo-controlled studies. *Arthritis Rheum*. 2008;58(8):2443-52.

150. Kapur S, Bonk ME. Rilonacept (arcalyst), an interleukin-1 trap for the treatment of cryopyrin-associated periodic syndromes. *P t*. 2009;34(3):138-41.

151. Van Cutsem E, Shitara K, Deng W, Vaury A, Tseng L, Wang X, et al. Gevokizumab, an interleukin-1 β (IL-1 β) monoclonal antibody (mAb), in metastatic colorectal cancer (mCRC), metastatic gastroesophageal cancer (mGEC) and metastatic renal cell carcinoma (mRCC): "first-in-cancer" phase Ib study. *Annals of Oncology*. 2019;30(Supplement_4).

152. Knickelbein JE, Tucker WR, Bhatt N, Armbrust K, Valent D, Obiyor D, et al. Gevokizumab in the Treatment of Autoimmune Non-necrotizing Anterior Scleritis: Results of a Phase I/II Clinical Trial. *Am J Ophthalmol*. 2016;172:104-10.

153. Tugal-Tutkun I, Kadayifcilar S, Khairallah M, Lee S, Ozdal P, Ozyazgan Y, et al. Safety and Efficacy of Gevokizumab in Patients with Behcet's Disease Uveitis: Results of an Exploratory Phase 2 Study. *Ocul Immunol Inflamm*. 2017;25(1):62-70.

154. Ramadan KM, Eswedi HA, El-Agnaf MR. Schnitzler syndrome: a case report of successful treatment using the anti-CD20 monoclonal antibody rituximab. *Br J Dermatol*. 2007;156(5):1072-4.

155. Asli B, Bienvenu B, Cordoliani F, Brouet JC, Uzunhan Y, Arnulf B, et al. Chronic urticaria and monoclonal IgM gammopathy (Schnitzler syndrome): report of 11 cases treated with pefloxacin. *Arch Dermatol*. 2007;143(8):1046-50.

156. Kastritis E, Katoulis A, Terpos E, Panayiotides I, Gavriatopoulou M, Dimopopoulos MA. Schnitzler's syndrome: increased levels of bone formation and angiogenesis factors are reduced after successful pefloxacin treatment. *Clin Lymphoma Myeloma*. 2008;8(6):359-62.

157. Sebba A. Tocilizumab: the first interleukin-6-receptor inhibitor. *Am J Health Syst Pharm*. 2008;65(15):1413-8.

158. Jones G, Ding C. Tocilizumab: a review of its safety and efficacy in rheumatoid arthritis. *Clin Med Insights Arthritis Musculoskelet Disord*. 2010;3:81-9.

159. Canna SW, Girard C, Malle L, de Jesus A, Romberg N, Kelsen J, et al. Life-threatening NLRP4-associated hyperinflammation successfully treated with IL-18 inhibition. *J Allergy Clin Immunol*. 2017;139(5):1698-701.

160. Dalhoff A, Shalit I. Immunomodulatory effects of quinolones. *Lancet Infect Dis*. 2003;3(6):359-71.

161. Aouba A, Pressiat C, Pricopi M, Georgin-Lavialle S, Boue F, Lievre-Castilla MA, et al. Complete remission of Schnitzler syndrome and Waldenstrom macroglobulinemia under rituximab-cyclophosphamide-dexamethasone. *Dermatology*. 2015;230(1):18-22.

162. Eiling E, Moller M, Kreiselmaier I, Brasch J, Schwarz T. Schnitzler syndrome: treatment failure to rituximab but response to anakinra. *J Am Acad Dermatol*. 2007;57(2):361-4.
163. Cascavilla N, Bisceglia M, D'Arena G. Successful treatment of Schnitzler's syndrome with anakinra after failure of rituximab trial. *Int J Immunopathol Pharmacol*. 2010;23(2):633-6.
164. Tinazzi E, Puccetti A, Patuzzo G, Sorleto M, Barbieri A, Lunardi C. Schnitzler syndrome, an autoimmune-autoinflammatory syndrome: report of two new cases and review of the literature. *Autoimmun Rev*. 2011;10(7):404-9.
165. Liu X, Pichulik T, Wolz OO, Dang TM, Stutz A, Dillen C, et al. Human NACHT, LRR, and PYD domain-containing protein 3 (NLRP3) inflammasome activity is regulated by and potentially targetable through Bruton tyrosine kinase. *J Allergy Clin Immunol*. 2017;140(4):1054-67.e10.
166. Mensa-Vilaro A, Teresa Bosque M, Magri G, Honda Y, Martinez-Banaclocha H, Casorran-Berges M, et al. Late onset cryopyrin-associated periodic syndrome due to myeloid-restricted somatic NLRP3 mosaicism. *Arthritis Rheumatol*. 2016.
167. Rowczenio DM, Gomes SM, Aróstegui JI, Mensa-Vilaro A, Omoyinmi E, Trojer H, et al. Late-Onset Cryopyrin-Associated Periodic Syndromes Caused by Somatic NLRP3 Mosaicism—UK Single Center Experience. *Front Immunol*. 2017;8.
168. Aksentijevich I, Putnam CD, Remmers EF, Mueller JL, Le J, Kolodner RD, et al. The clinical continuum of cryopyrinopathies: novel CIAS1 mutations in North American patients and a new cryopyrin model. *Arthritis Rheum*. 2007;56(4):1273-85.
169. Franklin BS, Bossaller L, De Nardo D, Ratter JM, Stutz A, Engels G, et al. The adaptor ASC has extracellular and 'prionoid' activities that propagate inflammation. *Nat Immunol*. 2014;15(8):727-37.
170. Bowman RL, Busque L, Levine RL. Clonal Hematopoiesis and Evolution to Hematopoietic Malignancies. *Cell Stem Cell*. 2018;22(2):157-70.
171. Wiedmeier JE, Kato C, Zhang Z, Lee H, Dunlap J, Nutt E, et al. Clonal hematopoiesis as determined by the HUMARA assay is a marker for acquired mutations in epigenetic regulators in older women. *Exp Hematol*. 2016;44(9):857-65.e5.
172. Klepin HD. Myelodysplastic Syndromes and Acute Myeloid Leukemia in the Elderly. *Clin Geriatr Med*. 2016;32(1):155-73.
173. Qian L, Shen J, Cen J, Yin W, Ma Y. Myelodysplastic syndrome with neutrophilic panniculitis: A report of two cases and a literature review. *Oncol Lett*. 2015;9(4):1954-6.
174. Fain O, Braun T, Stirnemann J, Fenaux P. Systemic and autoimmune manifestations in myelodysplastic syndromes. *Rev Med Interne*. 2011;32(9):552-9.
175. Mekinian A, Grignano E, Braun T, Decaux O, Liozon E, Costedoat-Chalumeau N, et al. Systemic inflammatory and autoimmune manifestations associated with myelodysplastic syndromes and chronic myelomonocytic leukaemia: a French multicentre retrospective study. *Rheumatology (Oxford)*. 2016;55(2):291-300.
176. Arranz L, Arriero MDM, Villatoro A. Interleukin-1beta as emerging therapeutic target in hematological malignancies and potentially in their complications. *Blood Rev*. 2017;31(5):306-17.
177. de Mooij CEM, Netea MG, van der Velden W, Blijlevens NMA. Targeting the interleukin-1 pathway in patients with hematological disorders. *Blood*. 2017;129(24):3155-64.
178. Hemmati S, Haque T, Gritsman K. Inflammatory Signaling Pathways in Preleukemic and Leukemic Stem Cells. *Front Oncol*. 2017;7:265.
179. Basiorka AA, McGraw KL, Eksioğlu EA, Chen X, Johnson J, Zhang L, et al. The NLRP3 inflammasome functions as a driver of the myelodysplastic syndrome phenotype. *Blood*. 2016;128(25):2960-75.
180. Sallman DA, Cluzeau T, Basiorka AA, List A. Unraveling the Pathogenesis of MDS: The NLRP3 Inflammasome and Pyroptosis Drive the MDS Phenotype. *Front Oncol*. 2016;6.
181. Hoffman HM, Broderick L. The role of the inflammasome in patients with autoinflammatory diseases. *J Allergy Clin Immunol*. 2016;138(1):3-14.
182. Treon SP, Xu L, Yang G, Zhou Y, Liu X, Cao Y, et al. MYD88 L265P somatic mutation in Waldenstrom's macroglobulinemia. *N Engl J Med*. 2012;367(9):826-33.

183. Varettoni M, Arcaini L, Zibellini S, Boveri E, Rattotti S, Riboni R, et al. Prevalence and clinical significance of the MYD88 (L265P) somatic mutation in Waldenstrom's macroglobulinemia and related lymphoid neoplasms. *Blood*. 2013;121(13):2522-8.
184. Ngo VN, Young RM, Schmitz R, Jhavar S, Xiao W, Lim KH, et al. Oncogenically active MYD88 mutations in human lymphoma. *Nature*. 2011;470(7332):115-9.
185. Yu X, Li W, Deng Q, Li L, Hsi ED, Young KH, et al. MYD88 L265P Mutation in Lymphoid Malignancies. *Cancer Res*. 2018;78(10):2457-62.
186. Mulla E, Neame R. Delayed development of the IgM paraprotein in Schnitzler's syndrome. *Scand J Rheumatol*. 2015;44(6):521-2.
187. Blotta S, Tassone P, Prabhala RH, Tagliaferri P, Cervi D, Amin S, et al. Identification of novel antigens with induced immune response in monoclonal gammopathy of undetermined significance. *Blood*. 2009;114(15):3276-84.
188. Preuss KD, Held G, Kubuschok B, Hung CZ, Malatsidze N, Wagner M, et al. Identification of antigenic targets of paraproteins by expression cloning does not support a causal role of chronic antigenic stimulation in the pathogenesis of multiple myeloma and MGUS. *Int J Cancer*. 2007;121(2):459-61.
189. Swiecicki PL, Hegerova LT, Gertz MA. Cold agglutinin disease. *Blood*. 2013;122(7):1114-21.
190. Hatjiharissi E, Ngo H, Leontovich AA, Leleu X, Timm M, Melhem M, et al. Proteomic analysis of waldenstrom macroglobulinemia. *Cancer Res*. 2007;67(8):3777-84.
191. Beyer NH, Lueking A, Kowald A, Frederiksen JL, Heegaard NH. Investigation of autoantibody profiles for cerebrospinal fluid biomarker discovery in patients with relapsing-remitting multiple sclerosis. *J Neuroimmunol*. 2012;242(1-2):26-32.
192. Auger I, Balandraud N, Rak J, Lambert N, Martin M, Roudier J. New autoantigens in rheumatoid arthritis (RA): screening 8268 protein arrays with sera from patients with RA. *Ann Rheum Dis*. 2009;68(4):591-4.
193. Zhu H, Luo H, Yan M, Zuo X, Li QZ. Autoantigen Microarray for High-throughput Autoantibody Profiling in Systemic Lupus Erythematosus. *Genomics Proteomics Bioinformatics*. 2015;13(4):210-8.
194. de Brito Rocha S, Baldo DC, Andrade LEC. Clinical and pathophysiologic relevance of autoantibodies in rheumatoid arthritis. *Adv Rheumatol*. 2019;59(1):2.
195. Rosenfeld AM, Meng W, Chen DY, Zhang B, Granot T, Farber DL, et al. Computational Evaluation of B-Cell Clone Sizes in Bulk Populations. *Front Immunol*. 2018;9.
196. Berg JM, Tymoczko JL, Stryer L. Diversity Is Generated by Gene Rearrangements. *Biochemistry: W H Freeman*; 2002.
197. Lipsker D, Spehner D, Drillien R, Schmitt P, Cribier B, Heid E, et al. Schnitzler syndrome: heterogeneous immunopathological findings involving IgM-skin interactions. *Br J Dermatol*. 2000;142(5):954-9.
198. Petrikos L, Kyrtsionis MC, Roumelioti M, Georgiou G, Efthymiou A, Tzenou T, et al. Clonotypic analysis of immunoglobulin heavy chain sequences in patients with Waldenstrom's macroglobulinemia: correlation with MYD88 L265P somatic mutation status, clinical features, and outcome. *Biomed Res Int*. 2014;2014:809103.
199. Kastner DL. Hereditary periodic fever syndromes. *Hematology Am Soc Hematol Educ Program*. 2005:74-81.
200. Goldbach-Mansky R. Current Status of Understanding the Pathogenesis and Management of Patients With NOMID/CINCA. *Curr Rheumatol Rep*. 2011;13(2):123-31.
201. Goldbach-Mansky R, Kastner DL. Autoinflammation: The prominent role of IL-1 in monogenic autoinflammatory diseases and implications for common illnesses. *J Allergy Clin Immunol*. 2009;124(6):1141-51.
202. He Y, Hara H, Nunez G. Mechanism and Regulation of NLRP3 Inflammasome Activation. *Trends Biochem Sci*. 2016;41(12):1012-21.

203. Agostini L, Martinon F, Burns K, McDermott MF, Hawkins PN, Tschopp J. NALP3 forms an IL-1beta-processing inflammasome with increased activity in Muckle-Wells autoinflammatory disorder. *Immunity*. 2004;20(3):319-25.
204. Kummer JA, Broekhuizen R, Everett H, Agostini L, Kuijk L, Martinon F, et al. Inflammasome components NALP 1 and 3 show distinct but separate expression profiles in human tissues suggesting a site-specific role in the inflammatory response. *J Histochem Cytochem*. 2007;55(5):443-52.
205. Dick MS, Sborgi L, Ruhl S, Hiller S, Broz P. ASC filament formation serves as a signal amplification mechanism for inflammasomes. *Nat Commun*. 2016;7:11929.
206. Nalbantoglu S, Tanyolac B, Berdeli A. Apoptosis-associated speck-like protein containing a CARD (ASC) expression profiles in familial Mediterranean fever (FMF) patients with different MEFV mutation patterns. *Scand J Rheumatol*. 2013;42(2):159-62.
207. Miao EA, Rajan JV, Aderem A. Caspase-1 induced pyroptotic cell death. *Immunol Rev*. 2011;243(1):206-14.
208. Rubartelli A. Redox control of NLRP3 inflammasome activation in health and disease. *J Leukoc Biol*. 2012;92(5):951-8.
209. Eitel J, Suttorp N, Opitz B. Innate immune recognition and inflammasome activation in *listeria monocytogenes* infection. *Front Microbiol*. 2010;1:149.
210. Tschopp J, Schroder K. NLRP3 inflammasome activation: The convergence of multiple signalling pathways on ROS production? *Nat Rev Immunol*. 2010;10(3):210-5.
211. Arsenic R, Treue D, Lehmann A, Hummel M, Dietel M, Denkert C, et al. Comparison of targeted next-generation sequencing and Sanger sequencing for the detection of PIK3CA mutations in breast cancer. *BMC Clin Pathol*. 2015;15:20.
212. Curci PL, Sonnante G. How a Small Double-Stranded Trick Can Mislead Sanger Sequencing. *J Biomol Tech*. 2015;26(3):80-2.
213. Ben-Zvi I, Herskovizh C, Kukuy O, Kassel Y, Grossman C, Livneh A. Familial Mediterranean fever without MEFV mutations: a case-control study. *Orphanet J Rare Dis*. 2015;10:34.
214. Baroja-Mazo A, Martin-Sanchez F, Gomez AI, Martinez CM, Amores-Iniesta J, Compan V, et al. The NLRP3 inflammasome is released as a particulate danger signal that amplifies the inflammatory response. *Nat Immunol*. 2014;15(8):738-48.
215. de Torre-Minguela C, Mesa Del Castillo P, Pelegrin P. The NLRP3 and Pypin Inflammasomes: Implications in the Pathophysiology of Autoinflammatory Diseases. *Front Immunol*. 2017;8:43.
216. Kerr N, Lee SW, Perez-Barcena J, Crespi C, Ibanez J, Bullock MR, et al. Inflammasome proteins as biomarkers of traumatic brain injury. *PLoS One*. 2018;13(12):e0210128.
217. Keane RW, Dietrich WD, de Rivero Vaccari JP. Inflammasome Proteins As Biomarkers of Multiple Sclerosis. *Front Neurol*. 2018;9:135.
218. Basiorka AA, McGraw KL, Abbas-Aghababazadeh F, McLemore AF, Vincelette ND, Ward GA, et al. Assessment of ASC specks as a putative biomarker of pyroptosis in myelodysplastic syndromes: an observational cohort study. *Lancet Haematol*. 2018.
219. Head SR, Komori HK, LaMere SA, Whisenant T, Van Nieuwerburgh F, Salomon DR, et al. Library construction for next-generation sequencing: overviews and challenges. *Biotechniques*. 2014;56(2):61-4, 6, 8, passim.
220. Lis JT, Schleif R. Size fractionation of double-stranded DNA by precipitation with polyethylene glycol. *Nucleic Acids Res*. 1975;2(3):383-9.
221. BioCat. EpiNext DNA Library Preparation Kit (Illumina), 24 reactions: / Impressum; 2017 [Available from: <https://www.biocat.com/products/P-1051-24-EP>].
222. Blankenberg D, Hillman-Jackson J. Analysis of next-generation sequencing data using Galaxy. *Methods Mol Biol*. 2014;1150:21-43.
223. Kuri P, Schieber NL, Thumberger T, Wittbrodt J, Schwab Y, Leptin M. Dynamics of in vivo ASC speck formation. *J Cell Biol*. 2017;216(9):2891-909.
224. Dinarello CA. Biologic basis for interleukin-1 in disease. *Blood*. 1996;87(6):2095-147.

225. Pizzirani C, Falzoni S, Govoni M, La Corte R, Donadei S, Di Virgilio F, et al. Dysfunctional inflammasome in Schnitzler's syndrome. *Rheumatology (Oxford)*. 2009;48(10):1304-8.
226. Magyari L, Varszegi D, Kovesdi E, Sarlos P, Farago B, Javorhazy A, et al. Interleukins and interleukin receptors in rheumatoid arthritis: Research, diagnostics and clinical implications. *World J Orthop*. 2014;5(4):516-36.
227. Ciccarelli F, De Martinis M, Ginaldi L. An update on autoinflammatory diseases. *Curr Med Chem*. 2014;21(3):261-9.
228. Shah N, Kammermeier J, Elawad M, Glocker EO. Interleukin-10 and interleukin-10-receptor defects in inflammatory bowel disease. *Curr Allergy Asthma Rep*. 2012;12(5):373-9.
229. Gu Y, Yang J, Ouyang X, Liu W, Li H, Bromberg J, et al. Interleukin 10 suppresses Th17 cytokines secreted by macrophages and T cells. *Eur J Immunol*. 2008;38(7):1807-13.
230. Toutilou I, Galeotti C, Rossi-Semerano L, Hentgen V, Piram M, Kone-Paut I. The expanding spectrum of rare monogenic autoinflammatory diseases. *Orphanet J Rare Dis*. 2013;8:162.
231. Kawasaki Y, Oda H, Ito J, Niwa A, Tanaka T, Hijikata A, et al. Identification of a High-Frequency Somatic NLRC4 Mutation as a Cause of Autoinflammation by Pluripotent Cell-Based Phenotype Dissection. *Arthritis Rheumatol*. 2017;69(2):447-59.
232. Vince JE, Silke J. The intersection of cell death and inflammasome activation. *Cell Mol Life Sci*. 2016;73(11-12):2349-67.
233. Pierini R, Juruj C, Perret M, Jones CL, Mangeot P, Weiss DS, et al. AIM2/ASC triggers caspase-8-dependent apoptosis in Francisella-infected caspase-1-deficient macrophages. *Cell Death Differ*. 2012;19(10):1709-21.
234. Warner N, Nunez G. MyD88: a critical adaptor protein in innate immunity signal transduction. *J Immunol*. 2013;190(1):3-4.
235. Lord KA, Hoffman-Liebermann B, Liebermann DA. Complexity of the immediate early response of myeloid cells to terminal differentiation and growth arrest includes ICAM-1, Jun-B and histone variants. *Oncogene*. 1990;5(3):387-96.
236. Fiedler K, Kokai E, Bresch S, Brunner C. MyD88 is involved in myeloid as well as lymphoid hematopoiesis independent of the presence of a pathogen. *Am J Blood Res*. 2013;3(2):124-40.
237. Vanaja SK, Rathinam VA, Fitzgerald KA. Mechanisms of inflammasome activation: recent advances and novel insights. *Trends Cell Biol*. 2015;25(5):308-15.
238. Hoesel B, Schmid JA. The complexity of NF-kappaB signaling in inflammation and cancer. *Mol Cancer*. 2013;12:86.
239. Takeda K, Akira S. TLR signaling pathways. *Semin Immunol*. 2004;16(1):3-9.
240. Cataisson C, Salcedo R, Hakim S, Moffitt BA, Wright L, Yi M, et al. IL-1R-MyD88 signaling in keratinocyte transformation and carcinogenesis. *J Exp Med*. 2012;209(9):1689-702.
241. Andreakos E, Sacre SM, Smith C, Lundberg A, Kiriakidis S, Stonehouse T, et al. Distinct pathways of LPS-induced NF-kappa B activation and cytokine production in human myeloid and nonmyeloid cells defined by selective utilization of MyD88 and Mal/TIRAP. *Blood*. 2004;103(6):2229-37.
242. Patkar N, Subramanian PG, Deshpande P, Ghodke K, Tembhare P, Mascarenhas R, et al. MYD88 mutant lymphoplasmacytic lymphoma/Waldenstrom macroglobulinemia has distinct clinical and pathological features as compared to its mutation negative counterpart. *Leuk Lymphoma*. 2015;56(2):420-5.
243. Martinez-Lopez A, Curiel-Olmo S, Mollejo M, Cereceda L, Martinez N, Montes-Moreno S, et al. MYD88 (L265P) somatic mutation in marginal zone B-cell lymphoma. *Am J Surg Pathol*. 2015;39(5):644-51.
244. Ansell SM, Hodge LS, Secreto FJ, Manske M, Braggio E, Price-Troska T, et al. Activation of TAK1 by MYD88 L265P drives malignant B-cell Growth in non-Hodgkin lymphoma. *Blood Cancer J*. 2014;4:e183.

245. Sallmyr A, Fan J, Rassool FV. Genomic instability in myeloid malignancies: increased reactive oxygen species (ROS), DNA double strand breaks (DSBs) and error-prone repair. *Cancer Lett.* 2008;270(1):1-9.
246. Koefler HP, Leong G. Preleukemia: one name, many meanings. *Leukemia.* 2017;31(3):534-42.
247. Steensma DP, Bejar R, Jaiswal S, Lindsley RC, Sekeres MA, Hasserjian RP, et al. Clonal hematopoiesis of indeterminate potential and its distinction from myelodysplastic syndromes. *Blood.* 2015;126(1):9-16.
248. Busque L, Patel JP, Figueroa ME, Vasanthakumar A, Provost S, Hamilou Z, et al. Recurrent somatic TET2 mutations in normal elderly individuals with clonal hematopoiesis. *Nat Genet.* 2012;44(11):1179-81.
249. Gribnau J, Barakat T. X-chromosome inactivation and its implications for human disease. *BioRxiv.* 2017.
250. Lyon MF. Gene action in the X-chromosome of the mouse (*Mus musculus* L.). *Nature.* 1961;190:372-3.
251. Zuo T, Wang L, Morrison C, Chang X, Zhang H, Li W, et al. FOXP3 is an X-linked breast cancer suppressor gene and an important repressor of the HER-2/ErbB2 oncogene. *Cell.* 2007;129(7):1275-86.
252. Busque L, Gilliland DG. X-inactivation analysis in the 1990s: promise and potential problems. *Leukemia.* 1998;12(2):128-35.
253. Abkowitz JL, Taboada M, Shelton GH, Catlin SN, Guttorp P, Kiklevich JV. An X chromosome gene regulates hematopoietic stem cell kinetics. *Proc Natl Acad Sci U S A.* 1998;95(7):3862-6.
254. Genovese G, Kahler AK, Handsaker RE, Lindberg J, Rose SA, Bakhoum SF, et al. Clonal hematopoiesis and blood-cancer risk inferred from blood DNA sequence. *N Engl J Med.* 2014;371(26):2477-87.
255. Jaiswal S, Fontanillas P, Flannick J, Manning A, Grauman PV, Mar BG, et al. Age-Related Clonal Hematopoiesis Associated with Adverse Outcomes. *N Engl J Med.* 2014;371(26):2488-98.
256. Xu L, Hunter ZR, Yang G, Zhou Y, Cao Y, Liu X, et al. MYD88 L265P in Waldenstrom macroglobulinemia, immunoglobulin M monoclonal gammopathy, and other B-cell lymphoproliferative disorders using conventional and quantitative allele-specific polymerase chain reaction. *Blood.* 2013;121(11):2051-8.
257. Growkova K, Kufova Z, Sevcikova T, Filipova J, Kascak M, Jelinek T, et al. Diagnostic Tools of Waldenstroms Macroglobulinemia - Best Possibilities for Non-invasive and Long-term Disease Monitoring. *Klin Onkol.* 2017;30(Supplementum2):81-91.
258. Mach-Pascual S, Legare RD, Lu D, Kroon M, Neuberg D, Tantravahi R, et al. Predictive value of clonality assays in patients with non-Hodgkin's lymphoma undergoing autologous bone marrow transplant: a single institution study. *Blood.* 1998;91(12):4496-503.
259. Allen RC, Zoghbi HY, Moseley AB, Rosenblatt HM, Belmont JW. Methylation of HpaII and HhaI sites near the polymorphic CAG repeat in the human androgen-receptor gene correlates with X chromosome inactivation. *Am J Hum Genet.* 1992;51(6):1229-39.
260. Lau AW, Brown CJ, Penaherrera M, Langlois S, Kalousek DK, Robinson WP. Skewed X-chromosome inactivation is common in fetuses or newborns associated with confined placental mosaicism. *Am J Hum Genet.* 1997;61(6):1353-61.
261. Varettoni M, Zibellini S, Arcaini L, Boveri E, Rattotti S, Pascutto C, et al. MYD88 (L265P) mutation is an independent risk factor for progression in patients with IgM monoclonal gammopathy of undetermined significance. *Blood.* 2013;122(13):2284-5.
262. Mori N, Ohwashi M, Yoshinaga K, Mitsushashi K, Tanaka N, Teramura M, et al. L265P mutation of the MYD88 gene is frequent in Waldenstrom's macroglobulinemia and its absence in myeloma. *PLoS One.* 2013;8(11):e80088.
263. Chilton PM, Embry CA, Mitchell TC. Effects of Differences in Lipid A Structure on TLR4 Pro-Inflammatory Signaling and Inflammasome Activation. *Front Immunol.* 2012;3:154.

264. Schroder K, Tschopp J. The inflammasomes. *Cell*. 2010;140(6):821-32.
265. Franchi L, Munoz-Planillo R, Nunez G. Sensing and reacting to microbes through the inflammasomes. *Nat Immunol*. 2012;13(4):325-32.
266. Zhan C, Qi R, Wei G, Guven-Maiorov E, Nussinov R, Ma B. Conformational dynamics of cancer-associated MyD88-TIR domain mutant L252P (L265P) allosterically tilts the landscape toward homo-dimerization. *Protein Eng Des Sel*. 2016;29(9):347-54.
267. Sikora KA, Bennett JR, Vyncke L, Deng Z, Tsai WL, Pauwels E, et al. Germline gain-of-function myeloid differentiation primary response gene-88 (MYD88) mutation in a child with severe arthritis. *J Allergy Clin Immunol*. 2018;141(5):1943-7.e9.
268. Donovan KA, Lacy MQ, Gertz MA, Lust JA. IL-1beta expression in IgM monoclonal gammopathy and its relationship to multiple myeloma. *Leukemia*. 2002;16(3):382-5.
269. McKerrell T, Park N, Chi J, Collord G, Moreno T, Ponstingl H, et al. JAK2 V617F hematopoietic clones are present several years prior to MPN diagnosis and follow different expansion kinetics. *Blood Adv*. 2017;1(14):968-71.
270. Ma X. Epidemiology of myelodysplastic syndromes. *Am J Med*. 2012;125(7 Suppl):S2-5.
271. Wang ES. Treating acute myeloid leukemia in older adults. *Hematology Am Soc Hematol Educ Program*. 2014;2014(1):14-20.
272. Thota S, Viny AD, Makishima H, Spitzer B, Radivoyevitch T, Przychodzen B, et al. Genetic alterations of the cohesin complex genes in myeloid malignancies. *Blood*. 2014;124(11):1790-8.
273. Kim JS, He X, Orr B, Wutz G, Hill V, Peters JM, et al. Intact Cohesion, Anaphase, and Chromosome Segregation in Human Cells Harboring Tumor-Derived Mutations in STAG2. *PLoS Genet*. 2016;12(2):e1005865.
274. Solomon DA, Kim T, Diaz-Martinez LA, Fair J, Elkahloun AG, Harris BT, et al. Mutational inactivation of STAG2 causes aneuploidy in human cancer. *Science*. 2011;333(6045):1039-43.
275. Challen GA, Sun D, Jeong M, Luo M, Jelinek J, Berg JS, et al. Dnmt3a is essential for hematopoietic stem cell differentiation. *Nat Genet*. 2011;44(1):23-31.
276. Koya J, Kataoka K, Sato T, Bando M, Kato Y, Tsuruta-Kishino T, et al. DNMT3A R882 mutants interact with polycomb proteins to block haematopoietic stem and leukaemic cell differentiation. *Nat Commun*. 2016;7:10924.
277. Pan F, Wingo TS, Zhao Z, Gao R, Makishima H, Qu G, et al. Tet2 loss leads to hypermutagenicity in haematopoietic stem/progenitor cells. *Nat Commun*. 2017;8:15102.
278. Mekinian A, Dervin G, Lapidus N, Kahn JE, Terriou L, Liozon E, et al. Biologics in myelodysplastic syndrome-related systemic inflammatory and autoimmune diseases: French multicenter retrospective study of 29 patients. *Autoimmun Rev*. 2017;16(9):903-10.
279. Cotter PD, May A, Fitzsimons EJ, Houston T, Woodcock BE, al-Sabah AI, et al. Late-onset X-linked sideroblastic anemia. Missense mutations in the erythroid delta-aminolevulinate synthase (ALAS2) gene in two pyridoxine-responsive patients initially diagnosed with acquired refractory anemia and ringed sideroblasts. *J Clin Invest*. 1995;96(4):2090-6.
280. Braunstein M, Ozcelik T, Bagislar S, Vakil V, Smith EL, Dai K, et al. Endothelial progenitor cells display clonal restriction in multiple myeloma. *BMC Cancer*. 2006;6:161.
281. Pathak S, Rowczenio DM, Owen RG, Doody GM, Newton DJ, Taylor C, et al. Exploratory study of MYD88 L265P, rare NLRP3 variants and clonal hematopoiesis prevalence in patients with Schnitzler's Syndrome. *Arthritis Rheumatol*. 2019.
282. Jackson DA, ElSawa SF. Factors regulating immunoglobulin production by normal and disease-associated plasma cells. *Biomolecules*. 2015;5(1):20-40.
283. Rodriguez-Zhurbenko N, Quach TD, Hopkins TJ, Rothstein TL, Hernandez AM. Human B-1 Cells and B-1 Cell Antibodies Change With Advancing Age. *Front Immunol*. 2019;10:483.
284. Lobo PI. Role of Natural Autoantibodies and Natural IgM Anti-Leucocyte Autoantibodies in Health and Disease. *Front Immunol*. 2016;7:198.
285. Murphy C, Devine T, O'Kennedy R. Technology advancements in antibody purification. *Antibody Technology Journal*. 2019;6:17-32.

286. Cambier JC, Butler JE. A rapid method for the purification of immunoglobulin M (IgM) from the sera of certain mammalian species. *Prep Biochem.* 1974;4(1):31-46.
287. Fassina G, Ruvo M, Palombo G, Verdoliva A, Marino M. Novel ligands for the affinity-chromatographic purification of antibodies. *J Biochem Biophys Methods.* 2001;49(1-3):481-90.
288. Reymond Sutandy F, Qian J, Chen CS, Zhu H. Overview of Protein Microarrays. *Curr Protoc Protein Sci.* 2013;0 27:Unit-27 1.
289. Ekins RP. Multi-analyte immunoassay. *J Pharm Biomed Anal.* 1989;7(2):155-68.
290. Kastritis E, Leblond V, Dimopoulos MA, Kimby E, Staber P, Kersten MJ, et al. Waldenstrom's macroglobulinaemia: ESMO Clinical Practice Guidelines for diagnosis, treatment and follow-up. *Ann Oncol.* 2018;29(Supplement_4):iv41-iv50.
291. Agathangelidis A, Darzentas N, Hadzidimitriou A, Brochet X, Murray F, Yan XJ, et al. Stereotyped B-cell receptors in one-third of chronic lymphocytic leukemia: a molecular classification with implications for targeted therapies. *Blood.* 2012;119(19):4467-75.
292. Brazdilova K, Plevova K, Skuhrova Francova H, Kockova H, Borsky M, Bikos V, et al. Multiple productive IGH rearrangements denote oligoclonality even in immunophenotypically monoclonal CLL. *Leukemia.* 2018;32(1):234-6.
293. Porath J, Maisano F, Belew M. Thiophilic adsorption--a new method for protein fractionation. *FEBS Lett.* 1985;185(2):306-10.
294. Madadlou A, O'Sullivan S, Sheehan D. Fast protein liquid chromatography. *Methods Mol Biol.* 2011;681:439-47.
295. Gautam S, Loh KC. Immunoglobulin-M purification--challenges and perspectives. *Biotechnol Adv.* 2011;29(6):840-9.
296. Hutchens TW. Thiophilic adsorption chromatography. *Methods Mol Biol.* 1992;11:1-15.
297. Hu S, Song G, Neiswinger J, Zhu H. Proteins on the HuProt array are well folded. Johns Hopkins: CDI Laboratories.
298. Bagnara D, Squillario M, Kipling D, Mora T, Walczak AM, Da Silva L, et al. A Reassessment of IgM Memory Subsets in Humans. *J Immunol.* 2015;195(8):3716-24.
299. Ayoglu B, Mitsios N, Kockum I, Khademi M, Zandian A, Sjoberg R, et al. Anoctamin 2 identified as an autoimmune target in multiple sclerosis. *Proc Natl Acad Sci U S A.* 2016;113(8):2188-93.
300. Brahms H, Raymackers J, Union A, de Keyser F, Meheus L, Luhrmann R. The C-terminal RG dipeptide repeats of the spliceosomal Sm proteins D1 and D3 contain symmetrical dimethylarginines, which form a major B-cell epitope for anti-Sm autoantibodies. *J Biol Chem.* 2000;275(22):17122-9.
301. Arroyo-Avila M, Santiago-Casas Y, McGwin G, Jr., Cantor RS, Petri M, Ramsey-Goldman R, et al. Clinical associations of anti-Smith antibodies in PROFILE: a multi-ethnic lupus cohort. *Clin Rheumatol.* 2015;34(7):1217-23.
302. Yuan F, Wei F, Huang H, Xue Y, Guo P, You Y. The Predictive Value of Autoantibody Spectrum on Organ Damage in Patients With Systemic Lupus Erythematosus. *Arch Rheumatol.* 2019;34(2).
303. Gonzalez CM, Lopez-Longo FJ, Monteagudo I, Grau R, Rodriguez-Mahou M, St-Cyr C, et al. Antiribonucleoprotein antibodies in children with human immunodeficiency virus infection: comparative study with childhood-onset systemic lupus erythematosus. *Pediatr AIDS HIV Infect.* 1996;7(6):401-8.
304. Sundar K, Jacques S, Gottlieb P, Villars R, Benito ME, Taylor DK, et al. Expression of the Epstein-Barr virus nuclear antigen-1 (EBNA-1) in the mouse can elicit the production of anti-dsDNA and anti-Sm antibodies. *J Autoimmun.* 2004;23(2):127-40.
305. Kawamoto N, Yamada A, Ohkouchi S, Maeda T, Tanaka S, Hashimoto T, et al. IgG reactive to CTL-directed epitopes of self-antigens is either lacking or unbalanced in atopic dermatitis patients. *Tissue Antigens.* 2003;61(5):352-61.

306. Parker CE, Nguyen TM, Segal D, MacDonald JK, Chande N. Low dose naltrexone for induction of remission in Crohn's disease. *Cochrane Database Syst Rev.* 2018;4:Cd010410.
307. Parkitny L, Younger J. Reduced Pro-Inflammatory Cytokines after Eight Weeks of Low-Dose Naltrexone for Fibromyalgia. *Biomedicines.* 2017;5(2).
308. Ludwig MD, Turel AP, Zagon IS, McLaughlin PJ. Long-term treatment with low dose naltrexone maintains stable health in patients with multiple sclerosis. *Mult Scler J Exp Transl Clin.* 2016;2:2055217316672242.
309. Turel AP, Oh KH, Zagon IS, McLaughlin PJ. Low Dose Naltrexone for Treatment of Multiple Sclerosis: A Retrospective Chart Review of Safety and Tolerability. *J Clin Psychopharmacol.* 2015;35(5):609-11.
310. Yang J, Xu Z, Sui M, Han J, Sun L, Jia X, et al. Co-Positivity for Anti-dsDNA, -Nucleosome and -Histone Antibodies in Lupus Nephritis Is Indicative of High Serum Levels and Severe Nephropathy. *PLoS One.* 2015;10(10):e0140441.
311. Abreu-Velez AM, Howard MS. Collagen IV in Normal Skin and in Pathological Processes. *N Am J Med Sci.* 2012;4(1):1-8.
312. Vasoo S. Drug-induced lupus: an update. *Lupus.* 2006;15(11):757-61.
313. Araujo-Fernandez S, Ahijon-Lana M, Isenberg DA. Drug-induced lupus: Including anti-tumour necrosis factor and interferon induced. *Lupus.* 2014;23(6):545-53.
314. Petty RE, Hunt DW, Rosenberg AM. Antibodies to type IV collagen in rheumatic diseases. *J Rheumatol.* 1986;13(2):246-53.
315. Mackel AM, DeLustro F, DeLustro B, Fudenberg HH, LeRoy EC. Immune response to connective tissue components of the basement membrane. *Connect Tissue Res.* 1982;10(3-4):333-43.
316. Flaegstad T, Fredriksen K, Dahl B, Traavik T, Rekvig OP. Inoculation with BK virus may break immunological tolerance to histone and DNA antigens. *Proc Natl Acad Sci U S A.* 1988;85(21):8171-5.
317. Pestronk A, Choksi R, Logigian E, Al-Lozi MT. Sensory neuropathy with monoclonal IgM binding to a trisulfated heparin disaccharide. *Muscle Nerve.* 2003;27(2):188-95.
318. Kritzman J, Kunkel HG, McCarthy J, Mellors RC. Studies of a Waldenstrom-type macroglobulin with rheumatoid factor properties. *J Lab Clin Med.* 1961;57:905-17.
319. Stone MJ, Merlini G, Pascual V. Autoantibody activity in Waldenstrom's macroglobulinemia. *Clin Lymphoma.* 2005;5(4):225-9.
320. Kurowska W, Kuca-Warnawin EH, Radzikowska A, Maslinski W. The role of anti-citrullinated protein antibodies (ACPA) in the pathogenesis of rheumatoid arthritis. *Cent Eur J Immunol.* 2017;42(4):390-8.
321. Gul A. Dynamics of Inflammatory Response in Autoinflammatory Disorders: Autonomous and Hyperinflammatory States. *Front Immunol.* 2018;9:2422.
322. Kriangkum J, Motz SN, Mack T, Beiggi S, Baigorri E, Kuppusamy H, et al. Single-Cell Analysis and Next-Generation Immuno-Sequencing Show That Multiple Clones Persist in Patients with Chronic Lymphocytic Leukemia. *PLoS One.* 2015;10(9):e0137232.
323. Tan YG, Wang YQ, Zhang M, Han YX, Huang CY, Zhang HP, et al. Clonal Characteristics of Circulating B Lymphocyte Repertoire in Primary Biliary Cholangitis. *J Immunol.* 2016;197(5):1609-20.
324. Darzentas N, Stamatopoulos K. Stereotyped B cell receptors in B cell leukemias and lymphomas. *Methods Mol Biol.* 2013;971:135-48.
325. Hershberg U, Luning Prak ET. The analysis of clonal expansions in normal and autoimmune B cell repertoires. *Philos Trans R Soc Lond B Biol Sci.* 2015;370(1676).
326. Truck J, Ramasamy MN, Galson JD, Rance R, Parkhill J, Lunter G, et al. Identification of antigen-specific B cell receptor sequences using public repertoire analysis. *J Immunol.* 2015;194(1):252-61.
327. Chiorazzi N, Ferrarini M. Cellular origin(s) of chronic lymphocytic leukemia: cautionary notes and additional considerations and possibilities. *Blood.* 2011;117(6):1781-91.

328. Darzentas N, Hadzidimitriou A, Murray F, Hatzi K, Josefsson P, Laoutaris N, et al. A different ontogenesis for chronic lymphocytic leukemia cases carrying stereotyped antigen receptors: molecular and computational evidence. *Leukemia*. 2010;24(1):125-32.
329. Chaudhary N, Wesemann DR. Analyzing Immunoglobulin Repertoires. *Front Immunol*. 2018;9.
330. Femand JP, Bridoux F, Dispenzieri A, Jaccard A, Kyle RA, Leung N, et al. Monoclonal gammopathy of clinical significance: a novel concept with therapeutic implications. *Blood*. 2018.
331. Arcila ME, Yu W, Syed M, Kim H, Maciag L, Yao J, et al. Establishment of Immunoglobulin Heavy (IGH) Chain Clonality Testing by Next-Generation Sequencing for Routine Characterization of B-Cell and Plasma Cell Neoplasms. *J Mol Diagn*. 2019;21(2):330-42.
332. Janeway C. *The generation of diversity in immunoglobulins*: Garland Science; 2001 2001.
333. Calis JJ, Rosenberg BR. Characterizing immune repertoires by high throughput sequencing: strategies and applications. *Trends Immunol*. 2014;35(12):581-90.
334. Vettermann C, Schlissel MS. Allelic exclusion of immunoglobulin genes: models and mechanisms. *Immunol Rev*. 2010;237(1):22-42.
335. DeWitt WS, Lindau P, Snyder TM, Sherwood AM, Vignali M, Carlson CS, et al. A Public Database of Memory and Naive B-Cell Receptor Sequences. *PLoS One*. 2016;11(8):e0160853.
336. Langerak AW, Groenen PJ, Bruggemann M, Beldjord K, Bellan C, Bonello L, et al. EuroClonality/BIOMED-2 guidelines for interpretation and reporting of Ig/TCR clonality testing in suspected lymphoproliferations. *Leukemia*. 2012;26(10):2159-71.
337. Polonelli L, Ponton J, Elguezal N, Moragues MD, Casoli C, Pilotti E, et al. Antibody complementarity-determining regions (CDRs) can display differential antimicrobial, antiviral and antitumor activities. *PLoS One*. 2008;3(6):e2371.
338. Sela-Culang I, Kunik V, Ofra Y. The structural basis of antibody-antigen recognition. *Front Immunol*. 2013;4:302.
339. Chothia C, Lesk AM. Canonical structures for the hypervariable regions of immunoglobulins. *J Mol Biol*. 1987;196(4):901-17.
340. Chothia C, Lesk AM, Tramontano A, Levitt M, Smith-Gill SJ, Air G, et al. Conformations of immunoglobulin hypervariable regions. *Nature*. 1989;342(6252):877-83.
341. Davies DR, Cohen GH. Interactions of protein antigens with antibodies. *Proc Natl Acad Sci U S A*. 1996;93(1):7-12.
342. D'Angelo S, Ferrara F, Naranjo L, Erasmus MF, Hraber P, Bradbury ARM. Many Routes to an Antibody Heavy-Chain CDR3: Necessary, Yet Insufficient, for Specific Binding. *Front Immunol*. 2018;9:395.
343. Ralph DK, Matsen FA. Consistency of VDJ Rearrangement and Substitution Parameters Enables Accurate B Cell Receptor Sequence Annotation. *PLoS Comput Biol*. 2016;12(1).
344. Kovaltsuk A, Krawczyk K, Galson JD, Kelly DF, Deane CM, Truck J. How B-Cell Receptor Repertoire Sequencing Can Be Enriched with Structural Antibody Data. *Front Immunol*. 2017;8:1753.
345. Davis MM. The evolutionary and structural 'logic' of antigen receptor diversity. *Semin Immunol*. 2004;16(4):239-43.
346. Racanelli V, Brunetti C, De Re V, Caggiari L, De Zorzi M, Leone P, et al. Antibody V(h) repertoire differences between resolving and chronically evolving hepatitis C virus infections. *PLoS One*. 2011;6(9):e25606.
347. Martin DA, Bradl H, Collins TJ, Roth E, Jack HM, Wu GE. Selection of Ig mu heavy chains by complementarity-determining region 3 length and amino acid composition. *J Immunol*. 2003;171(9):4663-71.
348. Miqueu P, Guillet M, Degauque N, Dore JC, Soullillou JP, Brouard S. Statistical analysis of CDR3 length distributions for the assessment of T and B cell repertoire biases. *Mol Immunol*. 2007;44(6):1057-64.

349. Zemlin M, Klinger M, Link J, Zemlin C, Bauer K, Engler JA, et al. Expressed murine and human CDR-H3 intervals of equal length exhibit distinct repertoires that differ in their amino acid composition and predicted range of structures. *J Mol Biol.* 2003;334(4):733-49.
350. Rene C, Prat N, Thuizat A, Broctawik M, Avinens O, Eliaou JF. Comprehensive characterization of immunoglobulin gene rearrangements in patients with chronic lymphocytic leukaemia. *J Cell Mol Med.* 2014;18(6):979-90.
351. Baptista MJ, Calpe E, Fernandez E, Colomo L, Cardesa-Salzman TM, Abrisqueta P, et al. Analysis of the IGHV region in Burkitt's lymphomas supports a germinal center origin and a role for superantigens in lymphomagenesis. *Leuk Res.* 2014;38(4):509-15.
352. Kriangkum J, Motz SN, Debes Marun CS, Lafarge ST, Gibson SB, Venner CP, et al. Frequent occurrence of highly expanded but unrelated B-cell clones in patients with multiple myeloma. *PLoS One.* 2013;8(5):e64927.
353. Hong B, Wu Y, Li W, Wang X, Wen Y, Jiang S, et al. In-Depth Analysis of Human Neonatal and Adult IgM Antibody Repertoires. *Front Immunol.* 2018;9:128.
354. Martin VG, Wu YB, Townsend CL, Lu GH, O'Hare JS, Mozeika A, et al. Transitional B Cells in Early Human B Cell Development - Time to Revisit the Paradigm? *Front Immunol.* 2016;7:546.
355. Tonegawa S. Somatic generation of antibody diversity. *Nature.* 1983;302(5909):575-81.
356. Wu YC, Kipling D, Leong HS, Martin V, Ademokun AA, Dunn-Walters DK. High-throughput immunoglobulin repertoire analysis distinguishes between human IgM memory and switched memory B-cell populations. *Blood.* 2010;116(7):1070-8.
357. Adderson EE, Shackelford PG, Quinn A, Wilson PM, Cunningham MW, Insel RA, et al. Restricted immunoglobulin VH usage and VDJ combinations in the human response to Haemophilus influenzae type b capsular polysaccharide. Nucleotide sequences of monospecific anti-Haemophilus antibodies and polyspecific antibodies cross-reacting with self antigens. *J Clin Invest.* 1993;91(6):2734-43.
358. Varettoni M, Zibellini S, Capello D, Arcaini L, Rossi D, Pascutto C, et al. Clues to pathogenesis of Waldenstrom macroglobulinemia and immunoglobulin M monoclonal gammopathy of undetermined significance provided by analysis of immunoglobulin heavy chain gene rearrangement and clustering of B-cell receptors. *Leuk Lymphoma.* 2013;54(11):2485-9.
359. Boes M. Role of natural and immune IgM antibodies in immune responses. *Mol Immunol.* 2000;37(18):1141-9.
360. Kaveri SV, Silverman GJ, Bayry J. Natural IgM in immune equilibrium and harnessing their therapeutic potential. *J Immunol.* 2012;188(3):939-45.
361. Czajkowsky DM, Shao Z. The human IgM pentamer is a mushroom-shaped molecule with a flexural bias. *Proc Natl Acad Sci U S A.* 2009;106(35):14960-5.
362. Cooper NR. The classical complement pathway: activation and regulation of the first complement component. *Adv Immunol.* 1985;37:151-216.
363. Elkon KB, Silverman GJ. Naturally occurring autoantibodies to apoptotic cells. *Adv Exp Med Biol.* 2012;750:14-26.
364. Chong BF, Tseng LC, Lee T, Vasquez R, Li QZ, Zhang S, et al. IgG and IgM autoantibody differences in discoid and systemic lupus patients. *J Invest Dermatol.* 2012;132(12):2770-9.
365. Podolska MJ, Biermann MH, Maueroder C, Hahn J, Herrmann M. Inflammatory etiopathogenesis of systemic lupus erythematosus: an update. *J Inflamm Res.* 2015;8:161-71.
366. Ichinohe T, Miyama T, Kawase T, Honjo Y, Kitaura K, Sato H, et al. Next-Generation Immune Repertoire Sequencing as a Clue to Elucidate the Landscape of Immune Modulation by Host-Gut Microbiome Interactions. *Front Immunol.* 2018;9:668.
367. van Dongen JJ, Langerak AW, Bruggemann M, Evans PA, Hummel M, Lavender FL, et al. Design and standardization of PCR primers and protocols for detection of clonal immunoglobulin and T-cell receptor gene recombinations in suspect lymphoproliferations: report of the BIOMED-2 Concerted Action BMH4-CT98-3936. *Leukemia.* 2003;17(12):2257-317.

368. Georgiou G, Ippolito GC, Beausang J, Busse CE, Wardemann H, Quake SR. The promise and challenge of high-throughput sequencing of the antibody repertoire. *Nat Biotechnol.* 2014;32(2):158-68.
369. Alamyar E, Duroux P, Lefranc MP, Giudicelli V. IMGT((R)) tools for the nucleotide analysis of immunoglobulin (IG) and T cell receptor (TR) V-(D)-J repertoires, polymorphisms, and IG mutations: IMGT/V-QUEST and IMGT/HighV-QUEST for NGS. *Methods Mol Biol.* 2012;882:569-604.
370. Lefranc MP. From IMGT-ONTOLOGY DESCRIPTION axiom to IMGT standardized labels: for immunoglobulin (IG) and T cell receptor (TR) sequences and structures. *Cold Spring Harb Protoc.* 2011;2011(6):614-26.
371. Lefranc MP, Pommie C, Ruiz M, Giudicelli V, Foulquier E, Truong L, et al. IMGT unique numbering for immunoglobulin and T cell receptor variable domains and Ig superfamily V-like domains. *Dev Comp Immunol.* 2003;27(1):55-77.
372. Lefranc MP, Pommie C, Kaas Q, Duprat E, Bosc N, Guiraudou D, et al. IMGT unique numbering for immunoglobulin and T cell receptor constant domains and Ig superfamily C-like domains. *Dev Comp Immunol.* 2005;29(3):185-203.
373. Lefranc MP. IMGT unique numbering for the variable (V), constant (C), and groove (G) domains of IG, TR, MH, IgSF, and MhSF. *Cold Spring Harb Protoc.* 2011;2011(6):633-42.
374. Wang HW, Raffeld M. Molecular assessment of clonality in lymphoid neoplasms. *Semin Hematol.* 2019;56(1):37-45.
375. Lange MD, Huang L, Yu Y, Li S, Liao H, Zemlin M, et al. Accumulation of VH Replacement Products in IgH Genes Derived from Autoimmune Diseases and Anti-Viral Responses in Human. *Front Immunol.* 2014;5:345.
376. Małecka A, Trøen G, Tierens A, Østlie I, Małecki J, Randen U, et al. Immunoglobulin heavy and light chain gene features are correlated with primary cold agglutinin disease onset and activity. *Haematologica.* 2016;101(9):e361-4.
377. Kim S, Park I, Park SG, Cho S, Kim JH, Ipper NS, et al. Generation, Diversity Determination, and Application to Antibody Selection of a Human Naive Fab Library. *Mol Cells.* 2017;40(9):655-66.
378. Elhanati Y, Sethna Z, Marcou Q, Callan CG, Jr., Mora T, Walczak AM. Inferring processes underlying B-cell repertoire diversity. *Philos Trans R Soc Lond B Biol Sci.* 2015;370(1676).
379. Parameswaran P, Liu Y, Roskin KM, Jackson KK, Dixit VP, Lee JY, et al. Convergent antibody signatures in human dengue. *Cell Host Microbe.* 2013;13(6):691-700.
380. Child FJ, Woolford AJ, Calonje E, Russell-Jones R, Whittaker SJ. Molecular analysis of the immunoglobulin heavy chain gene in the diagnosis of primary cutaneous B cell lymphoma. *J Invest Dermatol.* 2001;117(4):984-9.
381. Agathangelidis A, Sutton LA, Hadzidimitriou A, Tresoldi C, Langerak AW, Belessi C, et al. Immunoglobulin Gene Sequence Analysis In Chronic Lymphocytic Leukemia: From Patient Material To Sequence Interpretation. *J Vis Exp.* 2018(141).
382. Lefranc MP. IMGT, the international ImMunoGeneTics database. *Nucleic Acids Res.* 2001;29(1):207-9.
383. IJspeert H, van Schouwenburg PA, van Zessen D, Pico-Knijnenburg I, Stubbs AP, van der Burg M. Antigen Receptor Galaxy: A User-Friendly, Web-Based Tool for Analysis and Visualization of T and B Cell Receptor Repertoire Data. *J Immunol.* 2017;198(10):4156-65.
384. Burnet FM. The immunological significance of the thymus: an extension of the clonal selection theory of immunity. *Australas Ann Med.* 1962;11:79-91.
385. Sekiguchi DR, Eisenberg RA, Weigert M. Secondary heavy chain rearrangement: a mechanism for generating anti-double-stranded DNA B cells. *J Exp Med.* 2003;197(1):27-39.
386. IJspeert H, Wentink M, van Zessen D, Driessen GJ, Dalm VA, van Hagen MP, et al. Strategies for B-cell receptor repertoire analysis in primary immunodeficiencies: from severe combined immunodeficiency to common variable immunodeficiency. *Front Immunol.* 2015;6:157.
387. Fink K. Can We Improve Vaccine Efficacy by Targeting T and B Cell Repertoire Convergence? *Front Immunol.* 2019;10:110.

388. Tak PP, Doorenspleet ME, de Hair MJH, Klarenbeek PL, van Beers-Tas MH, van Kampen AHC, et al. Dominant B cell receptor clones in peripheral blood predict onset of arthritis in individuals at risk for rheumatoid arthritis. *Ann Rheum Dis*. 2017;76(11):1924-30.
389. Reddy ST, Ge X, Miklos AE, Hughes RA, Kang SH, Hoi KH, et al. Monoclonal antibodies isolated without screening by analyzing the variable-gene repertoire of plasma cells. *Nat Biotechnol*. 2010;28(9):965-9.
390. Baumer C, Fisch E, Wedler H, Reinecke F, Korfhage C. Exploring DNA quality of single cells for genome analysis with simultaneous whole-genome amplification. *Sci Rep*. 2018;8(1):7476.
391. Crombie J, Davids MS. IGHV mutational status testing in chronic lymphocytic leukemia. *Am J Hematol*. 2017;92(12):1393-7.
392. Kyte J, Doolittle RF. A simple method for displaying the hydropathic character of a protein. *J Mol Biol*. 1982;157(1):105-32.
393. Jimenez C, Sebastian E, Chillon MC, Giraldo P, Mariano Hernandez J, Escalante F, et al. MYD88 L265P is a marker highly characteristic of, but not restricted to, Waldenstrom's macroglobulinemia. *Leukemia*. 2013;27(8):1722-8.
394. Lee YN, Frugoni F, Dobbs K, Tirosh I, Du L, Ververs FA, et al. Characterization of T and B cell repertoire diversity in patients with RAG deficiency. *Sci Immunol*. 2016;1(6).
395. George D, Mallery P. *SPSS for Windows Step by Step: A Simple Guide and Reference* 10 ed. Boston, USA.: Pearson; 2010.
396. Shi B, Yu J, Ma L, Ma Q, Liu C, Sun S, et al. Short-term assessment of BCR repertoires of SLE patients after high dose glucocorticoid therapy with high-throughput sequencing. *Springerplus*. 2016;5:75.
397. Liu S, Hou XL, Sui WG, Lu QJ, Hu YL, Dai Y. Direct measurement of B-cell receptor repertoire's composition and variation in systemic lupus erythematosus. *Genes Immun*. 2017;18(1):22-7.
398. Matsuda F, Ishii K, Bourvagnet P, Kuma K, Hayashida H, Miyata T, et al. The complete nucleotide sequence of the human immunoglobulin heavy chain variable region locus. *J Exp Med*. 1998;188(11):2151-62.
399. Ciric B, VanKeulen V, Rodriguez M, Kyle RA, Gertz MA, Pease LR. Clonal evolution in Waldenstrom macroglobulinemia highlights functional role of B-cell receptor. *Blood*. 2001;97(1):321-3.
400. Kriangkum J, Taylor BJ, Treon SP, Mant MJ, Belch AR, Pilarski LM. Clonotypic IgM V/D/J sequence analysis in Waldenstrom macroglobulinemia suggests an unusual B-cell origin and an expansion of polyclonal B cells in peripheral blood. *Blood*. 2004;104(7):2134-42.
401. Li L, Wang XH, Banerjee S, Volsky B, Williams C, Virland D, et al. Different pattern of immunoglobulin gene usage by HIV-1 compared to non-HIV-1 antibodies derived from the same infected subject. *PLoS One*. 2012;7(6):e39534.
402. Martin-Jimenez P, Garcia-Sanz R, Balanzategui A, Alcoceba M, Ocio E, Sanchez ML, et al. Molecular characterization of heavy chain immunoglobulin gene rearrangements in Waldenstrom's macroglobulinemia and IgM monoclonal gammopathy of undetermined significance. *Haematologica*. 2007;92(5):635-42.
403. Tabibian-Keissar H, Hazanov L, Schiby G, Rosenthal N, Rakovsky A, Michaeli M, et al. Aging affects B-cell antigen receptor repertoire diversity in primary and secondary lymphoid tissues. *Eur J Immunol*. 2016;46(2):480-92.
404. Vergani S, Korsunsky I, Mazzarello AN, Ferrer G, Chiorazzi N, Bagnara D. Novel Method for High-Throughput Full-Length IGHV-D-J Sequencing of the Immune Repertoire from Bulk B-Cells with Single-Cell Resolution. *Front Immunol*. 2017;8:1157.
405. Kosmidis P, Bonzheim I, Dufke C, Colak S, Hentrich T, Schroeder C, et al. Next generation sequencing of the clonal IGH rearrangement detects ongoing mutations and interfollicular trafficking in in situ follicular neoplasia. *PLoS One*. 2017;12(6):e0178503.

406. Katsibardi K, Braoudaki M, Papathanasiou C, Karamolegou K, Tzortzatou-Stathopoulou F. Clinical significance of productive immunoglobulin heavy chain gene rearrangements in childhood acute lymphoblastic leukemia. *Leuk Lymphoma*. 2011;52(9):1751-7.
407. Li A, Rue M, Zhou J, Wang H, Goldwasser MA, Neuberg D, et al. Utilization of Ig heavy chain variable, diversity, and joining gene segments in children with B-lineage acute lymphoblastic leukemia: implications for the mechanisms of VDJ recombination and for pathogenesis. *Blood*. 2004;103(12):4602-9.
408. Sudhakar N, Rajkumar T, Rajalekshmy KR, Nancy NK. Characterization of clonal immunoglobulin heavy (IGH) V-D-J gene rearrangements and the complementarity-determining region in South Indian patients with precursor B-cell acute lymphoblastic leukemia. *Blood Res*. 2017;52(1):55-61.
409. Kirsch I, Vignali M, Robins H. T-cell receptor profiling in cancer. *Mol Oncol*. 2015;9(10):2063-70.
410. Sun G, Qiu L, Cheng Z, Pan W, Qiu J, Zou C, et al. Association of the characteristics of B- and T-cell repertoires with papillary thyroid carcinoma. *Oncol Lett*. 2018;16(2):1584-92.
411. Wang L, Dai Y, Liu S, Lai L, Yan Q, Chen H, et al. Assessment of variation in B-cell receptor heavy chain repertoire in patients with end-stage renal disease by high-throughput sequencing. *Ren Fail*. 2019;41(1):1-13.
412. Yu L, Guan Y. Immunologic Basis for Long HCDR3s in Broadly Neutralizing Antibodies Against HIV-1. *Front Immunol*. 2014;5:250.
413. Larimore K, McCormick MW, Robins HS, Greenberg PD. Shaping of human germline IgH repertoires revealed by deep sequencing. *J Immunol*. 2012;189(6):3221-30.
414. Giles I, Lambrianides N, Latchman D, Chen P, Chukwuocha R, Isenberg D, et al. The critical role of arginine residues in the binding of human monoclonal antibodies to cardiolipin. *Arthritis Res Ther*. 2005;7(1):R47-56.
415. Townsend CL, Laffy JM, Wu YB, Silva O'Hare J, Martin V, Kipling D, et al. Significant Differences in Physicochemical Properties of Human Immunoglobulin Kappa and Lambda CDR3 Regions. *Front Immunol*. 2016;7:388.
416. Ademokun A, Wu YC, Martin V, Mitra R, Sack U, Baxendale H, et al. Vaccination-induced changes in human B-cell repertoire and pneumococcal IgM and IgA antibody at different ages. *Aging Cell*. 2011;10(6):922-30.
417. Mroczek ES, Ippolito GC, Rogosch T, Hoi KH, Hwangpo TA, Brand MG, et al. Differences in the composition of the human antibody repertoire by B cell subsets in the blood. *Front Immunol*. 2014;5:96.
418. Petrova VN, Muir L, McKay PF, Vassiliou GS, Smith KGC, Lyons PA, et al. Combined Influence of B-Cell Receptor Rearrangement and Somatic Hypermutation on B-Cell Class-Switch Fate in Health and in Chronic Lymphocytic Leukemia. *Front Immunol*. 2018;9:1784.
419. Gachard N, Parrens M, Soubeyran I, Petit B, Marfak A, Rizzo D, et al. IGHV gene features and MYD88 L265P mutation separate the three marginal zone lymphoma entities and Waldenstrom macroglobulinemia/lymphoplasmacytic lymphomas. *Leukemia*. 2013;27(1):183-9.
420. Henriques A, Rodriguez-Caballero A, Nieto WG, Langerak AW, Criado I, Lecrevisse Q, et al. Combined patterns of IGHV repertoire and cytogenetic/molecular alterations in monoclonal B lymphocytosis versus chronic lymphocytic leukemia. *PLoS One*. 2013;8(7):e67751.
421. Foreman AL, Lemercier B, Lim A, Kourlisky P, Kenny T, Gershwin ME, et al. VH gene usage and CDR3 analysis of B cell receptor in the peripheral blood of patients with PBC. *Autoimmunity*. 2008;41(1):80-6.
422. Bashford-Rogers RJM, Smith KGC, Thomas DC. Antibody repertoire analysis in polygenic autoimmune diseases. *Immunology*. 2018;155(1):3-17.
423. Mockridge CI, Chapman CJ, Spellerberg MB, Sheth B, Fleming TP, Isenberg DA, et al. Sequence analysis of V(4-34)-encoded antibodies from single B cells of two patients with systemic lupus erythematosus (SLE). *Clin Exp Immunol*. 1998;114(1):129-36.

424. Kraj P, Friedman DF, Stevenson F, Silberstein LE. Evidence for the overexpression of the VH4-34 (VH4.21) Ig gene segment in the normal adult human peripheral blood B cell repertoire. *J Immunol.* 1995;154(12):6406-20.
425. Schickel JN, Glauzy S, Ng YS, Chamberlain N, Massad C, Isnardi I, et al. Self-reactive VH4-34-expressing IgG B cells recognize commensal bacteria. *J Exp Med.* 2017;214(7):1991-2003.
426. Pugh-Bernard AE, Silverman GJ, Cappione AJ, Villano ME, Ryan DH, Insel RA, et al. Regulation of inherently autoreactive VH4-34 B cells in the maintenance of human B cell tolerance. *J Clin Invest.* 2001;108(7):1061-70.
427. Tiumentseva M, Morozova V, Zakabunin A, Korobko D, Malkova N, Filipenko M, et al. Use of the VH6-1 gene segment to code for anti-interleukin-18 autoantibodies in multiple sclerosis. *Immunogenetics.* 2016;68(4):237-46.
428. Soderstrom I, van Dijk-Hard I, Feld S, Hillorn V, Holmberg D, Lundkvist I. Altered VH6-D-JH repertoire in human insulin-dependent diabetes mellitus and autoimmune idiopathic thrombocytopenic purpura. *Eur J Immunol.* 1999;29(9):2853-62.
429. Merchionne F, Procaccio P, Dammacco F. Waldenstrom's macroglobulinemia. An overview of its clinical, biochemical, immunological and therapeutic features and our series of 121 patients collected in a single center. *Crit Rev Oncol Hematol.* 2011;80(1):87-99.
430. Treon SP, Xu L, Hunter Z. MYD88 Mutations and Response to Ibrutinib in Waldenstrom's Macroglobulinemia. *N Engl J Med.* 2015;373(6):584-6.
431. Varettoni M, Zibellini S, Defrancesco I, Ferretti VV, Rizzo E, Malcovati L, et al. Pattern of somatic mutations in patients with Waldenstrom macroglobulinemia or IgM monoclonal gammopathy of undetermined significance. *Haematologica.* 2017;102(12):2077-85.
432. Martin V, Wu YC, Kipling D, Dunn-Walters D. Ageing of the B-cell repertoire. *Philos Trans R Soc Lond B Biol Sci.* 2015;370(1676).
433. Yao X, Li H, Leng SX. Inflammation and immune system alterations in frailty. *Clin Geriatr Med.* 2011;27(1):79-87.
434. Kyle RA, Larson DR, Therneau TM, Dispenzieri A, Kumar S, Cerhan JR, et al. Long-Term Follow-up of Monoclonal Gammopathy of Undetermined Significance. *N Engl J Med.* 2018;378(3):241-9.
435. Paiva B, Corchete LA, Vidriales MB, Garcia-Sanz R, Perez JJ, Aires-Mejia I, et al. The cellular origin and malignant transformation of Waldenstrom macroglobulinemia. *Blood.* 2015;125(15):2370-80.
436. Gameiro A, Gouveia M, Pereira M, Tellechea O, Goncalo M. Clinical characterization and long-term follow-up of Schnitzler syndrome. *Clin Exp Dermatol.* 2016;41(5):461-7.